Università degli Studi di Padova

Dipartimento di Scienze Chimiche

Ph.D. course in: Science and Engineering of Materials and Nanostructures (**SIMN**), XXXIV cycle

The application of a sacrificial Al anode in simplified *e*ATRP

Applicazione di un anodo sacrificale di Al in eATRP semplificata

Thesis written with the financial contribution of China Scholarship Council (CSC)

Coordinator: Prof.Giovanni Mattei

Supervisor: Prof. Abdirisak Ahmed Isse

Ph.D. student: Jie Luo

October. 2021

Table of Contents

Abstract

Polymeric materials (including natural and artificial polymers) have a long history in the life of mankind, natural polymers such as wood and cotton being used for ages. Starting from the last century, polymer chemistry received rapid development with chemists' huge efforts. During this period, several synthesis approaches were deeply investigated and developed. Radical polymerization attracted attention for a long time, but with the significant weakness of broad molecular weight distribution. Recently, controlled radical polymerization (CRP) processes were achieved, allowing the production of polymers with low dispersity by minimizing termination reactions. Thus, a wide variety of CRP methods known as Reversible Deactivation Radical Polymerization (RDRP) were developed.

Among them, atom transfer radical polymerization (ATRP) is the most robust and versatile method that affords polymers of predefined molecular weight, narrow molecular weight distributions, and advanced macromolecular architectures as well as extension of chain lifetime. Despite these obvious advantages, the conventional ATRP suffers from several issues. For example, radical termination leads to the depletion of the activator species (for instance, $[Cu^{I}L]^{+}$) and thus large amounts of catalyst are needed in the system to control the polymerization. Therefore, in the past decades, several methods have been developed to regenerate activators using chemical reactions or physical stimuli that allow spatial and temporal regulation of controlled polymerizations.

Electrochemically mediated ATRP (*e*ATRP), usually performed in a two-compartment cell with Pt electrodes, is one of the popular ATRP methods. The regeneration of the activator is achieved by adjustment of the applied current or applied potential. A significant improvement of the traditional setup was achieved by using inexpensive non noble metals as cathode materials. Also, the two-compartment cell was replaced with an undivided cell with a sacrificial aluminum anode. However, there are still some unclear mechanisms about the effects of metal ions released from the sacrificial anode on catalyst stability and polymerization efficiency. These issues have been addressed in this thesis work and the obtained results will be presented as described below.

Chapter I is a review on the long development history of RDRP and simultaneously introduces several controlled radical polymerization methods such as NMP, OMRP, RAFT and ATRP. The mechanisms and development of these processes and various fundamental characteristics, including reaction components, kinetics, most relevant parameters and obtainable polymeric materials are presented.

Chapter II provides a detailed description of the development of *e*ATRP and progresses on the understanding of its dynamics and determination of several important parameters. Subsequently, simplified *e*ATRP (*se*ATRP) is introduced with special emphasis on some unclear issues about the effects of the anodic dissolution of Al on the stability and performance of copper-based catalysts, a subject that was deeply investigated during the PhD thesis and will be fully treated in **Chapters IV-VIII**.

The used reagents, instruments and corresponding principles, and related experimental methods are listed in **Chapter III**.

Chapter IV discusses the influences of Al^{3+} ions generated from anodic dissolution of Al wire on two widely used ATRP catalysts ($[Cu^{II}L]^{2+}$, L= TPMA and Me_6TREN) in three selected common organic solvents (DMF, DMSO, and MeCN). Both voltametric analysis and evolution of UV-vis-NIR spectra proved that TPMA forms more stable complexes with Cu^{2+} and Cu^{+} than with Al^{3+} in DMF and DMSO. Also $[Cu^{II}TPMA]^{2+}$ is stable in MeCN containing Al^{3+} ions, but $[Cu^{I}TPMA]^{+}$ is destroyed via replacement of Cu^{+} by Al^{3+}. Conversely, copper complexes coordinated

with Me_6TREN suffer from a competition between Al^{3+} and Cu ions for Me_6TREN in all investigated solvents. The ligand showed higher affinity for Al^{3+} than for Cu^{2+} and Cu^{+}. However, addition of enough ligand to form complexes with both Al and Cu ions could effectively suppress the competition and allow maintaining the stability of $[Cu^{II}L]^{2+}$ in the studied solvents.

Investigations on the problem of competition between Al^{3+} and Cu^{2+} were extended to typical ATRP conditions for *n*-butyl acrylate (*n*-BA), i.e., 50 vol% *n*-BA in DMF, DMSO, or MeCN and during *se*ATRP of the monomer. **Chapter V** describes the results of this study, which confirmed the results obtained in pure solvents. The negative interference of Al^{3+} ions during *e*ATRP could be suppressed by adding excess amine ligand. Using a two-fold excess of Br^{-} without excess ligand, as another potential pathway to suppress the competition, was found to be beneficial although it could not fully restore the efficiency of the Cu catalysts.

Besides organic media, investigations on the effects of anodic dissolution of Al were also carried out in aqueous solutions, as discussed in **Chapter VI**. In this system, no remarkable changes occurred to $[Cu^{II}TPMA]^{2+}$ stability, while a significant fraction of $[Cu^{II}Me_6TREN]^{2+}$ disappeared through exchange of the ligand with Al^{3+} and reduction of Cu^{2+} and $[Cu^{II}Me_6TREN]^{2+}$ by active Al. Reduction of Cu^{2+} to metallic Cu by Al was proved by the UV-vis-NIR spectra of the complexes and SEM-EDX characterization of the Al surface. The competitive equilibria between Cu and Al ions for the ligands were effectively suppressed by adding excess ligand over Cu^{2+}.

In **Chapter VII**, we also took account of the pH effects caused by the formation of aluminum hydroxides during the anodic dissolution process. Decreased pH due to Al^{3+} hydrolysis caused a small amount of $[Cu^{II}TPMA]^{2+}$ to undergo ligand protonation and hence dissociation, and nearly complete decomposition of $[Cu^{II}Me_6TREN]^{2+}$ followed by Cu^{2+} reduction to form Cu^{0} on the Al surface. When more Me_6TREN was added to the solution, the initial pH could be restored but not $[Cu^{II}Me_6TREN]^{2+}$; only a small amount of the Cu^{2+} survived reduction in the presence of Al and could be restored as $[Cu^{II}Me_6TREN]^{2+}$ when excess ligand was added. Performing the polymerization in aqueous media, the addition of excess ligand significantly improved polymerization

parameters.

In **Chapter VIII**, the possibility of using low-cost Na_2CO_3 to suppress the competitive equilibria triggered by anodic dissolution of Al was explored. Addition of Na_2CO_3 not only could effectively suppress the competitive complexation equilibria involving Al^{3+} and copper complexes in both organic solvents (DMF, DMSO, and MeCN) and aqueous media, but was also capable of recovering the pH in aqueous solutions and hence effectively enhance the polymerization rate. It is important to note that the amount of CO_3^{2-} must be strictly controlled with respect to Al^{3+} ions, otherwise, it can combine with $[Cu^{II}Me_6TREN]^{2+}$ to form a new more stable complex $[CO_3Cu^{II}Me_6TREN]$ with a more negative redox potential.

Chapter I

Introduction

Because of the change of lifestyle and the development of science and technology, polymers have experienced a revolutionary change in both materials and synthesis techniques. The earliest record of the usage of polymer materials by human being can be traced back to the Christian era.[1] The concept of 'polymer' was first introduced in 1833 by Jöns Jakob Berzelius and then polymer chemistry received rapid development since 1922.[2] Nowadays, indeed, the utilization of polymer materials is commonplace in our daily lives involving materials like plastic, rubber, coatings, fiber, adhesives, functional polymer materials, biopolymer materials, etc. Some chemists surprisingly found that only a small fraction of polymer materials come from the nature, such as natural rubber, wool, cotton, and spider webbing, with absolutely advantageous and

distinctive features. Thus, the improvement of polymerization technology could afford people a wide range of alternatives because of its low cost, easy synthesis, good quality, and environmentally friendly performance. However, the majority of commercial polymeric materials are obtained via conventional step growth or ionic polymerizations, which are limited by two main factors: poorly controlled architectures and broad molecular weight distribution.[3-5]

Free radical polymerization has also been known for a long time but development of the process rapidly grew in the period from 1910s to ~1950s.[6] **Scheme 1.1** presents a general radical polymerization mechanism: i) radical generation–initiation, ii) radical propagation, iii) chain transfer, and iv) chain termination.[3-4, 7-8]

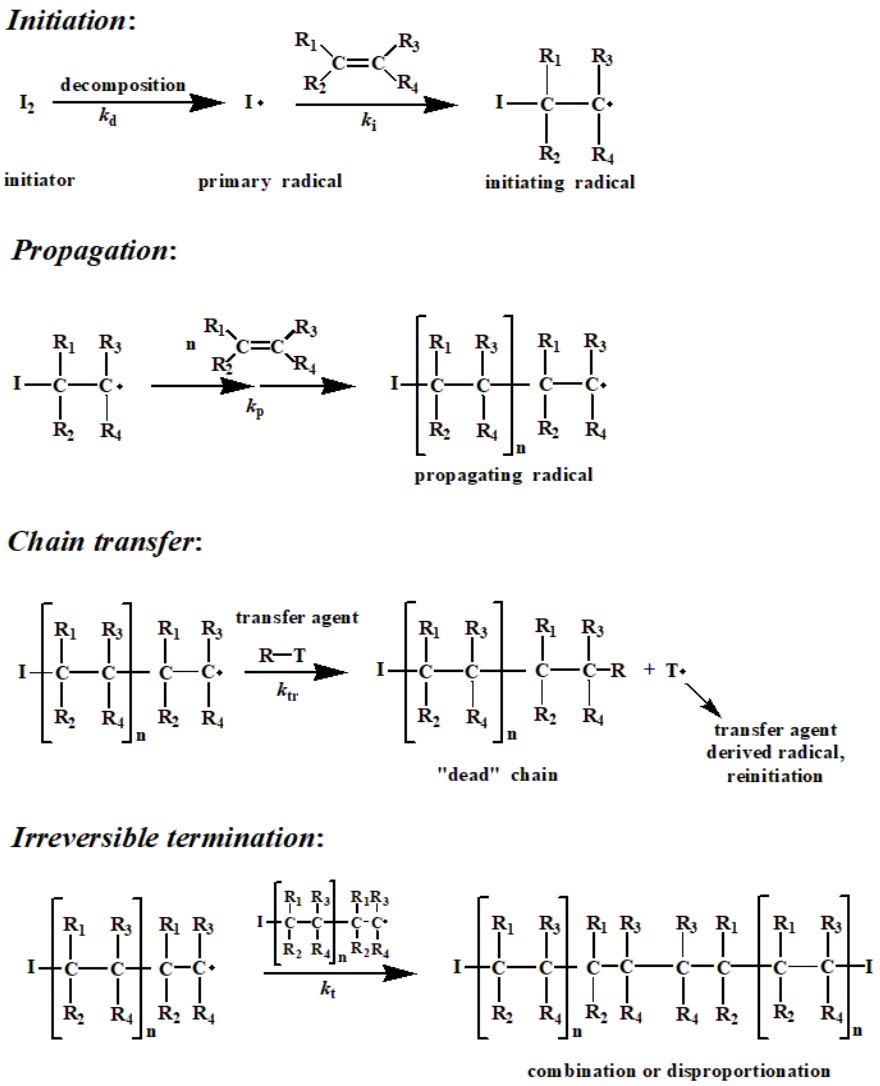

Scheme 1.1 Mechanism of normal free radical polymerization

For a radical polymerization process, the concentration of the primary radicals is very important; it is strongly related to the initiation rate constant (k_i) and efficiency (f).[7, 9] In the presence of a vinyl-based monomer, radicals successfully add to a C=C double bond to form a propagating chain radical. Mostly, the chain growth reaction is facile (typically $k_p > 10^2$ $M^{-1}s^{-1}$) and highly exothermic. The propagation rate relies on monomer property,[10-12] chain length,[13-15] and solvent nature.[16-17] Most rate coefficients of individual steps in free radical polymerization have already been extracted by pulsed laser photolysis (PLP).[18-20] The inevitable termination reaction results in the formation of inactive polymer end-functionalities and a broad distribution. As shown in **Scheme 1.1**, when a macroradical reacts with a transfer agent (R-T), a new radical and a 'dead' polymer chain are generated. In a free radical polymerization, termination by chain transfer stops the constant growth of the polymer and induces the experimental molecular weight to be lower than predicted. Various types of transfer reactions, such as transfer to monomer,[21-23] initiator,[24-25] transfer agents,[26-28] solvent or polymer,[29-31] can occur causing the end-functionality of the propagating radicals to become inactive. From the 1960s to early 1970s, great progress on free radical selectivity and reaction has been made via computational models and synthetic experiments,[32-39] to understand better the reactivity of radicals and monomers. The main factors that govern the reactivity include radical stability, and polar, steric and thermodynamic effects.[40-41]

In fact, as early as 1936, the problems of chain transfer and termination in anionic polymerization of styrene and butadiene were avoided by addition of metallo-organic compounds reported by Ziegler.[42] In 1953, Flory proposed and defined for the first time the features of a living radical polymerization (LRP) in vinyl monomers, and three years later, "living polymerization" was coined by Szwarc.[43-45] In 1982 Ostu and co-authors introduced the "iniferter" concept and built a model for LRP.[46-47] Subsequently, a range of effective strategies were developed to diminish radical chain termination and other undesired reactions.[48-49] It is worth noting that, among them controlled/living radical polymerization (CLRP) has attracted a great deal of interest due to the advantages of higher selective monomer scope and moderate eco-friendly reaction

conditions.[50-56] Simultaneously, numerous improvements have been made by radical polymerization chemists and several distinct techniques will be briefly introduced in the following section.

1.1 Characteristics of Reversible-Deactivation Radical Polymerizations (RDRP)

1.1.1 Fundamental mechanism

From 1990s to the present day, radical polymerization technology was revitalized and is still attracting much attention.[3] A range of effective approaches has been developed which differ in reaction mechanisms, reagents, and reaction conditions. For all practical purposes, these methods are not truly living since irreversible termination inevitably occurs according to different pathways involving various side reactions such as rearrangements, disproportions, fragmentations, end-functionality decomposition, etc. Hence, in 2010, the international union of pure and applied chemistry (IUPAC), a worldwide authority on chemical nomenclature and terminology, recommended to use reversible-deactivation radical polymerization (RDRP) as a professional term for these polymerization methods.[57]

***Reversible termination* (*deactivation*):**

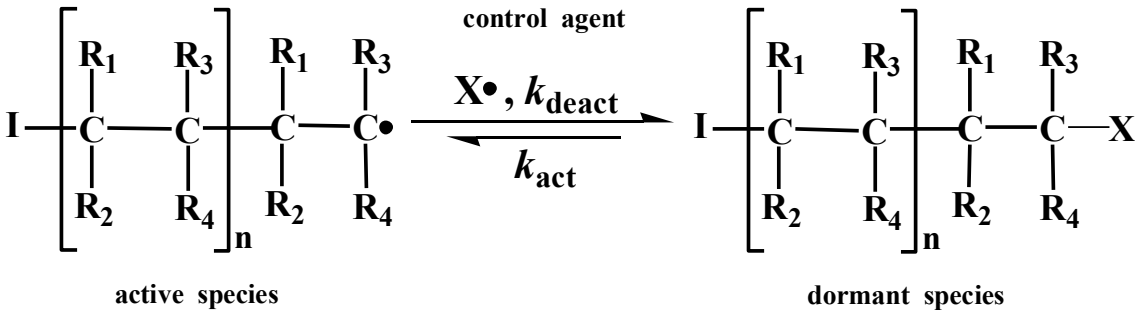

Scheme 1.2 Reversible termination process

Slow initiation (k_i), fast growth or propagation (k_p), and rapid termination (k_t) are

the distinct kinetic features of traditional free radical polymerizations (**Scheme 1.1**). In general, free radicals are generated directly from initiator decomposition by photoirradiation or thermolysis at high temperature. Moreover, the lifetime of free radicals is as short as ca. 1s. The rapid bimolecular termination reaction induces the concentration of inactive end-functional groups to increase and limits further extension of the polymer chains in the presence of additional monomer units. Compared to conventional radical polymerization, RDRP equilibrium is achieved with the aid of a control agent ($X^{\bullet}$) (**Scheme 1.2**).[56] A rapid dynamic equilibrium between active and dormant species is crucial for all RDRP systems, which ensures that all propagating species have equal opportunities for growth. To reach dynamic equilibrium, in addition, fast initiation as compared to chain growth or propagation (k_p), and lower concentration of active propagating species [P_n•] than dormant chains [P_n-X] (typically [P_n•]/[P_n-X] < 10^{-5}) are necessary.[58-61] The radical-radical termination rate is proportional to the square of radical concentration (i.e., $k_t \propto [P_n\bullet]^2$). As such, the irreversible termination of active radicals can be drastically reduced by lowering P_n• concentration. In fact, the activation rate is much lower than the deactivation rate, so that the period of inactivity (dormant state) is much longer than the period of propagation in CRP. Each time a chain is activated, it propagates for a very short time adding to few monomer units before it is deactivated back to the dormant state. This intermittent sequence of activation/deactivations steps elongates the lifetime of the growing chains from *ca*. 1s to several hours.[62] As a result, the overall lifetime of propagating active radical species can be extended to even several days. It allows continuous production of well-defined and architecturally diverse polymers with low molecular weight distribution.

As shown in **Scheme 1.2**, the role of the control agent cannot be overlooked. The stability and orthogonal property of the control agent guarantee the polymerization to be continuously controllable and alive.[4] The active propagating radicals (P_n•) quickly deactivate to dormant species in the presence of a control agent to reach the RDRP equilibrium. The end-functionality of dormant species (P_n-X) not only permits all polymer chains to be extended in the presence of another monomer, but also allows a linear growth of molecular weight with monomer consumption. However, a small

fraction of active chains unavoidably undergoes radical-radical termination during the polymerization. Finally, a broad range of functional polymers with well-defined architectures, predetermined molecular weights and low dispersity are obtained.

1.1.2 Development and characteristics

Since early 1990s, different strategies have been utilized and improved for the development of CRPs. All these methods rely on the introduction of a control reagent that reacts with the propagating radicals via reversible deactivation, thereby converting them to dormant chains. Depending on the mechanism and IUPAC recommendations, three broadly categorized systems can be distinguished. The first is (a) stable radical mediated polymerization (SRMP), which is based on a dissociation-recombination mechanism, in particular, best represented by nitroxide-mediated (radical) polymerization (NMP or NMRP; IUPAC recommended to use "aminoxyl" instead of "nitroxide", i.e. AMRP, although it did not receive popularity), and some organometallic-mediated radical polymerization **(**OMRP) processes. The other two are (b) atom transfer radical polymerization (ATRP), which involves a reversible atom or group transfer catalyzed usually, though not exclusively, by transition-metal complexes, and (c) degenerative-transfer radical polymerization (DTRP), which involves a degenerative transfer (DT) of a group (or atom), exemplified by reversible addition-fragmentation chain transfer (RAFT), and some organometallic-mediated radical polymerization **(**OMRP) processes, as shown in **Scheme 1.3**.

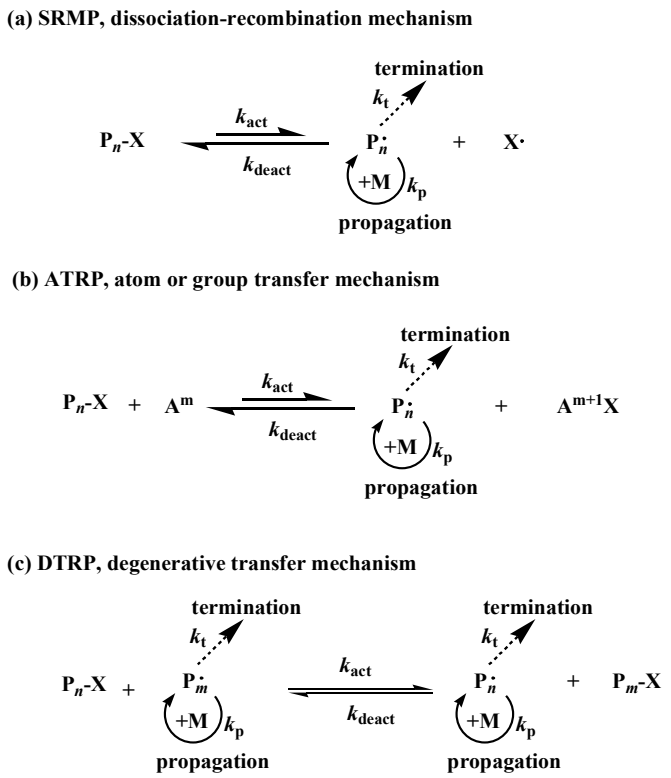

Scheme 1.3 The fundamental mechanisms of the three most common RDRPs.

1.1.3 Nitroxide-mediated polymerization (NMP)

A general NMP is comprised of initiation, propagation, and termination steps. The original NMP was discovered by Solomon and Rizzardo at the Commonwealth Scientific and Industrial Research Organization (CSIRO) in 1985.[63] The second seminal contribution was by Georges *et al*. who demonstrated the synthesis of polystyrene (PS) with a narrow dispersity and predictable molecular weight via NMP.[52] In detail, benzoyl peroxide (BPO) and 2,2,6,6-tetramethyl-l-piperidinyloxy (TEMPO, **Scheme 1.4**) were used as initiator and capturing agent (persistent nitroxide radical), respectively. Continually heating the reaction mixture from 35 °C to 123 °C for more than 70 h yielded PS with a dispersity of 1.26. **Scheme 1.5** illustrates the reaction mechanism. The carbon-oxygen bond (-C-ONR_1R_2) of an alkoxyamine is cleaved (with a dissociation constant k_d) to a carbon-centered transient radical (P_n•) and a stable nitroxide persistent radical (R_2R_1NO•) at elevated temperatures. The highly reactive P_n• can either add to a vinyl monomer unit to afford a new chain radical or cross-couple

with a nitroxide radical (k_c) to regenerate a dormant alkoxyamine, which will later undergo thermal self-initiation. The new active propagating radical chain can again either reversibly recombine with the nitroxide or react with another monomer unit. Moreover, as the end-functional group is still living after the reaction has been stopped, chain growth and polymerization will be recovered upon the addition of a new monomer to yield a copolymer. Significantly, the persistent radicals cannot terminate themselves but only cross-couple with the new growing polymer chain. The unavoidable termination (k_t) of the growing transient radicals finally leads to an irreversible accumulation of the persistent radical. An important consequence of persistent radical accumulation is a shift of the disassociation/association ($K=k_d/k_c$) equilibrium toward the dormant species, thus significantly reducing the polymerization rate until a new pseudo-equilibrium state is reached. This effect, which somehow tends to regulate the polymerization rate, is termed "persistent radical effect" (PRE).[9, 64-68] Fischer *et al*. and Goto and Fukuda showed that the persistent radical concentration progressively increases with time ($[R_2R_1NO\bullet] \propto t^{1/3}$) while the transient radical concentration decreases with time ($[P_n\bullet] \propto t^{-1/3}$) during the quasi-equilibrium stage.[61, 65-67, 69]

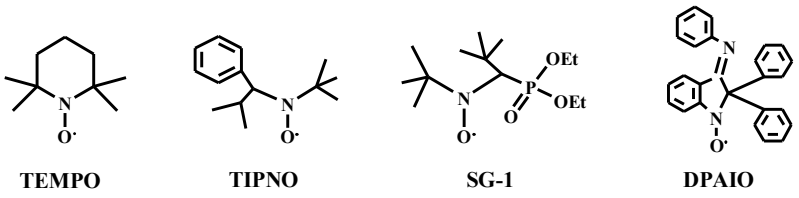

Scheme 1.4 Structures of some commonly used nitroxides in NMP.

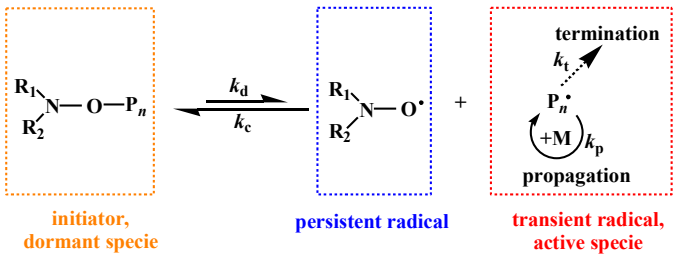

Scheme 1.5 The mechanisms of NMP.

Although some nitroxide radicals such as TEMPO are commercially available, the process suffers from several serious drawbacks: i) the progressive decrease of transient radical concentration results in a drastic reduction of polymerization rate; ii) poor monomer selectivity except styrenic monomers; iii) high polymerization temperature and long reaction time; iv) better polymerization control with unimolecular initiators than bimolecular hybrid systems; v) solvent effect.[67, 70-72] To solve these problems, several TEMPO-based derivatives or TEMPO-like structures such as morpholone and piperazinone-based nitroxides as well as alkoxyamines were introduced into NMP**.** The substitution of R_1 or (and) R_2 with bulky groups has a positive effect on lowering the bond dissociation energy (BDE) of -C-ONR_1R_2; some examples are 2,2,5-trimethyl-4-phenyl-3-azahexane-N-oxyl (TIPNO), *N*-tert-butyl-*N*-(l-diethylphosphono-2,2-dimethylpropyl) (SG-1 or DEPN), 2,2-diphenyl-3-phenylimino-2,3-dihydroindol-1-yloxyl (DPAIO) (**Scheme 1.4**).[67, 73-78] The versatile nature of these nitroxides can be used to control the polymerization of a wide range of monomers such as styrene, acrylates, acrylonitrile, acrylamides, dienes, etc. to prepare polymers with accurate control of molecular weights and low dispersity. However, despite many efforts including the synthesis of unimolecular initiator alkoxyamines, polymerization rate improvement and lowering the reaction temperature are still open problems.

In the past decade, a robust electrochemical technique was successfully introduced in the controlled radical polymerization field.[79] Zhang *et al*. carried out an electrochemical study on the oxidation of alkoxyamines. Combining experiments with digital simulations, they proved that oxidation follows an $EC_{irr}E$ mechanism: i) electrochemical step, i.e., one-electron oxidation of an alkoxyamine species; ii) an irreversible chemical reaction, assisted by electrostatic catalysis, involving dissociation of the radical cation to TEMPO and a carbocation; iii) a second electrochemical step involving oxidation of TEMPO generated in ii).[80] Although polymerization was not investigated in this outstanding work, the introduction of electrochemical skills in NMP will be believably achieved in the future.

1.1.4 Organometallic-mediated radical polymerization (OMRP)

The application of metal species to mediate polymerization has a long history. Ziegler and co-workers were the first to develop metal compounds for mediating polymerization.[42, 81-83] Metal-based catalyst systems rapidly came into chemists' sight for the development of RDRP. In 1992, Wayland *et al*. reported the first example of organometallic-mediated radical polymerization (OMRP) of acrylate based on a porphyrin complex of rhodium exposed to visible light.[84] However, side reactions such as uncontrolled polymerization reinitiation and radical-radical termination resulted in a broad distribution of polymer molecular weight. To understand better the process and eliminate these drawbacks, it became clear that fundamental mechanistic studies were necessary. Depending on the type of metal complex used as a catalyst, polymerization temperature, and characteristics of additives, two main OMRP mechanisms were identified as shown in **Scheme 1.6**. In the reversible termination (RT) mechanism, a fast and reversible homolytic cleavage of a weak metal-carbon bond is the core of the process. Conventional free radical initiators are used to generate active radicals through homolytic dissociation, which can either react reversibly with the metal complex to generate dormant species with a weak metal-carbon bond or add to a vinyl monomer to form new active propagating chain radicals. The latter can again react either with the metal complex or with the monomer; eventually the equilibrium of activation and reversible deactivation is reached and the process proceeds through repetitive activation-propagation-deactivation steps. The transition metal complex in this process acts as a trapping agent for the growing radicals and mediates the polymerization.

Alternatively, the active radical, generated as in the initial step of RT, can react with the metal complex to form an active propagating chain in a degenerative transfer (DT) process **(Scheme 1.6 b**). In this case, the metal complex continuously alternates between two propagating chains, the deactivation of one radical chain through degenerative transfer simultaneously activating another radical.

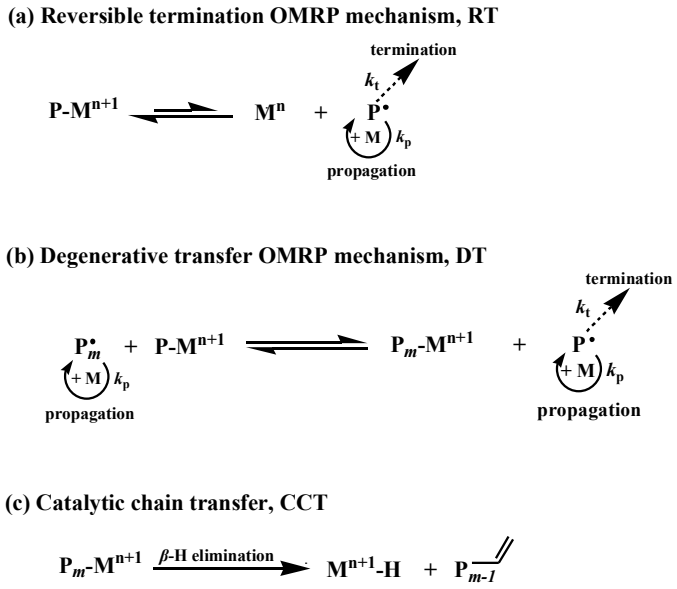

Scheme 1.6 The interplay of metal-assisted polymerization processes in OMRP.

While in general these two mechanisms co-exist in one OMRP, the contribution of the DT pathway is significant only if the content of generated active chains in the system is higher than the metal complex concentration. Therefore, if the usual radical initiators are used, a long induction period during which time the radicals are converted to a dormant organometallic species is observed in DT OMRP.[85] Fine-tuning of the BDE of the metal-carbon bond is essential because irreversible radical trapping may occur if strong metal-carbon bonds are formed. On the other hand, formation of very weak metal-carbon bonds may cause the occurrence of massive side reactions. One of the typical side reactions observed in OMRP is the non-living process of catalytic chain transfer (CCT). It corresponds to the formation of an olefin-terminated polymer chain and a high valance state metal-hydride compound species, the latter being generated by *β*-hydrogen elimination of a high valance state metal-alkyl dormant species, as shown in **Scheme 1.6 c**. An alternative pathway of CCT is the abstraction of H atom from the active growing chain radical by the metal complex to generate a metal hydride and a polymer chain terminating with a carbon-carbon double bond. In both cases, the metal hydride reacts with the monomer to generate the metal at a lower oxidation state together with a new propagating radical. What is certain, however, is that the *β*-hydrogen elimination occurs especially in iron (III)-based systems for methyl

methacrylate and styrene polymerizations.[86-87]

Many transition metal compounds were developed in the last two decades for OMRP, including for instance cobalt-mediated radical polymerization (CMRP), organotellurium-mediated radical polymerization (TERP), organostibine-mediated radical polymerization (SBRP), organobismuthine-mediated radical polymerization (BIRP), and also various other metals such as Mo, Os, Ti, Cr, V, Ni, Pd, etc.[77, 85, 88] CMRP is one of the most successful OMRP techniques. It is worth noting that BDE of Co-alkyl bonds is quite low (100 $kJ \cdot mol^{-1}$) so that homolytic dissociation is fast while the coupling of Co complexes with carbon centered radicals is a diffusion-controlled reaction.[89] Thus, CMRP of acrylate is faster than polymerization by NMP with alkoxyamine. Well-controlled polymer weight and narrow distribution can be reached in OMRP in the presence of a transition metal complex with TEMPO or its derivates. Due to the versatility of transition metal catalyst systems, the scope of OMRP is quite wide, covering a large variety of monomers including acrylates, vinyl esters, styrenes, *N*,*N*-dimethylacrylamide, 2-dimethylaminoethyl acrylate, *N*-isopropylacrylamide, acrylonitrile, vinylpyrrolidone, etc.[72, 85-86, 88] Some limitations of OMRP, which represent obstacles to its industrialization, are the high cost of the metal complex and its removal from the polymer. In addition, a better understanding of the interplay of several mechanisms is essential to allow the design of more efficient catalyst systems and the achievement of precise topology, targeted molecular weights and low dispersity.

1.1.5 Reversible addition-fragmentation chain transfer (RAFT)

RAFT, one of the most used RDRP methodologies, based on degenerate-transfer radical polymerization (DTRP or DT), has broadened the field of free radical polymerization.[57, 60, 68] It does not need to obey PRE and does not use a metal complex. The active radical chain (P_n•) reacts with a dormant species (P_m-X) to form an intermediate radical (P_m-XZY•-P_n), through a reversible addition process. The intermediate radical then further undergoes a fragmentation step to form a dormant species and a new propagating radical (P_m•). X can be an atom (e.g., iodine transfer

polymerization, termed ITP), a vinyl function group or an unsaturated thio compound (e.g., xanthates). This interesting case of two-steps reversible addition-fragmentation transfer process formally termed RAFT (**Scheme 1.7**) was first reported in 1998 by Moad, Rizzardo and co-workers at the Commonwealth Scientific and Industrial Research Organization (CSIRO), using thiocarbonyl thio as RAFT agents.[54, 57, 90-91] Contemporarily, another polymerization method based on the same mechanism with macromolecular design by interchange of xanthate (named MADIX, which is more suitable for less-activated monomers) was reported.[92] Well-controlled RAFT over molecular weights and dispersity is provided by chain transfer agents (CTA) such as dithioesters, trithiocarbonates, xanthates, dithiocarbamates, and organometallic RAFT agents (M-RAFT, in which M = tungsten, molybdenum, or chromium).[93-94] At the beginning of the polymerization, initiators are activated to generate radicals by irradiation over a wide range of temperatures. The ensuing radicals start propagation by adding to the monomer but after a short period of propagation (P_n•) they add to a CTA (species **1** in **Scheme 1.7**) with a rate constant k_{add}. The structure of the CTA with Z, R and X/Y standing for an activating group such as an ester or an aryl group, the homolytic leaving group and S determine the polymerization rate as well as length of polymer chains and dispersity. The Z group affects the reactivity of the C=X bond and the stability of the intermediate radical **2**, which fragments to form a new CTA **3** (β-scission, k_β) and a new radical R• (**Scheme 1.7 a**). The new radical R• is capable of reacting with the monomer to generate a new active radical chain P_m•, as illustrated in **Scheme 1.7 b**. Subsequently, the new CTA **3** and the active species P_m• are immediately subject to a reversible addition process again followed by the release of a new intermediate radical **4**, which fragments to a dormant species containing P_m and an active radical chain P_n• (**Scheme 1.7 c**). Ideally, the reactivity and the stability of the new active radical P_m• should be similar to or better than that of P_n• to keep a high transfer efficiency compared to propagation rate, otherwise the process will face numerous negative effects on polymerization rate.[68] A steady-state with a high exchange coefficient is beneficial to ensure that all P_m• and P_n• species have equal opportunities to keep growing in the short time scale of this process and obtain a narrow

molecular weight distribution. Slow addition of the monomer into the system is another potential way to achieve low dispersity.[9, 60, 68]

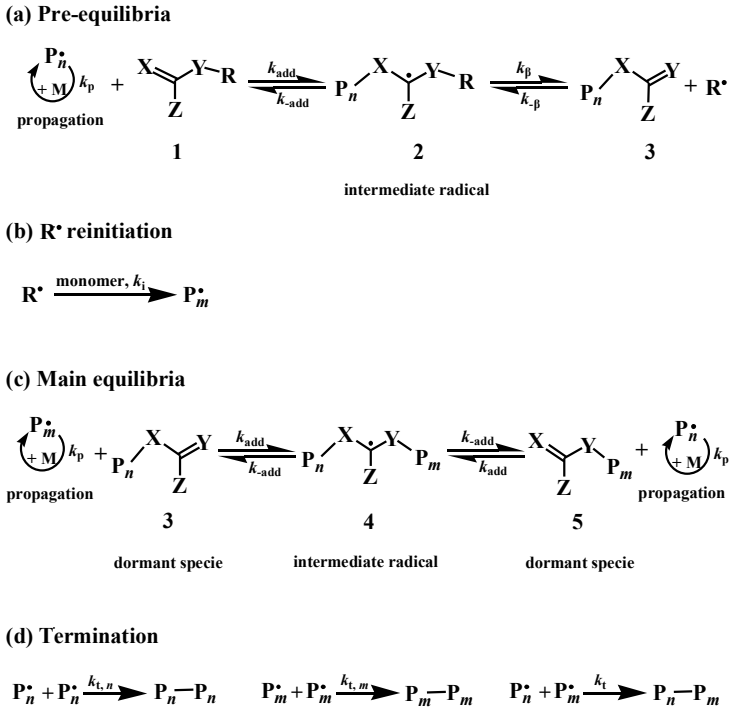

Scheme 1.7 Mechanism of RAFT polymerization showing pre-equilibrium, reinitiation, main equilibrium and termination steps.

The success of RAFT polymerization strongly relies on the choice of the unsaturated CTA with particular attention to both Z and R groups. The structure of the Z group must be chosen to activate the double bond (C=X) of the CTA towards radical addition but at the same time not provide too great stabilizing influence on the adduct radical. For instance, -Ph could enhance the polymerization of styrene and MA but retard the polymerization of acrylates and inhibit reaction of vinyl esters. Conversely, $–NR_2$ in dithiocarbamates or –OR in xanthates is good for vinyl esters but inefficient for styrene. The steric and electronic factors together affect the leaving ability of the R group, the steric effect being more important. A highly stable intermediate radical could contribute to reduce the fragmentation rate, hindering the establishment of a steady state for the propagating radicals. RAFT polymerizations of a wide range of monomers were successfully investigated in bulk, organic or aqueous solutions, emulsion, miniemulsion,

and suspension systems, to prepare polymers with various architectures. In addition, an increased stability of the intermediate radical could lead to an increase of its concentration, which may ultimately result in irreversible radical–radical terminations (**Scheme 1.7 d**). Although not always detectable, there are some odd phenomena for intermediate radical terminations under some circumstances.[9, 95-96]

In the last half decade, electrochemically mediated RAFT (*e*RAFT) has been investigated as a powerful and versatile RDRP technique for polymerization.[97-102] Wang *et al*. used direct electroreduction of benzoyl peroxide (BPO) or 4-bromobenzenediazonium tetrafluoroborate ($BrPhN_2^+$) to form aryl radicals, acting as initiators for RAFT polymerization of MA.[97] However, polymerizations were unsuccessful because of rapid passivation of the electrodes. Then, electroreduction of the CTA was attempted to generate propagating radicals but also this approach did not give satisfactory results since the reduction process resulted in the formation of carbanions by a two-electron transfer process. Lorandi *et al*. mitigated the negative effect of CTA decomposition during electroreduction through the introduction of tetraphenylporphyrin (TPP) as an auxiliary mediator.[98] A slow but controlled *e*RAFT of *n*-butyl acrylate (BA) in DMF or DMSO at 25 °C was obtained. After 6h, while the monomer conversion only reached to 17%, the polymer dispersity was as low as 1.22. It is probable that the steric hindrance of TPP structure minimized the coupling between the radical anion of TPP and the radicals generated from the partial CTA decomposition. Subsequently, Strover *et al*. systematically studied the relationship between CTA reduction potentials and different Z and R groups via cyclic voltammetry (CV) to establish a predominant reduction mechanism of CTAs.[100] It is worth noting that Bray *et al*. employed an amphiphilic block polymer as a macro RAFT agent (CTA), sodium formaldehyde sulfoxylate (SFS) as a chemical reductant, Fe-EDTA complex as reduction mediator, and ammonium persulfate (APS) as an oxidant and source of sulfate radical anion as initiating radicals to achieve styrene polymerization in emulsion via *e*RAFT.[99] Emulsion *e*RAFT polymerization gave pretty rapid polymerization of styrene at ambient temperature with low dispersity. In addition, photo-RAFT and photoinduced electron transfer RAFT (PET-RAFT) polymerization have revolutionized

polymer chemistry.[103-107] Alternatively, Qiao *et al*. in 2017 proposed ultrasonication of aqueous media as a means to generate hydroxyl radicals for polymerization, which was coined sono-RAFT.[108]

RAFT quickly became widely used and was further studied in the last two decades. According to the statistics of RAFT-related literature and patent inventions, as shown in **Figure 1.1**, RAFT is now arguably one of the most convenient and versatile RDRP methods.

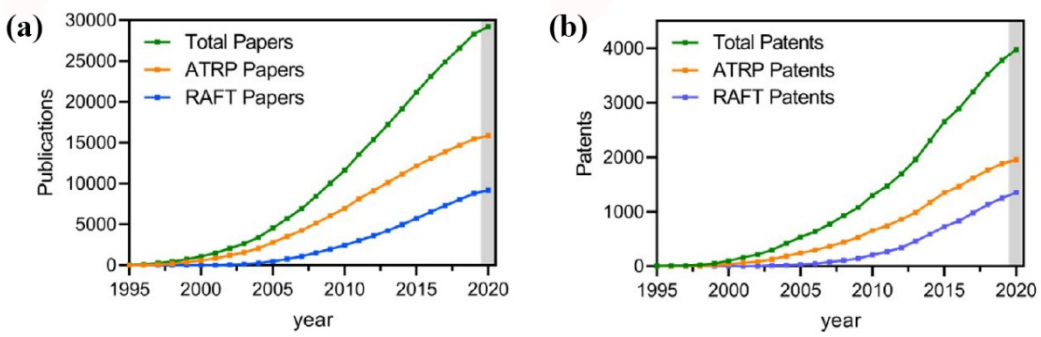

Figure 1.1 Cumulative publications and inventions relating to ATRP and RAFT polymerization during the period of 1995 ~ 2020.[4]

1.1.6 Atom transfer radical polymerization (ATRP)

In approximate chronological order of CRP development, atom transfer radical polymerization (ATRP) was reported prior to RAFT and after NMP. This method, however, revolutionized the field of free radical polymerization. In 1995, Sawamoto *et al*.,[109] and Wang and Matyjasewski[53, 110] independently reported metal-catalyzed RDRP processes that operated through an atom transfer radical addition process. Since then, ATRP quickly attracted much attention and became the method of choice for the synthesis of polymers with a range of architectures and compositions.[111] A clear indication of this success is the high number of annual publications, as illustrated in **Figure 1.1**. During the last fifteen years, an explosive increase has been observed in the number of publications on ATRP, including a dramatic increase in the number of patent applications. A substantial body of work was progressively carried out on various

aspects of ATRP, including the thermodynamics of the process and its components, catalyst system improvement, initiation mechanism, monomer adaptability, solvent effects, though not exclusively, and the employment of external stimuli (e.g., light, electrochemical, mechanochemical, biological, etc.). Therefore, these achievements will be carefully addressed in the following sub-sections.

The first report on the addition of halocarbons (RX) to an alkene double bond in a radical chain process was made by Kharasch *et al*. in 1945.[112] The overall process can be catalyzed by a transition metal complex (M^n-X) through the transfer of a halogen atom; it was then termed as atom transfer radical addition (ATRA).[113] The first purposeful use of ATRA in polymer synthesis was in the production of telomers in 1990.[114] The first reports of ATRP, which clearly displayed the characteristics of living polymerization, appeared in 1995.[53, 109-110] ATRP then rapidly grew and became one of the most popular and widely used RDRP methods. The widespread use of ATRP is due to numerous advantages of this method: catalytic amounts (ppm amounts) of transition metal complexes or even metal-free catalysts are used; many initiators and ligands are commercially available; a large range of monomers can be polymerized; the choice of end-functionalization group is flexible; a wide range of temperatures and various reaction media can be employed; polymers with different composition, topology and complex architecture can be prepared by ATRP, especially using recently developed advanced methods based on external stimuli, which is not possible for the other CRP methods.

1.1.6.1 General ATRP description: mechanism and setup

ATRP is a controlled reversible deactivation radical polymerization in which the deactivation of the radicals involves a reversible transfer of an atom or a group catalyzed, though not exclusively, by transition metal complexes. In an efficient ATRP system, a fast and reversible homolytic cleavage of a carbon-halogen bond in a dormant alkyl halide (P_n-X) species is activated (k_{act}) by a transition metal complex (M^n/L, where M^n is a transition metal with an oxidation number n, and L is a polyamine ligand) at a

low oxidation state to form a carbon centered radical (P_n•) and the transition metal complex at a higher oxidation state (X-M^{n+1}/L). The active radical can either reversibly react with the transition metal-halide complex to form a dormant polymer chain and the original transition metal complex (k_{deact}) or add to a vinyl monomer to form a new active propagating radical, as illustrated in **Scheme 1.8**. The latter can either react with the monomer or with X-M^{n+1}/L and eventually a dynamic equilibrium of reversible activation/deactivation is reached. The ATRP equilibrium is well-shifted to the left in favor of the dormant species so that radical-radical termination is kinetically hampered because of low propagating radical concentration. Like NMP, ATRP is regulated through the persistent radical effect (PRE) in which the X-M^{n+1}/L species plays the role of a persistent (stable) radical.

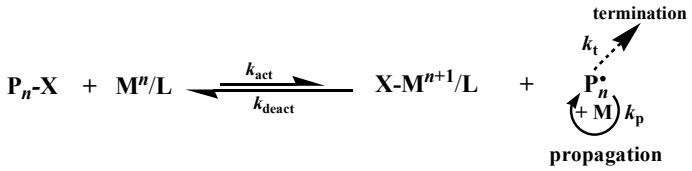

Scheme 1.8 General mechanism of ATRP

Besides radical-radical coupling or disproportionation, other termination pathways such as catalytic radical termination (CRT) via formation of an organometallic species as in OMRP have been reported. In principle, depending on the structure of dormant species and type of metal catalyst, probably both ATRP and OMRP mechanisms can contribute to the polymerization control simultaneously. For example, an OMRP equilibrium can be established in a situation where the catalyst M^n/L can react with radicals P_n• with the formation of the corresponding organometallic species P_n-M^{n+1}/L (**Scheme 1.6 a**). If the organometallic species is unstable and readily dissociates back to M^n/L and P_n•, the OMRP mechanism will not have a significant contribution to the overall polymerization control. If instead, a relatively stable organometallic species is formed, OMRP mechanism will operate along with ATRP, both mechanisms contributing to the overall polymerization control. However, in the other extreme case, where the organometallic compound is very stable (and is formed

rapidly), the activation of P_n-X will be followed by the formation of the organometallic species and, due to the inability of the latter to be dissociated, the reaction will stop without polymer generation after the initiator is consumed completely; in this case, M^n/L acts as a radical trap.

A well-controlled ATRP reaches rapidly the equilibrium of the reversible activation and deactivation ($K_{ATRP} = k_{act}/k_{deact}$, **eq. 1-1**) and obeys the PRE rule.[77, 115] Usually, K_{ATRP} is small (10^{-4}~10^{-9}), which ensures a low radical concentration and minimizes termination reactions.[116] The ATRP equilibrium can be expressed as a combination of four reversible reactions: oxidation of the metal complex (i.e., electron transfer), electron affinity of the halogen atom, bond homolysis of the alkyl halide and association of the halide ion to M^{n+1}/L (i.e., halidophilicity).[117] Therefore, understanding how the initiator and catalyst interact reveals important information about the polymerization. As in any other radical process, a true ‘‘living’’ radical polymerization cannot be achieved (owing to the bimolecular radical termination, i.e., coupling or disproportionation, k_t) although the large majority of chains (typically, > 90%) are ‘living’. The ‘dead’ chains (or terminated chains) cannot be reactivated and do not grow any further due to the loss of ω-chain end functionality. Moreover, high level of termination can result in the accumulation of the deactivator, leading to polymerizations that essentially stop with low conversion and poor dispersity. The dead chain fraction (DCF, defined in **eq. 1-2**) depends on many factors, e.g., the temperature, monomer property and conversion (conv.), the targeted degree of polymerization, and the initial concentration of initiator. The rate of ATRP (R_p), (**eq. 1-3**), like that of any other radical polymerization, depends on k_p and on the concentrations of monomer ([M]) and growing radical ([P_n•]).[115, 118] Polymers with narrow molecular weight distributions ($Đ$ or M_w/M_n) are obtained by ATRP, whereby more uniform polymer chains are provided by higher concentrations of deactivator ([X-M^{n+1}/L]) and by higher monomer conversions, as shown by **eq. 1-4.** The efficiency of deactivation, which is responsible for the degree of polymerization control, depends on the value of k_{deact} and also on the concentration of the deactivator. Since [X-M^{n+1}/L] normally increases due to the PRE, ATRP can be viewed as a ‘‘self-regulating’’ system.

$$K_{ATRP} = \frac{k_{act}}{k_{deact}} = \frac{[P_n\bullet]\cdot[X\text{-}M^{n+1}/L]}{[P_n\text{-}X]_0\cdot[M^n/L]} \quad (1\text{-}1)$$

$$DCF = \frac{[T]}{[P_n\text{-}X]_0} = \frac{2k_t\cdot[\ln(1\text{-}conv.)]^2}{[P_n\text{-}X]_0\cdot k_p^2\cdot t} \quad (1\text{-}2)$$

$$R_p = k_p\cdot[M]\cdot[P_n\bullet] = k_p\cdot K_{ATRP}\cdot\frac{[M]\cdot[M^n/L]\cdot[P_n\text{-}X]_0}{[X\text{-}M^{n+1}/L]} \quad (1\text{-}3)$$

$$Đ = \frac{M_w}{M_n} \approx 1+\left(\frac{k_p\cdot[P_n\text{-}X]_0}{k_{deact}\cdot[X\text{-}M^{n+1}/L]}\right)\cdot\left(\frac{2}{conv.}\text{-}1\right) \quad (1\text{-}4)$$

An important issue that has to be emphasized here is related to the general setup of ATRP, which often involves a Schlenk tube system used for deoxygenation and several other glassware for storing degassed reagents, and sometimes an oil bath for heating to high temperatures. The potential risks one has to consider include explosion, which could happen at any moment during deoxygenation, which is done by evacuation and backfilling with N_2 several times, or in the heating period, burns, splash of hot liquid on people's skin, etc. Moreover, the polymerization rate drastically decreases or even the reaction stops if the Schlenk line is opened to air (O_2 traps radicals and oxidizes the catalyst). Therefore, simplification and improvement of ATRP setup is another important field of study with particular attention to increase the oxygen tolerance of the system. In the following sections, the properties of the various components of an ATRP system will be described with emphasis on the positive and negative effects of each element on polymerization.

1.1.6.2 Basic components: initiators, catalysts, monomers and solvents

Sawamoto *et al*. reported the polymerization of MMA with carbon tetrachloride as initiator, $RuCl_2(PPh_3)_3$ as a catalyst and $MeAl(ODBP)_2$ (ODBP = 2,6-di-tert-butylphenoxide) as a co-catalyst,[109] while Wang and Matyjaszewski reported well-controlled polymerizations of styrene and (meth)acrylates by using 1-phenylethyl halide (1-PEX, X = Cl or Br) as initiator and CuX/2,2'-bipyridine as a catalyst.[53, 110] Thus, the basic components of a successful ATRP system should contain an initiator, a

catalyst, a monomer, and, if necessary, other components such as solvent or additives, and should be performed at an appropriate temperature. Therefore, understanding the role of each component of ATRP is crucial for obtaining well-defined polymers as well as for potentially expanding the scope of ATRP. Thus, separate sections will be dedicated to each of these basic components.

1.1.6.3 Initiators

According to **eq. 1-1**, the equilibrium between active and dormant species is maintained through a reversible activation/deactivation process. Both the activation of the C–X bond in P_n-X and deactivation of the $P_n^{\bullet}$ back to a dormant species involve electron transfer processes. It is necessary to understand the mechanism of such processes to guide initiator selection for an optimal ATRP. The mechanism of the activation step in ATRP has been the subject of several studies and it is well-understood now that it proceeds by an inner-sphere electron transfer (ISET) pathway concerted with an atom transfer (AT).[5, 119-124] The initiator is usually an alkyl halide (RX or a macromolecular species P_n-X, X = Cl, Br, I). However, pseudohalogens such as N_3, SCN, CN, etc., can also be transferred to a transition metal complex (M^n/L) through a bridged transition state (e.g., P_n····X····M^n/L).[119, 125-126] This process yields a metal complex with a halide ion coordinated to the metal at a higher oxidation state (X-M^{n+1}/L) together with a free radical, which can add to monomer molecules (propagation, k_p). Subsequently, the propagating chain radical abstracts a halogen atom from X-M^{n+1}/L, reforming the dormant halogen-capped polymer chain, P_n-X. In the homolytic ISET step, the BDE of C-X bond in P_n-X depends on the nature of X. In this case, the C-X reactivity decreases in the following order: I > Br > Cl.[121-122]

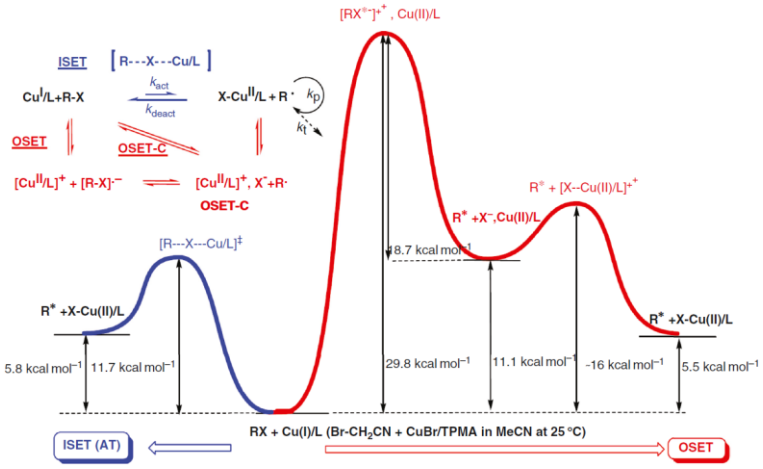

Figure 1.2 Comparison of the energy profiles associated with the ISET-AT and OSET-C processes for the reaction between MeCN-Br and $[Cu^{I}TPMA]^{+}$ in MeCN at 25°C.[124]

Besides ISET, several other pathways have been considered for the electron transfer between RX and M^{n}/L, taking into consideration that the reductive cleavage mechanism of alkyl halides has two different mechanisms: stepwise or concerted (**Figure 1.2**).[116, 121-122, 124, 127] One possible reaction is an outer-sphere electron transfer yielding M^{n+1}/L and a radical anion RX•$^{-}$ intermediate, which then decomposes to a free radical and a halide ion (OSET- SW).[121, 127] Another possibility is an outer-sphere electron transfer involving concerted reductive cleavage of the C-X bond (OSET-C). Through thermodynamic analysis combining computational data with experimental results, Gennaro's and Matyjaszewski's groups concluded that neither OSET-SW nor OSET-C occurs in ATRP.[5, 68, 120, 122, 124, 128-130] In particular, electron transfer to alkyl halides typically used as initiators in ATRP never produces intermediate radical anions, even in polar solvents such as MeCN and DMF. **Figure 1.2** compares the free energy profiles for the activation of $BrCH_2CN$ by CuBr/TPMA in MeCN at 25 °C via ISET and OSET-C processes. It is shown that OSET should have an energy barrier ~18 kcal mol^{-1} higher than the experimentally measured value, and the predicted rate of OSET-C process is ~10 orders of magnitude lower than the experimentally measured value, confirming the ISET pathway.[124, 129-130]

A special case of ATRP is a system based on metallic copper in the presence of an

amine ligand. Percec and co-workers proposed a mechanism based on outer-sphere electron transfer and coined the term single electron transfer LRP (SET-LRP).[127] The proposed mechanism relies on OSET-SW, whereby the P_n-X bond dissociation occurs through the formation and decomposition of a radical anion intermediate derived from the dormant species. In this polymerization, Cu^0 and the initiator act as an electron donor and an electron acceptor, respectively. In practice, however, the alkyl halides preferentially react with Cu^I species which has a much higher reactivity than Cu^0, although the latter initially activates the initiator, thus starting the reaction, and continues to slowly react with P_nX only as a supplemental activator.[131-133] It has to be emphasized again that electron transfer to alkyl halides does not produce radical anion intermediates and therefore any mechanism based OSET-SW, including SET-LRP, should be discarded.

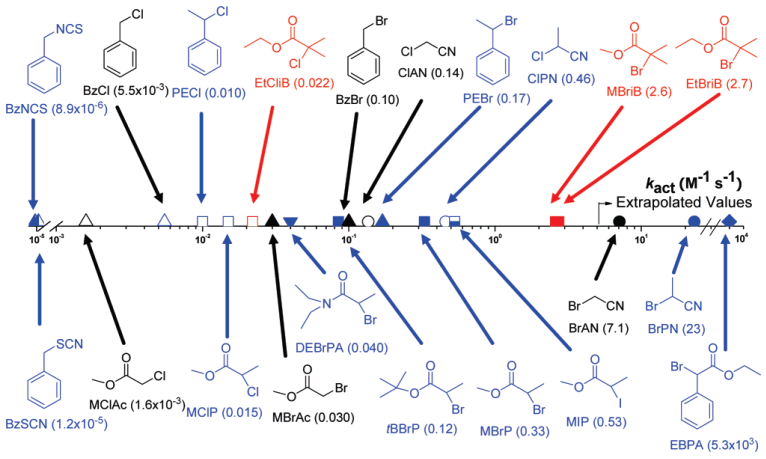

Figure 1.3 ATRP activation rate constants for various initiators with Cu^IX/PMDETA (X=Br or Cl) in MeCN at 35 °C.[125]

In ATRP, the main role of the alkyl halide (RX) species is to fix the number of initiated chains. According to **eq. 1-3**, the polymerization rate R_p is proportional to the concentration of P_n-X. Moreover, the molecular weight (M_w) is inversely proportional to the initial concentration of the initiator. To choose a good initiator, the structure of the alkyl group (R or P_n) should be considered first. Other important factors that are worth consideration are BDE of the C-X bond, the nucleophilicity of X^-, the Lewis

acidity of the metal complex chosen as a catalyst, the solvent polarity, and the polymerization temperature. As illustrated in **Figure 1.3**, the activity of the initiator depends on the structure of alkyl group and the electron-withdrawing groups attached to the C-X bond and follows the order: tertiary > secondary > primary and phenyl ester > cyanide > ester > benzyl > amide. RX reactivity depends also on the leaving group, following the order: I > Br > Cl ≫ SCN ≈ NCS.[116, 125, 134]

1.1.6.4 Catalysts

The activity of the catalyst is crucial in terms of controlling the polymerization. An "ideal" ATRP catalyst should be not only very stable and active, but also should maintain its activity when used at a very low concentration (~ppm). Sawamoto *et al*. first attempted polymerization of MMA by employing a 10 mM ruthenium complex in toluene at 60 °C.[109] After 4h, the monomer conversion reached 90% yielding a high molecular weight (~ 10 000) polymer with low *Đ* (1.3~1.4). Wang and Matyjaszewski used various initiators and a CuX/bpy catalyst at a ratio of R-X/CuX/bpy = 1/1/3 (X = Br, Cl) for the polymerization of styrene, various acrylates and methyl methacrylate at different temperatures, obtaining polymers with $M_n \approx 10^5$ and *Đ* as low as 1.1.[110] The most commonly used ATRP catalysts are Cu complexes with nitrogen-based polydentate ligands, owing to their availability, low cost, and stability of both activator and deactivator complexes in many solvents. The structure of the amine ligand plays a key role in tuning the activity of the catalyst.[116, 128, 134-136]

There are some rules for the selection of a good ATRP catalyst: i) it must have an accessible one-electron redox couple able to undergo a reversible atom transfer reaction; ii) the metal center must have a free position for a new ligand (i.e. X^-); iii) its affinity for radicals must be low, otherwise, *β*-H elimination (CCT) and the formation of organometallic compound might take place; iv) the metal should be a weak Lewis acid to avoid initiator or P_n-X ionization; v) the metal center should not activate by an outer-sphere electron transfer pathway; vi) last but not the least, the exchange between the dormant and active species must be fast.[118] The equilibrium between activation and

deactivation steps of the ATRP (**Scheme 1.7**) is affected by ligands through both polar (electronic interactions with the metal ion center) and steric effects (bulky ligands). The most common catalysts are complexes based on copper(II/I) halide and nitrogen-based ligands. The optimum ratio of ligand to copper in ATRP mainly depends on the ligand structure and small structural changes may lead to large differences in catalyst activity. For instance, the best ratio of bidentate bpy to copper should be equal to 2:1, while only 1:1 is necessary for the tetradentate ligands.[7] It is noteworthy that while CuX_2/bpy is soluble in polar solvents such as MeCN, it is less soluble in nonpolar solvents. Therefore, bpy derivatives with long alkyl chains were prepared to increase the catalyst solubility in nonpolar polymerization media and also to modify its activity. Certain multidentate ligands coordinate well both Cu(I) and Cu(II) forming complexes with good solubility in both polar and nonpolar media. Examples of such ligands include *N*,*N*,*N*′,*N*′-tetramethylethylenediamine (TMEDA), tris[2-aminoethyl]amine (TREN), tetraazacyclotetradecane (Cyclam), 1,4,8,11-tetraazacyclotetradecane (Me_4Cyclam), *N*,*N*,*N*',*N*',*N*''-pentamethyldiethylenetriamine (PMDETA), 1,1,4,7,10,10-hexamethyl triethylenetetramine (HMTETA), tris(2-pyridylmethyl)amine (TPMA) and tris[2-(dimethylamino)ethyl]amine (Me_6TREN).[7, 68] The activity increases with the number of nitrogens coordinated to copper and with their electron donating ability. A good σ-donor and π-acceptor ligand can stabilize the metal very well. Matyjaszewski *et al*. determined the activation rate constants of Cu^I complexes with a large number of nitrogen-based ligands in the activation reaction of ethyl α-bromoisobutyrate (EBiB) in MeCN in the presence of TEMPO as a radical trapping agent (**Figure 1.4**).[128, 134-136] Several general 'rules' pertaining to Cu^I-based catalyst activity were derived from these investigations: (1) nitrogen-based ligands form Cu(I) complexes with good activity in ATRP in contrast to sulfur, oxygen, or phosphorus ligands, which form less active complexes; (2) the number of N atoms and the structure of the ligand strongly influence the activity, i.e., tetradentate (cyclic-bridged) > tetradentate (branched) > tetradentate (cyclic) > tridentate > tetradentate (linear) > bidentate > monodentate ligands; (3) the activity of ligands depend upon the N nature following the order: pyridine-containing ligands ≥ aliphatic alkyl amine > imine; (4) activity also depends on steric hindrance;

(5) catalyst activity depends also on other factors such as solvent type and temperature.

Until now, despite copper is the most commonly used transition metal catalyst for conducting conventional ATRP, a range of other metals including Ti, Mo, Re, Fe, Ru, Os, Rh, Co, Ni, and Pd have also been successfully employed.[7, 68, 77, 118, 126, 137] It should be noted that all of these successful systems benefit from a vast variety of potential ligands that can be used to further modulate catalyst activity.

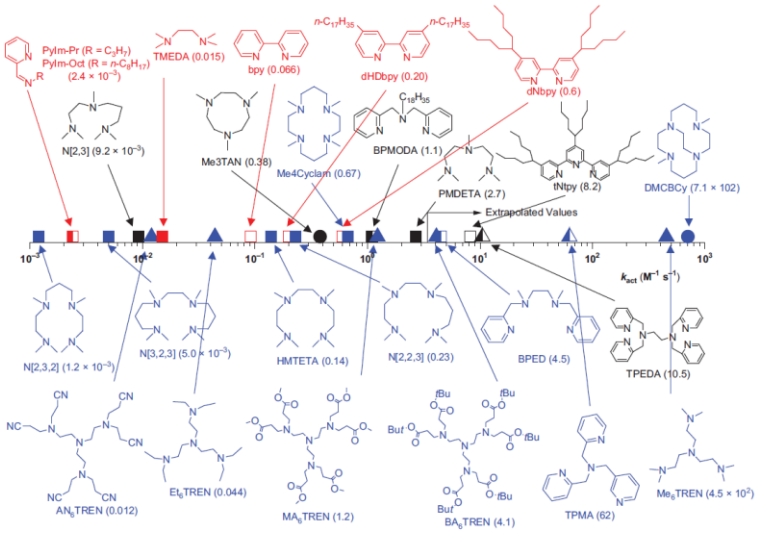

Figure 1.4 Activation rate constants of Cu^{I} complexes derived from various *N*-donor ligands in the reaction with EBiB in MeCN at 35 °C.[135]

1.1.6.5 Monomers and solvents

The rapid progress and flexibility of ATRP have allowed a variety of vinyl monomers to be polymerized to obtain polymeric materials with diverse topologies, predetermined molecular weight and narrow dispersity. The initial range of monomers that could be polymerized by ATRP included (meth)acrylates, styrene, acrylonitrile, (meth)acrylamides, vinylpyridines, ionic type monomers and other monomers containing a multitude of groups.[2, 4, 68, 118, 126, 129-130, 137] However, less conjugated monomers are difficult to polymerize in a controlled way, which is most probably due to the difficulty in the activation step of their less reactive carbon-halogen bonds. Block copolymers can be easily prepared by ATRP but the process requires that monomers

are polymerized following an appropriate sequence based on their order of reactivity: acrylonitrile > methacrylates > acrylates ≈ styrene > acrylamides >> vinyl chloride > vinyl acetate.[68, 129]

The solvent nature also has a remarkable influence on activation rate and equilibrium constant in ATRP, although the effect is less pronounced as compared to initiator and ligand effects.[138-140] Furthermore, a broad range of solvents are accessible including organic solvents, water, ionic liquids, emulsion, and even supercritical carbon dioxide.[129] To explore the effect of solvent on ATRP activation, Matyjaszewski *et al*. reported k_{act} and K_{ATRP} values for the reaction of $[Cu^{I}HMTETA]^{+}$ with EBiB and MBiB, respectively, in a wide range of solvents. The catalyst was most active in DMSO and least active in acetone with ~30-fold and ~80-fold enhancement in k_{act} and K_{ATRP}, respectively, from acetone to DMSO. The activation rate constant does not correlate with the dielectric constant of the solvent. In addition, the effect of monomers on k_{act} and K_{ATRP} was investigated at different monomer to solvent volume ratios. Both k_{act} and K_{ATRP} decreased as the solvent volume in the mixture solution was decreased, indicating that a medium effect is operative.[139] However, K_{ATRP} dropped much faster than k_{act} as a result of increased k_{deact} with increasing monomer fraction. Wang *et al.* measured K_{ATRP} at different solvent/monomer ratios for ATRP of MA with TPMA or Me_6TREN as the ligand in MeCN and DMSO.[140] A much steeper decline of K_{ATRP} was observed in DMSO than in MeCN and was ascribed to the decreasing polarity order: DMSO > MeCN > MA. To quantitatively analyze the effect of the solvent, several approaches including thermodynamic cycles, quantum chemical calculations, and targeted experiments were employed.[138] The higher the solvent polarity used in ATRP, the higher the k_{act} as well as the lower the k_{deact}, ultimately resulting in a higher equilibrium constant. The solvent effects were quantified by a Kamlet−Taft linear solvation energy relationship and a plot of experimental log K_{ATRP} values versus predicted values in terms of the Kamlet−Taft relationship is shown in **Figure 1.5.** The linear solvation energy relationship was applied to a large selection of organic solvents and water with a catalyst activity spanning over seven orders of magnitude. Nonspecific solvent−solute

interactions mainly account for solvent effects on k_{act}.[139] It was found that log K_{ATRP} in aqueous solutions was ~ 3 orders of magnitude higher than in organic solutions. The formation of H bonds, Lewis acid-base adducts with copper, and the competition between the ligand, solvent, and/or monomer to coordinate copper cannot be neglected as one or some of them might result in an increase in the overall rate of polymerization.[126, 137-139, 141]

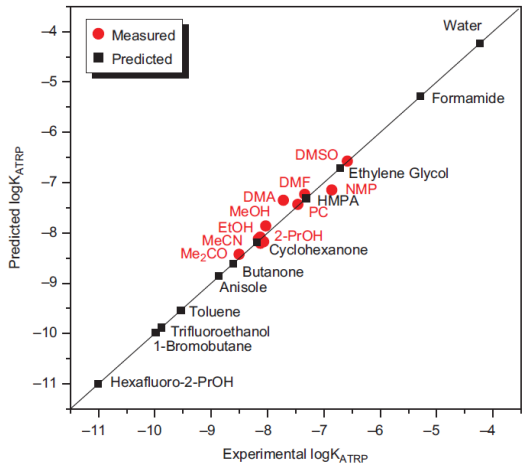

Figure 1.5 A plot of log K_{ATRP} values for Cu^{I}Br/HMTETA + MBiB against values predicted by the Kamlet–Taft relationship.[138]

1.1.6.6 Other factors affecting ATRP rate

Besides type of initiator, catalyst, monomer and solvent, as described above, other factors such as temperature, pressure and various additives also affect polymerization rate. A multitude of outstanding works were carried out to boost the rate of ATRP by addition of certain additives, like metal alkoxides (Al, Ti, and Sn-based alkoxides), zerovalent metals such as Cu, Fe, Mg and Zn, phenols, benzoic acid, alkylamines, pyridine, water, and phase-transfer agents.[118, 126, 130] In addition, there are some other possibilities for accelerating polymerization rate with narrow $Đ$ by tuning reaction conditions like the polymerization temperature and pressure. Higher temperature could increase k_p much more than k_t because of the lower activation energy of termination.[142] Pressure is another key parameter. Both K_{ATRP} and k_p apparently increase at high

pressure, and this favorable effect is not counterbalanced by an increase in dispersity.[143-144] As such, according to **eq. 1-2**, the dead chain fraction (DCF) could significantly decrease due to the high propagation rate at high temperature and pressure, thus indirectly allowing to prolong the retention of chain-end functionalities for different topologies.

1.1.7 Development of advanced ATRP methods

Although ATRP is a robust and versatile technique for radical polymerization, there are still some limitations in the widely used Cu-based ATRP. For instance, the initiation process always starts with air sensitive Cu^{I} at relatively high concentrations with the obvious trouble of intolerance to oxygen or other oxidants. Other problems include catalyst removal, polymer purification, side reactions (radical-radical termination or disproportionation, fragmentation, end-functionality decomposition, etc.), and the complicated setup (with some safety risks as explained in **1.1.6.1**). Various advanced methods of ATRP aiming to avoid starting with Cu^{I} and reducing the catalyst load to ppm level or even making the process metal-free or ligand- and solvent-free have been developed and are nowadays commonly used.[4-5, 129, 145-147]

1.1.7.1 Reverse ATRP and SR&NI ATRP

Reverse ATRP was developed to avoid starting with air sensitive Cu^{I} catalysts; the process starts with an air stable Cu^{II} complex (deactivator), which is converted *in situ* to the activator by reaction of the deactivator with a standard free radical from a radical initiator such as 2,2'-azobisisobutirronitrile (AIBN).[148] However, this process could only be used for the preparation of homopolymers and not for other more complicated architectures unless a polymeric precursor of radicals could be prepared. Furthermore, other unfavorable features such as long reaction time, high catalyst concentration and high temperature limit the wide application of reverse ATRP.

Simultaneous reverse and normal initiation (SR&NI) ATRP was then developed to use a low concentration of active catalyst complex with addition of a relatively larger

amount of alkyl halide initiator concurrently with a small amount of a conventional radical initiator (e.g., AIBN).[149] The reaction starts with the decomposition of the conventional radical source. SR&NI ATRP has been successfully conducted in aqueous heterogeneous media such as miniemulsion and could afford polymers of various architecture. Despite these advantages, on the other hand, a drawback of SR&NI ATRP is the introduction of a small fraction of polymer chains generated from the direct initiation of radical initiator, which is an issue in a highly functionalized or pure segmented copolymer.[62, 77]

1.1.7.2 Activators regenerated by electron transfer (ARGET) ATRP

Another technique toward reducing the amount of catalyst needed in ATRP is activators generated by electron transfer (AGET) ATRP.[77, 129, 140] This method employs a variety of reducing agents including Sn^{II} compounds, ascorbic acid, phenols, thiophenols, hydrazine, glucose, etc., and can be successfully carried out in the presence of a limited amount of air, in different solvents as well as in bulk and in miniemulsion. ARGET ATRP is an improvement over SR&NI ATRP; it was developed as an extension of AGET ATRP, which was first reported in 2006.[150-153] In ARGET ATRP, the role of the reducing agent should be limited to generating the activator by electron transfer, while the number of growing chains is determined by the initiator, RX. For copper-based ATRP, a Cu^{II} complex is reversibly reduced by the reducing agent to generate a Cu^{I} complex able to activate the C-X bond in the initiator. Polymerization is therefore triggered when the reducing agent activates the catalyst in the presence of initiator and monomer. If the quantity of the reducing agent is large enough to reduce not only the starting Cu^{II} but also the Cu^{II} species arising from radical termination, the polymerization can proceed until the monomer is consumed completely or the reaction is stopped. Thus, a low concentration of Cu^{II} is needed for the synthesis of 'pure' polymers, and some catalyst-induced side reactions are greatly reduced. However, some reducing agents may induce undesired side reactions involving the ligand, solvent or monomer.[77, 146]

1.1.7.3 Supplemental activator and reducing agent (SARA) ATRP

SARA ATRP uses low toxicity reducing agents including zerovalent metals (in the form of powder, turnings, wire, mesh, film, etc.) such as Cu, Fe, Mn, Zn, and Ag as well as eco-friendly inorganic sulfites such as sodium dithionite ($Na_2S_2O_4$), sodium metabisulfite ($Na_2S_2O_5$), sodium bisulfite ($NaHSO_3$), and sodium carbonate (Na_2CO_3).[129, 145, 154-155] Besides acting as a reducing agent for the reduction of deactivators, zerovalent metals can also act as supplemental activators by a direct reaction with chain-ends of alkyl halides. In the case of Cu^0 as the reducing agent in Cu-based ATRP, the process is sometimes called SET LRP, a name coined by Percec [121, 127] who proposed a mechanism based on outer-sphere electron transfer (see **1.1.6.3**). However, various groups have presented a series of arguments and experimental evidence invalidating the SET LRP mechanism. [120, 122, 124-125] According to the mechanism of Percec, Cu^0 is the main activator of C-X, while Cu^I rapidly and completely undergoes disproportionation. In addition, the reaction between Cu^0 and RX occurs by an OSET mechanism producing intermediate radical anions, $RX^{\bullet-}$. Both these assumptions were shown to be wrong. Disproportionation/comproportionation between Cu^I, Cu^0 and Cu^{II} is a relatively slow process rather than 'instantaneous', and disproportionation is only partial in most systems, while comproportionation dominates. Moreover, the formation of an intermediate radical anion is not viable due to the absence any covalent bond feature between carbon-centered radical and associated anion leaving group.

Effective surface contact is an important factor for SARA ATRP with zerovalent metals and, in general, a big contact area could boost the polymerization rate. Additionally, use of a zerovalent metal such Cu^0 is favorable for catalyst preparation, removal, and recyclability (excluding powder).[137] However, several limitations are also present. For instance, the presence of a thin and less reactive oxide layer on the metal surface can slow the initial polymerization rate. Also, the problem of metal powder removal after polymerization and the use of expensive ligands (e.g., TPMA or Me_6TREN) are important issues. Despite these drawbacks, SARA ATRP was also

employed for surface-initiated polymerization, which is known as SARA SI-ATRP.[156] In addition, a temporal control on polymerization can be introduced by inserting the metal into the solution (polymerization "on") or lifting it out of the solution (polymerization "off").

1.1.7.4 Initiators for continuous activator regeneration (ICAR) ATRP

ICAR ATRP is another strategy to reduce the concentration of the metal catalyst used in the polymerization with the introduction of a small amount of a free radical initiator (e.g., AIBN).[157] Like SR&NI ATRP and reverse ATRP, one limitation of ICAR ATRP is in the synthesis of block copolymers, because the propagating radicals originate from the free radical initiator, not from a dormant polymer chain, and as such will generate only homopolymer chains. The radical generation rate is favored by the radical initiator decomposition rate (k_i), thus the polymerization rate in ICAR ATRP is dictated by the rate of free radical initiator decomposition. The slow generation of radicals in ICAR ATRP, via either chemical reaction (i.e., self-initiation) or physical stimuli (e.g., thermal, light, etc.) methods, continuously reduces the deactivator to regenerate the activator together with dormant species. As such, a low concentration of catalyst (<100 ppm or less) is needed in ICAR ATRP. In practice, the rate of the process is controlled by tuning the rate and concentration of radicals. Moreover, the polymerization rate, the molecular weight and $Đ$ are controlled by K_{ATRP} and k_{deact}, or are dependent upon the catalyst.[4, 129, 137, 145, 157] The most used catalysts are Cu or Fe-based systems in a range of solvents including organic solvents, ionic liquids, and water. A main limitation in ICAR is that new chains are continuously formed as long as the free radical initiator is present in solution.

1.1.8 ATRP methods based on external stimuli

Besides the chemical methods described in the previous sections (addition of additives like a radical initiator, reducing agents, a zerovalent metal, etc.), several physical methods based on external stimuli such as light, ultrasound, and electric

current have been recently developed. These methods include electrochemically mediated polymerization (*e*ATRP), photochemically mediated polymerization (photoATRP), and mechanically mediated procedures (mechanoATRP or sonoATRP).[4-5, 105, 129, 145-146, 158-160] *e*ATRP is one of the most popular methods for polymerization. Since it was used as the principal method of investigation in my thesis, only a brief introduction of *e*ATRP will be included in this chapter, whereas a full description on the state of the art, development history, and applications of *e*ATRP will be provided in a dedicated chapter of the thesis (**Chapter II**).

1.1.8.1 Photochemically mediated polymerization, photoATRP

The use of photoATRP to activate and control ATRP has attracted considerable attention due to the abundance and easy availability of light source, low cost, and environmentally friendly nature of the method. Moreover, it offers tremendous possibilities for temporal and spatial control during polymerization simply by turning the light on or off. Conventional photochemical reactions including both unimolecular dissociation (type I, for instance, (2,4,6 trimethylbenzoyl) diphenylphosphine oxide, TMDPO, 2,2-dimethoxy-2-phenyl acetophenone, DMPA) and a bimolecular process (type II, for instance, camphorquinone (CQ) and benzhydrol (Bzh) or benzophenone (BP)) are performed in the presence of photoinitiators and photosensitizers under UV-vis light irradiation, as shown in **Scheme 1.9**. Guan and Smart were the first to report the significance of light in ATRP in 2000 showing that irradiation not only accelerated the polymerization but also allowed lowering catalyst concentration.[161] Subsequently, Kwak and Matyjaszewski reported the first photoATRP with the aid of UV-irradiated dithiocarbamate in the presence of ppm amounts of a copper catalyst.[162] To better understand the mechanism of photoATRP, different aspects of the process, including the role of initiators, catalyst system (e.g., Cu, Fe, Ru, Au, Ir, etc.), ligand structure, solvent, different light source and temporal control were investigated.[2, 145-146, 163-172] One of the most important factors was found to be the type of ligand and its molar ratio with respect to the deactivator. As in other low-ppm ATRP methods (reverse,

SR&NI, and ICAR), the rate of polymerization in photoATRP depends on the radical generation rate and can be tuned by varying the light source (brightness, optical path, and wavelength), and the amount of metal catalyst and ligand.

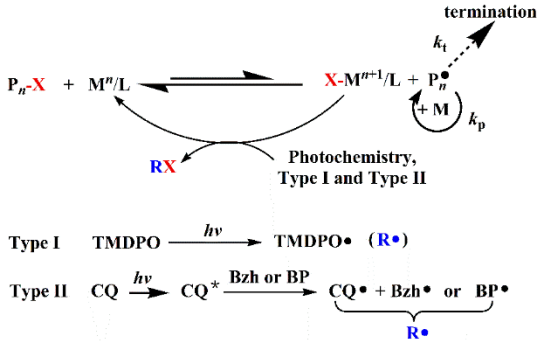

Scheme 1.9 Mechanistic scheme for photoinduced ATRP

Further, metal-free photoATRP was developed by using organic photoredox catalysts under irradiation with an oxidative quenching process.[173-178] It's completely different from photoATRP based on metal catalysts in which, for instance, the regeneration of the Cu^I activator is achieved by photochemical reduction of a Cu^{II} complex via a reductive quenching process in the presence of excess ligand. Apart from the low catalyst loading, some advantages of metal-mediated photoATRP are increased lifetime of chain-end functionality, rapid polymerization and easy preparation of polymers with diverse topologies. However, metal-free photoATRP is more limited and requires appropriate selection of monomer and solvent. For example, according to recent investigations, metal-free photoATRP provides good control for MA but less efficient control for acrylic and styrenic monomers.[2] Moreover, the range of currently available catalysts is rather limited.

1.1.8.2 Mechanochemically mediated procedures, mechanoATRP or sonoATRP

Ultrasound is the latest method to transfer electrons and regenerate the activators in an ATRP system.[108, 179-184] In contrast to the conventional ultrasound-mediated radical polymerizations that utilized the force-induced cleavage of labile bonds,

mechano-ATRP is based on piezochemical initiation of polymerization, whereby mechanical energy is converted into chemical energy.[145] Esser-Kahn *et al*. [183]and Matyjaszewski *et al*.[184] in 2017 independently used commercially available barium titanate ($BaTiO_3$) and zinc oxide (ZnO) piezoelectric nanoparticles as transducers, respectively. However, it was noted that the temporal control for these systems was not ideal as the polymerization slightly continued even during the 'off' periods.[2] Pan *et al*. who recently reviewed externally controlled ATRP concluded that the following factors need be considered for the improvement of mechanoATRP: employing transducers with larger dielectric constants, higher concentration of transducers, smaller particles with geometric defects (e.g, distortion), and addition of surfactants to keep homogenous dispersion.[145]

1.1.8.3 Electrochemical Control of ATRP

Electroanalytical methods are environmentally benign, hugely versatile and widely used in many fields.[79, 185] Cyclic voltammetry (CV), linear sweep voltammetry (LSV), chronoamperometry (CA) as well as chronopotentiometry (CP) are the most frequently used methods of electroanalysis for characterizing catalysts.

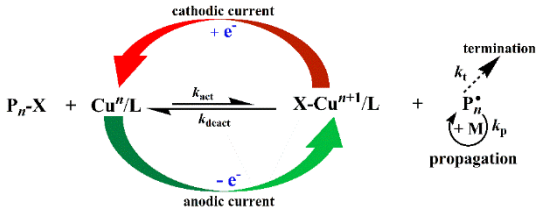

Scheme 1.10 Mechanism of *e*ATRP. Application of an anodic or a cathodic current allows to oxidize or reduce the catalyst, respectively.

Electrochemically mediated ATRP (abbreviated *e*ATRP) is a new procedure for continuously controlling the ratio of activator to deactivator under vigorous stirring.[79] It is similar to ARGET and ICAR ATRP in that it allows the use of only ppm amounts of catalyst, with continuous regeneration of the activator by reduction at an electrode surface. The regeneration of the Cu^I activator and polymerization rate in *e*ATRP can be

strictly controlled through adjustment of the applied potential or current. In addition, *e*ATRP allows temporal control of polymerization: electroreduction of the catalyst to its lower oxidation state triggers polymerization, whereas oxidation back to the higher oxidation state stops the reaction (**Scheme 1.10**). This can be easily done by adjusting the applied potential to a value appropriate for catalyst reduction or oxidation to switch on or switch off the process. *e*ATRP was shown to be an excellent tool for the synthesis of polymers with various predesigned architectures and narrow $Đ$ as well as predetermined molecular weight in a wide range of solvents. From an economic standpoint, it is very important to employ inexpensive electrode materials (carbon or non-noble metals and alloys, for example, stainless steel) to replace rare and expensive materials such as Pt as alternative cathodic or anodic electrodes or both of them. Thus, the conventional divided cell was replaced with an undivided one with a sacrificial anode. Several achievements were reported by the research groups of Matyjaszewski and Gennaro.[186-187] However, to date, nobody systematically explored the effect of a sacrificial anode such as Al used in an undivided cell on the performances of various $[Cu^{II}L]^{2+}$ (L= TPMA or Me_6TREN) complexes in *e*ATRP in different solvents. This important issue was the main subject of study of this thesis and details of the investigations and the obtained results will be presented in **Chapters IV-VIII**.

1.2 Conclusions

The versatility and unprecedented success of control over radical polymerization made RDRP the preeminent method of synthesis of polymers with well-defined architecture and composition, predetermined molecular weights and low dispersity. In the last two decades, many advanced approaches such as NMP, ATRP and RAFT were developed and improved. NMP relies on spontaneous homolytic cleavage of a covalent bond. Despite NMP provides several advantages for the preparation of specific polymers, as shown in **Figure 1.6**, several inherent limitations in NMP have led to the more widespread use of other two polymerization methods (ATRP and RAFT) in polymer synthesis, as indicated in **Figure 1.1**. Both NMP and ATRP processes rely on

PRE, while methods based on DT such as RAFT follow a conventional radical polymerization with a steady state established by balancing initiation and termination rates rather than a reversible activation/deactivation process.

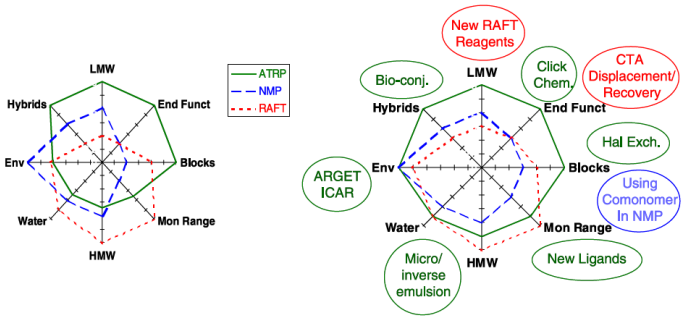

Figure 1.6 Comparison of NMP, ATRP and RAFT.[68]

It is indisputable that Cu-catalyzed ATRP is a powerful and robust radical polymerization technique for the preparation of polymers with precisely predesigned structure, multi end-functionality, and high molecular weight as well as narrow *Đ*. There are, however, still many features that remain unexplored up to now and need to be looked at in more detail. For instance, the dead chains that are inevitably formed during the reaction, setup improvement for scale-up production, product purification, and cost and environmental issues are still restricting wide application of ATRP in the industry. In contrast to traditional ATRP, several advanced methods including *e*ATRP, photoATRP and mechanoATRP, which use ppm amounts of air-stable catalysts and allow temporal control of polymerization, are widely used at the laboratory scale. Today, *e*ATRP can be used for the polymerization of diverse monomers while the technique is compatible with a range of solvents. In particular, the development of a simplified *e*ATRP setup allowed easier access to rapid and controlled polymerizations for the fabrication of multi-functional polymers.

References

[1**]**. Peng, H.; Sun, X.; Weng, W.; Fang, X., *Polymer Materials for Energy and Electronic Applications*. Academic Press: 2016.
[2**]**. Parkatzidis, K.; Wang, H. S.; Truong, N. P.; Anastasaki, A., Recent developments and future challenges in controlled radical polymerization: a 2020 update. *Chem* **2020**.
[3**]**. Webster, O. W., Living polymerization methods. *Science* **1991,** *251* (4996), 887-893.
[4**]**. Corrigan, N.; Jung, K.; Moad, G.; Hawker, C. J.; Matyjaszewski, K.; Boyer, C., Reversible-deactivation radical polymerization (Controlled/living radical polymerization): From discovery to materials design and applications. *Progress in Polymer Science* **2020**, 101311.
[5**]**. Isse, A. A.; Gennaro, A., Electrochemistry for Atom Transfer Radical Polymerization. *The Chemical Record*. **2021**.
[6**]**. Morawetz, H., *Polymers: the origins and growth of a science*. 2002.
[7**]**. Moad, G.; Solomon, D. H., *The chemistry of radical polymerization*. Elsevier: 2006.
[8**]**. Tedder, J. M., Which factors determine the reactivity and regioselectivity of free radical substitution and addition reactions? *Angewandte Chemie International Edition in English* **1982,** *21* (6), 401-410.
[9**]**. Ehlers, F.; Barth, J.; Vana, P., Kinetics and Thermodynamics of Radical Polymerization. In *Fundamentals of Controlled/Living Radical Polymerization*, Royal Society of Chemistry Cambridge: 2013; pp 1-59.
[10**]**. Asua, J. M.; Beuermann, S.; Buback, M.; Castignolles, P.; Charleux, B.; Gilbert, R. G.; Hutchinson, R. A.; Leiza, J. R.; Nikitin, A. N.; Vairon, J. P., Critically evaluated rate coefficients for free-radical polymerization, 5. *Macromolecular Chemistry and Physics* **2004,** *205* (16), 2151-2160.
[11**]**. Dervaux, B.; Junkers, T.; Schneider-Baumann, M.; Du Prez, F. E.; Barner-Kowollik, C., Propagation rate coefficients of isobornyl acrylate, tert-butyl acrylate and 1-ethoxyethyl acrylate: A high frequency PLP-SEC study. *Journal of Polymer Science Part A: Polymer Chemistry* **2009,** *47* (23), 6641-6654.
[12**]**. Beuermann, S.; Buback, M.; Davis, T. P.; García, N.; Gilbert, R. G.; Hutchinson, R. A.; Kajiwara, A.; Kamachi, M.; Lacík, I.; Russell, G. T., Critically Evaluated Rate Coefficients for Free-Radical Polymerization, 4. *Macromolecular Chemistry and Physics* **2003,** *204* (10), 1338-1350.
[13**]**. Olaj, O. F.; Vana, P.; Zoder, M.; Kornherr, A.; Zifferer, G., Is the rate constant of chain propagation kp in radical polymerization really chain-length independent? *Macromolecular rapid communications* **2000,** *21* (13), 913-920.
[14**]**. Olaj, O. F.; Zoder, M.; Vana, P.; Kornherr, A.; Schnöll-Bitai, I.; Zifferer, G., Chain length dependence of chain propagation revisited. *Macromolecules* **2005,** *38* (5), 1944-1948.
[15**]**. Heuts, J. P.; Russell, G. T.; Smith, G. B.; van Herk, A. M. In *The Importance of Chain-Length Dependent Kinetics in Free-Radical Polymerization: A Preliminary*

Guide, Macromolecular symposia, Wiley Online Library: 2007; pp 12-22.
[16**]**. Zammit, M. D.; Davis, T. P.; Willett, G. D.; O'Driscoll, K. F., The effect of solvent on the homo-propagation rate coefficients of styrene and methyl methacrylate. *Journal of Polymer Science Part A: Polymer Chemistry* **1997,** *35* (11), 2311-2321.
[17**]**. Coote, M. L.; Davis, T. P.; Klumperman, B.; Monteiro, M. J., A mechanistic perspective on solvent effects in free-radical copolymerization. **1998**.
[18**]**. Beuermann, S.; Buback, M., Rate coefficients of free-radical polymerization deduced from pulsed laser experiments. *Progress in Polymer Science* **2002,** *27* (2), 191-254.
[19**]**. Aleksandrov, A.; Genkin, V. N.; Kitaĭ, M.; Smirnova, I.; Sokolov, V., Kinetics of laser-initiated polymerization and molecular-weight distribution of the resultant polymer. *Soviet Journal of Quantum Electronics* **1977,** *7* (5), 547.
[20**]**. Gilbert, R. G., Critically-evaluated propagation rate coefficients in free radical polymerizations I. Styrene and methyl methacrylate (Technical Report). *Pure and applied chemistry* **1996,** *68* (7), 1491-1494.
[21**]**. Mayo, F. R.; Gregg, R.; Matheson, M. S., Chain Transfer in the Polymerization of Styrene. VI. Chain Transfer with Styrene and Benzoyl Peroxide; the Efficiency of Initiation and the Mechanism of Chain Termination1. *Journal of the American Chemical Society* **1951,** *73* (4), 1691-1700.
[22**]**. Baysal, B.; Tobolsky, A. V., Rates of initiation in vinyl polymerization. *Journal of Polymer Science* **1952,** *8* (5), 529-541.
[23**]**. Bartlett, P. D.; Altschul, R., The polymerization of allyl compounds. II. Preliminary kinetic study of the peroxide-induced polymerization of allyl acetate. *Journal of the American Chemical Society* **1945,** *67* (5), 816-822.
[24**]**. Pryor, W. A.; Lee, A.; Witt, C., Reactions of Radicals. IX. t-Butyl Peroxide. *Journal of the American Chemical Society* **1964,** *86* (20), 4229-4234.
[25**]**. May Jr, J. A.; Smith, W. B., Polymer studies by gel permeation chromatography. II. Kinetic parameters for styrene polymerizations. *The Journal of Physical Chemistry* **1968,** *72* (1), 216-221.
[26**]**. Nair, C. R.; Clouet, G.; Chaumont, P., Functionalization of PMMA by a functional "iniferter": Kinetics of polymerization of MMA using N, N′-diethyl-N, N′-bis (2-hydroxyethyl) thiuram disulfide. *Journal of Polymer Science Part A: Polymer Chemistry* **1989,** *27* (6), 1795-1809.
[27**]**. Kaloforov, N. Y.; Borsig, E., Transfer reactions in radical polymerization of styrene in acetone–chloroform mixture. *Journal of Polymer Science: Polymer Chemistry Edition* **1973,** *11* (10), 2665-2680.
[28**]**. Gleixner, G.; Breitenbach, J. W.; Olaj, O. F., Kettenübertragung durch tetrabromkohlenstoff bei der polymerisation von styrol und von vinylacetat. *Die Makromolekulare Chemie: Macromolecular Chemistry and Physics* **1977,** *178* (8), 2249-2255.
[29**]**. Britton, D.; Heatley, F.; Lovell, P. A., Chain transfer to polymer in free-radical bulk and emulsion polymerization of vinyl acetate studied by NMR spectroscopy. *Macromolecules* **1998,** *31* (9), 2828-2837.
[30**]**. Lim, D.; Wichterle, O., Chain transfer of polymer in radical polymerization.

Journal of Polymer Science **1958,** *29* (120), 579-584.
[31**]**. Schulz, V. G.; Stein, D., Über die verzweigung des polyvinylacetats. I. Die bestimmung der übertragungskonstante des polymeren nach der methode der „α-polymeren" . *Die Makromolekulare Chemie: Macromolecular Chemistry and Physics* **1962,** *52* (1), 1-22.
[32**]**. Bamford, C.; Jenkins, A., The reactivity of free radicals. *Journal of Polymer Science* **1961,** *53* (158), 149-155.
[33**]**. Bamford, C.; Jenkins, A. D., Patterns of free radical reactivity. Part 3. *Transactions of the Faraday Society* **1963,** *59*, 530-539.
[34**]**. Borsig, E.; Lazar, M.; Čapla, M., Polymerization of methyl methacrylate initiated by 3.3. 4.4-tetraphenyl hexane and 1.1. 2.2-tetraphenyl cyclopentane. *Die Makromolekulare Chemie: Macromolecular Chemistry and Physics* **1967,** *105* (1), 212-222.
[35**]**. Szwarc, M., Carbanions, living polymers, and electron transfer processes. **1968**.
[36**]**. Borsig, E.; Lazar, M.; Čapla, M.; Florián, Š., Reinitiation reactions of poly (methyl methacrylate) with labile bound fragments of initiator. *Die Angewandte Makromolekulare Chemie: Applied Macromolecular Chemistry and Physics* **1969,** *9* (1), 89-95.
[37**]**. Olaj, O., Zur Kinetik der spontanen und der durch extrem kleine Starterkonzentrationen initiierten radikalischen Polymerisation des Styrols. *Monatshefte für Chemie-Chemical Monthly* **1971,** *102* (3), 648-671.
[38**]**. Smith, S.; Hubin, A. J., The preparation and chemistry of dicationically active polymers of tetrahydrofuran. *Journal of Macromolecular Science—Chemistry* **1973,** *7* (7), 1399-1413.
[39**]**. Hawthorne, D. G.; Johns, S. R.; Solomon, D. H.; Willing, R. I., The cyclopolymerization of N-Allyl-N-methyl (2-substituted allyl) amines. The structure of the polymers and low molecular weight products. *Australian Journal of Chemistry* **1976,** *29* (9), 1955-1974.
[40**]**. Evans, M.; Polanyi, M., Further considerations on the thermodynamics of chemical equilibria and reaction rates. *Transactions of the Faraday Society* **1936,** *32*, 1333-1360.
[41**]**. Bell, R. P., The theory of reactions involving proton transfers. *Proceedings of the Royal Society of London. Series A-Mathematical and Physical Sciences* **1936,** *154* (882), 414-429.
[42**]**. Ziegler, K., The importance of alkali metallo-organic compounds for synthesis. *Angew Chem* **1936,** *49*, 499-502.
[43**]**. Flory, P. J., *Principles of polymer chemistry*. Cornell University Press: 1953.
[44**]**. Szwarc, M.; Levy, M.; Milkovich, R., Polymerization initiated by electron transfer to monomer. A new method of formation of block polymers1. *Journal of the American Chemical Society* **1956,** *78* (11), 2656-2657.
[45**]**. SZWARC, M., 'Living'polymers. *Nature* **1956,** *178* (4543), 1168-1169.
[46**]**. Otsu, T.; Yoshida, M., Role of initiator-transfer agent-terminator (iniferter) in radical polymerizations: Polymer design by organic disulfides as iniferters. *Die Makromolekulare Chemie, Rapid Communications* **1982,** *3* (2), 127-132.

[47**]**. Otsu, T.; Yoshida, M.; Tazaki, T., A model for living radical polymerization. *Die Makromolekulare Chemie, Rapid Communications* **1982,** *3* (2), 133-140.
[48**]**. Otsu, T.; Yoshida, M., Efficient synthesis of two or multi component block copolymers through living radical polymerization with polymeric photoiniferters. *Polymer Bulletin* **1982,** *7* (4), 197-203.
[49**]**. Błedzki, A.; Braun, D.; Titzschkau, K., Polymerisationsauslösung mit substituierten ethanen, 6. Polymerisation von methylmethacrylat mit verschiedenen tetraphenylethanen. *Die Makromolekulare Chemie: Macromolecular Chemistry and Physics* **1983,** *184* (4), 745-754.
[50**]**. Matyjaszewski, K.; Gaynor, S.; Greszta, D.; Mardare, D.; Shigemoto, T., 'Living'and controlled radical polymerization. *Journal of Physical Organic Chemistry* **1995,** *8* (4), 306-315.
[51**]**. Greszta, D.; Matyjaszewski, K., Mechanism of controlled/"living" radical polymerization of styrene in the presence of nitroxyl radicals. Kinetics and simulations. *Macromolecules* **1996,** *29* (24), 7661-7670.
[52**]**. Georges, M. K.; Veregin, R. P.; Kazmaier, P. M.; Hamer, G. K., Narrow molecular weight resins by a free-radical polymerization process. *Macromolecules* **1993,** *26* (11), 2987-2988.
[53**]**. Wang, J.-S.; Matyjaszewski, K., Controlled/" living" radical polymerization. atom transfer radical polymerization in the presence of transition-metal complexes. *Journal of the American Chemical Society* **1995,** *117* (20), 5614-5615.
[54**]**. Chiefari, J.; Chong, Y.; Ercole, F.; Krstina, J.; Jeffery, J.; Le, T. P.; Mayadunne, R. T.; Meijs, G. F.; Moad, C. L.; Moad, G., Living free-radical polymerization by reversible addition− fragmentation chain transfer: the RAFT process. *Macromolecules* **1998,** *31* (16), 5559-5562.
[55**]**. Wayland, B. B.; Poszmik, G.; Mukerjee, S. L.; Fryd, M., Living radical polymerization of acrylates by organocobalt porphyrin complexes. *Journal of the American Chemical Society* **1994,** *116* (17), 7943-7944.
[56**]**. Gaynor, S. G.; Wang, J.-S.; Matyjaszewski, K., Controlled radical polymerization by degenerative transfer: effect of the structure of the transfer agent. *Macromolecules* **1995,** *28* (24), 8051-8056.
[57**]**. Jenkins, A. D.; Jones, R. G.; Moad, G., Terminology for reversible-deactivation radical polymerization previously called" controlled" radical or" living" radical polymerization (IUPAC Recommendations 2010). *Pure and Applied Chemistry* **2009,** *82* (2), 483-491.
[58**]**. Matyjaszewski, K., Ranking living systems. *Macromolecules* **1993,** *26* (7), 1787-1788.
[59**]**. Matyjaszewski, K., Introduction to living polymeriz. Living and/or controlled polymerization. *Journal of Physical Organic Chemistry* **1995,** *8* (4), 197-207.
[60**]**. Shipp, D. A., Reversible-deactivation radical polymerizations. *Polymer Reviews* **2011,** *51* (2), 99-103.
[61**]**. Goto, A.; Fukuda, T., Kinetics of living radical polymerization. *Progress in Polymer Science* **2004,** *29* (4), 329-385.
[62**]**. Matyjaszewski, K.; Sumerlin, B. S.; Tsarevsky, N. V., *Progress in controlled*

radical polymerization: materials and applications. ACS Publications: 2012.
[63**]**. Solomon, D. H.; Rizzardo, E.; Cacioli, P., Polymerization process and polymers produced thereby. Google Patents: 1986.
[64**]**. Fischer, H., Unusual selectivities of radical reactions by internal suppression of fast modes. *Journal of the American Chemical Society* **1986,** *108* (14), 3925-3927.
[65**]**. Fischer, H., The persistent radical effect in "living" radical polymerization. *Macromolecules* **1997,** *30* (19), 5666-5672.
[66**]**. Fischer, H., The persistent radical effect in controlled radical polymerizations. *Journal of Polymer Science Part A: Polymer Chemistry* **1999,** *37* (13), 1885-1901.
[67**]**. Fischer, H., The persistent radical effect: a principle for selective radical reactions and living radical polymerizations. *Chemical reviews* **2001,** *101* (12), 3581-3610.
[68**]**. Braunecker, W. A.; Matyjaszewski, K., Controlled/living radical polymerization: Features, developments, and perspectives. *Progress in Polymer Science* **2007,** *32* (1), 93-146.
[69**]**. Souaille, M.; Fischer, H., Kinetic conditions for living and controlled free radical polymerizations mediated by reversible combination of transient propagating and persistent radicals: The ideal mechanism. *Macromolecules* **2000,** *33* (20), 7378-7394.
[70**]**. Hawker, C. J.; Barclay, G. G.; Orellana, A.; Dao, J.; Devonport, W., Initiating systems for nitroxide-mediated "living" free radical polymerizations: synthesis and evaluation. *Macromolecules* **1996,** *29* (16), 5245-5254.
[71**]**. Hawker, C. J.; Bosman, A. W.; Harth, E., New polymer synthesis by nitroxide mediated living radical polymerizations. *Chemical reviews* **2001,** *101* (12), 3661-3688.
[72**]**. Benoit, D.; Harth, E.; Helms, B.; Rees, I.; Vestberg, R.; Rodlert, M.; Hawker, C. In *Controlled/Living Radical Polymerization—Progress in ATRP, NMP, and RAFT (K. Matyjaszewski, Ed.)*, ACS Symposium Series, 2000; p 123.
[73**]**. Rizzardo, E.; Solomon, D. H., On the Origins of Nitroxide Mediated Polymerization (NMP) and Reversible Addition–Fragmentation Chain Transfer (RAFT). *Australian Journal of Chemistry* **2012,** *65* (8), 945-969.
[74**]**. Grubbs, R. B., Nitroxide-mediated radical polymerization: limitations and versatility. *Polymer Reviews* **2011,** *51* (2), 104-137.
[75**]**. Benoit, D.; Grimaldi, S.; Robin, S.; Finet, J.-P.; Tordo, P.; Gnanou, Y., Kinetics and mechanism of controlled free-radical polymerization of styrene and n-butyl acrylate in the presence of an acyclic β-phosphonylated nitroxide. *Journal of the American Chemical Society* **2000,** *122* (25), 5929-5939.
[76**]**. Benoit, D.; Chaplinski, V.; Braslau, R.; Hawker, C. J., Development of a universal alkoxyamine for "living" free radical polymerizations. *Journal of the American Chemical Society* **1999,** *121* (16), 3904-3920.
[77**]**. Tsarevsky, N. V.; Sumerlin, B. S., *Fundamentals of controlled/living radical polymerization*. Royal Society of Chemistry: 2013.
[78**]**. Grimaldi, S.; Finet, J.-P.; Le Moigne, F.; Zeghdaoui, A.; Tordo, P.; Benoit, D.; Fontanille, M.; Gnanou, Y., Acyclic β-phosphonylated nitroxides: a new series of counter-radicals for "living"/controlled free radical polymerization. *Macromolecules* **2000,** *33* (4), 1141-1147.
[79**]**. Magenau, A. J.; Strandwitz, N. C.; Gennaro, A.; Matyjaszewski, K.,

Electrochemically mediated atom transfer radical polymerization. *Science* **2011,** *332* (6025), 81-4.
[80**]**. Zhang, L.; Laborda, E.; Darwish, N.; Noble, B. B.; Tyrell, J. H.; Pluczyk, S.; Le Brun, A. P.; Wallace, G. G.; Gonzalez, J.; Coote, M. L., Electrochemical and electrostatic cleavage of alkoxyamines. *Journal of the American Chemical Society* **2018,** *140* (2), 766-774.
[81**]**. Ziegler, K., Belgian Patent 533,362, 1954. *Google Scholar There is no corresponding record for this reference*.
[82**]**. Ziegler, K.; Holzkamp, E.; Breil, H.; Martin, H., Das mülheimer normaldruck-polyäthylen-verfahren. *Angewandte chemie* **1955,** *67* (19-20), 541-547.
[83**]**. Cecchin, G.; Morini, G.; Piemontesi, F., Ziegler-Natta Catalysts. *Kirk-Othmer Encyclopedia of Chemical Technology* **2000**.
[84**]**. Wayland, B. B.; Poszmik, G.; Fryd, M., Metalloradical reactions of rhodium (II) porphyrins with acrylates: reduction, coupling, and photopromoted polymerization. *Organometallics* **1992,** *11* (11), 3534-3542.
[85**]**. Allan, L. E.; Perry, M. R.; Shaver, M. P., Organometallic mediated radical polymerization. *Progress in polymer science* **2012,** *37* (1), 127-156.
[86**]**. Gridnev, A. A.; Ittel, S. D., Catalytic chain transfer in free-radical polymerizations. *Chemical Reviews* **2001,** *101* (12), 3611-3660.
[87**]**. Shaver, M. P.; Allan, L. E.; Rzepa, H. S.; Gibson, V. C., Correlation of Metal Spin State with Catalytic Reactivity: Polymerizations Mediated by α-Diimine–Iron Complexes. *Angewandte Chemie* **2006,** *118* (8), 1263-1266.
[88**]**. Hurtgen, M.; Detrembleur, C.; Jerome, C.; Debuigne, A., Insight into organometallic-mediated radical polymerization. *Polymer Reviews* **2011,** *51* (2), 188-213.
[89**]**. Halpern, J. In thermodynamics and kinetics of transition-metal alkyl homolytic bond-dissociation processes, ACS Symposium Series, *Amer. Chemical. Soc.* 1155 16th ST, NW, Washington, DC 20036: 1990; pp 100-112.
[90**]**. Semsarilar, M.; Perrier, S., 'Green'reversible addition-fragmentation chain-transfer (RAFT) polymerization. *Nature chemistry* **2010,** *2* (10), 811.
[91**]**. Le, T.; Moad, G.; Rizzardo, E.; Thang, S., Polymerization with living characteristics with controlled dispersity, polymers prepared thereby, and chain-transfer agents used in the same. *USA Patent* **1998**.
[92**]**. Corpart, P.; Charmot, D.; Biadatti, T.; Zard, S.; Michelet, D., Method for block copolymer synthesis by controlled radical polymerization. *Pat. Num. WO* **1998,** *98*, 9858974.
[93**]**. Geagea, R.; Destarac, M.; Mazieres, S.; Stefak, R. In *RAFT polymerization mediated by an organometallic thiocarbonyl thio transfer agent*, RAFT polymerization mediated by an organometallic thiocarbonyl thio transfer agent, 2009.
[94**]**. Geagea, R.; Ladeira, S.; Mazières, S.; Destarac, M., Chromium and molybdenum pentacarbonyl complexes of phosphinocarbodithioates: synthesis, molecular structure and behaviour in RAFT polymerisation. *Chemistry–A European Journal* **2011,** *17* (13), 3718-3725.
[95**]**. Monteiro, M. J.; de Brouwer, H., Intermediate radical termination as the

mechanism for retardation in reversible addition− fragmentation chain transfer polymerization. *Macromolecules* **2001,** *34* (3), 349-352.
[96**]**. Klumperman, B.; van den Dungen, E. T.; Heuts, J. P.; Monteiro, M. J., RAFT-Mediated Polymerization—A Story of Incompatible Data? *Macromolecular rapid communications* **2010,** *31* (21), 1846-1862.
[97**]**. Wang, Y.; Fantin, M.; Park, S.; Gottlieb, E.; Fu, L.; Matyjaszewski, K., Electrochemically Mediated Reversible Addition-Fragmentation Chain-Transfer Polymerization. *Macromolecules* **2017,** *50* (20), 7872-7879.
[98**]**. Lorandi, F.; Fantin, M.; Shanmugam, S.; Wang, Y.; Isse, A. A.; Gennaro, A.; Matyjaszewski, K., Toward Electrochemically Mediated Reversible Addition–Fragmentation Chain-Transfer (eRAFT) Polymerization: Can Propagating Radicals Be Efficiently Electrogenerated from RAFT Agents? *Macromolecules* **2019,** *52* (4), 1479-1488.
[99**]**. Bray, C.; Li, G.; Postma, A.; Strover, L. T.; Wang, J.; Moad, G., Initiation of RAFT Polymerization: Electrochemically Initiated RAFT Polymerization in Emulsion (Emulsion eRAFT), and Direct PhotoRAFT Polymerization of Liquid Crystalline Monomers. *Australian Journal of Chemistry* **2020**.
[100**]**. Strover, L. T.; Cantalice, A.; Lam, J. Y.; Postma, A.; Hutt, O. E.; Horne, M. D.; Moad, G., Electrochemical behavior of thiocarbonylthio chain transfer agents for RAFT polymerization. *ACS Macro Letters* **2019,** *8* (10), 1316-1322.
[101**]**. Sang, W.; Xu, M.; Yan, Q., Coenzyme-catalyzed electro-RAFT polymerization. *ACS Macro Letters* **2017,** *6* (12), 1337-1341.
[102**]**. Wang, Y.; Fantin, M.; Matyjaszewski, K., Synergy between electrochemical ATRP and RAFT for polymerization at low copper loading. *Macromolecular rapid communications* **2018,** *39* (12), 1800221.
[103**]**. Phommalysack-Lovan, J.; Chu, Y.; Boyer, C.; Xu, J., PET-RAFT polymerisation: towards green and precision polymer manufacturing. *Chemical communications* **2018,** *54* (50), 6591-6606.
[104**]**. Allegrezza, M. L.; Konkolewicz, D., PET-RAFT Polymerization: Mechanistic Perspectives for Future Materials. *ACS Macro Letters* **2021,** *10* (4), 433-446.
[105**]**. Liu, Z.; Zhang, G.; Lu, W.; Huang, Y.; Zhang, J.; Chen, T., UV light-initiated RAFT polymerization induced self-assembly. *Polymer Chemistry* **2015,** *6* (34), 6129-6132.
[106**]**. Hu, L.; Hao, Q.; Wang, L.; Cui, Z.; Fu, P.; Liu, M.; Qiao, X.; Pang, X., The in situ “grafting from” approach for the synthesis of polymer brushes on upconversion nanoparticles via NIR-mediated RAFT polymerization. *Polymer Chemistry* **2021,** *12* (4), 545-553.
[107**]**. Zhou, Y.; Zhang, Z.; Reese, C. M.; Patton, D. L.; Xu, J.; Boyer, C.; Postma, A.; Moad, G., Selective and Rapid Light-Induced RAFT Single Unit Monomer Insertion in Aqueous Solution. *Macromolecular rapid communications* **2020,** *41* (1), 1900478.
[108**]**. McKenzie, T. G.; Colombo, E.; Fu, Q.; Ashokkumar, M.; Qiao, G. G., Sono-RAFT polymerization in aqueous medium. *Angewandte Chemie International Edition* **2017,** *56* (40), 12302-12306.
[109**]**. Kato, M.; Kamigaito, M.; Sawamoto, M.; Higashimura, T., Polymerization of

methyl methacrylate with the carbon tetrachloride/dichlorotris-(triphenylphosphine) ruthenium (II)/methylaluminum bis (2, 6-di-tert-butylphenoxide) initiating system: possibility of living radical polymerization. *Macromolecules* **1995,** *28* (5), 1721-1723.
[110**]**. Wang, J.-S.; Matyjaszewski, K., Controlled/" living" radical polymerization. Halogen atom transfer radical polymerization promoted by a Cu (I)/Cu (II) redox process. *Macromolecules* **1995,** *28* (23), 7901-7910.
[111**]**. Patten, T. E.; Xia, J.; Abernathy, T.; Matyjaszewski, K., Polymers with very low polydispersities from atom transfer radical polymerization. *Science* **1996,** *272* (5263), 866-868.
[112**]**. Kharasch, M.; Jensen, E. V.; Urry, W., Addition of carbon tetrachloride and chloroform to olefins. *Science* **1945,** *102* (2640), 128-128.
[113**]**. Minisci, F., Free-radical additions to olefins in the presence of redox systems. *Accounts of Chemical Research* **1975,** *8* (5), 165-171.
[114**]**. Ameduri, B.; Boutevin, B., Synthesis of chlorinated telechelic oligomers. 1. Telomerization of nonconjugated dienes with functional telogens. *Macromolecules* **1990,** *23* (9), 2433-2439.
[115**]**. Matyjaszewski, K.; Davis, T. P., *Handbook of radical polymerization*. John Wiley & Sons: 2003.
[116**]**. Tang, W.; Tsarevsky, N. V.; Matyjaszewski, K., Determination of equilibrium constants for atom transfer radical polymerization. *Journal of the American Chemical Society* **2006,** *128* (5), 1598-1604.
[117**]**. Matyjaszewski, K., *Advances in controlled/living radical polymerization*. ACS Publications: 2003.
[118**]**. Matyjaszewski, K., *Controlled radical polymerization*. American Chemical Society: 1998.
[119**]**. Matyjaszewski, K., Radical nature of Cu-catalyzed controlled radical polymerizations (atom transfer radical polymerization). *Macromolecules* **1998,** *31* (15), 4710-4717.
[120**]**. Isse, A. A.; Gennaro, A.; Lin, C. Y.; Hodgson, J. L.; Coote, M. L.; Guliashvili, T., Mechanism of carbon-halogen bond reductive cleavage in activated alkyl halide initiators relevant to living radical polymerization: theoretical and experimental study. *J Am Chem Soc* **2011,** *133* (16), 6254-64.
[121**]**. Guliashvili, T.; Percec, V., A comparative computational study of the homolytic and heterolytic bond dissociation energies involved in the activation step of ATRP and SET-LRP of vinyl monomers. *Journal of Polymer Science Part A: Polymer Chemistry* **2007,** *45* (9), 1607-1618.
[122**]**. Isse, A. A.; Gennaro, A., Homogeneous reduction of haloacetonitriles by electrogenerated aromatic radical anions: determination of the reduction potential of• CH2CN. *The Journal of Physical Chemistry A* **2004,** *108* (19), 4180-4186.
[123**]**. Isse, A. A.; Bortolamei, N.; De Paoli, P.; Gennaro, A., On the mechanism of activation of copper-catalyzed atom transfer radical polymerization. *Electrochimica Acta* **2013,** *110*, 655-662.
[124**]**. Lin, C. Y.; Coote, M. L.; Gennaro, A.; Matyjaszewski, K., Ab initio evaluation of the thermodynamic and electrochemical properties of alkyl halides and radicals and

their mechanistic implications for atom transfer radical polymerization. *Journal of the American Chemical Society* **2008,** *130* (38), 12762-12774.
[125**]**. Tang, W.; Matyjaszewski, K., Effects of initiator structure on activation rate constants in ATRP. *Macromolecules* **2007,** *40* (6), 1858-1863.
[126**]**. Kamigaito, M.; Ando, T.; Sawamoto, M., Metal-catalyzed living radical polymerization. *Chemical Reviews* **2001,** *101* (12), 3689-3746.
[127**]**. Percec, V.; Guliashvili, T.; Ladislaw, J. S.; Wistrand, A.; Stjerndahl, A.; Sienkowska, M. J.; Monteiro, M. J.; Sahoo, S., Ultrafast synthesis of ultrahigh molar mass polymers by metal-catalyzed living radical polymerization of acrylates, methacrylates, and vinyl chloride mediated by SET at 25 C. *Journal of the American Chemical Society* **2006,** *128* (43), 14156-14165.
[128**]**. Matyjaszewski, K.; Göbelt, B.; Paik, H.-j.; Horwitz, C. P., Tridentate nitrogen-based ligands in Cu-based ATRP: a structure− activity study. *Macromolecules* **2001,** *34* (3), 430-440.
[129**]**. Matyjaszewski, K., Atom transfer radical polymerization (ATRP): current status and future perspectives. *Macromolecules* **2012,** *45* (10), 4015-4039.
[130**]**. Matyjaszewski, K.; Spanswick, J., Copper-Mediated Atom Transfer Radical Polymerization. **2012**.
[131**]**. Matyjaszewski, K.; Tsarevsky, N. V.; Braunecker, W. A.; Dong, H.; Huang, J.; Jakubowski, W.; Kwak, Y.; Nicolay, R.; Tang, W.; Yoon, J. A., Role of Cu0 in controlled/"living" radical polymerization. *Macromolecules* **2007,** *40* (22), 7795-7806.
[132**]**. Konkolewicz, D.; Wang, Y.; Krys, P.; Zhong, M.; Isse, A. A.; Gennaro, A.; Matyjaszewski, K., SARA ATRP or SET-lRP. end of controversy? *Polymer Chemistry* **2014,** *5* (15), 4396-4417.
[133**]**. Lorandi, F.; Fantin, M.; Isse, A. A.; Gennaro, A., RDRP in the presence of Cu0: The fate of Cu (I) proves the inconsistency of SET-LRP mechanism. *Polymer* **2015,** *72*, 238-245.
[134**]**. Tang, W.; Kwak, Y.; Braunecker, W.; Tsarevsky, N. V.; Coote, M. L.; Matyjaszewski, K., Understanding atom transfer radical polymerization: effect of ligand and initiator structures on the equilibrium constants. *Journal of the American Chemical Society* **2008,** *130* (32), 10702-10713.
[135**]**. Tang, W.; Matyjaszewski, K., Effect of ligand structure on activation rate constants in ATRP. *Macromolecules* **2006,** *39* (15), 4953-4959.
[136**]**. Xia, J.; Zhang, X.; Matyjaszewski, K., The effect of ligands on copper-mediated atom transfer radical polymerization. ACS Publications: 2000.
[137**]**. Ayres, N., Atom transfer radical polymerization: a robust and versatile route for polymer synthesis. *Polymer Reviews* **2011,** *51* (2), 138-162.
[138**]**. Braunecker, W. A.; Tsarevsky, N. V.; Gennaro, A.; Matyjaszewski, K., Thermodynamic components of the atom transfer radical polymerization equilibrium: quantifying solvent effects. *Macromolecules* **2009,** *42* (17), 6348-6360.
[139**]**. Horn, M.; Matyjaszewski, K., Solvent effects on the activation rate constant in atom transfer radical polymerization. *Macromolecules* **2013,** *46* (9), 3350-3357.
[140**]**. Wang, Y.; Kwak, Y.; Buback, J.; Buback, M.; Matyjaszewski, K., Determination of ATRP equilibrium constants under polymerization conditions. *ACS Macro Letters*

2012, *1* (12), 1367-1370.
[141**]**. Min, K.; Matyjaszewski, K., Atom transfer radical polymerization in aqueous dispersed media. *Open Chemistry* **2009,** *7* (4), 657-674.
[142**]**. Seeliger, F.; Matyjaszewski, K., Temperature effect on activation rate constants in ATRP: new mechanistic insights into the activation process. *Macromolecules* **2009,** *42* (16), 6050-6055.
[143**]**. Morick, J.; Buback, M.; Matyjaszewski, K., Effect of pressure on activation–deactivation equilibrium constants for ATRP of methyl methacrylate. *Macromolecular Chemistry and Physics* **2012,** *213* (21), 2287-2292.
[144**]**. Buback, M.; Morick, J., Equilibrium Constants and Activation Rate Coefficients for Atom Transfer Radical Polymerizations at Pressures up to 2 500 Bar. *Macromolecular Chemistry and Physics* **2010,** *211* (19), 2154-2161.
[145**]**. Pan, X.; Fantin, M.; Yuan, F.; Matyjaszewski, K., Externally controlled atom transfer radical polymerization. *Chemical Society Reviews* **2018,** *47* (14), 5457-5490.
[146**]**. Krys, P.; Matyjaszewski, K., Kinetics of Atom Transfer Radical Polymerization. *European Polymer Journal* **2017,** *89*, 482-523.
[147**]**. Wang, J.; Xie, X.; Xue, Z.; Fliedel, C.; Poli, R., Ligand-and solvent-free ATRP of MMA with FeBr 3 and inorganic salts. *Polymer Chemistry* **2020,** *11* (7), 1375-1385.
[148**]**. Wang, J.-S.; Matyjaszewski, K., " Living"/controlled radical polymerization. Transition-metal-catalyzed atom transfer radical polymerization in the presence of a conventional radical initiator. *Macromolecules* **1995,** *28* (22), 7572-7573.
[149**]**. Gromada, J.; Matyjaszewski, K., Simultaneous reverse and normal initiation in atom transfer radical polymerization. *Macromolecules* **2001,** *34* (22), 7664-7671.
[150**]**. Jakubowski, W.; Min, K.; Matyjaszewski, K., Activators regenerated by electron transfer for atom transfer radical polymerization of styrene. *Macromolecules* **2006,** *39* (1), 39-45.
[151**]**. Jakubowski, W.; Matyjaszewski, K., Activators regenerated by electron transfer for atom-transfer radical polymerization of (meth) acrylates and related block copolymers. *Angewandte Chemie International Edition* **2006,** *45* (27), 4482-4486.
[152**]**. Jakubowski, W.; Matyjaszewski, K., Activator generated by electron transfer for atom transfer radical polymerization. *Macromolecules* **2005,** *38* (10), 4139-4146.
[153**]**. Min, K.; Gao, H.; Matyjaszewski, K., Preparation of homopolymers and block copolymers in miniemulsion by ATRP using activators generated by electron transfer (AGET). *Journal of the American Chemical Society* **2005,** *127* (11), 3825-3830.
[154**]**. Braidi, N.; Buffagni, M.; Ghelfi, F.; Parenti, F.; Gennaro, A.; Isse, A. A.; Bedogni, E.; Bonifaci, L.; Cavalca, G.; Ferrando, A., ARGET ATRP of styrene in EtOAc/EtOH using only Na2CO3 to promote the copper catalyst regeneration. *Journal of Macromolecular Science, Part A* **2021,** *58* (6), 376-386.
[155**]**. Abreu, C. M.; Mendonça, P. V.; Serra, A. n. C.; Popov, A. V.; Matyjaszewski, K.; Guliashvili, T.; Coelho, J. F., Inorganic sulfites: Efficient reducing agents and supplemental activators for atom transfer radical polymerization. *Acs Macro Letters* **2012,** *1* (11), 1308-1311.
[156**]**. Yan, J.; Pan, X.; Wang, Z.; Lu, Z.; Wang, Y.; Liu, L.; Zhang, J.; Ho, C.; Bockstaller, M. R.; Matyjaszewski, K., A fatty acid-inspired tetherable initiator for

surface-initiated atom transfer radical polymerization. *Chemistry of Materials* **2017,** *29* (11), 4963-4969.
[157**]**. Matyjaszewski, K.; Jakubowski, W.; Min, K.; Tang, W.; Huang, J.; Braunecker, W. A.; Tsarevsky, N. V., Diminishing catalyst concentration in atom transfer radical polymerization with reducing agents. *Proceedings of the National Academy of Sciences* **2006,** *103* (42), 15309-15314.
[158**]**. Dadashi-Silab, S.; Doran, S.; Yagci, Y., Photoinduced electron transfer reactions for macromolecular syntheses. *Chemical reviews* **2016,** *116* (17), 10212-10275.
[159**]**. Chen, M.; Zhong, M.; Johnson, J. A., Light-controlled radical polymerization: mechanisms, methods, and applications. *Chemical reviews* **2016,** *116* (17), 10167-10211.
[160**]**. Chmielarz, P.; Fantin, M.; Park, S.; Isse, A. A.; Gennaro, A.; Magenau, A. J. D.; Sobkowiak, A.; Matyjaszewski, K., Electrochemically mediated atom transfer radical polymerization (*e*ATRP). *Progress in Polymer Science* **2017,** *69*, 47-78.
[161**]**. Guan, Z.; Smart, B., A remarkable visible light effect on atom-transfer radical polymerization. *Macromolecules* **2000,** *33* (18), 6904-6906.
[162**]**. Kwak, Y.; Matyjaszewski, K., Photoirradiated atom transfer radical polymerization with an alkyl dithiocarbamate at ambient temperature. *Macromolecules* **2010,** *43* (12), 5180-5183.
[163**]**. Mosnáček, J.; Ilčíková, M. t., Photochemically mediated atom transfer radical polymerization of methyl methacrylate using ppm amounts of catalyst. *Macromolecules* **2012,** *45* (15), 5859-5865.
[164**]**. Tasdelen, M. A.; Ciftci, M.; Yagci, Y., Visible light-induced atom transfer radical polymerization. *Macromolecular Chemistry and Physics* **2012,** *213* (13), 1391-1396.
[165**]**. Ciftci, M.; Tasdelen, M. A.; Yagci, Y., Sunlight induced atom transfer radical polymerization by using dimanganese decacarbonyl. *Polymer Chemistry* **2014,** *5* (2), 600-606.
[166**]**. Dadashi-Silab, S.; Atilla Tasdelen, M.; Yagci, Y., Photoinitiated atom transfer radical polymerization: Current status and future perspectives. *Journal of Polymer Science Part A: Polymer Chemistry* **2014,** *52* (20), 2878-2888.
[167**]**. Ribelli, T. G.; Konkolewicz, D.; Bernhard, S.; Matyjaszewski, K., How are radicals (re) generated in photochemical ATRP? *Journal of the American Chemical Society* **2014,** *136* (38), 13303-13312.
[168**]**. Ribelli, T. G.; Konkolewicz, D.; Pan, X.; Matyjaszewski, K., Contribution of photochemistry to activator regeneration in ATRP. *Macromolecules* **2014,** *47* (18), 6316-6321.
[169**]**. Pan, X.; Lamson, M.; Yan, J.; Matyjaszewski, K., Photoinduced metal-free atom transfer radical polymerization of acrylonitrile. *ACS Macro Letters* **2015,** *4* (2), 192-196.
[170**]**. Pan, X.; Malhotra, N.; Simakova, A.; Wang, Z.; Konkolewicz, D.; Matyjaszewski, K., Photoinduced atom transfer radical polymerization with ppm-level Cu catalyst by visible light in aqueous media. *Journal of the American Chemical Society* **2015,** *137* (49), 15430-15433.
[171**]**. Pan, X.; Fang, C.; Fantin, M.; Malhotra, N.; So, W. Y.; Peteanu, L. A.; Isse, A.

A.; Gennaro, A.; Liu, P.; Matyjaszewski, K., Mechanism of photoinduced metal-free atom transfer radical polymerization: experimental and computational studies. *Journal of the American Chemical Society* **2016,** *138* (7), 2411-2425.
[172**]**. Zhang, T.; Gieseler, D.; Jordan, R., Lights on! A significant photoenhancement effect on ATRP by ambient laboratory light. *Polymer Chemistry* **2016,** *7* (4), 775-779.
[173**]**. Kreutzer, J.; Yagci, Y., Metal free reversible-deactivation radical polymerizations: advances, challenges, and opportunities. *Polymers* **2018,** *10* (1), 35.
[174**]**. Treat, N. J.; Sprafke, H.; Kramer, J. W.; Clark, P. G.; Barton, B. E.; Read de Alaniz, J.; Fors, B. P.; Hawker, C. J., Metal-free atom transfer radical polymerization. *Journal of the American Chemical Society* **2014,** *136* (45), 16096-16101.
[175**]**. Miyake, G. M.; Theriot, J. C., Perylene as an organic photocatalyst for the radical polymerization of functionalized vinyl monomers through oxidative quenching with alkyl bromides and visible light. *Macromolecules* **2014,** *47* (23), 8255-8261.
[176**]**. Singh, V. K.; Yu, C.; Badgujar, S.; Kim, Y.; Kwon, Y.; Kim, D.; Lee, J.; Akhter, T.; Thangavel, G.; Park, L. S., Highly efficient organic photocatalysts discovered via a computer-aided-design strategy for visible-light-driven atom transfer radical polymerization. *Nature Catalysis* **2018,** *1* (10), 794-804.
[177**]**. Lim, C.-H.; Ryan, M. D.; McCarthy, B. G.; Theriot, J. C.; Sartor, S. M.; Damrauer, N. H.; Musgrave, C. B.; Miyake, G. M., Intramolecular charge transfer and ion pairing in N, N-diaryl dihydrophenazine photoredox catalysts for efficient organocatalyzed atom transfer radical polymerization. *Journal of the American Chemical Society* **2017,** *139* (1), 348-355.
[178**]**. Theriot, J. C.; Lim, C.-H.; Yang, H.; Ryan, M. D.; Musgrave, C. B.; Miyake, G. M., Organocatalyzed atom transfer radical polymerization driven by visible light. *Science* **2016,** *352* (6289), 1082-1086.
[179**]**. Wang, Z.; Pan, X.; Yan, J.; Dadashi-Silab, S.; Xie, G.; Zhang, J.; Wang, Z.; Xia, H.; Matyjaszewski, K., Temporal control in mechanically controlled atom transfer radical polymerization using low ppm of Cu catalyst. *ACS Macro Letters* **2017,** *6* (5), 546-549.
[180**]**. Wang, Z.; Wang, Z.; Pan, X.; Fu, L.; Lathwal, S.; Olszewski, M.; Yan, J.; Enciso, A. E.; Wang, Z.; Xia, H., Ultrasonication-induced aqueous atom transfer radical polymerization. *ACS Macro Letters* **2018,** *7* (3), 275-280.
[181**]**. Collins, J.; McKenzie, T. G.; Nothling, M. D.; Ashokkumar, M.; Qiao, G. G., High frequency sonoATRP of 2-hydroxyethyl acrylate in an aqueous medium. *Polymer Chemistry* **2018,** *9* (19), 2562-2568.
[182**]**. Collins, J.; McKenzie, T. G.; Nothling, M. D.; Allison-Logan, S.; Ashokkumar, M.; Qiao, G. G., Sonochemically initiated RAFT polymerization in organic solvents. *Macromolecules* **2018,** *52* (1), 185-195.
[183**]**. Mohapatra, H.; Kleiman, M.; Esser-Kahn, A. P., Mechanically controlled radical polymerization initiated by ultrasound. *Nature Chemistry* **2017,** *9* (2), 135-139.
[184**]**. Wang, Z.; Pan, X.; Li, L.; Fantin, M.; Yan, J.; Wang, Z.; Wang, Z.; Xia, H.; Matyjaszewski, K., Enhancing mechanically induced ATRP by promoting interfacial electron transfer from piezoelectric nanoparticles to Cu catalysts. *Macromolecules* **2017,** *50* (20), 7940-7948.

[185**]**. Qiu, J.; Matyjaszewski, K.; Thouin, L.; Amatore, C., Cyclic voltammetric studies of copper complexes catalyzing atom transfer radical polymerization. *Macromolecular Chemistry and Physics* **2000,** *201* (14), 1625-1631.
[186**]**. Park, S.; Chmielarz, P.; Gennaro, A.; Matyjaszewski, K., Simplified electrochemically mediated atom transfer radical polymerization using a sacrificial anode. *Angew Chem Int Ed Engl* **2015,** *54* (8), 2388-92.
[187**]**. Lorandi, F.; Fantin, M.; Isse, A. A.; Gennaro, A., Electrochemically mediated atom transfer radical polymerization of n-butyl acrylate on non-platinum cathodes. *Polymer Chemistry* **2016,** *7* (34), 5357-5365.

Chapter II

Electrochemically mediated ATRP (*e*ATRP)

2.1 General description

Thus far, the research shows that robust and versatile ATRP is one of the most successful RDRP methods for vinyl monomers in a well-controlled polymerization. As mentioned in **Chapter I,** several significant drawbacks boosted the further developments of these RDRP methods. For instance, few examples that are worth of mentioning are the negative effect of PRE in NMP and the required strict reaction conditions (high temperature, long reaction period, and the development of initiators), the complicated interplay of several mechanisms (RT, DT, and CCT) along with the

severe restriction of the organometallic complex system in the field of OMRP, and the undesired kinetic behaviors in RAFT polymerization due to the impacts of CTA structure. On the other hand, various advanced approaches of ATRP (Reverse, SR&NI, ICAR, ARGET, and SARA) were developed with the aim of avoiding starting with highly air-sensitive Cu^{I} and (or) reducing the catalyst load to ppm level. However, there are still some limitations like the difficult control of the concentration of radicals from the conventional initiator (AIBN) and strict reaction conditions (high temperature for initiator decomposition and special setup and hence complicated deoxygenation process) as well as some side products generated from the oxidization of reducing agents. Moreover, the reducing agent and its oxidation products must be removed at the end of the reaction, and this purification step increases the cost of polymer production. In particular, ATRP can be triggered by electrochemistry, light, and mechanical force with lower catalyst loadings, which allows for temporal and spatial control of the reaction.[1-9] Despite these advantages in photo-ATRP and mechono-ATRP, the use of schlenk line (SL) system with complicated and strict deoxygenation processes,[10-18] risks related with optical radiation, noise pollution, long polymerization time (over 15 h),[10-11, 18-23] low conversion (<80%),[10, 12, 17-18, 20-26] and the addition of a large amount of costly ligands (at least four-folds with respect to copper),[13, 16-17, 19, 24, 27-29] still limit large scale applications of these methods. Some of these problems arise from the long induction periods needed for the activation of the dormant species,[12, 18, 20, 27] and reactions of some intermediate species (CO_3• or Zn^{2+}), generated during the ultrasonication process, with the ligand.[13, 29] Thus, from an industrial point of view, they appear to be inappropriate for process scale-up.

Electrochemically mediated ATRP (*e*ATRP, **Scheme 2.1**) offers multiple readily adjustable parameters, e.g., applied current, potential, and total charge passed, to manipulate polymerization rate by controlling the desired concentration of activator and deactivator species at the working electrode surface.[3-4, 30] The most used *e*ATRP setup is a three-electrode cell, consisting of a working electrode (WE), a counter electrode (CE) and a reference electrode (RE). This setup allows obtaining cyclic voltammetry (CV) profile of the catalyst. CV analysis has been widely used to investigate the redox

properties and the activity of ATRP copper catalysts together with the mechanism of the cleavage of carbon-halogen bonds.[31-47]

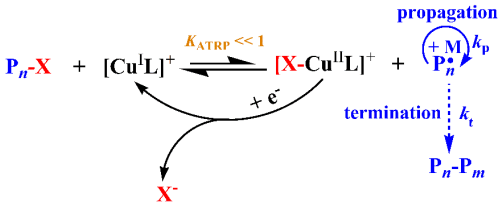

Scheme 2.1 Schematic representation of the mechanism for electrochemical control of ATRP.

In a traditional copper-catalyzed ATRP, the deactivator Cu^{II} complex coordinated with a polydentate amine ligand and a halogen ion is reduced at the working electrode to generate $[XCu^{I}L]$ when an appropriate potential (E_{app}) or current is applied. Subsequently, the reduced catalyst is dispersed throughout the bulk reaction mixture by vigorous stirring. Simultaneously, dissociation of $[XCu^{I}L]$ complex results in the formation of the activator complex $[Cu^{I}L]^+$ and free halide ions. The activator activates the dormant species (an activated alkyl halide initiator, R-X, or a macromolecule initiator with a C-X end-functionality, P_n–X) by a reductive cleavage of the C-X bond, resulting in the regeneration of the deactivator ($[XCu^{II}L]^+$) and formation of propagating radicals. The active propagating radical chains can be either reversibly deactivated back to dormant species (P_nX) by $[XCu^{II}L]^+$ or react with the monomer. Termination is limited due to the low instantaneous radical concentration. Continuous regeneration of the activator and hence the rate of polymerization (R_p, **eq. 1-3, Chapter I**) can be controlled by adjusting the E_{app}. Moreover, the $C_{Cu^{II}}/C_{Cu^{I}}$ ratio at the electrode surface is related to the Nernst equation:

$$E_{app} = E_{1/2} + \frac{RT}{nF} \ln \frac{C_{Cu^{II}}}{C_{Cu^{I}}} \quad \textbf{(2-1)}$$

Additionally, the electrolysis can be carried out under both potentiostatic conditions and galvanostatic conditions.[48-52] The galvanostatic mode is simpler than the potentiostatic one and requires a two-electrode system (WE and CE) instead of a

three-electrode setup. Various polymer architectures including homopolymers, block copolymers and star polymers have been successfully synthesized by *e*ATRP. [3-4, 53] The method was also applied for the synthesis of multi-functional polymers[4, 53-55] and in various fields such as biology,[56-62] energy storage,[63-65] electrocatalysis,[66-67] and surface modification.[54, 58, 65, 68-71]

2.2 Investigations on dynamics and parameters

Typically, a well-controlled *e*ATRP reaction mixture consists of a stable transition metal catalyst,[47, 72-75] high activity initiator,[72, 76] monomer, solvent,[48, 50, 77-81] and an electrolyte.[3] A fundamental characteristic of the system is that the deactivation rate constant (k_{deact}) is much higher than the activation rate constant (k_{act}) so that $K_{ATRP} = k_{act}/k_{deact} \ll 1$. Also, the choice of the applied potential (E_{app}) or current (I_{app}) is very important. Other factors that affect the polymerization are temperature,[3, 48, 67, 82-83] pH,[84-85] stirring rate,[52] nature of the electrode materials,[50, 52] and the ability of oxygen tolerance.[86]

2.2.1 Most relevant parameters and kinetics

2.2.1.1 Cyclic voltammetry of copper complexes

Both Cu^{I} and Cu^{II} complexes (**Scheme 2.2**) play an important role in the ATRP equilibrium and affect the polymerization rate (R_p),[30, 52] according to **eqs. 1-1 and 1-3**. Hence, the relative stability constants (β^{II}, β^{I}) of Cu^{II} and Cu^{I} amine complexes as well as the relative association constants of $[Cu^{II}L]^{2+}$ and $[Cu^{I}L]^{+}$ with halide ions (K_X^{II}, K_X^{I}) are very important parameters that can be evaluated through cyclic voltammetry.[33] Voltammetric techniques are also widely used to determine activation rate constants.[34, 78, 87-91] The standard potentials (E^{e}) of the $[Cu^{II}L]^{2+}/[Cu^{I}L]^{+}$ and $[XCu^{II}L]^{+}/[XCu^{I}L]$ couples can be estimated from cyclic voltammetry as the half-sum of cathodic and anodic peak potentials, $E^{e} \approx E_{1/2} = (E_{pc} + E_{pa})/2$, in which E_{pc} and E_{pa} represent the cathodic and anodic peak potentials,

respectively. Significantly, according to **eqs 2-2** and **2-3**, the $E_{1/2}$ values obtained from CV of copper complexes strongly depend on the nature of the ligand and of the halogen atom. As such, ligands combining with solvated copper(II) ions to form stable complexes with high β^{II} and β^{I} and low K_{ATRP} should be chosen. The standard potential of the redox couple $[XCu^{II}L]^+/[XCu^{I}L]$ relies on the relative affinity of Cu^{II} and Cu^{I} for the halide ion (halidophilicity). A high K_X^I results in high $[XCu^{I}L]$ concentration, which slows polymerization because it is inactive and must first dissociate to provide the needed binary $[Cu^{I}L]^+$ complex. Conversely, a catalyst with K_X^{II} higher than K_X^{I} is favorable for the deactivation process and boosts polymerization control. In general, K_X^{II} is much higher than K_X^{I} with a broad range of up to ~5 orders of magnitude.[33, 36, 67, 84, 92-93] Moreover, $E^{\Theta}_{XCu^{II}L/XCu^{I}L}$ increases in the following order for X: F < Cl ~ pseudo-halide < Br < I.[87, 94] The differences between the standard potentials of the redox couples Cu^{2+}/Cu^{+}, $[Cu^{II}L]^{2+}/[Cu^{I}L]^{+}$ and $[XCu^{II}L]^{+}/[XCu^{I}L]$ depend on the values of β^{II}, β^{I}, K_X^{II} and K_X^{I}, which are related to the structure of the ligand and the type of halogen atom and are affected by solvent and solvent/monomer mixtures.[3, 31-33, 36, 45, 52, 67, 72-73, 77-78, 81, 87, 95-98] TPMA and Me_6TREN are among the most used ligands as they give very stable and highly active copper complexes (**Figure 1.4**). Therefore, complexes with these ligands were chosen as the main catalysts studied in my thesis.

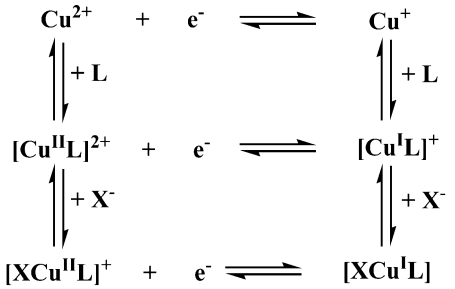

Scheme 2.2 Redox and complexation equilibria involving Cu^{II} and Cu^{I} species with amine ligands (L) and X= Cl^- or Br^-.

$$E^{\Theta}_{Cu^{II}L/Cu^{I}L} = E^{\Theta}_{Cu^{II}/Cu^{I}} + \frac{RT}{nF}\ln\frac{\beta^{I}}{\beta^{II}} \quad \textbf{(2-2)}$$

$$E^{\Theta}_{XCu^{II}L/XCu^{I}L} = E^{\Theta}_{Cu^{II}L/Cu^{I}L} + \frac{RT}{nF}\ln\frac{K^{I}}{K^{II}} \quad \textbf{(2-3)}$$

On the other hand, the catalytic activity of the copper complex has to be taken into consideration by the addition of an alkyl halide initiator to the reaction mixture containing monomer and solvent. Examples of typical voltammetric changes after initiator addition are shown for some complexes in **Figure 2.1**. The cathodic peak current increases while the anodic peak decreases in intensity and completely disappears in some cases.

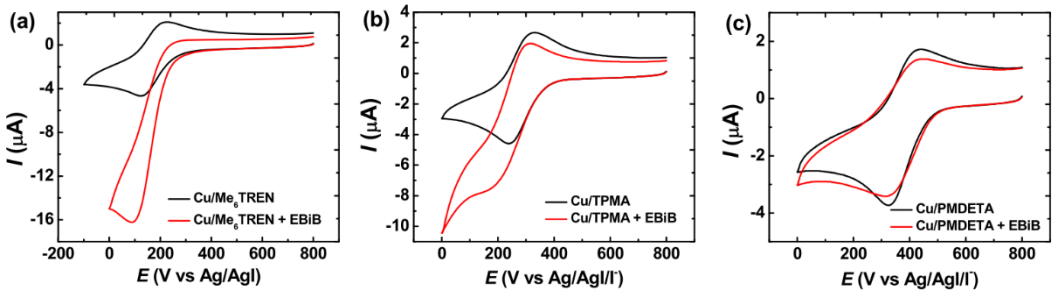

Figure 2.1 Cyclic voltammetry of $[BrCu^{II}L]^{+}$ (L = Me_6TREN **(a)**, TPMA **(b)** or PMDETA **(c)**) in the absence (black line) and presence (red line) of ethyl 2-bromoisobutyrate (EBiB) in 56% (v/v) *n*-butyl acrylate (*n*-BA) in DMF, with 0.2 M Bu_4NClO_4 as supporting electrolyte at $T = 44$ °C.[52]

The increase of the cathodic current in **Figure 2.1** can be explained by the regeneration of $[BrCu^{II}L]^{+}$ via the typical catalytic EC mechanism (an electron transfer followed by a chemical reaction).[3, 30, 99-100] The electrochemically generated $[BrCu^{I}L]$ dissociates to $[Cu^{I}L]^{+}$ and Br^{-} near the electrode surface, followed by reaction of $[Cu^{I}L]^{+}$ with the initiator RBr to give $R^{\bullet}$ and $[BrCu^{II}L]^{+}$ (**Scheme 2.3**). A portion of the $[BrCu^{II}L]^{+}$ thus regenerated returns to the electrode to be reduced again. The cathodic current is thereby enhanced, whereas the anodic current decreases, because $[BrCu^{I}L]$ is partially (or completely) lost due to chemical reactions in solution. Furthermore, the catalytic efficiency of $[BrCu^{II}L]^{+}$ can be preliminarily evaluated by the cathodic peak

current in the presence of initiator. The voltammetric pattern of $[Cu^{II}PMDETA]^{2+}$ was not modified by the addition of excess ethyl 2-bromoisobutyrate (EBiB) in the working solution, while a remarkable catalytic enhancement was observed when Me_6TREN and TPMA were used as ligands, clearly indicating that fast activation processes occur with Cu complexes of these ligands.

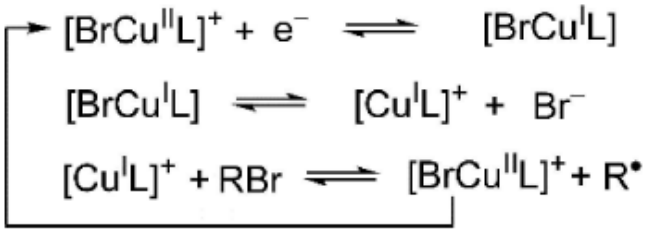

Scheme 2.3 Electrocatalytic reduction of RBr initiator by $[Cu^{I}L]^{+}$.[98]

2.2.1.2 Copper(I) disproportionation

Disproportionation or combination reactions occur not only in radical reactions [101] but also Cu^{I} species may be involved in disproportionation/comproportionation equilibria in different media.[36, 84, 102-106] Although Cu^{+} ions are capable of forming stable complexes in the presence of polyamine ligands,[33, 84] they may undergo disproportionation to generate more stable $[Cu^{II}L]^{2+}$ species. Bare Cu^{+} ions are not stable in aqueous media; they disproportionate to metallic Cu^{0} and Cu^{2+} ions (**eq. 2-4**) with a disproportionation constant $K_{disp} = 10^{6}$.[107] Disproportionation can occur also in the presence of a ligand (L) (**eq. 2-5**) albeit with a much lower disproportionation constant K^{*}_{disp} (10^{-4}~10^{2} in water).[84] Moreover, the disproportionation rate (k_{disp}) of $[Cu^{I}L]^{+}$ strongly depends on the nature of the ligand,[36, 84] solvent,[36, 102-103, 105] and pH.[84]

$$\mathbf{2\ Cu^{+} \rightleftharpoons Cu^{2+} + Cu^{0}},\ K_{disp} \qquad \textbf{(2-4)}$$

$$\mathbf{2\ [Cu^{I}L]^{+} \rightleftharpoons [Cu^{II}L]^{2+} + Cu^{0} + L},\ \boldsymbol{K_{disp}^{*}} \qquad \textbf{(2-5)}$$

Gennaro and Matyjaszewski *et al*. concluded that the disproportionation constant of $[Cu^{I}L]^{+}$ in water is much higher than in organic solvents, and activation of alkyl halides is much faster (≥ 2 orders of magnitude) than disproportionation.[36, 102-106] Typically, the disproportionation rate constant, k_{disp}, decreases by 1~2 orders of magnitude when the pH is raised from 6 to 10 in water, which is probably due to the stabilization of Cu^{I} by the formation of a hydroxide coordinated complex $[Cu^{I}L(OH)]$. **Figure 2.2 a, b** shows decay of the limiting current recorded on a rotating disk electrode for the oxidation of $[Cu^{I}TPMA]^{+}$ at pH 6 and 10, and the kinetic analysis of the data for k_{disp} determination. However, disproportionation is kinetically minimized during polymerization. This is due to a drastic lowering of $[Cu^{I}L]^{+}$ concentration by the activation reaction, resulting in a dramatic drop of disproportionation rate. These findings confirm that also in aqueous media, ATRP in the presence of metallic copper proceeds through SARA ATRP, not SET-LRP (Single Electron Transfer-Living Radical Polymerization).[105-106] Similar results were also found for $[Cu^{I}L]^{+}$ in DMSO and DMSO/MA: disproportionation is always in competition with RX activation by $[Cu^{I}L]^{+}$, but the latter is always much favored and the ratio between activation and disproportion rates ($\upsilon_{act}/\upsilon_{disp}$) exceeds 10^2 (**Figure 2.2 c**).[36]

Apart from the type of solvent and pH in water, the nature of the ligand also shows a remarkable influence on k_{disp}. In the case of the ligands TPMA, Me_6TREN and PMDETA, K_{disp} increases in the order TPMA < Me_6TREN < PMDETA. The disproportionation appears to be negligible for $[Cu^{I}TPMA]^{+}$ in contrast to $[Cu^{I}PMDETA]^{+}$ which is highly unstable, undergoing rapid disproportionation to Cu^{II} and Cu^{0}. Also $[Cu^{I}Me_6TREN]^{+}$ has a relatively high disproportionation rate constant although its K_{disp} is not very high. **Figure 2.2 d** presents a visual observation of the disproportionation of $[Cu^{I}Me_6TREN]^{+}$ in water. A purple-red-colored Cu^{0} precipitate was obtained after 1 h when 0.5 mmol of CuBr were mixed with 0.5 mmol of Me_6TREN in 5 mL of water.[104]

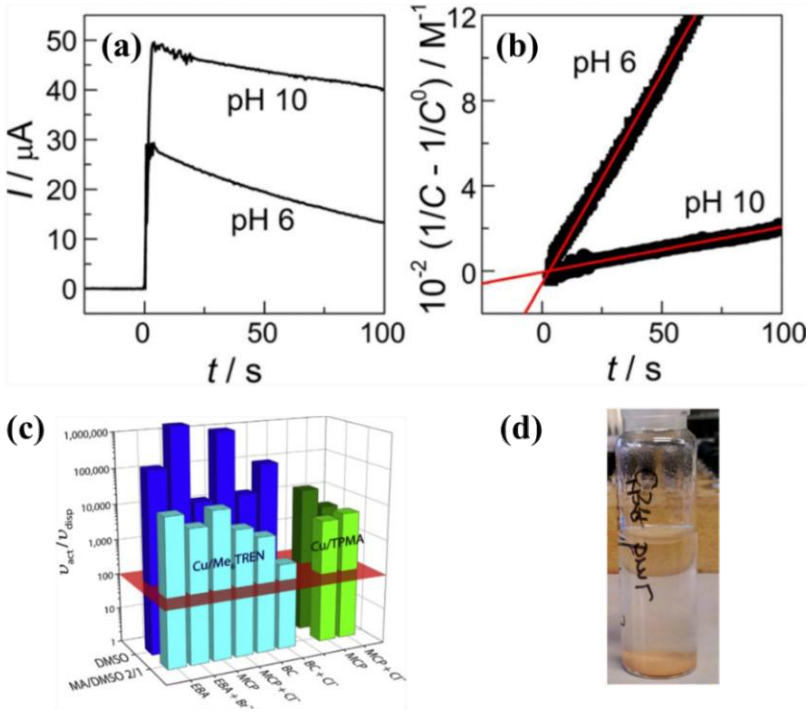

Figure 2.2 (a) Decay of the limiting current of $[Cu^{I}TPMA]^{+}$ oxidation at $E = -0.2$ V vs SCE with time, recorded in H_2O + 0.1 M Et_4NBF_4 on a RDE; $C^0_{[Cu^{I}TPMA]^{+}} = 0.5$ mM at pH 6, $C^0_{[Cu^{I}TPMA]^{+}} = 1$ mM at pH 10; **(b)** Regression analysis of the data.[84] **(c)** $\upsilon_{act}/\upsilon_{disp}$ ratio for various complex/ligand combinations in DMSO and methyl acrylate/DMSO (2/1, v/v).[36] **(d)** Visual observation of the disproportionation of CuBr/Me_6TREN (0.5 mmol each) in 5 mL of H_2O.[104]

Disproportionation is one of the main side reactions in aqueous ATRP and might be in severe competition with the activation reaction. Therefore, for a good catalytic system, both the selected initiator and the dormant species formed during polymerization should have activation rate constants (k_{act}) that are much higher than the disproportionation rate constant (k_{disp}) of Cu(I).

2.2.1.3 Determination of activation and deactivation rate constants and ATRP equilibrium constant

The equilibrium constant of ATRP, K_{ATRP}, is defined by the ratio between the rate constants of activation, k_{act}, and deactivation, k_{deact}, $K_{ATRP} = k_{act}/k_{deact}$. These constants

are affected by many factors including the nature of the catalyst,[72] initiator, solvent,[77] the monomer/solvent ratio, temperature[108] and pressure[109]. A substantial body of work has been done to accurately determine such constants for various catalyst/initiator systems via diverse approaches based on electrochemistry, gas-chromatography, HPLC, NMR, EPR, and UV-Vis spectroscopy.[3, 37, 72, 76, 90, 110-115] Among them, voltammetric techniques proved to be very convenient and versatile and have been widely used for the determination of K_{ATRP} and k_{act} due to the required small amount of reactants, and the highly accurate values determined in a short time. k_{deact} was determined by independently measuring k_{act} and K_{ATRP}.

The activation process of an alkyl halide initiator, which involves the breaking of the C-X bond through Inner Sphere Electron Transfer or Atom Transfer (ISET-AT) pathway,[7, 46, 96] results in the formation of a radical and the metal complex at a higher oxidation state. To make the ATRP activation reaction kinetically irreversible, a good radical scavenger such as 2,2,6,6-tetramethylpiperidine-1-oxyl (TEMPO) must be added in a large excess with respect to $[Cu^{I}L]^{+}$. In these conditions, the deactivation reaction is outrun by reaction of the radical with TEMPO and the activation step becomes the rate-determining step of the whole process (**Scheme 2.4**).

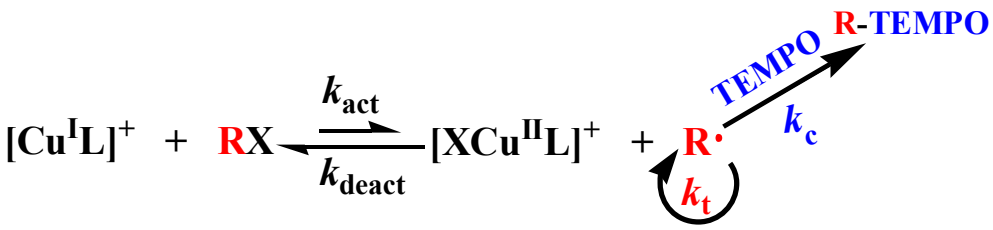

Scheme 2.4 Mechanism of RX reduction by $[Cu^{I}L]^{+}$ in the presence of TEMPO.

A wide variety of reliable electrochemical methods of k_{act} determination have recently been developed. Chronoamperometry on a rotating disk electrode (RDE) was employed to determine k_{act} in various solvents through monitoring the current decay versus time for the oxidation of $[Cu^{I}L]^{+}$ at an appropriate constant applied potential E_{app}, (**Figure 2.3 a, b**). If the reaction is performed in the presence of a large excess of RX over $[Cu^{I}L]^{+}$, the data can be analyzed according to a pseudo-first order rate law (**eq.**

2-6). This method enabled to measure k_{act} values in the range from 10^{-3} to 10^{3} M^{-1} s^{-1} and was applied in organic solvents,[34, 88, 90-91, 99, 116] water,[78] and ionic liquid[117] as well as in various solvent/monomer mixtures.[36, 77, 89]

$$\ln \frac{C^0_{[Cu^I]^+}}{C_{[Cu^I]^+}} = k_{act}[RX]_0 \qquad (2\text{-}6)$$

Cyclic voltammetry was used to study fast activation reactions with $k_{act} > 5\times10^3$ M^{-1} s^{-1}. Homogeneous redox catalysis (HRC) occurs when $[XCu^{II}L]^+$ is reduced in the presence of RX and TEMPO.[78, 118] A series of voltammograms of the catalyst are recorded in the presence of TEMPO before and after addition of RX at different concentrations. The degree of catalysis, defined as the ratio between the peak currents measured before ($I_{pc,0}$) and after (I_{pc}) the addition of RX, i.e., $I_{pc}/I_{pc,0}$, is related to a dimensionless kinetic parameter λ, defined by **eq. 2-7**.[3, 78, 87, 119]

$$\lambda = \frac{R\,T\,k_{act}C_{cat}}{F\,v} \qquad (2\text{-}7)$$

$I_{pc}/I_{pc,0}$, depends also on the ratio between the concentrations of RX and catalyst, known as the excess factor, γ = [RX]/[catalyst], as shown in **Figure 2.3 c, d**. The activation rate constant is determined by fitting of the experimental data of $I_{pc}/I_{pc,0}$ as a function of scan rate and excess factor. This method was used to determine k_{act} values spanning from 10^1 to 10^6 M^{-1} s^{-1} in acetonitrile and in aqueous media.

On the other hand, if the activation of RX by $[Cu^IL]^+$ is extremely fast, a special voltammetric pattern with splitting of the cathodic peak into an irreversible pre-peak and the usual peak couple of the catalyst is observed. This situation is known as total catalysis and the potential of the pre-peak is given by **eq. 2-8**.[78]

$$E_p = E^{\Theta}_{[Cu^{II}L]^{2+}/[Cu^{I}L]^{+}} - 0.409\frac{RT}{F} + \frac{RT}{2F}\ln\left(\frac{RT(C_{[Cu^{II}L]^{2+}}}{vC_{RX}}k_{act}\right)^2 \qquad (2\text{-}8)$$

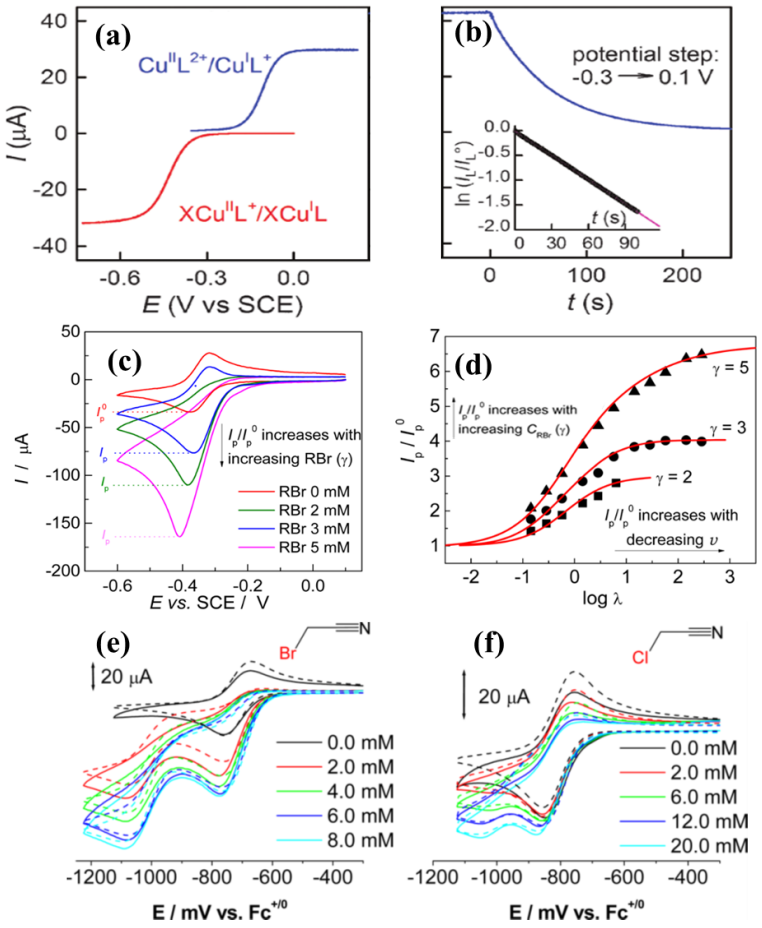

Figure 2.3 (a) Voltammograms for the oxidation of 1 mM $[Cu^{I}L]^{+}$ and reduction of 1 mM $[ClCu^{II}L]^{+}$ in MeCN + 0.1 M Et_4NBF_4 at a rotating disc electrode at $\upsilon = 5$ mVs^{-1} and $\omega = 2500$ rpm. **(b)** Chronoamperometry of 1 mM $[Cu^{I}L]^{+}$ in the presence of 20 mM $PhCH_2Cl$ and 10 mM TEMPO; inset: kinetic analysis according to a pseudo-first-order rate law.[34] **(c)** Background subtracted CVs of 10^{-3} M $[Cu^{II}TPMA]^{2+}$ in H_2O + 0.1 M Et_4NBF_4, recorded at a glassy carbon electrode in the absence and presence of oligo(ethylene oxide) 2-bromopropionate (OEOBP) at different concentrations at $\upsilon =$ 0.5 Vs^{-1}. **(d)** Fitting of the experimental values of $I_p/I_{p,0}$ (black squares) on the theoretical curves (red lines), for the system $[Cu^{II}TPMA]^{2+}$/OEOBP in water with 10^{-3} M $[Cu^{II}L]^{2+}$ at various γ ratios.[78] Cyclic voltammetry of 1.0 mM $[BrCu^{II}TPMA]Br$ in the presence of bromoacetonitrile **(e)** or chloroacetonitrile **(f)** + 0.1 M Et_4NClO_4 in MeCN at 25 °C. Solid curves are the experimental data and broken lines the simulated data.[37]

In this case, k_{act} can be calculated directly from **eq. 2-8** by using E_p values measured at various concentrations of RX and/or scan rates. For instance, for the activation of 2-hydroxyethyl 2-bromoisobutyrate (HEBiB) by $[Cu^{I}Me_6TREN]^+$ in water, a rate constant as high as 2.6×10^7 M^{-1} s^{-1} was measured under total catalysis conditions.[78]

Besides these electrochemical methods, k_{act} of both slow and fast ATRP systems was determined by digital simulations of CV.[37, 78, 90-91, 99, 120-121] It was successfully applied to various systems, such as $[Cu^{II}TPMA]^{2+}$ + HEBiB and $[Cu^{II}TPMA]^{2+}$ + OEOBP in water. Interestingly, it was found that the presence of the monomer negatively affects k_{act} in water much more than it does in polar organic solvents (such as DMSO or DMF).

Cyclic voltammetry with digital simulation was also used to investigate the formation of organometallic species $[R{-}Cu^{II}L]^+$ (**eq. 2-9**) in ATRP.[37, 120-121] The presence of this species was observed via spectroscopic and electrochemical techniques, **(Figure 2.3 e, f)**, showing that its role in ATRP depends on the structure of the initiator and catalyst, and the nature of the solvent. Interestingly, the rate constants obtained from the simulation indicated that the formation of the organometallic species is very fast ($1.6 \sim 3.6 \times 10^7$ $M^{-1}s^{-1}$), whereas its dissociation is much slower. This method allows determination of k_{act}, regardless of whether the system allows formation of an organometallic species or not, by simply working in the presence of a radical scavenger such as TEMPO so that the radicals are quantitively trapped before they react with $[Cu^{I}L]^+$ to generate the organometallic complex.

$$[Cu^{I}L]^+ + R\cdot \rightleftharpoons [RCu^{II}L]^+ \qquad (2\text{-}9)$$

Conversely, the accurate measurement of k_{deact} is usually difficult because the rate of the deactivation reaction approaches the diffusion-controlled limit ($k_{deact} \approx 10^7{-}10^8$ M^{-1} s^{-1}) and the radical $R^{\bullet}$ cannot be isolated nor its concentration can be quantified in situ due to the termination side reactions. Bernhardt's group determined the rate constants of some deactivation reactions by cyclic voltammetry combined with digital

simulation.[90, 120] First, the determination of k_{act} was done through recording the voltammetric pattern of a copper catalyst + RX in the presence of TEMPO in DMSO or MeCN, coupled with digital simulation. Subsequently, the same experiment was repeated in the absence of TEMPO and simulated by using the just calculated k_{act}, while refining the k_{deact} value ($0.86 \sim 1.8 \times 10^8$ M^{-1} s^{-1}).

It is worth noting that k_{deact} in DMSO is ~2 orders of magnitude lower than that in MeCN.[72] Besides k_{act} and k_{deact}, the determination of K_{ATRP} can also be achieved by digital simulation of CV or by chronoamperometry at a rotating disk electrode with data analysis according to modified Fischer's equations for the persistent radical effect.[37, 90, 110, 122-123] Determination of reliable K_{ATRP} values requires measurement in the absence of halide ions to avoid the formation of inactive Cu^I species such as $[Cu^IX_2]^-$ and $[XCu^IL]$. K_{ATRP} values in pure solvents or solvent/monomer mixtures spanning in a wide range of $10^{-9} \sim 1$ were obtained.

2.2.1.4 Applied potential or current

Electrochemical polymerization was carried out in a three-electrode setup and strictly controlled by applied electrochemical parameters, such as potential and current, which were selected based on the electrochemical properties of the used catalyst. Conventionally, the divided electrochemical cell is composed mainly of a big area platinum (Pt) WE, a separated Pt CE, and a RE. In some cases, the divided cell can be changed to a simplified undivided cell by replacing the expensive Pt electrode with a sacrificial Al anode.[48-50, 124-125] According to **eq. 1-3**, the polymerization rate (R_p) is directly proportional to the ratio between the concentrations of $[Cu^IL]^+$ and $[XCu^{II}L]^+$ in solution, which can be modulated through the applied overpotential, η ($\eta = E_{app} - E_{1/2}$). An example of the effect of η on the current passing through the electrodes is presented in **Figure 2.4 a** for *e*ATRP of *n*-butyl acrylate (*n*-BA) catalyzed by $[BrCu^{II}TPMA]^+$.[52] Upon addition of EBiB, both the CV and LSV patterns presented an amplified cathodic current, which is consistent with a catalytic mechanism. Polymerization was started by applying a fixed potential (E_{app}) close to or more

negative than $E_{1/2}$ and as shown in **Figure 2.4 b**, the lower the applied overpotential (more negative η), the higher the polymerization rate. A linear increase of M_n and good control with low dispersity were always obtained (**Figure 2.4 c)**. In general, the lower the E_{app}, the larger the initial current and the faster the reduction rate and hence the polymerization rate. This is because a more negative η establishes a lower $C_{Cu^{II}}/C_{Cu^{I}}$ ratio, which enhances the rate of activation on one side, while it decreases the rate of deactivation on the other side. However, once a sufficiently negative η (< -0.125 V) is applied, the rate of $[BrCu^{II}TPMA]^+$ reduction becomes limited by mass transport. Under such conditions, R_p becomes independent of η and is not further enhanced. In addition, the total consumed charge can be used to estimate the extent of radical–radical termination during *e*ATRP.[51, 85, 126-127] Regardless of the applied potential, fast decay of the current was observed in the early stages of polymerization under potentiostatic mode of electrolysis.

The decrease of the current suggested the possibility of a galvanostatic process using at least two current steps chosen on account of the mean current recorded during a potentiostatic experiment. The RE can be eliminated when a galvanostatic mode is used, and therefore, *e*ATRP can be conducted using a simplified two-electrode system (**Figure 2.4 d**). In order to carry out a galvanostatic *e*ATRP, appropriate current values must be selected, which can be rationalized from previously conducted potentiostatic experiments. Initially, Magenau *et al*. and Park *et al*. utilized a two-stage current program (**Figure 2.4 e**) to rapidly convert the vast majority of $[BrCu^{II}L]^+$ to $[Cu^{I}L]^+$,[49, 52] trigging *e*ATRP. The length of the constant current step is somewhat critical. When the applied current values were maintained for long periods, the effective potential of the working electrode drifted to more negative potentials, leading to the appearance of a purple-red copper deposit on the WE, as the insert photograph in **Figure 2.4 d** shows. To improve polymerization control and avoid undesirable Cu deposition, a multi-step current procedure was developed and applied to the reaction mixture (**Figure 2.4 f**).

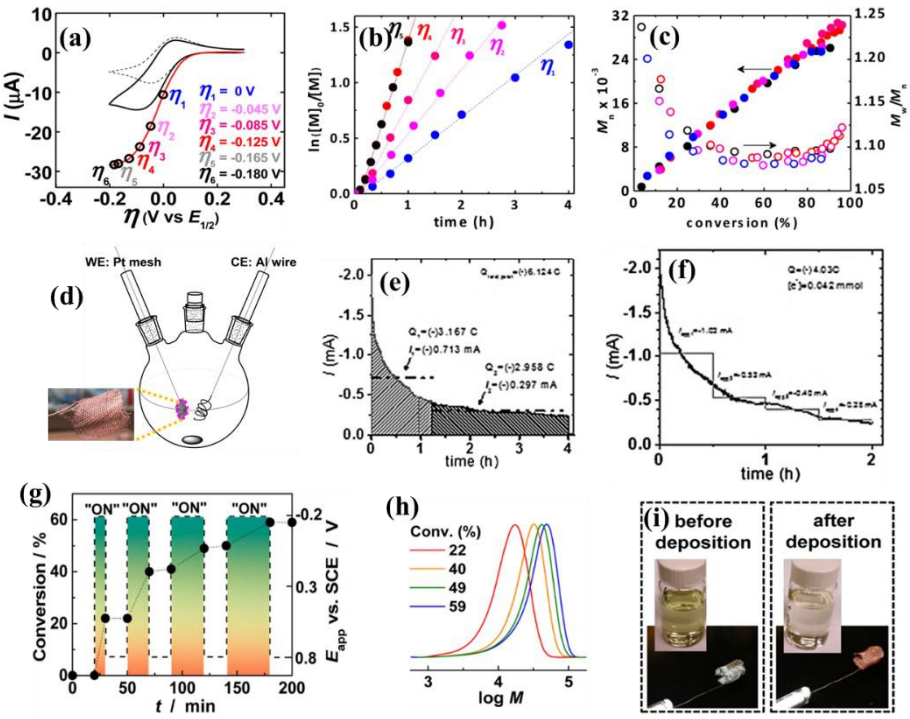

Figure 2.4 (a) Voltammetry of $[BrCu^{II}TPMA]^+$ in the absence (dotted line) and presence of excess EBiB without stirring (black solid line) or under vigorous stirring (solid red line), recorded at 0.05 V s^{-1}. Circles indicate E_{app}, expressed as $\eta = E_{app} - E_{1/2}$, used in *e*ATRP experiments. **(b)** Effect of the E_{app} on the first-order plots of polymerization rate, **(c)** M_n and M_w/M_n versus conversion. Reaction conditions: $[BA]/[EBiB]/[BrCu^{II}TPMA]^+ = 300/1/0.09$, $[Bu_4NClO_4] = 0.2$ M, [BA]=3.9 M in DMF, T= 44 °C, V_{tot} = 23 mL, and ω = 875 rpm.[52] **(d)** Galvanostatic *se*ATRP set up; the insert graph is copper deposited on a Pt mesh WE. **(e)** Chronoamperometry recorded during a potentiostatic *e*ATRP; the dotted lines indicate the applied current values chosen for a galvanostatic two-stage *e*ATRP and **(f)** chronoamperometry for a potentiostatic *e*ATRP showing the values of applied current to be used in a multi-step galvanostatic *se*ATRP.[49] **(g-h)** *e*ATRP of 10% MAA (v/v) in water at pH = 0.9 and T =25 °C, $MAA/RX/CuCl_2/TPMA/NaCl = 200/1/0.1/0.4/29$: **(g)** Variation of conversion (full circles) and applied potential (dashed lines) with time during *e*ATRP of MAA (no potential was applied in the first 20 min); **(h)** Evolution of MW with monomer conversion, after each step at E_{app} = −0.2 V vs SCE.[85] **(i)** Images of crude polymerization mixture and Pt working electrode, before and after copper deposition.[52]

Temporal control of polymerization was achieved by switching η from negative to sufficiently positive values (**Figure 2.4 g**).[85] Application of a positive overpotential caused rapid oxidation of $[Cu^{I}L]^{+}$ to $[Cu^{II}L]^{2+}$, which quickly stopped the polymerization. Complete reinitiation was achieved after switching again η to a negative value, confirming the preservation of dormant ATRP chain ends. *e*ATRP allowed very accurate temporal control, as the example of *e*ATRP of 10% MAA (v/v) in water in **Figure 2.4 g, h** demosntrates.[85] Without application of an oxidation potential, polymerization would slowly decelerate due to radical termination and not due to the direct oxidation of the catalyst. All chains were effectively reinitiated after each "ON" step, proving the livingness of the process. On the other hand, another advantage of *e*ATRP is the possibility of catalyst removal at the end of the polymerization through applying a sufficiently negative potential to further reduce Cu^{I} to Cu^{0}, as seen in **Figure 2.4 i**.[52] All Cu was eventually deposited on the cathode. Subsequently, the catalyst was regenerated by anodic stripping of Cu^{0} in the presence of the ligand.

2.2.1.5 Others relevant aspects of *e*ATRP

The polymerization rate can be roughly adjusted by the $C_{[Cu^{I}L]^{+}}/C_{[XCu^{II}L]^{+}}$ ratio as shown in **eq. 1-3**, which is controlled by the applied potential. In addition, Magenau *et al*. systemically evaluated the effects of various factors on *e*ATRP.[52] For example, the nature of the catalyst complex has a great influence on the ATRP equilibrium constant K_{ATRP}, and further affects R_P if various catalysts are compared by applying a fixed value of η. As such, with reference to **Figure 2.5 a**, the rate of polymerization rate decreases in the order Me_6TREN > TPMA > PMDETA, which matches the order of reactivity of $[Cu^{I}L]^{+}$ with RX.[91] The dispersity depends on the applied potential. A clear evidence of the effect of E_{app} on the dispersity is shown in **Figure 2.5 b** for PMDETA. When a less negative potential was applied, the amount of deactivator $[XCu^{II}L]^{+}$ was relatively increased and thus the dispersity decreased. Based on **eq. 1-4**, polymer dispersity is inversely proportional to the concentration of $[XCu^{II}L]^{+}$.

Therefore, as expected, increasing the deactivator concentration induced a slight decrease of R_p and a remarkable improvement of $Đ$, especially at high monomer conversion (**Figure 2.5 c, d**).[52] In the *e*ATRP of *n*-BA in DMF, a homogeneous polymer with designed molecular weight and narrow distribution was obtained even in the presence of ppm level of $[BrCu^{II}TPMA]^+$.[3, 7, 127-129]

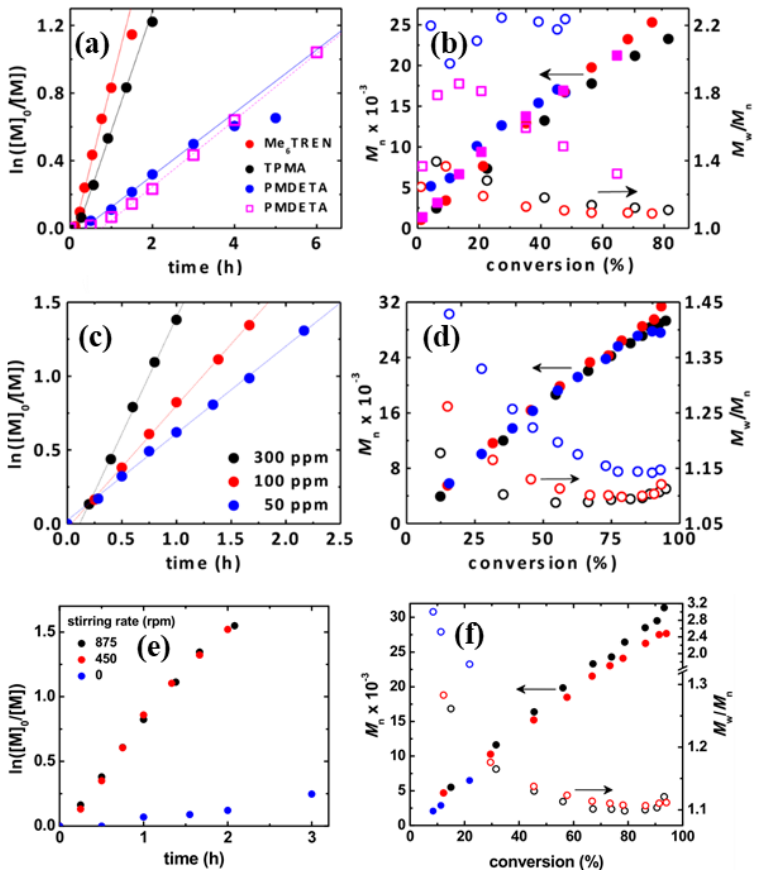

Figure 2.5 First-order kinetic plots **(a, c, e)** and evolution of M_n and M_w/M_n versus conversion **(b, d, f)** under various conditions: *n*-BA/EBiB/$Cu(OTf)_2$/L/TBABr = 300/1/*x*/0.03/0.03 in DMF + 0.2 M Bu_4NClO_4 at T = 45 °C; **(a, b)** L = Me_6TREN, TPMA, and PMDETA, η = −0.180 V, x = 0.03 (circles) or η = −0.125 V, x = 0.09 (squares); **(c, d)** L = TPMA, η = −0.125 V, x = 0.09, 0.03, and 0.015; **(e, f)** L = TPMA, η = −0.125 V, x = 0.03.[52]

Additionally, since reduction of the catalyst occurs only on the WE surface, vigorous stirring is necessary to maintain a fixed $C_{[Cu^{I}L]^+}/C_{[XCu^{II}L]^+}$ ratio and homogeneous distribution of the activator as well as deactivator species in the working

solution during polymerization (**Figure 2.5 e, f**).[52] Moreover, stirring can also prevent the deposition of the growing chains at the WE surface, especially, when an insoluble polymer is generated in the solution (e.g. the polymerization of *n*-BA in DMSO).[130] The influence of the distance between WE and CE on the $C_{[Cu^{I}L]^{+}}/C_{[XCu^{II}L]^{+}}$ ratio control should be considered as well, in particular, for the preparation of polymeric surfaces through surface-initiated *e*ATRP (SI- *e*ATRP).[69, 131]

The choice of the solvent also plays a crucial role in *e*ATRP; in general, K_{ATRP} in aqueous solutions is much higher than in commonly used organic solvents such as DMSO, DMF, and MeCN.[3, 77-78, 83-84, 127, 132] The polymerization in DMSO is faster in comparison to reactions conducted in DMF and MeCN because of higher K_{ATRP} in this solvent with respect to the others.[7, 36, 53, 91, 93, 96, 133] In aqueous solutions, the stability of the catalyst is sensitive to pH changes because of amine ligand protonation at low pH and coordination of hydroxide ions to the copper catalyst at high pH.[3, 84-85, 132, 134] As the catalyst is prone to ligand protonation, dissociation of the complex and Cu^{I} disproportionation can occur, leading to inefficient ATRP catalysis. On the other hand, high K_{ATRP} provides high concentration of radicals, which enhances the possibility of radical termination reactions. Therefore, a small overpotential must be applied to suppress these negative aspects and harness a well-controlled polymerization. Additionally, *e*ATRP in non-conventional media such as miniemulsions and ionic liquids has also been developed, especially for nonpolar monomers.[3-4, 51, 80-81, 117, 135-136]

Polymerization of acrylic or methacrylic acids is one of the biggest challenges for ATRP due to the side reaction of intramolecular cyclization, which leads to the loss of the C-X chain-end functionality.[7, 85, 137] In addition, chain extension from terminal halogen functionalized polymers (for example, acrylate and/or methacrylate based block copolymers) composed of less active monomers with a more active monomer is significantly affected by the low initiation efficiency of the macroinitiator.[98, 136, 138] The solution to the problem in both of these situations involves, among various other expedients, switching of the chain-end halogen from C–Br to C–Cl because of the higher affinity of Cu^{II} for Cl^{-} than Br^{-} and the lower reactivity of C-Cl than C-Br.[7, 85,

[98, 127, 136-139] The kinetic mismatch observed in some co-polymerizations was overcome by using high concentrations of $CuCl_2$/L during chain extension. More recently, a method known as catalytic halogen exchange (cHE) that does not need high catalyst concentration was reported. [98, 136] Chain extensions with more active monomers were successfully achieved by using low concentration of $[Cu^{II}L]^{2+}$ (≤ 1 mM) with excess Cl^- high enough to convert all the starting Br-capped macronitiator (P_n–Br) to P_n-Cl.

*e*ATRP is also affected by the temperature and supporting electrolyte.[3, 108, 140-142] Reaction temperature was found to have an important effect in aqueous ATRP, especially for *N*,*N*-dimethylacrylamide (DMA) polymerization.[140-141, 143-144] *e*ATRP is also affected by the supporting electrolyte. A decrease in the rate of polymerization was noted when the concentration of supporting electrolyte was decreased in potentiostatic *e*ATRP, which can be explained as a consequence of an increased solution resistance. In addition, the use of chloride or bromide salts acting as both electrolyte and halide source was adopted in aqueous media to increase the concentration of the deactivator $[XCu^{II}L]^+$.[3, 33, 84-85, 145]

2.3 Simplified *e*ATRP (*se*ATRP): setup and principal features

The vast majority of ATRP experiments are performed in a schlenk line (SL) system, with safety and several other issues that have been previously described.[146-147] A substantial body of work was performed to develop more efficient ATRP methods that avoid the use of air-sensitive low oxidation state catalyst through the application of external physical stimuli; even metal-free methods and some approaches aimed to improve the oxygen tolerance of the process have been developed.

Figure 2.6 represents the traditional three-electrode setup used for both the electrochemical characterization of the catalytic system and the *e*ATRP process. The *e*ATRP reaction setup consists of a five-neck jacketed flask equipped with a magnetic stirring element, inert gas purging system, and a water jacket temperature control system. The flask necks are fitted with a RE (e.g., Ag|AgX/X^- for organic solvents and saturated calomel electrode (SCE) for aqueous solutions), a WE (e.g., a Pt mesh or a

glassy carbon (GC) disc), a CE (e.g., a Pt gauze or plate), an inlet/outlet port for degassing, and an inlet/outlet port for samples and reagents. For all CV measurements, in general, a Pt or GC electrode can be used as the WE, while separation of the CE is not strictly necessary. For polymerization, a Pt mesh with a big area is used as WE, whereas the CE is a Pt mesh or a graphite rod separated from the working solution through a glass frit filled with a conductive solution and a methylcellulose gel, saturated with an adequate electrolyte.

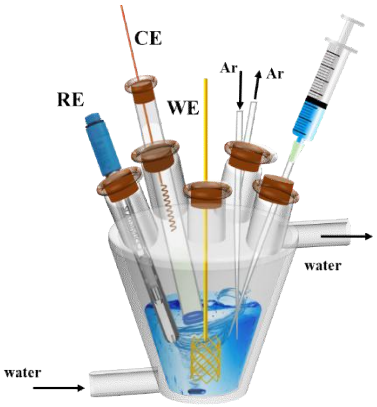

Figure 2.6 A conventional *e*ATRP setup and reactor

2.3.1 *se*ATRP using a sacrificial counter electrode

Several modifications and simplifications of the *e*ATRP setup from the original three-electrode setup have been developed for partial removal of the noble Pt electrodes. Park *et al*. reported that the two-compartment reactor can be simplified by using a sacrificial Al anode, termed as simplified *e*ATRP (*se*ATRP).[49] *se*ATRP does not require the separation of cathodic and anodic compartments, and the Al electrode can be directly inserted into the reaction mixture. Furthermore, the ohmic drop caused by the separation between anodic and cathodic compartments is avoided, bringing a beneficial energy saving.[3, 48, 50, 133] Therefore, the anodic dissolution becomes the oxidation of the electrode itself, which releases Al^{3+} ions into the solution. It has been reported that the effects of Al^{3+} on the catalyst stability and polymerization control could be neglected when $CuBr_2$/TPMA (1/2 or 1/1 of molar ratio) was used as a catalyst for the synthesis of diverse topology polymers in DMF and miniemulsion, such as

homopolymers, copolymers, block polymers, star polymers, and polymer brushes via *se*ATRP or SI-ATRP.[22, 49, 54, 71, 124-125, 129, 133, 135, 148-160] The polymerizations carried out in an undivided cell showed linear increase of MW with conversion and low $Đ$ throughout the reactions just as *e*ATRP in conventional, divided three-electrode cells. Nevertheless, an excess of ligand was required when Me_6TREN was used; with this ligand, a severe competition between Al^{3+} ions and copper ions occurs during electrolysis in DMF or DMSO.[48, 133] Galvanostatic *e*ATRP was also investigated in an undivided cell by a multistep current procedure, chosen on the basis of a chronoamperometry recorded during a potentiostatic *e*ATRP on Pt.[48-49, 55, 124-125, 129, 150-151, 153-155, 157-158]

Despite great achievements were obtained on process optimization, limited attention was devoted to investigations on the mechanism of action of Al^{3+} in the polymerization medium and its impact on the stability and performance of copper-based ATRP catalysts in organic media. In addition, besides using excess ligand, efficient and cost-effective approaches for eliminating or avoiding the competition phenomenon need to be explored.

2.3.2 *se*ATRP using non platinum electrodes

Extremely expensive and rare Pt material, as shown in **Table 2.1**, is often used as both cathode and anode in *e*ATRP because of its good electronic conduction and chemical inertness. However, this electrode material acts only as an electron carrier for catalyst reduction and is not directly involved in the polymerization process. Therefore, Pt can be replaced by any other cost-effective material, such as Al (**Table 2.1**), who is a good conductor and stable in the electrochemical potential window of interest for the *e*ATRP process. In order to achieve complete removal of Pt from the two-compartment cell, because this type of setup with expensive electrode materials is not appealing for industrial implementation of *e*ATRP, many efforts have been made in aqueous solutions, DMF, or DMSO.[48, 50, 133] Au, glassy carbon (GC), Ti, Ni, NiCr (80/20, wt%) alloy, and 304 stainless steel (SS304) were examined as cathodes in aqueous *e*ATRP of OEOMA

with $[Cu^{II}TPMA]^{2+}$.[50] The results show a good performance by Au and GC, both in terms of monomer conversion and polymer weight distribution, whereas an initial induction period was observed with Ti, NiCr alloy and SS304, during which no appreciable polymerization occurred. This induction period was attributed to the presence of a passivating oxide layer on the surfaces of such materials. Indeed, no induction period was observed when a pre-electrolysis of $[XCu^{II}L]^{+}$ was applied to generate the activator and concurrently clean the electrode surface by removal of surface oxides.

Table 2.1 The market information comparison between Al and Platinum wires

Companies	Alfa Aesar		Sigma-Aldrich	
Products	Al wire	Platinum wire	Al wire	Platinum wire
Specification (metals basis)	1.0 mm, 99+%, 250 m	0.5 mm, 99.95%, 100 cm	1.0 mm, 99.5%, 10 m	0.5 mm, 99.9%, 4 g
Price	~ 0.5 €/g	~195.25 €/g	~ 7.0 €/g	~ 320 €/g

* The data are taken from the websites of Alfa Aesar and Sigma-Aldrich companies.

Aqueous *e*ATRP with non-noble metal cathodes were investigated also in an undivided cell with a sacrificial Al anode in the presence of a 2-fold excess of TPMA with respect to Cu^{2+}, thus totally removing Pt from the system. The competition between Al^{3+} and Cu^{2+} or Cu^{+} for the TPMA ligand can possibly hamper polymerization, compared to the same synthesis in a divided cell with separated anodic and cathodic compartments. However, a detailed explanation of the phenomenon was not provided in that study.[50]

Furthermore, various cathode materials including Pt, GC, Fe, Au, SS304, and NiCr alloy were investigated for the polymerization of *n*-BA in DMF with $[BrCuMe_6TREN]^{+}$ complex as well.[48] WE materials were effectively cleaned by a series of procedures including both physical and chemical methods with the aim of removing oxide layers from the surface and avoid any induction period during polymerization. Finally, with 1 mM $Cu(OTf)_2$ and a two-fold excess (2 mM) of Me_6TREN, well-controlled polymerizations were obtained in an undivided cell with a sacrificial Al anode under

both potentiostatic and galvanostatic conditions. Conversely, when the same *e*ATRP experiment was performed in an undivided cell with an Al anode but without excess Me_6TREN (1 mM), polymerization was slow and stopped after 68% conversion. In addition, a purple-red deposit on the working electrode was observed at the end of the experiment. This clearly indicated decomposition of the Cu complex with the formation of a metallic copper deposit as a consequence of a competition between Al^{3+} ions and Cu^{2+} and Cu^{+} ions for Me_6TREN. These competitive equilibria were also confirmed by drastic changes of the voltammetric pattern of the Cu complex in the presence of Al^{3+} generated from the electrolysis of Al in situ in bulk solution. When 1 mM Al^{3+} was added to a 1 mM solution of $[Cu^{II}Me_6TREN]^{2+}$, the peak couple of the Cu complex lost reversibility showing only a cathodic peak with significantly reduced current intensity. Clearly, the concentration of $[Cu^{II}Me_6TREN]^{2+}$ decreased after Al^{3+} addition, while the reduced complex $[Cu^{I}Me_6TREN]^{+}$ became unstable. However, the original voltametric pattern of $[Cu^{II}Me_6TREN]^{2+}$ was almost recovered by further addition of excess ligand.

Well-controlled *se*ATRP polymerizations of various monomers such as *n*-butyl acrylate (*n*-BA), methyl methacrylate (MMA) and styrene (S) were also achieved with copper catalysts in an SS304 reactor in which the scaffold of the cell acted as a cathode in combination with a sacrificial Al anode.[133] In detail, a 2-fold excess of ligand (i.e., TPMA, Me_6TREN, and TREN) over $CuBr_2$ was used for galvanostatic *se*ATRP of *n*-BA, MMA, and S in DMF or ethanol in order to suppress the effect of Al^{3+} ions on the stability of Cu catalysts. Notwithstanding such achievements, the various possible competitions occurring in the presence of Al^{3+} in each solvent were not deeply investigated. What is certain, however, is that release of metal ions from the SS304 WE into the polymerization solution was negligible in all tested solvents.

These studies have shown that inexpensive electrode materials can be used in a simplified *e*ATRP in an undivided cell with the possibility of scale-up, especially if a galvanostatic mode is employed. It is important to note that the selected electrode material should be stable (e.g., no corrosion) and inert with a wide electrochemical potential window. Furthermore, it should not directly activate C–X bonds. In addition, problems like surface passivation, induction period, low monomer conversion, and

slow polymerization rate must also be considered and overcome. Summarily, these achievements represent a significant step toward the scale-up and the commercialization of this polymerization technique even though some further improvements are required.

2.4 Aim of this thesis

Based on these investigations about simplified electrochemically mediated ATRP above, the aim of this work is to systematically uncover the mechanism of interference of Al^{3+} ions generated by anodic dissolution of a sacrificial Al anode on copper catalysts with two widely used ligands, TPMA and Me_6TREN, in different media including organic solvents and aqueous solutions. Electrochemical methods (cyclic voltammetry (CV), linear sweep voltammetry (LSV), chronoamperometry (CA), etc.) were used as principal tools of investigation, corroborated by UV-Vis-NIR spectroscopy and some other characterization techniques. Possible methods of solving the competition issues were also investigated, in order to make *se*ATRP a cost-effective, environmentally friendly process more appealing for scale-up applications in the industrial field. Thus, the research project of the thesis addressed the following points.

Firstly, this work was to mainly investigate: i) the interactions between Al^{3+} ions generated from the electrolysis of Al and ligands (TPMA and Me_6TREN); ii) the influence of metallic Al on the stability of free solvated Cu^{2+} ions and copper complexes used as catalysts; iii) the influence of Al^{3+} on the stability of $[Cu^{II}L]^{2+}$ and $[Cu^{I}L]^{+}$; iv) the $[BrCu^{II}L]^{+}$ stability and Al^{3+} effect in typical ATRP conditions; v) the potentiostatic *e*ATRP of *n*-BA in three selected organic media (DMF, DMSO, and MeCN) in divided and undivided cells; vi) the possible solutions for eliminating the competition between Al^{3+} and copper ions for the amine ligand.

In addition, the simplified *e*ATRP setup was investigated also in aqueous solutions. The various issues that were investigated include: i) the interactions between Al^{3+} generated from the electrolysis of Al and ligands (TPMA and Me_6TREN); ii) the influence of anodic dissolution of Al process on the stability of free solvated Cu^{2+} ions

and copper complexes, and on solution pH; iii) the simulation of only pH effects on the catalyst stability in typical ATRP conditions and the effects of only Al^{3+} ions on catalyst stability in buffered typical ATRP mixtures; iv) kinetic investigations of the reaction of activated Al with Cu^{2+} and $[Cu^{II}L]^{2+}$ species; v) potentiostatic *e*ATRP of OEOMA and DMA in divided and undivided cells in water; vi) possible solutions to the problem of the competition between Al^{3+} and copper ions for the ligand.

Finally, instead of adding expensive ligands in excess, other cost-effective approaches were evaluated to suppress or eliminate the negative effects of Al^{3+} ions during polymerization in both organic solvents and aqueous solutions by the addition of inorganic sodium salts containing different anions. Before using these salts in *se*ATRP, the influences of the anions on the stability of copper catalysts were investigated in different media.

References

[1**]**. Chen, M.; Zhong, M.; Johnson, J. A., Light-controlled radical polymerization: mechanisms, methods, and applications. *Chemical reviews* **2016,** *116* (17), 10167-10211.
[2**]**. Dadashi-Silab, S.; Doran, S.; Yagci, Y., Photoinduced electron transfer reactions for macromolecular syntheses. *Chemical reviews* **2016,** *116* (17), 10212-10275.
[3**]**. Chmielarz, P.; Fantin, M.; Park, S.; Isse, A. A.; Gennaro, A.; Magenau, A. J. D.; Sobkowiak, A.; Matyjaszewski, K., Electrochemically mediated atom transfer radical polymerization (*e*ATRP). *Progress in Polymer Science* **2017,** *69*, 47-78.
[4**]**. Matyjaszewski, K., Advanced Materials by Atom Transfer Radical Polymerization. *Adv Mater* **2018,** *30* (23), e1706441.
[5**]**. Corrigan, N.; Jung, K.; Moad, G.; Hawker, C. J.; Matyjaszewski, K.; Boyer, C., Reversible-deactivation radical polymerization (Controlled/living radical polymerization): From discovery to materials design and applications. *Progress in Polymer Science* **2020**, 101311.
[6**]**. Parkatzidis, K.; Wang, H. S.; Truong, N. P.; Anastasaki, A., Recent developments and future challenges in controlled radical polymerization: a 2020 update. *Chem* **2020**.
[7**]**. Isse, A. A.; Gennaro, A., Electrochemistry for Atom Transfer Radical Polymerization. *The Chemical Record* **2021**.
[8**]**. Zaborniak, I.; Chmielarz, P., Ultrasound-Mediated Atom Transfer Radical Polymerization (ATRP). *Materials (Basel)* **2019,** *12* (21).
[9**]**. Pan, X.; Tasdelen, M. A.; Laun, J.; Junkers, T.; Yagci, Y.; Matyjaszewski, K., Photomediated controlled radical polymerization. *Progress in Polymer Science* **2016,** *62*, 73-125.
[10**]**. Konkolewicz, D.; Schröder, K.; Buback, J.; Bernhard, S.; Matyjaszewski, K., Visible Light and Sunlight Photoinduced ATRP with ppm of Cu Catalyst. *ACS Macro Letters* **2012,** *1* (10), 1219-1223.
[11**]**. McKenzie, T. G.; Wong, E. H. H.; Fu, Q.; Sulistio, A.; Dunstan, D. E.; Qiao, G. G., Controlled Formation of Star Polymer Nanoparticles via Visible Light Photopolymerization. *ACS Macro Letters* **2015,** *4* (9), 1012-1016.
[12**]**. Pan, X.; Lamson, M.; Yan, J.; Matyjaszewski, K., Photoinduced Metal-Free Atom Transfer Radical Polymerization of Acrylonitrile. *ACS Macro Letters* **2015,** *4* (2), 192-196.
[13**]**. Wang, Z.; Pan, X.; Li, L.; Fantin, M.; Yan, J.; Wang, Z.; Wang, Z.; Xia, H.; Matyjaszewski, K., Enhancing Mechanically Induced ATRP by Promoting Interfacial Electron Transfer from Piezoelectric Nanoparticles to Cu Catalysts. *Macromolecules* **2017,** *50* (20), 7940-7948.
[14**]**. Wang, Z.; Pan, X.; Yan, J.; Dadashi-Silab, S.; Xie, G.; Zhang, J.; Wang, Z.; Xia, H.; Matyjaszewski, K., Temporal control in mechanically controlled atom transfer radical polymerization using low ppm of Cu catalyst. *ACS Macro Letters* **2017,** *6* (5), 546-549.

[15**]**. Wang, Z.; Wang, Z.; Pan, X.; Fu, L.; Lathwal, S.; Olszewski, M.; Yan, J.; Enciso, A. E.; Wang, Z.; Xia, H., Ultrasonication-induced aqueous atom transfer radical polymerization. *ACS Macro Letters* **2018,** *7* (3), 275-280.
[16**]**. Dadashi-Silab, S.; Lorandi, F.; DiTucci, M. J.; Sun, M.; Szczepaniak, G.; Liu, T.; Matyjaszewski, K., Conjugated Cross-linked Phenothiazines as Green or Red Light Heterogeneous Photocatalysts for Copper-Catalyzed Atom Transfer Radical Polymerization. *J Am Chem Soc* **2021,** *143* (25), 9630-9638.
[17**]**. Hao, Q.; Qiao, L.; Shi, G.; He, Y.; Cui, Z.; Fu, P.; Liu, M.; Qiao, X.; Pang, X., Effect of nitrogen type on carbon dot photocatalysts for visible-light-induced atom transfer radical polymerization. *Polymer Chemistry* **2021,** *12* (20), 3060-3066.
[18**]**. Pan, X.; Malhotra, N.; Zhang, J.; Matyjaszewski, K., Photoinduced Fe-based atom transfer radical polymerization in the absence of additional ligands, reducing agents, and radical initiators. *Macromolecules* **2015,** *48* (19), 6948-6954.
[19**]**. Kutahya, C.; Schmitz, C.; Strehmel, V.; Yagci, Y.; Strehmel, B., Near-Infrared Sensitized Photoinduced Atom-Transfer Radical Polymerization (ATRP) with a Copper(II) Catalyst Concentration in the ppm Range. *Angew Chem Int Ed Engl* **2018,** *57* (26), 7898-7902.
[20**]**. Dadashi-Silab, S.; Pan, X.; Matyjaszewski, K., Photoinduced Iron-Catalyzed Atom Transfer Radical Polymerization with ppm Levels of Iron Catalyst under Blue Light Irradiation. *Macromolecules* **2017,** *50* (20), 7967-7977.
[21**]**. Zaborniak, I.; Chmielarz, P., Temporally Controlled Ultrasonication-Mediated Atom Transfer Radical Polymerization in Miniemulsion. *Macromolecular Chemistry and Physics* **2019,** *220* (17), 1900285.
[22**]**. Zaborniak, I.; Surmacz, K.; Chmielarz, P., Synthesis of sugar-based macromolecules via sono-ATRP in miniemulsion. *Polymers for Advanced Technologies* **2020,** *31* (9), 1972-1979.
[23**]**. Pan, X.; Malhotra, N.; Dadashi-Silab, S.; Matyjaszewski, K., A simplified Fe-based photoATRP using only monomers and solvent. *Macromolecular rapid communications* **2017,** *38* (13), 1600651.
[24**]**. Kütahya, C.; Wang, P.; Li, S.; Liu, S.; Li, J.; Chen, Z.; Strehmel, B., Carbon dots as a promising green photocatalyst for free radical and ATRP-based radical photopolymerization with blue LEDs. *Angewandte Chemie International Edition* **2020,** *59* (8), 3166-3171.
[25**]**. Ni, B.; Wang, D.; Zhang, H.; Li, P.; Niu, T., Visible Light Controlled Polymerization of Azide-Derived Monomers: A Facile, Metal-Free PET-ATRP Route to Construct Azide Polymers. *Macromolecular Chemistry and Physics* **2019,** *220* (7), 1800529.
[26**]**. Zhou, M.-J.; He, F.; Wu, H.; Wang, G.-X.; Liu, L.-C.; Xu, W., Photo-induced ATRP of MMA without ligands in ionic liquid. *Iranian Polymer Journal* **2017,** *26* (3), 205-211.
[27**]**. Yan, W.; Dadashi-Silab, S.; Matyjaszewski, K.; Spencer, N. D.; Benetti, E. M., Surface-Initiated Photoinduced ATRP: Mechanism, Oxygen Tolerance, and Temporal Control during the Synthesis of Polymer Brushes. *Macromolecules* **2020,** *53* (8), 2801-2810.

[28]. Rolland, M.; Whitfield, R.; Messmer, D.; Parkatzidis, K.; Truong, N. P.; Anastasaki, A., Effect of Polymerization Components on Oxygen-Tolerant Photo-ATRP. *ACS Macro Letters* **2019,** *8* (12), 1546-1551.
[29]. Wang, Z.; Lorandi, F.; Fantin, M.; Wang, Z.; Yan, J.; Wang, Z.; Xia, H.; Matyjaszewski, K., Atom Transfer Radical Polymerization Enabled by Sonochemically Labile Cu-carbonate Species. *ACS Macro Letters* **2019,** *8* (2), 161-165.
[30]. Magenau, A. J.; Strandwitz, N. C.; Gennaro, A.; Matyjaszewski, K., Electrochemically mediated atom transfer radical polymerization. *Science* **2011,** *332* (6025), 81-4.
[31]. Navon, N.; Golub, G.; Cohen, H.; Paoletti, P.; Valtancoli, B.; Bencini, A.; Meyerstein, D., Design of Ligands That Stabilize Cu(I) and Shift the Reduction Potential of the Cu(II/I) Couple Cathodically in Aqueous Solutions. *Inorg Chem* **1999,** *38* (15), 3484-3488.
[32]. Ambundo, E. A.; Deydier, M.-V.; Grall, A. J.; Aguera-Vega, N.; Dressel, L. T.; Cooper, T. H.; Heeg, M. J.; Ochrymowycz, L. A.; Rorabacher, D. B., Influence of Coordination Geometry upon Copper(II/I) Redox Potentials. Physical Parameters for Twelve Copper Tripodal Ligand Complexes. *Inorganic Chemistry* **1999,** *38* (19), 4233-4242.
[33]. Bortolamei, N.; Isse, A. A.; Di Marco, V. B.; Gennaro, A.; Matyjaszewski, K., Thermodynamic Properties of Copper Complexes Used as Catalysts in Atom Transfer Radical Polymerization. *Macromolecules* **2010,** *43* (22), 9257-9267.
[34]. De Paoli, P.; Isse, A. A.; Bortolamei, N.; Gennaro, A., New insights into the mechanism of activation of atom transfer radical polymerization by Cu (I) complexes. *Chemical Communications* **2011,** *47* (12), 3580-3582.
[35]. Arnaboldi, S.; Gennaro, A.; Isse, A. A.; Mussini, P. R., The solvent effect on the electrocatalytic cleavage of carbon-halogen bonds on Ag and Au. *Electrochimica Acta* **2015,** *158*, 427-436.
[36]. Lorandi, F.; Fantin, M.; Isse, A. A.; Gennaro, A., RDRP in the presence of Cu0: The fate of Cu (I) proves the inconsistency of SET-LRP mechanism. *Polymer* **2015,** *72*, 238-245.
[37]. Zerk, T. J.; Bernhardt, P. V., Organo-Copper(II) Complexes as Products of Radical Atom Transfer. *Inorg Chem* **2017,** *56* (10), 5784-5792.
[38]. Isse, A. A.; Falciola, L.; Mussini, P. R.; Gennaro, A., Relevance of electron transfer mechanism in electrocatalysis: the reduction of organic halides at silver electrodes. *Chemical communications* **2006,** (3), 344-346.
[39]. Isse, A. A.; De Giusti, A.; Gennaro, A.; Falciola, L.; Mussini, P. R., Electrochemical reduction of benzyl halides at a silver electrode. *Electrochimica acta* **2006,** *51* (23), 4956-4964.
[40]. Isse, A. A.; Gottardello, S.; Durante, C.; Gennaro, A., Dissociative electron transfer to organic chlorides: electrocatalysis at metal cathodes. *Physical Chemistry Chemical Physics* **2008,** *10* (17), 2409-2416.
[41]. Isse, A. A.; Mussini, P. R.; Gennaro, A., New insights into electrocatalysis and dissociative electron transfer mechanisms: the case of aromatic bromides. *The Journal of Physical Chemistry C* **2009,** *113* (33), 14983-14992.

[42**]**. Gennaro, A.; Isse, A. A.; Bianchi, C. L.; Mussini, P. R.; Rossi, M., Is glassy carbon a really inert electrode material for the reduction of carbon–halogen bonds? *Electrochemistry communications* **2009,** *11* (10), 1932-1935.
[43**]**. Isse, A. A.; Berzi, G.; Falciola, L.; Rossi, M.; Mussini, P. R.; Gennaro, A., Electrocatalysis and electron transfer mechanisms in the reduction of organic halides at Ag. *Journal of Applied Electrochemistry* **2009,** *39* (11), 2217-2225.
[44**]**. Bortolamei, N.; Isse, A. A.; Gennaro, A., Estimation of standard reduction potentials of alkyl radicals involved in atom transfer radical polymerization. *Electrochimica acta* **2010,** *55* (27), 8312-8318.
[45**]**. Isse, A. A.; Lin, C. Y.; Coote, M. L.; Gennaro, A., Estimation of standard reduction potentials of halogen atoms and alkyl halides. *The Journal of Physical Chemistry B* **2011,** *115* (4), 678-684.
[46**]**. Isse, A. A.; Gennaro, A.; Lin, C. Y.; Hodgson, J. L.; Coote, M. L.; Guliashvili, T., Mechanism of carbon-halogen bond reductive cleavage in activated alkyl halide initiators relevant to living radical polymerization: theoretical and experimental study. *J Am Chem Soc* **2011,** *133* (16), 6254-64.
[47**]**. Isse, A. A.; Visona, G.; Ghelfi, F.; Roncaglia, F.; Gennaro, A., Electrochemical Approach to Copper-Catalyzed Reversed Atom Transfer Radical Cyclization. *Advanced Synthesis & Catalysis* **2015,** *357* (4), 782-792.
[48**]**. Lorandi, F.; Fantin, M.; Isse, A. A.; Gennaro, A., Electrochemically mediated atom transfer radical polymerization of n-butyl acrylate on non-platinum cathodes. *Polymer Chemistry* **2016,** *7* (34), 5357-5365.
[49**]**. Park, S.; Chmielarz, P.; Gennaro, A.; Matyjaszewski, K., Simplified electrochemically mediated atom transfer radical polymerization using a sacrificial anode. *Angew Chem Int Ed Engl* **2015,** *54* (8), 2388-92.
[50**]**. Fantin, M.; Lorandi, F.; Isse, A. A.; Gennaro, A., Sustainable Electrochemically-Mediated Atom Transfer Radical Polymerization with Inexpensive Non-Platinum Electrodes. *Macromol Rapid Commun* **2016,** *37* (16), 1318-22.
[51**]**. Fantin, M.; Chmielarz, P.; Wang, Y.; Lorandi, F.; Isse, A. A.; Gennaro, A.; Matyjaszewski, K., Harnessing the interaction between surfactant and hydrophilic catalyst to control *e*ATRP in miniemulsion. *Macromolecules* **2017,** *50* (9), 3726-2732.
[52**]**. Magenau, A. J. D.; Bortolamei, N.; Frick, E.; Park, S.; Gennaro, A.; Matyjaszewski, K., Investigation of Electrochemically Mediated Atom Transfer Radical Polymerization. *Macromolecules* **2013,** *46* (11), 4346-4353.
[53**]**. Matyjaszewski, K.; Tsarevsky, N. V., Macromolecular engineering by atom transfer radical polymerization. *J Am Chem Soc* **2014,** *136* (18), 6513-33.
[54**]**. Chmielarz, P.; Yan, J.; Krys, P.; Wang, Y.; Wang, Z.; Bockstaller, M. R.; Matyjaszewski, K., Synthesis of Nanoparticle Copolymer Brushes via Surface-Initiated *se*ATRP. *Macromolecules* **2017,** *50* (11), 4151-4159.
[55**]**. Chmielarz, P., Synthesis of pyridoxine-based eagle-shaped asymmetric star polymers through *se*ATRP. *Polymers for Advanced Technologies* **2017,** *28* (12), 1787-1793.
[56**]**. Hu, Y.; Yang, G.; Liang, B.; Fang, L.; Ma, G.; Zhu, Q.; Chen, S.; Ye, X., The fabrication of superlow protein absorption zwitterionic coating by electrochemically

mediated atom transfer radical polymerization and its application. *Acta Biomaterialia* **2015,** *13*, 142-149.
[57**]**. Hu, Q.; Wang, Q.; Sun, G.; Kong, J.; Zhang, X., Electrochemically Mediated Surface-Initiated de Novo Growth of Polymers for Amplified Electrochemical Detection of DNA. *Analytical Chemistry* **2017,** *89* (17), 9253-9259.
[58**]**. Ran, F.; Wang, Z.; Yang, Y.; Liu, Z.; Kong, L.; Kang, L., Nano vanadium nitride incorporated onto interconnected porous carbon via the method of surface-initiated electrochemical mediated ATRP and heat-treatment approach for supercapacitors. *Electrochimica Acta* **2017,** *258*, 405-413.
[59**]**. Hu, Q.; Wang, Q.; Jiang, C.; Zhang, J.; Kong, J.; Zhang, X., Electrochemically mediated polymerization for highly sensitive detection of protein kinase activity. *Biosensors and Bioelectronics* **2018,** *110*, 52-57.
[60**]**. Hu, Q.; Wang, Q.; Kong, J.; Li, L.; Zhang, X., Electrochemically mediated in situ growth of electroactive polymers for highly sensitive detection of double-stranded DNA without sequence-preference. *Biosensors and Bioelectronics* **2018,** *101*, 1-6.
[61**]**. Liu, Q.; Ma, K.; Wen, D.; Wang, Q.; Sun, H.; Liu, Q.; Kong, J., Electrochemically mediated ATRP (*e*ATRP) amplification for ultrasensitive detection of glucose. *Journal of Electroanalytical Chemistry* **2018,** *823*, 20-25.
[62**]**. Li, D.; Ahmed, M.; Khan, A.; Xu, L.; Walters, A. A.; Ballesteros, B.; Al-Jamal, K. T., Tailoring the Architecture of Cationic Polymer Brush-Modified Carbon Nanotubes for Efficient siRNA Delivery in Cancer Immunotherapy. *ACS Applied Materials & Interfaces* **2021**.
[63**]**. Manthiram, A.; Yu, X.; Wang, S., Lithium battery chemistries enabled by solid-state electrolytes. *Nature Reviews Materials* **2017,** *2* (4), 1-16.
[64**]**. Wang, X.; Kerr, R.; Chen, F.; Goujon, N.; Pringle, J. M.; Mecerreyes, D.; Forsyth, M.; Howlett, P. C., Toward high-energy-density lithium metal batteries: opportunities and challenges for solid organic electrolytes. *Advanced Materials* **2020,** *32* (18), 1905219.
[65**]**. Ran, F.; Wu, J.; Niu, X.; Li, D.; Nie, C.; Wang, R.; Zhao, W.; Zhang, W.; Chen, Y.; Zhao, C., A new approach for membrane modification based on electrochemically mediated living polymerization and self-assembly of N-tert-butyl amide- and β-cyclodextrin-involved macromolecules for blood purification. *Materials Science and Engineering: C* **2019,** *95*, 122-133.
[66**]**. Perazzolo, V.; Daniel, G.; Brandiele, R.; Picelli, L.; Rizzi, G. A.; Isse, A. A.; Durante, C., PEO-b-PS Block Copolymer Templated Mesoporous Carbons: A Comparative Study of Nitrogen and Sulfur Doping in the Oxygen Reduction Reaction to Hydrogen Peroxide. *Chemistry–A European Journal* **2021,** *27* (3), 1002-1014.
[67**]**. Trevisanello, E.; De Bon, F.; Daniel, G.; Lorandi, F.; Durante, C.; Isse, A. A.; Gennaro, A., Electrochemically mediated atom transfer radical polymerization of acrylonitrile and poly(acrylonitrile-b-butyl acrylate) copolymer as a precursor for N-doped mesoporous carbons. *Electrochimica Acta* **2018,** *285*, 344-354.
[68**]**. Li, B.; Yu, B.; Huck, W. T.; Zhou, F.; Liu, W., Electrochemically induced surface-initiated atom-transfer radical polymerization. *Angewandte Chemie International Edition* **2012,** *51* (21), 5092-5095.

[69**]**. Yan, J.; Li, B.; Yu, B.; Huck, W. T.; Liu, W.; Zhou, F., Controlled polymer-brush growth from microliter volumes using sacrificial-anode atom-transfer radical polymerization. *Angew Chem Int Ed Engl* **2013,** *52* (35), 9125-9.
[70**]**. Shida, N.; Koizumi, Y.; Nishiyama, H.; Tomita, I.; Inagi, S., Electrochemically Mediated Atom Transfer Radical Polymerization from a Substrate Surface Manipulated by Bipolar Electrolysis: Fabrication of Gradient and Patterned Polymer Brushes. *Angewandte Chemie International Edition* **2015,** *54* (13), 3922-3926.
[71**]**. Chmielarz, P.; Krys, P.; Wang, Z.; Wang, Y.; Matyjaszewski, K., Synthesis of Well-Defined Polymer Brushes from Silicon Wafers via Surface-Initiated *se*ATRP. *Macromolecular Chemistry and Physics* **2017,** *218* (11), 1700106.
[72**]**. Tang, W.; Kwak, Y.; Braunecker, W.; Tsarevsky, N. V.; Coote, M. L.; Matyjaszewski, K., Understanding atom transfer radical polymerization: effect of ligand and initiator structures on the equilibrium constants. *Journal of the American Chemical Society* **2008,** *130* (32), 10702-10713.
[73**]**. Tang, W.; Matyjaszewski, K., Effect of ligand structure on activation rate constants in ATRP. *Macromolecules* **2006,** *39* (15), 4953-4959.
[74**]**. Guo, J. K.; Zhou, Y. N.; Luo, Z. H., Kinetic Insights into the Iron-Based Electrochemically Mediated Atom Transfer Radical Polymerization of Methyl Methacrylate. *Macromolecules* **2016,** *49* (11), 4038-4046.
[75**]**. Guo, J.-K.; Zhou, Y.-N.; Luo, Z.-H., Kinetic insights into the iron-based electrochemically mediated atom transfer radical polymerization of methyl methacrylate. *Macromolecules* **2016,** *49* (11), 4038-4046.
[76**]**. Tang, W.; Matyjaszewski, K., Effects of initiator structure on activation rate constants in ATRP. *Macromolecules* **2007,** *40* (6), 1858-1863.
[77**]**. Horn, M.; Matyjaszewski, K., Solvent effects on the activation rate constant in atom transfer radical polymerization. *Macromolecules* **2013,** *46* (9), 3350-3357.
[78**]**. Fantin, M.; Isse, A. A.; Matyjaszewski, K.; Gennaro, A., ATRP in Water: Kinetic Analysis of Active and Super-Active Catalysts for Enhanced Polymerization Control. *Macromolecules* **2017,** *50* (7), 2696-2705.
[79**]**. Lorandi, F.; Fantin, M.; Isse, A. A.; Gennaro, A., Electrochemical triggering and control of atom transfer radical polymerization. *Current Opinion in Electrochemistry* **2018,** *8*, 1-7.
[80**]**. Guo, J.-K.; Zhou, Y.-N.; Luo, Z.-H., Electrochemically mediated ATRP process intensified by ionic liquid: A “flash” polymerization of methyl acrylate. *Chemical Engineering Journal* **2019,** *372*, 163-170.
[81**]**. Fantin, M.; Park, S.; Wang, Y.; Matyjaszewski, K., Electrochemical atom transfer radical polymerization in miniemulsion with a dual catalytic system. *Macromolecules* **2016,** *49* (23), 8838-8847.
[82**]**. Tsarevsky, N. V.; Sumerlin, B. S., *Fundamentals of controlled/living radical polymerization*. Royal Society of Chemistry: 2013.
[83**]**. De Bon, F.; Marenzi, S.; Isse, A. A.; Durante, C.; Gennaro, A., Electrochemically Mediated Aqueous Atom Transfer Radical Polymerization of N, N-Dimethylacrylamide. *ChemElectroChem* **2020,** *7* (6), 1378-1388.
[84**]**. Fantin, M.; Isse, A. A.; Gennaro, A.; Matyjaszewski, K., Understanding the

Fundamentals of Aqueous ATRP and Defining Conditions for Better Control. *Macromolecules* **2015,** *48* (19), 6862-6875.
[85**]**. Fantin, M.; Isse, A. A.; Venzo, A.; Gennaro, A.; Matyjaszewski, K., Atom Transfer Radical Polymerization of Methacrylic Acid: A Won Challenge. *J Am Chem Soc* **2016,** *138* (23), 7216-9.
[86**]**. Yeow, J.; Chapman, R.; Gormley, A. J.; Boyer, C., Up in the air: oxygen tolerance in controlled/living radical polymerisation. *Chemical Society Reviews* **2018,** *47* (12), 4357-4387.
[87**]**. Lorandi, F.; Fantin, M.; De Bon, F.; Isse, A. A.; Gennaro, A., Electrochemical Procedures To Determine Thermodynamic and Kinetic Parameters of Atom Transfer Radical Polymerization. In *Reversible Deactivation Radical Polymerization: Mechanisms and Synthetic Methodologies*, ACS Publications: 2018; pp 161-189.
[88**]**. Isse, A. A.; Bortolamei, N.; De Paoli, P.; Gennaro, A., On the mechanism of activation of copper-catalyzed atom transfer radical polymerization. *Electrochimica Acta* **2013,** *110*, 655-662.
[89**]**. Peng, C.-H.; Zhong, M.; Wang, Y.; Kwak, Y.; Zhang, Y.; Zhu, W.; Tonge, M.; Buback, J.; Park, S.; Krys, P., Reversible-deactivation radical polymerization in the presence of metallic copper. Activation of alkyl halides by Cu0. *Macromolecules* **2013,** *46* (10), 3803-3815.
[90**]**. Zerk, T. J.; Bernhardt, P. V., New method for exploring deactivation kinetics in copper-catalyzed atom-transfer-radical reactions. *Inorg Chem* **2014,** *53* (21), 11351-3.
[91**]**. Fantin, M.; Isse, A. A.; Bortolamei, N.; Matyjaszewski, K.; Gennaro, A., Electrochemical approaches to the determination of rate constants for the activation step in atom transfer radical polymerization. *Electrochimica Acta* **2016,** *222*, 393-401.
[92**]**. Golub, G.; Lashaz, A.; Cohen, H.; Paoletti, P.; Bencini, A.; Valtancoli, B.; Meyerstein, D., The effect of N-methylation of tetra-aza-alkane copper complexes on the axial binding of anions. *Inorganica chimica acta* **1997,** *255* (1), 111-115.
[93**]**. Luo, J.; Durante, C.; Gennaro, A.; Isse, A. A., Electrochemical study of the effect of Al3+ on the stability and performance of Cu-based ATRP catalysts in organic media. *Electrochimica Acta* **2021,** *388*, 138589.
[94**]**. Lanzalaco, S.; Fantin, M.; Scialdone, O.; Galia, A.; Isse, A. A.; Gennaro, A.; Matyjaszewski, K., Atom transfer radical polymerization with different halides (F, Cl, Br, and I): is the process "living" in the presence of fluorinated initiators? *Macromolecules* **2017,** *50* (1), 192-202.
[95**]**. Min, K.; Matyjaszewski, K., Atom transfer radical polymerization in aqueous dispersed media. *Open Chemistry* **2009,** *7* (4), 657-674.
[96**]**. Matyjaszewski, K., Atom transfer radical polymerization (ATRP): current status and future perspectives. *Macromolecules* **2012,** *45* (10), 4015-4039.
[97**]**. Isse, A. A.; Lorandi, F.; Gennaro, A., Electrochemical approaches for better understanding of atom transfer radical polymerization. *Current Opinion in Electrochemistry* **2019,** *15*, 50-57.
[98**]**. De Bon, F.; Isse, A. A.; Gennaro, A., Electrochemically Mediated Atom Transfer Radical Polymerization of Methyl Methacrylate: The Importance of Catalytic Halogen Exchange. *ChemElectroChem* **2019,** *6* (16), 4257-4265.

[99**]**. Bell, C. A.; Bernhardt, P. V.; Monteiro, M. J., A rapid electrochemical method for determining rate coefficients for copper-catalyzed polymerizations. *J Am Chem Soc* **2011,** *133* (31), 11944-7.
[100**]**. Bard, A. J.; Faulkner, L. R., Electrochemical Methods, 2nd ed. *John Wiley & Sons: New York* **2001**.
[101**]**. Ribelli, T. G.; Augustine, K. F.; Fantin, M.; Krys, P.; Poli, R.; Matyjaszewski, K., Disproportionation or combination? The termination of acrylate radicals in ATRP. *Macromolecules* **2017,** *50* (20), 7920-7929.
[102**]**. Harrisson, S.; Couvreur, P.; Nicolas, J., Comproportionation versus disproportionation in the initiation step of Cu (0)-mediated living radical polymerization. *Macromolecules* **2012,** *45* (18), 7388-7396.
[103**]**. Wang, Y.; Zhong, M.; Zhu, W.; Peng, C.-H.; Zhang, Y.; Konkolewicz, D.; Bortolamei, N.; Isse, A. A.; Gennaro, A.; Matyjaszewski, K., Reversible-deactivation radical polymerization in the presence of metallic copper. Comproportionation–disproportionation equilibria and kinetics. *Macromolecules* **2013,** *46* (10), 3793-3802.
[104**]**. Zhang, Q.; Wilson, P.; Li, Z.; McHale, R.; Godfrey, J.; Anastasaki, A.; Waldron, C.; Haddleton, D. M., Aqueous copper-mediated living polymerization: exploiting rapid disproportionation of CuBr with Me6TREN. *J Am Chem Soc* **2013,** *135* (19), 7355-63.
[105**]**. Konkolewicz, D.; Krys, P.; Góis, J. R.; Mendonca, P. V.; Zhong, M.; Wang, Y.; Gennaro, A.; Isse, A. A.; Fantin, M.; Matyjaszewski, K., Aqueous RDRP in the presence of Cu0: The exceptional activity of CuI confirms the SARA ATRP mechanism. *Macromolecules* **2014,** *47* (2), 560-570.
[106**]**. Konkolewicz, D.; Wang, Y.; Krys, P.; Zhong, M.; Isse, A. A.; Gennaro, A.; Matyjaszewski, K., SARA ATRP or SET-lRP. end of controversy? *Polymer Chemistry* **2014,** *5* (15), 4396-4417.
[107**]**. Ciavatta, L.; Ferri, D.; Palombari, R., On the equilibrium Cu2++ Cu (s)⇄ 2Cu+. *Journal of Inorganic and Nuclear Chemistry* **1980,** *42* (4), 593-598.
[108**]**. Seeliger, F.; Matyjaszewski, K., Temperature effect on activation rate constants in ATRP: new mechanistic insights into the activation process. *Macromolecules* **2009,** *42* (16), 6050-6055.
[109**]**. Buback, M.; Morick, J., Equilibrium Constants and Activation Rate Coefficients for Atom Transfer Radical Polymerizations at Pressures up to 2 500 Bar. *Macromolecular Chemistry and Physics* **2010,** *211* (19), 2154-2161.
[110**]**. Wang, Y.; Kwak, Y.; Buback, J.; Buback, M.; Matyjaszewski, K., Determination of ATRP equilibrium constants under polymerization conditions. *ACS Macro Letters* **2012,** *1* (12), 1367-1370.
[111**]**. Zerk, T. J.; Bernhardt, P. V., Solvent dependent anion dissociation limits copper(I) catalysed atom transfer reactions. *Dalton Transactions* **2013,** *42* (32), 11683–11694.
[112**]**. Goto, A.; Fukuda, T., Determination of the activation rate constants of alkyl halide initiators for atom transfer radical polymerization. *Macromolecular rapid communications* **1999,** *20* (12), 633-636.
[113**]**. Matyjaszewski, K.; Paik, H.-j.; Zhou, P.; Diamanti, S. J., Determination of activation and deactivation rate constants of model compounds in atom transfer radical

polymerization. *Macromolecules* **2001,** *34* (15), 5125-5131.
[114**]**. Soerensen, N.; Barth, J.; Buback, M.; Morick, J.; Schroeder, H.; Matyjaszewski, K., SP-PLP-EPR measurement of ATRP deactivation rate. *Macromolecules* **2012,** *45* (9), 3797-3801.
[115**]**. Matyjaszewski, K.; Gao, H.; Sumerlin, B. S.; Tsarevsky, N. V., *Reversible Deactivation Radical Polymerization: Mechanisms and Synthetic Methodologies*. American Chemical Society: 2018.
[116**]**. Schröder, K.; Mathers, R. T.; Buback, J.; Konkolewicz, D.; Magenau, A. J.; Matyjaszewski, K., Substituted tris (2-pyridylmethyl) amine ligands for highly active ATRP catalysts. *ACS Macro Letters* **2012,** *1* (8), 1037-1040.
[117**]**. Lorandi, F.; De Bon, F.; Fantin, M.; Isse, A. A.; Gennaro, A., Electrochemical characterization of common catalysts and initiators for atom transfer radical polymerization in [BMIm][OTf]. *Electrochemistry Communications* **2017,** *77*, 116-119.
[118**]**. Ribelli, T. G.; Fantin, M.; Daran, J. C.; Augustine, K. F.; Poli, R.; Matyjaszewski, K., Synthesis and Characterization of the Most Active Copper ATRP Catalyst Based on Tris[(4-dimethylaminopyridyl)methyl]amine. *J Am Chem Soc* **2018,** *140* (4), 1525-1534.
[119**]**. Andrieux, C.; Blocman, C.; Dumas-Bouchiat, J.; M'halla, F.; Saveant, J., Homogeneous redox catalysis of electrochemical reactions: Part V. Cyclic voltammetry. *Journal of Electroanalytical Chemistry and Interfacial Electrochemistry* **1980,** *113* (1), 19-40.
[120**]**. Melville, J. N.; Bernhardt, P. V., Electrochemical Exploration of Active Cu-Based Atom Transfer Radical Polymerization Catalysis through Ligand Modification. *Inorganic Chemistry* **2021**.
[121**]**. Fantin, M.; Lorandi, F.; Ribelli, T. G.; Szczepaniak, G.; Enciso, A. E.; Fliedel, C.; Thevenin, L.; Isse, A. A.; Poli, R.; Matyjaszewski, K., Impact of Organometallic Intermediates on Copper-Catalyzed Atom Transfer Radical Polymerization. *Macromolecules* **2019,** *52* (11), 4079-4090.
[122**]**. Lorandi, F.; Fantin, M.; Isse, A. A.; Gennaro, A.; Matyjaszewski, K., New protocol to determine the equilibrium constant of atom transfer radical polymerization. *Electrochimica Acta* **2018,** *260*, 648-655.
[123**]**. Tang, W.; Tsarevsky, N. V.; Matyjaszewski, K., Determination of equilibrium constants for atom transfer radical polymerization. *Journal of the American Chemical Society* **2006,** *128* (5), 1598-1604.
[124**]**. Chmielarz, P., Synthesis of α-d-glucose-based star polymers through simplified electrochemically mediated ATRP. *Polymer* **2016,** *102*, 192-198.
[125**]**. Chmielarz, P.; Park, S.; Sobkowiak, A.; Matyjaszewski, K., Synthesis of b-cyclodextrin-based star polymers via a simplified electrochemically mediated ATRP. *Polymer* **2016,** *88*, 36-42.
[126**]**. Wang, Y.; Zhong, M.; Zhang, Y.; Magenau, A. J.; Matyjaszewski, K., Halogen conservation in atom transfer radical polymerization. *Macromolecules* **2012,** *45* (21), 8929-8932.
[127**]**. Pan, X.; Fantin, M.; Yuan, F.; Matyjaszewski, K., Externally controlled atom transfer radical polymerization. *Chem Soc Rev* **2018,** *47* (14), 5457-5490.

[128**]**. Chmielarz, P.; Sobkowiak, A., Synthesis of poly (butyl acrylate) using an electrochemically mediated atom transfer radical polymerization. *Polimery* **2016,** *61* (9), 585-590.
[129**]**. Chmielarz, P.; Sobkowiak, A.; Matyjaszewski, K., A simplified electrochemically mediated ATRP synthesis of PEO-b-PMMA copolymers. *Polymer* **2015,** *77*, 266-271.
[130**]**. Boyer, C.; Atme, A.; Waldron, C.; Anastasaki, A.; Wilson, P.; Zetterlund, P. B.; Haddleton, D.; Whittaker, M. R., Copper(0)- mediated radical polymerisation in a self-generating biphasic system. *Polymer Chemistry* **2013,** *4* (1), 106-112.
[131**]**. Li, B.; Yu, B.; Huck, W. T. S.; Zhou, F.; Liu, W., Electrochemically Induced Surface-Initiated Atom-Transfer Radical Polymerization. *Angewandte Chemie International Edition* **2012,** *51* (21), 5092-5095.
[132**]**. dos Santos, N. A. C.; Lorandi, F.; Badetti, E.; Wurst, K.; Isse, A. A.; Gennaro, A.; Licini, G.; Zonta, C., Tuning the reactivity and efficiency of copper catalysts for atom transfer radical polymerization by synthetic modification of tris (2-methylpyridyl) amine. *Polymer* **2017,** *128*, 169-176.
[133**]**. De Bon, F.; Isse, A. A.; Gennaro, A., Towards scale-up of electrochemically-mediated atom transfer radical polymerization: Use of a stainless-steel reactor as both cathode and reaction vessel. *Electrochimica Acta* **2019,** *304*, 505-512.
[134**]**. Mincheva, R.; Paneva, D.; Mespouille, L.; Manolova, N.; Rashkov, I.; Dubois, P., Optimized water-based ATRP of an anionic monomer: Comprehension and properties characterization. *Journal of Polymer Science Part A: Polymer Chemistry* **2009,** *47* (4), 1108-1119.
[135**]**. Zaborniak, I.; Chmielarz, P., Miniemulsion switchable electrolysis under constant current conditions. *Polymers for Advanced Technologies* **2020,** *31* (11), 2806-2815.
[136**]**. De Bon, F.; Fantin, M.; Isse, A. A.; Gennaro, A., Electrochemically mediated ATRP in ionic liquids: controlled polymerization of methyl acrylate in [BMIm][OTf]. *Polymer Chemistry* **2018,** *9* (5), 646-655.
[137**]**. Lorandi, F.; Fantin, M.; Wang, Y.; Isse, A. A.; Gennaro, A.; Matyjaszewski, K., Atom Transfer Radical Polymerization of Acrylic and Methacrylic Acids: Preparation of Acidic Polymers with Various Architectures. *ACS Macro Letters* **2020,** *9* (5), 693-699.
[138**]**. Shipp, D. A.; Wang, J.-L.; Matyjaszewski, K., Synthesis of acrylate and methacrylate block copolymers using atom transfer radical polymerization. *Macromolecules* **1998,** *31* (23), 8005-8008.
[139**]**. Peng, C.-H.; Kong, J.; Seeliger, F.; Matyjaszewski, K., Mechanism of halogen exchange in ATRP. *Macromolecules* **2011,** *44* (19), 7546-7557.
[140**]**. Chmielarz, P.; Park, S.; Simakova, A.; Matyjaszewski, K., Electrochemically mediated ATRP of acrylamides in water. *Polymer* **2015,** *60*, 302-307.
[141**]**. De Bon, F.; Marenzi, S.; Isse, A. A.; Durante, C.; Gennaro, A., Electrochemically Mediated Aqueous Atom Transfer Radical Polymerization of N , N -Dimethylacrylamide. *ChemElectroChem* **2020,** *7* (6), 1378-1388.
[142**]**. Krys, P.; Matyjaszewski, K., Kinetics of Atom Transfer Radical Polymerization.

European Polymer Journal **2017,** *89*, 482-523.
[143**]**. Mircea Teodorescu; KrzysztofMatyjaszewski, Macromol. Rapid Commun_Controlled polymerization of DMAA by ATRP. *Macromol. Rapid Commun.* **2000,** *21* (4), 190-194.
[144**]**. Ding, S.; Radosz, M.; Shen, Y., Atom Transfer Radical Polymerization of N,N-Dimethylacrylamide. *Macromolecular Rapid Communications* **2004,** *25* (5), 632-636.
[145**]**. Bortolamei, N.; Isse, A. A.; Magenau, A. J.; Gennaro, A.; Matyjaszewski, K., Controlled aqueous atom transfer radical polymerization with electrochemical generation of the active catalyst. *Angewandte Chemie International Edition* **2011,** *50* (48), 11391-11394.
[146**]**. Frank, P.; General, P., Schlenk Line Design and Safety. Apr: 2011.
[147**]**. Chandra, T.; Zebrowski, J. P., Reactivity control using a Schlenk line. *Journal of Chemical Health & Safety* **2014,** *21* (3), 22-28.
[148**]**. Zaborniak, I.; Macior, A.; Chmielarz, P., Stimuli-Responsive Rifampicin-Based Macromolecules. *Materials* **2020,** *13* (17), 3843.
[149**]**. Chmielarz, P., Synthesis of multiarm star block copolymers via simplified electrochemically mediated ATRP. *Chemical Papers* **2016,** *71* (1), 161-170.
[150**]**. Chmielarz, P., Synthesis of cationic star polymers by simplified electrochemically mediated ATRP. *Express Polymer Letters* **2016,** *10* (10), 810-821.
[151**]**. Chmielarz, P., Cellulose-based graft copolymers prepared by simplified electrochemically mediated ATRP. *Express Polymer Letters* **2017,** *11* (2), 140-151.
[152**]**. Chmielarz, P.; Pacześniak, T.; Rydel-Ciszek, K.; Zaborniak, I.; Biedka, P.; Sobkowiak, A., Synthesis of naturally-derived macromolecules through simplified electrochemically mediated ATRP. *Beilstein Journal of Organic Chemistry* **2017,** *13*, 2466-2472.
[153**]**. Chmielarz, P., Synthesis of high molecular weight five-arm star polymers by improved electrochemically mediated atom transfer radical polymerization. *Polimery* **2017,** *62* (09), 642-649.
[154**]**. Chmielarz, P.; Sobkowiak, A., Ultralow ppm *se*ATRP synthesis of PEO-b-PBA copolymers. *Journal of Polymer Research* **2017,** *24* (5).
[155**]**. Zaborniak, I.; Chmielarz, P., Dually-functional riboflavin macromolecule as a supramolecular initiator and reducing agent in temporally-controlled low ppm ATRP. *Express Polymer Letters* **2020,** *14* (3), 235-247.
[156**]**. Zaborniak, I.; Chmielarz, P.; Martinez, M. R.; Wolski, K.; Wang, Z.; Matyjaszewski, K., Synthesis of high molecular weight poly(n-butyl acrylate) macromolecules via *se*ATRP: From polymer stars to molecular bottlebrushes. *European Polymer Journal* **2020,** *126*, 109566.
[157**]**. Chmielarz, P., Synthesis of inositol-based star polymers through low ppm ATRP methods. *Polymers for Advanced Technologies* **2017,** *28* (12), 1804-1812.
[158**]**. Chmielarz, P., Synthesis of naringin-based polymer brushes via *se*ATRP. *Polymers for Advanced Technologies* **2018,** *29* (1), 470-480.
[159**]**. Chmielarz, P.; Sobkowiak, A., Synthesis of urethane—acrylic multi-block copolymers via electrochemically mediated ATRP. *Chemical Papers* **2016,** *70* (9).
[160**]**. Flejszar, M.; Chmielarz, P.; Wolski, K.; Grześ, G.; Zapotoczny, S., Polymer

Brushes via Surface-Initiated Electrochemically Mediated ATRP: Role of a Sacrificial Initiator in Polymerization of Acrylates on Silicon Substrates. *Materials* **2020,** *13* (16), 3559.

Chapter III

Experimental section

3.1 Materials

Common solvents: *N*,*N*-Dimethylformamide (DMF, Sigma- Aldrich, 99.8%), Dimethyl Sulfoxide (DMSO, Sigma- Aldrich, 99.9%), Acetonitrile (MeCN, HPLC grade, Sigma-Aldrich, 99.9%), Tetrahydrofuran (THF, Carlo Erba, HPLC grade, not stabilized), Acetone (VWR, 99%), were used as received. Deionized water was double distilled in the presence of potassium permanganate ($KMnO_4$) to remove all possible contaminants.

Deuterated solvents: Deuterated chloroform ($CDCl_3$, Sigma Aldrich, 99.8 atom % D), Deuterium oxide (D_2O, Sigma Aldrich, 99.9 atom % D) for NMR spectroscopy were used as received.

Acids: Sulfuric acid (H_2SO_4, Sigma-Aldrich, 95.0-98.0%), Hydrochloric acid (HCl, Sigma- Aldrich, 37%) and Perchloric acid ($HClO_4$, Sigma-Aldrich, 70%) were used as received.

Ligands: Tris[2-(dimethylamino)ethyl]amine (Me_6TREN, Alfa Aesar, 98%) and Tris(2-pyridylmethyl) amine (TPMA, Alfa Aesar 98%) were used as received.

Initiators: methyl α-bromoisobutyrate (MBiB, Sigma-Aldrich, > 99%) and 2-hydroxyethyl 2-bromoisobutyrate (HEBiB, Sigma Aldrich, 95%) were used as received.

Monomers and purification procedures: *n*-Butyl acrylate (*n*-BA, Sigma-Aldrich, > 99%), Oligo (ethylene oxide) methyl ether methacrylate (OEOMA, Sigma-Aldrich, average M_w = 500) and Dimethylacrylamide (DMA, Sigma Aldrich, 99%) were purified by passing through a column filled with basic alumina (Al_2O_3, VWR chemicals) to remove polymerization inhibitors.

Other chemicals and purification procedures: Tetraethylammonium tetrafluoroborate (Et_4NBF_4, Alfa Aesar, 99%) was recrystallized from ethanol twice. Tetraethylammonium bromide (Et_4NBr, Sigma-Aldrich, 99%) and Tetraethylammonium chloride (Et_4NCl, Sigma-Aldrich, 98%) were recrystallized from acetone and from a mixture of ethanol/diethyl ether, respectively.[1] They were then dried in a vacuum oven at 70 °C for 48 h. Copper (II) trifluoromethanesulfonate ($Cu(OTf)_2$, Sigma-Aldrich, 98%), Tetrakis(acetonitrile)copper(I) tetrafluoroborate

($Cu(MeCN)_4BF_4$, Sigma Aldrich, 97%), Ferrocene (Acros Organics, 98%), Lithium bromide (LiBr, Sigma Aldrich, 99.9%), Potassium hydroxide (KOH, VWR, 86.7%), anhydrous Aluminum chloride ($AlCl_3$, Carlo Erba, 99.9%), Sodium chloride (NaCl, Fisher Scientific, 99.0%), Sodium bromide (NaBr, Fisher Scientific, 99.0%), Sodium iodide (NaI, Fluka, 99.0%), Sodium phosphate monobasic (NaH_2PO_4, Carlo Erba, 99.0%), Sodium phosphate dibasic (Na_2HPO_4, Sigma Aldrich, 99.0%), Sodium phosphate tribasic dodecahydrate ($Na_3PO_4 \cdot 12H_2O$, Carlo Erba, 98%), Sodium sulphate (Na_2SO_4, Riedel-de haen, 99%), Sodium carbonate (Na_2CO_3, Fluka, 99.5%), Sodium acetate (CH_3COONa, Carlo Erba, 99%), Sodium nitrate ($NaNO_3$, Carlo Erba, 99.5%) and Sodium perchlorate ($NaClO_4$, Sigma Aldrich, 98%) were used as received.

Buffer solution: When necessary, pH was adjusted to the desired values with buffers prepared from the tetraethyl ethylenediamine (TEEN, Alfa Aesar, 98%) and $HClO_4$. TEEN is a sterically hindered amine that is not able to form complexes with hydrated metal ions in aqueous solutions.[2] The standard buffer solutions with pH 7 and 4 (VWR) for pH-meter calibration were used as received.

3.2 Instruments and methods

3.2.1 Electrochemical measurements and activation of electrodes

Electrochemical experiments were carried out in a three-electrode cell by using a PARC 273A potentiostat/galvanostat (EG&G Princeton Applied Research) run by a PC with Echem software or in some cases an Autolab PGSTAT 30 potentiostat/galvanostat (EcoChemie, The Netherlands) run by a PC with GPES software, or an Autolab PGSTAT302N potentiostat/galvanostat, run by a PC with NOVA 2.1 software (EcoChemie, The Netherlands).

Cyclic voltammetry (CV), linear sweep voltammetry (LSV), and anodic dissolution of Al to prepare Al^{3+} ions were carried out in a five-neck cell with a double wall jacket through which water from a thermostatic bath (HAAKE E3) at 25 °C was continuously circulated. The working electrode (WE) and the counter electrode (CE)

used for CV were a glassy carbon (GC) disk, fabricated from a 3 mm diameter rod (Tokai GC-20) and a Pt wire, respectively. For LSV measurements carried out in **Chapters IV and VIII**, the working electrode (WE) and the counter electrode (CE) were a rotating disc electrode (RDE) with a glassy carbon tip of 3 mm diameter (Autolab, Eco-Chimie) and a Pt wire, respectively. For electrolysis of Al^{3+}, the WE and CE were aluminum wire (Al, d = 1.0 mm, Sigma-Aldrich, 99.999%) and Pt mesh separated from the working solution through a glass frit filled with a conductive solution and a methylcellulose gel saturated with Et_4NBF_4. The reference electrode (RE) was Ag|AgI in 0.1M *n*-Bu_4NI in DMF for organic solvents, whereas a saturated calomel electrode (SCE, Schott Instruments, Science-line, B2810) was used in aqueous solutions.

The pH of the aqueous solutions was measured using inoLab WTW pH-meter, equipped with a combined glass electrode (SenTix 61, full of 3 mol/L KCl), which was calibrated by two-points method in pH = 4 and 7 commercial buffer solutions before every experiment.

The glassy carbon (GC) disk working electrode used for cyclic voltammetry studies was fabricated from a 3 mm diameter GC rod. Initially, the electrode surface was polished to mirror finish with 1000, 2000 and 4000 grit silicon carbide papers, followed by 3.0, 1.0, and 0.25 μm diamond pastes (Struers). After each polishing step, the electrode was washed with abundant acetone and then ultrasonically (Branson 2200 Ultrasonic Cleaner) rinsed in ethanol for 5 min. Prior to each experiment, and whenever passivation of the electrode became apparent during the experiment, the electrode surface was cleaned by polishing with a 0.25 μm diamond paste followed by ultrasonic rinsing in ethanol. The Pt mesh electrode was electrochemically activated prior to each polymerization by cycling the potential from -0.7 to 1.0 V vs. $Hg|Hg_2SO_4$ at a scan rate of 0.2 V s^{-1} (100 cycles).[3]

3.2.2 *e*ATRP in divided and undivided cells

All potentiostatic *e*ATRP experiments were carried out in a seven-neck cell with a double wall jacket through which water from a thermostatic bath (HAAKE E3) at 50 °C,

25 °C or 0 °C was continuously circulated. A Pt mesh (Alfa Aesar, 99.9% metals basis, ca. 6 cm^2) was used as a WE, whereas the CE was either a graphite rod in a divided cell. The graphite rod or Platinum was separated from the working solution by a glass frit filled with a conductive solution and a methylcellulose gel saturated with Et_4NBF_4. The RE was Ag|AgI in 0.1M *n*-Bu_4NI in DMF for organic solvents, whereas a saturated calomel electrode (SCE, Schott Instruments, Science-line, B2810) was used in aqueous solution. The ferrocenium/ferrocene (Fc^+/Fc) redox couple was used as internal standard, added at the end of each characterization/kinetic experiment for the organic media.

For *e*ATRP performed in an undivided cell, the separated counter electrode used in divided cell was replaced by an activated Al wire. However, the influences of Al^{3+} ions released from anodic dissolution on activator and deactivator stabilities as well as the polymerization kinetic control were investigated.

3.2.3 Ultraviolet -visible-near infrared absorption spectroscopy

The UV - Vis - NIR measurements were carried out with an Agilent Cary 5000 spectrophotometer by using 10 mm optical path length quartz cuvettes. The obtained results were presented in **Chapters IV and VI**. Working solutions were taken from the various examined solutions in the absence and the presence of Al^{3+} ions. Based on the Beer-Lambert law,[4] **eq. 3-1**, the absorption intensity is proportional to substance concentration:

$$\boldsymbol{A = \varepsilon\, l\, C} \tag{3-1}$$

where $\boldsymbol{A}$ is the absorbance of a substance in solution, $\boldsymbol{\varepsilon}$ is molar absorptivity ($M^{-1}\cdot cm^{-1}$), $\boldsymbol{l}$ is the length of light path (cm), here it is 1.0 cm, $\boldsymbol{C}$ is the concentration of the substance (M).

3.2.4 Gel permeation chromatography (GPC)

Gel permeation chromatography (GPC) is a liquid chromatographic technique that separates individual polymer chains based on their size in solution; it is used to measure

the molecular weight (MW) distribution of natural and synthetic polymers. The MW distribution affects many of the physical properties of the polymers. The general mechanism is that polymer molecules are dissolved in solution in the form of spherical coils, the size of which depends on the MW. Then the coils are introduced into an eluent flowing through a column packed with insoluble porous beads. The size of the pores on the beads is similar to that of polymer coils, which can diffuse in and out of the pores. This results in large coils eluting first as they cannot fit in many pores, while smaller coils elute last. This size separation can then be used to calculate molecular weight by using a calibration curve constructed with polymer standards.

Number-average molecular weight (M_n) and dispersity ($Đ$) of the PBA were determined by an Agilent 1260 Infinity Gel Permeation Chromatograph (GPC), equipped with a refractive index detector (RID) and two PLgel Mixed-D columns (300 ×7.5 mm, 5 μm) connected in series. The column system was calibrated with 12 linear poly (methyl methacrylate) (PMMA) standards (M_n = 540~2210 000 g•mol^{-1}). The columns and detector were thermostated at 30 ˚C. THF at a flow rate of 1 mL/min was used as the eluent for PBA and the received data were presented in **Chapter V**. For POEOMA and PDMA in **Chapter VII**, the columns and detector were thermostated at 70 ˚C and 50 ˚C, respectively. A solution of 0.01M LiBr in DMF at a flow rate of 1 mL/min was used as the eluent. Samples for analysis were periodically withdrawn from the electrolysis cell and, before injection, were filtered through neutral alumina over a 200-nm PTFE membrane to remove the copper complexes.

3.2.5 Nuclear magnetic resonance (NMR) and monomer conversion determination

NMR spectroscopy is an analytical chemistry technique used in quality control and research for determining the content and purity of a sample as well as its molecular structure. ^{1}H and ^{13}C are the most commonly used nuclei. NMR spectroscopy can provide detailed and quantitative information on the functional groups, since the area under an NMR peak is usually proportional to the number of protons involved.[5]

Monomer conversion was quantitatively determined by ^{1}H NMR, **eq. 3-2**, with a

Bruker 200 MHz spectrometer.

$$\text{Monomer conv.} = \frac{C_0 - C_t}{C_0} \times 100\% \quad (3\text{-}2)$$

where the C_0 is the initial concentration of monomer, C_t is the residual concentration of monomer at the time t. C_t can be obtained through **eq. 3-3**,

$$C_t = \text{CCF} \times \frac{A_m}{N_m} \quad (3\text{-}3)$$

where CCF is concentration conversion factor related to the signals and concentration of an internal standard, **eq. 3-4**, which is assumed to be 100% pure. A_m and N_m are the integral area value and the number of the protons involved in the signals of the monomer unit, respectively.

$$\text{CCF} = C_s \times \frac{N_s}{A_s} \quad (3\text{-}4)$$

where C_s is the internal standard concentration (e.g., the solvent or supporting electrolyte), A_s and N_s stand for the integral area value and the number of the protons involved in the signal of the chosen standard substance, respectively. In particular, A_s value is usually defined as 1.0 because of the initial selection in the software.

Thus, according to **eqs. 3-2** to **3-4**, the monomer conversion can be obtained as follows:

$$\text{Monomer conv.} = \left(1 - \frac{C_s}{C_0} \times \frac{A_m}{A_s} \times \frac{N_s}{N_m}\right) \times 100\% \quad (3\text{-}5)$$

The signal of Et_4NBF_4, Et_4NBr or solvent was used as internal standard to determine monomer conversion. In **Chapter V**, samples of *n*-BA taken from the reaction mixture were diluted in $CDCl_3$ and analyzed at ambient temperature. In **Chapters VII** and **VIII,** Samples of OEOMA or DMA taken from the reaction mixture were diluted in D_2O and analyzed at ambient temperature.

3.2.6 Scanning electron microscopy (SEM) characterizations and elemental analysis

Scanning electron microscopy (SEM) images were performed with a Zeiss Sigma HD FE-SEM equipped with an INCAx-act PentaFET Precision spectrometer (Oxford Instruments) using primary beam acceleration voltages at 20 kV. The EDX elemental

analysis was evaluated and based on at least 5 different selected regions for each sample and the results were reported as average values, as shown in **Chapters VI and VII**.

References

[1**]**. Armarego, W. L., *Purification of laboratory chemicals*. Butterworth-Heinemann: 2017.
[2**]**. Yu, Q.; Kandegedara, A.; Xu, Y.; Rorabacher, D., Avoiding interferences from Good's buffers: a contiguous series of noncomplexing tertiary amine buffers covering the entire range of pH 3–11. *Analytical biochemistry* **1997,** *253* (1), 50-56.
[3**]**. Lorandi, F.; Fantin, M.; Isse, A. A.; Gennaro, A., Electrochemically mediated atom transfer radical polymerization of n-butyl acrylate on non-platinum cathodes. *Polymer Chemistry* **2016,** *7* (34), 5357-5365.
[4**]**. Swinehart, D. F., The beer-lambert law. *Journal of chemical education* **1962,** *39* (7), 333.
[5**]**. Malz, F.; Jancke, H., Validation of quantitative NMR. *Journal of pharmaceutical and biomedical analysis* **2005,** *38* (5), 813-823.

Chapter IV

Electrochemical study of the effect of Al^{3+} on Cu-based ATRP catalysts in organic media

Abstract

Copper-based catalysts play an important role in atom transfer radical polymerization (ATRP). Recently, a low-cost and simple electrochemical variant of ATRP, known as simplified electrochemically-mediated ATRP (*se*ATRP), has been developed, receiving a rapidly growing interest as it is applicable to a variety of monomers in a wide range of reaction media. *se*ATRP is performed in an undivided cell with a sacrificial anode such as aluminum, and the metal ions (e.g., Al^{3+}) released from the anode might affect the performance of the copper catalyst. In this connection, knowledge of the effect of Al^{3+} on the stability and performance of typical Cu catalysts is highly desired. In this study, the stability of Cu complexes with tris(2-(dimethylamino)ethyl) amine (Me_6TREN) or tris(2-pyridylmethyl)amine (TPMA), was investigated in DMF, DMSO, and MeCN by electrochemical methods and UV-vis-NIR spectroscopy. Both ligands form complexes with Al^{3+}, but in DMF and DMSO, TPMA binds more strongly to Cu^{2+} and Cu^{+} than Al^{3+}, whereas the opposite is true for Me_6TREN in all tested solvents.

Keywords: *e*ATRP, copper catalysts, ligands, stability, aluminum ions

4.1 Introduction

To date, a substantial body of approaches were investigated to develop reversible deactivation radical polymerization (RDRP) methods for the synthesis of polymers with a well-defined structure, low dispersity and predetermined composition.[1-3] Among these, the most widely used RDRP techniques are nitroxide mediated polymerization (NMP),[4] organometallic mediated radical polymerization (OMRP),[5-7] reversible addition-fragmentation chain-transfer (RAFT),[7-9] and atom transfer radical polymerization (ATRP).[10-15] However, ATRP has attracted much attention because of its robustness, simplicity and applicability to a wide range of monomers and reaction media.

ATRP is a simple process that utilizes a redox equilibrium between a solubilized stable transition metal catalyst and a halogen-capped dormant polymer chain (or an alkyl halide initiator), as shown in **Scheme 4.1**. The equilibrium constant (K_{ATRP}), defined by the relative rate constants of activation (k_{act}) and deactivation (k_{deact}), **eq. 4-1**, is typically very low.[16-18] Radical termination reactions are essentially eliminated due to the low instantaneous radical concentration. However, one obvious limitation of conventional ATRP is the large amount of catalyst used, which leads to polymers with a significant amount of residual copper complexes ($Cu^{I}L$, X-$Cu^{II}L$), and thus causes a cost increase for metal removal. To overcome this problem, various ATRP methods based on regenerable low catalyst load have been developed. The most important strategies that have been developed for regenerating the catalyst by reduction are activators regenerated by electron transfer (ARGET) ATRP,[19-22] supplemental activator and reducing agent (SARA) ATRP,[22-25] initiators for continuous activator regeneration (ICAR) ATRP,[26-28] photochemically mediated polymerization (photoATRP),[29-35] electrochemically-mediated ATRP (*e*ATRP),[36-41] and mechanochemically mediated procedures (mechanoATRP).[15, 42-44]

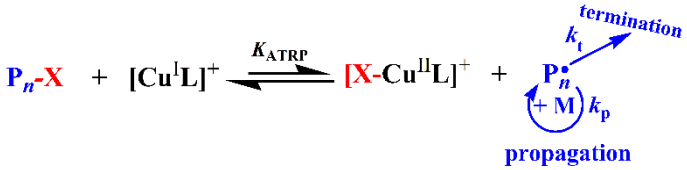

Scheme 4.1 Mechanism of traditional ATRP

$$K_{ATRP} = \frac{k_{act}}{k_{deact}} = \frac{[P_n\bullet]\cdot[X\text{-}Cu^{II}/L]}{[P_n\text{-}X]_0\cdot[Cu^{I}/L]} \ll 1 \quad (4\text{-}1)$$

$$R_P = k_p\,[M][P_n^\bullet] = k_p[M]\,K_{ATRP}\frac{[RX]\cdot[Cu^IL]^+}{[XCu^{II}L]^+} \quad (4\text{-}2)$$

Among the various advanced ATRP techniques, *e*ATRP has the unique advantage of avoiding formation of by-products arising from catalyst regeneration because electrons are directly used in place of chemical reducing agents. Moreover, the ratio of $[Cu^IL]^+/[XCu^{II}L]^+$ can be regulated by the applied potential or current, thus the overall rate of polymerization can be finely tuned by modulating the electrochemical stimulus parameters, **eq. 4-2**. Traditional *e*ATRP[45] was generally carried out in a three-electrode setup with expensive platinum (Pt) materials as working electrode (WE) and counter electrode (CE). In general, the CE compartment is separated from the WE. This two-compartment cell could be simplified to a single compartment one without any separator by the introduction of an Al sacrificial anode. This *e*ATRP setup is called simplified electrochemically-mediated ATRP (*se*ATRP).[46-50] Copper complexes with nitrogen amine ligands are the most used catalystsand prepared in situ by adding the ligand to a soluble copper salt. However, the Al^{3+} ions released from anodic dissolution of Al during polymerization might displace copper from the ligands, leading to loss of catalysis, as was previously reported for Me_6TREN in DMF and DMSO.[48-49] In a typical *se*ATRP experiment without excess ligand, polymerization progressively slows and stops after several hours at a moderate monomer conversion. The competition between Al and Cu ions for the ligand was not investigated, but addition of excess Me_6TREN with respect to the Cu^{2+} to provide sufficient ligand for the complexation of both Al^{3+} and Cu^{2+} ions during polymerization was proposed as a provisional solution to the problem.

Despite the practical importance of simplified *e*ATRP in undivided cells, to the best of our knowledge, there is no systematic investigation on the stability evolution of copper catalysts during polymerization in the presence of Al^{3+} ions in common organic media. Therefore, herein a series of experiments were designed and conducted to explore the effect of Al^{3+} ions on the stability of copper complexes with two widely used amine ligands, Me_6TRENTPMA, in three selected organic solvents (DMF, DMSO, and MeCN). The stability of both $[Cu^{II}L]^{2+}$ and $[Cu^{I}L]^{+}$ in the presence of increasing amounts Al^{3+} were evaluated by electrochemical methods and UV-vis-NIR spectroscopy.

4.2 Methodologies and procedures

4.2.1 Cyclic voltammetry (CV) measurements in the presence of Al^{3+}

Solutions of $[Cu^{II}L]^{2+}$ in the selected solvent + 0.1 M Et_4NBF_4 were always prepared in situ starting from 1 mM $Cu(OTf)_2$, followed by addition of the ligand (L, $[Cu^{II}]$:[L] = 1:1.05). Al^{3+} ions were introduced in the system by anodic dissolution of an Al wire immersed in the working solution containing the Cu complex while the cathode was immersed in a separated compartment containing only the electrolytic solution. The required amount of Al^{3+} (n mol) was prepared by applying a fixed anodic current until the passage of the theoretical charge, Q, according to $Q = 3nF$.[51] The effect of Al^{3+} on the voltammetric pattern of the complexes was often investigated by addition of increasing amounts of Al^{3+} until a two- to three-fold excess over $[Cu^{II}L]^{2+}$ was reached. The reproducibility of the results was less affected. Strictly speaking, the factors of GC passivation and the difference between the theoretical and real content of Al^{3+} released from the anodic dissolution process cannot be completely excluded. Fortunately, we only investigate the variation trends of different species in selected solvents. After each addition of Al^{3+}, therefore, a freshly polished GC electrode was used to record cyclic voltammetry. At the end of each experiment, the potential of the reference electrode (Ag/AgI/0.1 M n-Bu_4NI in DMF) was calibrated against the

ferrocenium/ferrocene couple (Fc^+/Fc) used as an internal standard.

4.2.2 UV- vis NIR absorption spectroscopy measurements

The interaction between Al^{3+} and ligands and the competition between Cu^{2+} and Al^{3+} ions for the ligands were also investigated by UV-vis-NIR spectroscopy. Typically, after every addition and CV analysis, a fixed volume of the solution was withdrawn immediately by a pipette into a 10 mm optical path length quartz cuvette. Subsequently, the UV-vis-NIR spectra of every sample were recorded by the utilization of air as internal standard and was repeated at least two times.

4.2.3 Linear sweep voltammetry (LSV) pattern measurements

Solutions of $[Cu^{I}L]^+$ in MeCN + 0.1 M Et_4NBF_4 in a tightly sealed cell were always prepared by addition of $Cu(MeCN)_4BF_4$, followed by adding the ligand (L, $[Cu^{II}]$:[L] = 1:1.05). To eliminate the effect of dioxygen, a flow of argon was maintained throughout the whole experiment. Al^{3+} ions were introduced in situ by anodic dissolution of an Al wire immersed in the working solution containing the Cu complex while the cathode was immersed in a separated compartment containing only the electrolytic solution. The required amount of Al^{3+} (n mol) was prepared by applying a fixed anodic current until the passage of the theoretical charge, Q, according to $Q = 3nF$.[51] In some experiments, Al^{3+} ions were added by a syringe from a stock solution prepared in advance by anodic dissolution of Al in MeCN + 0.1 M Et_4NBF_4. The effect of Al^{3+} on the voltammetric pattern of the complexes was often investigated by addition of increasing amounts of Al^{3+}. At the end of each experiment, the potential of the reference electrode (Ag/AgI/0.1 M n-Bu_4NI in DMF) was calibrated against the ferrocenium/ferrocene couple (Fc^+/Fc).

4.3 Results and discussion

4.3.1 Interaction between amine ligands and Al^{3+}

Copper complexes with nitrogen-based ligands such as TPMA and Me_6TREN have been extensively studied for their importance in ATRP and a great deal of information on their stability and chemical structure is available.[52-57] In contrast, there are no data on complexes of Al^{3+} with these ligands. We used cyclic voltammetry to investigate possible interactions of Al^{3+} ions with TPMA or Me_6TREN. Anodic dissolution of an Al wire was used to prepare in situ Al^{3+} ions hexacoordinated with six solvent molecules.[51]

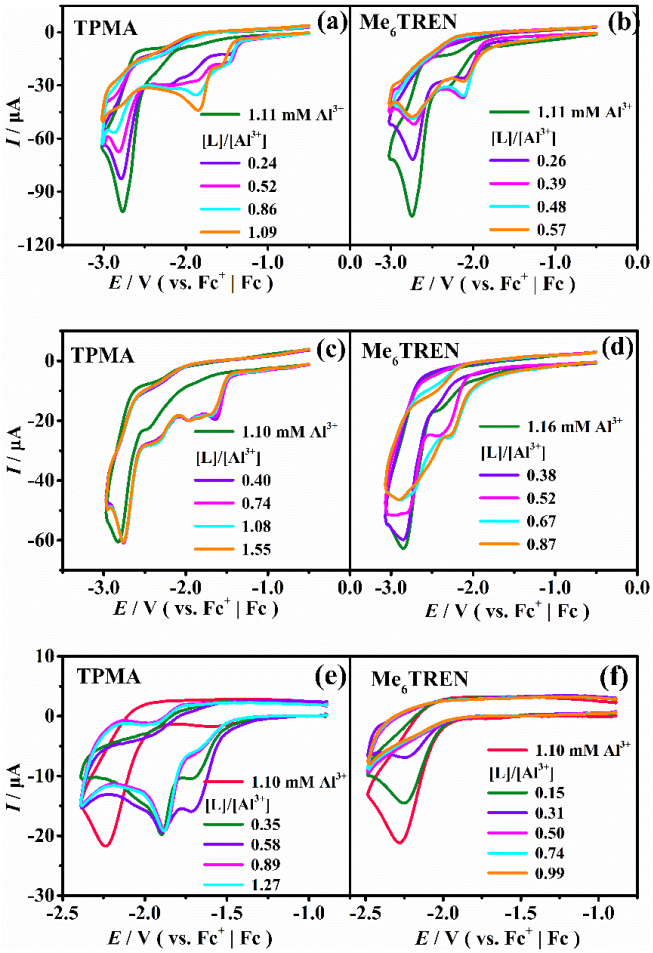

Figure 4.1 CVs of Al^{3+} in the absence and presence of amine ligands in MeCN **(a,b)**, DMF **(c,d)** or DMSO **(e,f)** with 0.1 M Et_4NBF_4 as the supporting electrolyte, recorded on a GC disk at $v = 0.2$ Vs^{-1}, $T = 25$ °C.

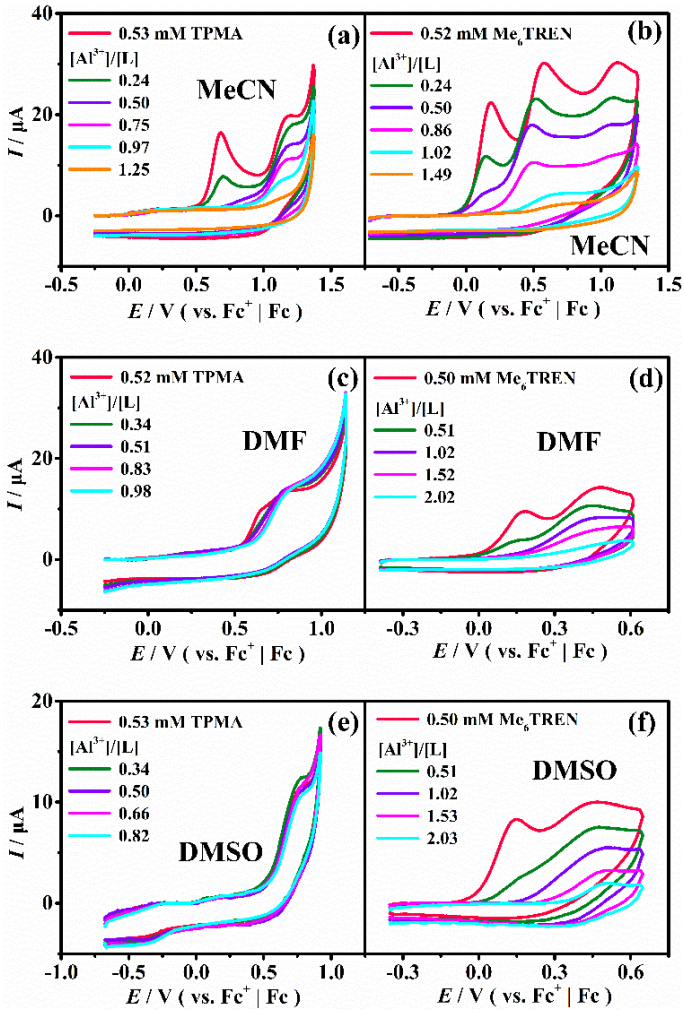

Figure 4.2 CVs of TPMA and Me_6TREN in different solvents with 0.1 M Et_4NBF_4 as the supporting electrolyte, recorded on a GC disk at $v = 0.2$ Vs^{-1} in the absence and the presence of Al^{3+} ions, $T = 25$ °C.

As shown in **Figure 4.1**, Al^{3+} exhibits a single irreversible reduction peak at a quite negative potential. This behavior was previously reported in DMF and assigned to $3e^-$ reduction to metallic Al, which causes gradual passivation of the GC disk.[51] When passivation was observed, the active electrode surface was regenerated by polishing. Addition of either TPMA or Me_6TREN, which do not display any reduction peaks in the investigated range of potentials, caused significant changes to the CV pattern of Al^{3+} (**Figure 4.1**). In MeCN, as shown in **Figure 4.1 a, b**, the reduction peak at -2.76 V decreased with increasing ligand concentration, while new reduction peaks, two for TPMA and one for Me_6TREN, appeared at less negative potentials. Similar changes

were observed also in DMF (**Figure 4.1 c, d**) and DMSO (**Figure 4.1 e, f**). This provides a clear evidence of the formation of new Al(III) species with the added ligands. These species undergo irreversible reduction processes that were not further investigated.

Evidence of the interaction of Al^{3+} ions with Me_6TREN and TPMA was gained also from changes on the voltametric pattern of the ligands. These compounds do not exhibit reduction peaks before the cathodic discharge of the background electrolyte. They do, however, undergo oxidation showing a variable number of anodic peaks, depending on type of ligand and solvent (**Figure 4.2**). In MeCN, as shown in **Figure 4.2 a, b**, addition of increasing amounts of Al^{3+} reduced the intensity of the anodic peaks of both ligands, which disappeared in the presence of excess Al^{3+} ions. Instead, this occurred only for Me_6TREN in DMF (**Figure 4.2 c, d**) and DMSO (**Figure 4.2 e, f**). Oxidation of the ligands (Me_6TREN in all solvents and TPMA in MeCN) becomes more difficult in the presence of Al^{3+} possibly because of stabilization through formation of complexes with the metal ion; their oxidation potentials shift to values beyond the accessible anodic potential window. The observed difference of behavior between TPMA and Me_6TREN agrees well with the results obtained for the reduction of Al^{3+} in the presence of the ligands. Both ligands form strong complexes with Al^{3+} in MeCN, whereas only Me_6TREN strongly coordinates Al^{3+} in DMF and DMSO.

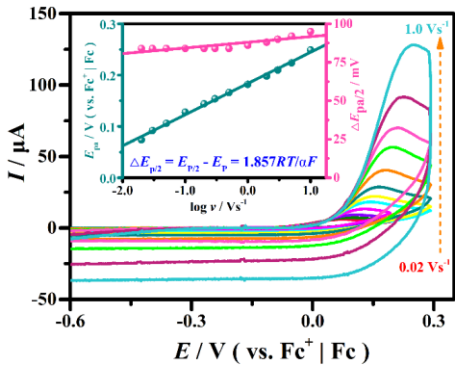

Figure 4.3 CVs of 0.5 mM Me_6TREN in MeCN + 0.1 M Et_4NBF_4, recorded on a GC disk at v = 0.2 Vs^{-1}, T = 25 °C. The inset shows dependence of E_p and $\triangle E_{p/2}$ on scan rate for the first peak of Me_6TREN.

Additionally, the first oxidation peak of the ligands was investigated at different sweep rates. The peak remains irreversible even at relatively high scan rates. To examine whether the absence of reversibility is due to sluggish electron transfer or chemical instability of the primary oxidation product, E_p and $\triangle E_{p/2} = E_p - E_{p/2}$ were analyzed as a function of v, obtaining a straight line for a plot of E_p vs. log v and roughly constant $\triangle E_{p/2}$ (**Figure 4.3**). The apparent transfer coefficient α calculated from the slope of the line and $\triangle E_{p/2}$ was 0.54 for Me_6TREN in MeCN. The values of α measured for Me_6TREN in DMSO and DMF were 0.49 and 0.54, respectively. Such α values, which were close to or higher than 0.5, indicate an oxidation mechanism under mixed kinetic control (between electron transfer and following chemical reaction). The values of α measured for TPMA were 0.53 in DMF, 0.26 in MeCN and 0.27 in DMSO. In this case, electron transfer from the ligand is irreversible in MeCN and DMSO, whereas the reaction is faster in DMF.

4.3.2 Effect of Al^{3+} on the stability of $[Cu^{II}L]^{2+}$

$[Cu^{II}L]^{2+}$ complexeswere prepared in situ by mixing equimolar amounts of $Cu(OTf)_2$ and the ligand. **Figure 4.4** shows CVs of $Cu(OTf)_2$ before and after addition of the amine ligand, and after further progressive addition of Al^{3+} ions. Typically, polyamine ligands such as Me_6TREN and TPMA strongly bind to Cu^+ and Cu^{2+} ions, with the formation of complexes of higher stability for Cu^{II} than Cu^I.[56, 58-59] The standard potential ($E^\ominus$) of the $[Cu^{II}L]^{2+}/[Cu^{I}L]^{+}$ couple can be estimated from cyclic voltammetry as the half-sum of the cathodic and anodic peak potentials, $E^\ominus \approx E_{1/2} = (E_{pc} + E_{pa})/2$, where E_{pc} and E_{pa} represent the cathodic and anodic peak potentials, respectively. $E^\ominus$ of $[Cu^{II}L]^{2+}/[Cu^{I}L]^{+}$ depends on the relative stability of $[Cu^{II}L]^{2+}$ and $[Cu^{I}L]^{+}$ complexes, according to **eq. 4-3:**

$$E^{\ominus}_{[Cu^{II}L]^{2+}/[Cu^{I}L]^{+}} = E^{\ominus}_{Cu^{2+}/Cu^{+}} - \frac{RT}{nF}\ln\frac{\beta^{II}}{\beta^{I}} \qquad (4\text{-}3)$$

where R is the universal gas constant, F is the Faraday constant, and β^{II} and β^{I} are the

stability constants of $[Cu^{II}L]^{2+}$ and $[Cu^{I}L]^{+}$, respectively. In all solvents, solvated Cu^{2+} ions showed a quasi-reversible peak couple with anodic to cathodic peak separation, i.e., $\Delta E_p = E_{pa} - E_{pc}$, in the range 86 – 160 mV at $\upsilon = 0.2$ Vs^{-1}. Addition of Me_6TREN or TPMA shifted the peak couple to more negative potentials, as shown in **Table 4.1**. This potential shift allowed to measure the ratio of β^{II}/β^{I}. In all solvents, β^{II} was much higher than β^{I} for both ligands. The negative shift of the peak couple indicates that both ligands form more stable complexes with Cu^{2+} than Cu^{+}, in good agreement with literature reports.[59-61] Also, the kinetics of electron transfer was enhanced on passing from solvated Cu^{2+} to $[Cu^{II}L]^{2+}$, with a decrease of ΔE_p from 86 – 160 mV to 78 – 84 mV.

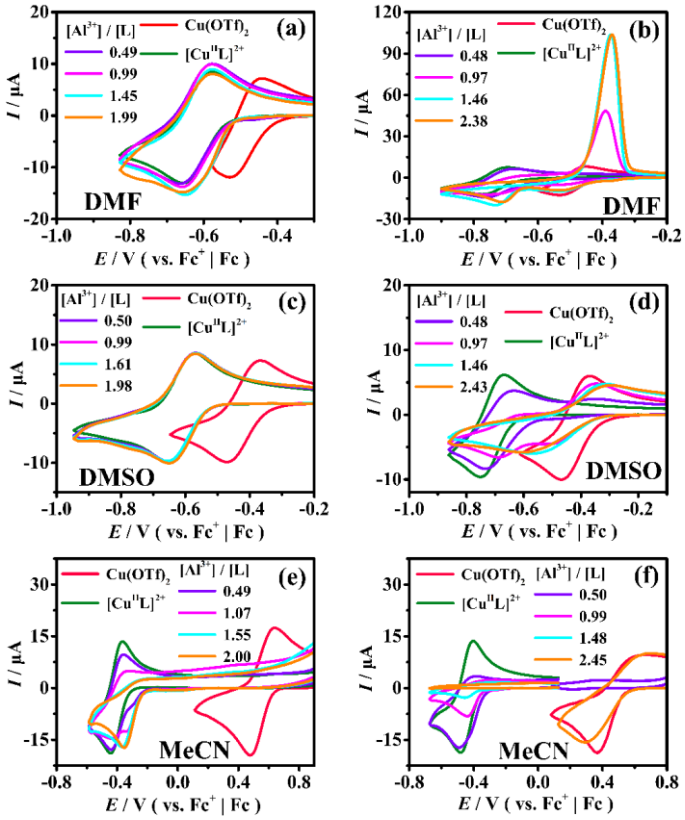

Figure 4.4 CVs of 1 mM $Cu(OTf)_2$ before and after addition of 1 equivalent of ligand to form $[Cu^{II}L]^{2+}$ and after further addition of Al^{3+} at different concentrations, recorded at $v = 0.2$ V s^{-1} on a GC disk in DMF **(a, b)**, DMSO **(c, d)** and MeCN **(e, f)**, with 0.1 M Et_4NBF_4 as the supporting electrolyte, $T = 25$ °C.

Addition of Al^{3+} to solutions of $[Cu^{II}L]^{2+}$ caused dramatic changes to the CV response of the copper complexes. Again, a difference of behavior was observed

between TPMA and Me_6TREN. No significant changes of both the voltametric patterns and $E^{\ominus}$ were observed when increasing amounts of Al^{3+} were added to $[Cu^{II}TPMA]^{2+}$ in either DMF or DMSO (**Figure 4.4 a, c** and **Table 4.1 entries 1, 3**). This points out that TPMA has a much higher affinity for Cu^{2+} ions than Al^{3+}, so that there is no competition for the ligand when both ions are present in solution. It is important to stress that $[Cu^{II}TPMA]^{2+}$ continued to exhibit a reversible peak couple after addition of Al^{3+} ions. This means that the ligand binds both Cu^{2+} and Cu^{+} better than Al^{3+}. In fact, as previously discussed, CV investigations did not show any significant interaction between Al^{3+} and TPMA (**Figure 4.1, 4.2**).

Table 4.1 Cyclic voltammetric data of $[Cu^{II}L]^{2+}$ in the absence and presence of Al^{3+}.[a]

Entry	Solvent	Ligands	Cu^{2+}/Cu^{+}	$[Cu^{II}L]^{2+}/[Cu^{I}L]^{+}$	β^{II}/β^{I}	$C_{Al^{3+}}$ / C_L			
			$E^{\ominus}$ (V)	$E^{\ominus}$ (V)		$E^{\ominus}$ (V)[b]	$E^{\ominus}$ (V)[c]	$E^{\ominus}$ (V)[d]	$E^{\ominus}$ (V)[e]
1	DMF	TPMA	-0.489	-0.617	1.5×10^{2}	-0.620	-0.619	-0.615	-0.615
2		Me_6TREN	-0.489	-0.735	1.4×10^{4}	-0.718	n/a	n/a	n/a
3	DMSO	TPMA	-0.425	-0.615	1.6×10^{3}	-0.610	-0.611	-0.611	-0.610
4		Me_6TREN	-0.425	-0.714	7.5×10^{4}	-0.684	n/a	n/a	n/a
5	MeCN	TPMA	0.616	-0.405	1.8×10^{17}	-0.398	-0.380	n/a	n/a
6		Me_6TREN	0.616	-0.442	7.5×10^{17}	-0.442	n/a	n/a	n/a

[a] Recorded at a glassy carbon working electrode, scan rate = 0.2 V/s, $E^{\ominus}$ (V) vs $Fc^{+}|Fc$;

[b] $C_{Al^{3+}}$ / C_L ~ 0.5, [c] $C_{Al^{3+}}$ / C_L ~ 1.0, [d] $C_{Al^{3+}}$ / C_L ~ 1.5, [e] $C_{Al^{3+}}$ / C_L ~ 2.0.

In contrast to the behavior observed in DMF and DMSO, addition of increasing amounts of Al^{3+} to a $[Cu^{II}TPMA]^{2+}$ solution in MeCN caused some changes (**Figure 4.4 e**). As the $[Al^{3+}]/[TPMA]$ ratio was increased from 0 to 2.0 for a fixed value of $[Cu^{2+}]$ = [TPMA] = 1 mM, the cathodic peak with E_p = -0.44 V was gradually replaced by a new one with E_p = -0.35 V, while the anodic peak completely disappeared. Obviously, Al^{3+} affects the stability the $[Cu^{II}L]^{2+}/[Cu^{I}L]^{+}$ redox couple but the presence of the cathodic peak even after excess Al^{3+} over $[Cu^{II}TPMA]^{2+}$ argues against dissociation of the latter to hand over the ligand to Al^{3+}. The absence of the peak couple with $E_{1/2}$ =

0.56 V, due to the quasi-reversible reduction of solvated Cu^{2+} ions, even in the presence of excess Al^{3+} ions confirms that exchange of the ligand between $[Cu^{II}TPMA]^{2+}$ and Al^{3+} does not occur. It is more likely that $[Cu^{I}TPMA]^{+}$ rather than $[Cu^{II}TPMA]^{2+}$ becomes unstable in the presence of Al^{3+} ions, so that the overall process underlying the irreversible cathodic peak involves reduction of $[Cu^{II}TPMA]^{2+}$ followed by ligand exchange between Cu^{+} and Al^{3+} (**eqs. 4-4, 4-5**). Note that the stoichiometry of Al(III) complexes with tetradentate amine ligands such as TPMA or Me_6TREN is not known. Here we simply assume 1:1 stoichiometry with solvent molecules binding to any remaining coordination sites of the metal. As such, it can be concluded that the stability of the complexes formed by Al^{3+} and copper ions with TPMA follows the order: $[Cu^{II}TPMA]^{2+} > [Al^{III}TPMA]^{3+} > [Cu^{I}TPMA]^{+}$.

$$[Cu^{II}TPMA]^{2+} + e^{-} \rightleftarrows [Cu^{I}TPMA]^{+} \quad (4\text{-}4)$$

$$[Cu^{I}TPMA]^{+} + Al^{3+} \rightleftarrows [Al^{III}TPMA]^{3+} + Cu^{+} \quad (4\text{-}5)$$

When Me_6TREN was used, the voltammetric pattern of $[Cu^{II}L]^{2+}$ was affected by Al^{3+} in all solvents (**Figure 4.4 b, d, f**). As the concentration of added Al^{3+} was increased, the reversible peak couple for $[Cu^{II}L]^{2+}/[Cu^{I}L]^{+}$ gradually decreased in current intensity until disappearance, while the peak couple for solvated Cu^{2+} ions appeared and increased in height. When the $[Al^{3+}]/[L]$ ratio was increased from 0.5 to 2.5 the reversible peak couple of $[Cu^{II}MeTREN]^{2+}/[Cu^{I}MeTREN]^{+}$ completely disappeared. The anodic peak for $[Cu^{I}Me_6TREN]^{+}$ oxidation disappeared in the presence of relatively low $[Al^{3+}]/[L]$ ratio in MeCN. These findings clearly point out that copper complexes in MeCN are not stable in the presence of Al^{3+} ions, following the stability order of $[Al^{III}Me_6TREN]^{3+} > [Cu^{II}Me_6TREN]^{2+} > [Cu^{I}Me_6TREN]^{+}$. Competitive equilibria leading to the displacement of Cu ions with Al^{3+} in the metal complex occur in solution (**eq. 4-6**). The resulting solvated Cu^{2+} ions exhibit their quasi-reversible peak couple in DMSO and MeCN (**Figure 4.4 d, f**).

$$[Cu^{II}Me_6TREN]^{2+} + Al^{3+} \rightleftarrows [Al^{III}Me_6TREN]^{3+} + Cu^{2+} \quad (4\text{-}6)$$

When Al^{3+} ions were added to $[Cu^{II}Me_6TREN]^{2+}$ in DMF, besides the cathodic

peak at -0.53 V for the reduction of Cu^{2+} to Cu^{+}, a second cathodic peak appeared around -0.72 V, followed by an intense anodic stripping peak at ca -0.37 V on scan reversal (**Figure 4.4 b**). The second cathodic peak is attributed to the reduction of Cu^{+} to metallic Cu which deposits on the electrode surface and therefore gives an anodic stripping peak upon oxidation in the reverse scan (**eqs. 4-7, 4-8**).

$$Cu^{+} + e^{-} \rightleftarrows Cu_{ads} \quad (4\text{-}7)$$

$$Cu_{ads} \rightleftarrows Cu^{2+} + 2e^{-} \quad (4\text{-}8)$$

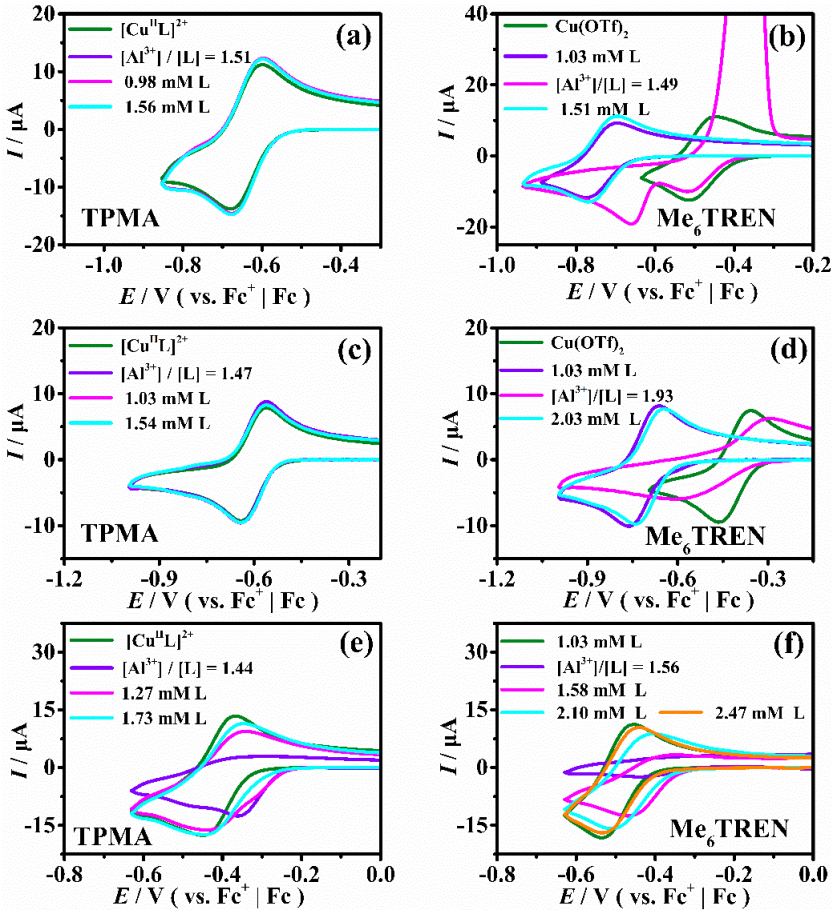

Figure 4.5 CVs of 1 mM $Cu(OTf)_2$ and 1 mM $[Cu^{II}L]^{2+}$ before and after stepwise addition of Al^{3+} and ligand (L), recorded at $\upsilon = 0.2$ V s^{-1} on a GC disk in DMF **(a-b)**, DMSO **(c-d)** and MeCN **(e-f)**, with 0.1 M Et_4NBF_4 as the supporting electrolyte, T = 25 °C.

Interestingly, when more ligand was added to $[Cu^{II}MeTREN]^{2+}$ solutions containing also Al^{3+}, the competitive complexation equilibria were satisfied for both

Cu^{2+} and Al^{3+} and almost full recovery of the electrochemical pattern of $[Cu^{II}MeTREN]^{2+}$ was observed (**Figure 4.5**).

4.3.3 Investigations of the effect of Al^{3+} on the stability of $[Cu^{I}L]^{+}$ in MeCN

In order to obtain more details on the mechanism of $[Cu^{I}L]^{+}$ disappearance in the presence of Al^{3+} in MeCN, cyclic voltammetry and linear sweep voltammetry of in-situ prepared $Cu^{I}L^{+}$ (L = TPMA or Me_6TREN) in MeCN + 0.1 M Et_4NBF_4 were performed at a glassy carbon RDE. **Figure 4.6** shows CVs of $Cu(I)(MeCN)_4BF_4$ in MeCN before and after addition of TPMA, and after further progressive addition of Al^{3+} ions and excess ligand. Note that the CVs were recorded starting from potentials were Cu(I) does not undergo oxidation and the forward scan goes in the positive direction. In MeCN, solvated Cu^{+} ions showed a quasi-reversible peak couple with anodic to cathodic peak separation, $\triangle E_p$ = 268 mV and $E_{1/2}$ = 0.542 mV at υ = 0.2 Vs^{-1}. After addition of 1 equivalent of TPMA to form $[Cu^{I}TPMA]^{+}$, the quasi-reversible peak couple at $E_{1/2}$ = 0.542 mV was replaced by a new couple with $E_{1/2}$ = -0.403 mV. Also, the kinetics of electron transfer was enhanced with a decrease of $\triangle E_p$ from 268 mV to 84 mV. The negative shift of the peak couple indicates that TPMA forms more stable complexes with Cu^{2+} than Cu^{+}, in good agreement with the previously discussed results. In the initial CV pattern of $[Cu^{I}TPMA]^{+}$, the negative current at the starting potential (-0.76 V) of the forward scan indicated the presence of $[Cu^{II}TPMA]^{2+}$, which undergoes reduction to $[Cu^{I}TPMA]^{+}$ at this potential. $[Cu^{II}TPMA]^{2+}$ probably arises from oxidation of $[Cu^{I}TPMA]^{+}$ by O_2, which adventitiously entered the cell during TPMA addition. Consecutive addition of Al^{3+} to the solution of $[Cu^{I}TPMA]^{+}$ by anodic dissociation of an Al wire immersed in the solution caused the anodic peak current to decrease gradually with the ratio of Al^{3+} to L, as shown in **Figure 4.6 a**. In addition, slight positive shifts of the cathodic peak with decrease of intensity were observed.

This set of CVs clearly show that at the end, nearly no Cu^{I} species either in the form of $[Cu^{I}L]^{+}$ or Cu^{+} was present as no anodic peak was observed. On the other hand, the cathodic peak for $[Cu^{II}L]^{2+}$ never disappeared, indicating that Cu^{I} undergoes

oxidation to Cu^{II} during the experiment. As inspection of **Figure 4.7** indicates, the dark yellow color typical of air-sensitive $[Cu^{I}TPMA]^{+}$ in MeCN,[62] decreased and eventually changed to green (**Figure 4.7 d**) after addition of a 2.5-fold excess of Al^{3+} over $[Cu^{I}L]^{+}$. This color variation during the whole electrolysis process demonstrated the potential generation of $[Cu^{II}TPMA]^{2+}$ complex. Indeed, after addition of excess TPMA, the multiple competitive equilibria were satisfied for both copper and aluminum ions and almost full recovery of the starting voltametric pattern was observed (**Figure 4.6 b**).

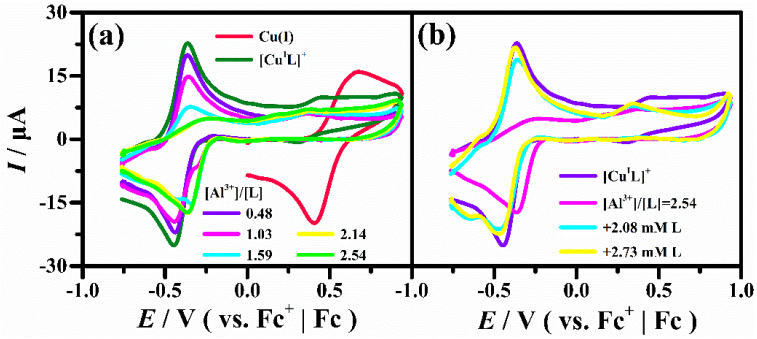

Figure 4.6 CVs of 1 mM $Cu(I)(MeCN)_4BF_4$ and 1 mM $[Cu^{I}TPMA]^{+}$ before and after stepwise addition of **(a)** Al^{3+} by anodic dissolution of Al and **(b)** TPMA, recorded at υ = 0.2 V s^{-1} on a GC disk in MeCN, with 0.1 M Et_4NBF_4 as the supporting electrolyte, T = 25 °C.

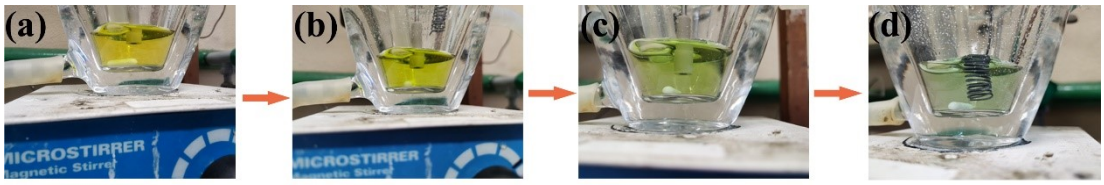

Figure 4.7 Digital photographs of 1 mM $[Cu^{I}TPMA]^{+}$ in MeCN at different stages of stepwise addition of Al^{3+} ions by anodic dissolution of an Al wire immersed in solution.

To further explore the mechanism of $[Cu^{I}L]^{+}$ conversion to $[Cu^{II}L]^{2+}$ upon Al^{3+} addition, a series of experiments were performed via various electrochemical methods. As was previously shown for investigations on ATRP initiation kinetics, the concentration of $[Cu^{I}L]^{+}$ can be easily monitored by chronoamperometry.[63] To avoid

possible interference of the Al wire, the method of Al^{3+} addition was changed: additions were made from a stock solution of Al^{3+} ions prepared in a separate experiment. Additionally, linear sweep voltammetry (LSV) at a RDE was used in place of cyclic voltammetry at a stationary electrode. **Figure 4.8** shows LSVs recorded for $[Cu^{I}L]^{+}$ before and after additions of Al^{3+} in MeCN. Before addition of Al^{3+}, a well-defined anodic wave was observed for $[Cu^{I}L]^{+}$ oxidation with L = TPMA or Me_6TREN (**Figure 4.8 a-c**). The quantity of $[Cu^{II}L]^{2+}$ present in solution was evaluated to be ca 3% of the total copper (**Figure 4.8 a, b**). Chronoamperometry under steady state conditions was used to monitor the decay of $[Cu^{I}L]^{+}$. This consists in an instantaneous shift of the potential of the RDE (at a fixed angular velocity) from an initial value (-1.0 V), where no oxidation process occurs at the electrode, to a value (0.1 V) in the plateau region where the electrode process has the maximum rate, producing a limiting current (I_L). Maintaining the system at this state for ca 480s, I_L remained substantially constant (**Figure 4.9 a**); according to the charge passed during this period, approximately 1% of $[Cu^{I}L]^{+}$ was oxidized to $[Cu^{II}L]^{2+}$ at the RDE. Subsequently, injecting a solution of Al^{3+} ions into the cell caused a steep decrease of I_L in a couple of seconds and then reached a stable region, as illustrated in **Figure 4.9 a**.

For the sake of comparison, the experiment was repeated by increasing the quantity of added Al^{3+} ions (1.6 mL instead of 0.5 mL of the stock solution). A similar behavior was observed but the limiting current drop was higher when a higher volume of Al^{3+} solution was injected (**Figure 4.9 b**). These I_L changes clearly indicate decrease of $[Cu^{I}L]^{+}$ concentration in solution. Indeed, I_L depends on $C_{[Cu^{I}L]^{+}}$ according to the Levich equation:[64]

$$I_L = 0.62nFAD^{2/3}v^{-1/6}\omega^{1/2}C_{[Cu^{I}L]^{+}} \quad (4\text{-}9)$$

where D is the diffusion coefficient of $[Cu^{I}L]^{+}$, n is the number of exchanged electrons, F is the Faraday constant, v is the kinematic viscosity and ω is the angular velocity of the RDE. **Figure 4.9 a, b** indicated that I_L dropped by about 50% and 100% after injectting 0.5 mL and 1.6 mL of 23 mM Al^{3+} ions in MeCN to $[Cu^{I}TPMA]^{+}$, respectively.

Loss of $[Cu^{I}TPMA]^{+}$ is also confirmed by solution color change from dark yellow of the starting solution to light yellow or transparent, as the inserts of **Figure 4.9 a, b** show.

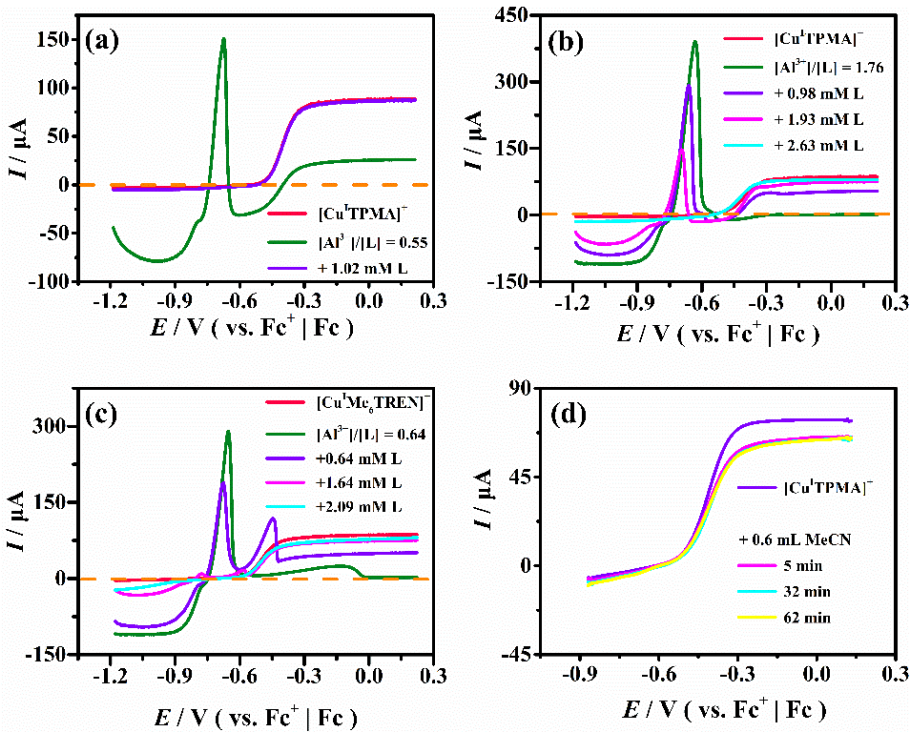

Figure 4.8 LSVs of 1 mM $[Cu^{I}L]^{+}$ in MeCN + 0.1 M Et_4NBF_4 (V = 20 mL), before and after addition of **(a)** 0.5 mL, **(b)** 1.6 mL, **(c)** 0.6 mL 23 mM Al^{3+} ions, and further excess of L, or **(d)** 0.6 mL of pure MeCN, recorded at v = 0.2 V s^{-1} on a glass carbon, v = 0.005 V s^{-1} and ω = 2500 rpm on a rotating disc electrode, T = 25 °C.

LSVs recorded after Al^{3+} addition to $[Cu^{I}TPMA]^{+}$ solutions are reported in **Figure 4.8 a, b**. When 0.5 mL of Al^{3+} solution was added, a decrease of about 50% of the anodic wave was observed, whereas addition of 1.6 mL in the second experiment caused complete disappearance of the wave. Furthermore, it is of interest to note that a new cathodic wave at $E_{1/2}$ = -0.815 V and an anodic striping peak at -0.65 V appeared after Al^{3+} addition (**Figure 4.8 a, b**). These new signals can be assigned to reduction of "free" Cu^{+} ions to metallic Cu that deposits on the electrode surface and is oxidized back to Cu^{+} by anodic stripping at -0.65 V.

Similar results were also found for $[Cu^{I}Me_6TREN]^{+}$. As illustrated in **Figure 4.8 c** and **Figure 4.9 c**. The initial current decreased instantaneously by about 80% when 0.4 mL of the Al^{3+} solution was injected. After this drop, the current remained constant,

but when 0.2 mL of 23 mM Al^{3+} solution in MeCN was added, I_L dropped to zero, indicating disappearnce of $[Cu^{I}L]^{+}$. LSV recorded after the second addition of Al^{3+} shows the cathodic wave assigned to Cu^{+} reduction and the associated anodic stripping of electrodeposited Cu^{0} (**Figure 4.8 c**).

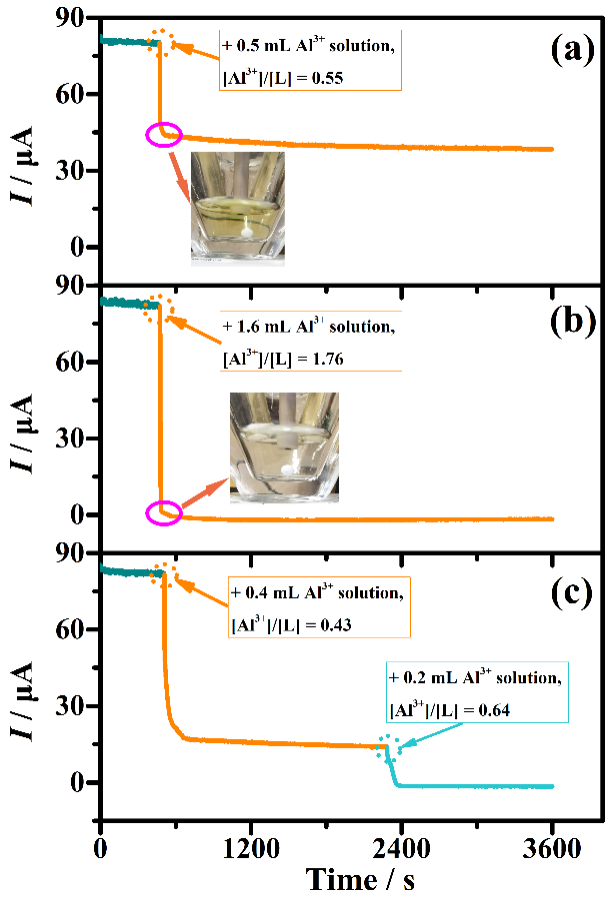

Figure 4.9 Chronoamperometry of 1 mM $[Cu^{I}L]^{+}$ in MeCN + 0.1 M Et_4NBF_4 at a rotating disc electrode at v = 0.005 V s^{-1} and ω = 2500 rpm for L = TPMA **(a,b)**, and Me_6TREN **(c)** before and after addition of Al^{3+} ions solution at different time points, T = 25 °C.

When excess ligand was added to solutions containing $[Cu^{I}L]^{+}$ and Al^{3+}, the LSV pattern of the starting $[Cu^{I}L]^{+}$ was almost fully restored (**Figure 4.8 a, b, c**). The recovered I_L was slightly lower than the starting value because of slight dilution due to the additions and some oxidation of $[Cu^{I}L]^{+}$ by O_2 introduced in the cell during solution injection. To check this last hypothesis, a blank experiment in which 0.6 mL of MeCN were added to a 1 mM solution of $[Cu^{I}L]^{+}$. A slight but instantaneous decrease of I_L, which then remained constant, was observed (**Figure 4.8 d**).

To sum up, all observations point to a rapid decomplexation of $[Cu^{I}L]^{+}$ when Al^{3+} ions are added. Some unknown Al(III) complex is formed while Cu^{+} ions go into solution and remain stable as solvated ions. When after Al^{3+} injection excess ligand, enough to make complexes with both Al^{3+} and Cu^{+} is added, $[Cu^{I}L]^{+}$ is reformed. As discussed in section **4.3.2**, CV investigations of $[Cu^{II}L]^{2+}$ with progressive addition of Al^{3+} have shown that Cu complexes with Me_6TREN are not stable in the presence of Al^{3+} in all selected solvents, whereas TPMA forms more stable complexes with Cu^{2+} and Cu^{+} than with Al^{3+} in DMF and DMSO. Also $[Cu^{II}TPMA]^{2+}$ is stable in MeCN containing Al^{3+}. However, Al^{3+} displaces Cu^{+} from its complex with TPMA in MeCN. Therefore, it is highly likely that *e*ATRP in undivided cells with Al anode will suffer from competitions between Al^{3+} released from the anode and Cu ions for Me_6TREN in all investigated solvents and TPMA only in MeCN.

4.3.4 UV-vis-NIR analysis of L, Cu^{2+}, and $[Cu^{II}L]^{2+}$ in the presence of Al^{3+}

On the other hand, as shown in **Figure 4.10**, the solution color of $[Cu^{II}Me_6TREN]^{2+}$ changed from dark green to colorless in DMF and DMSO or other color in MeCN when the $[Al^{3+}]/[L]$ ratio reached 1.5. Interestingly, the initial solution color was almost recovered upon adding excess ligand to guarantee enough ligand for both copper and aluminum ions. In contrast, no color changes were observed when Al^{3+} ions were added to solutions of the ligands. **Figure 4.11** also evidenced the absence of any significant absorption peak for TPMA or Me_6TREN in the presence of Al^{3+} in the UV-vis-NIR region from 350 to 1400 nm.

Some evidence of the formation of Al^{3+} complexes with TPMA and Me_6TREN at the detriment of $[Cu^{II}L]^{2+}$ can be obtained by analyzing changes of absorbance as a function of added Al^{3+} concentration. According to the Beer-Lambert law,[65] **eq. 4-11**, the absorption intensity is proportional to substance concentration:

$$\boldsymbol{A = \varepsilon\, l\, C} \tag{4-10}$$

where $\boldsymbol{A}$ is the absorbance of a substance in solution, $\boldsymbol{\varepsilon}$ is its molar absorptivity ($M^{-1}\cdot cm^{-1}$), $\boldsymbol{l}$ is the length of light path (cm), here it is 1.0 cm, $\boldsymbol{C}$ is the concentration of the

substance (M). Therefore, the loss of copper complexes due to the presence of Al^{3+} could be also evaluated through $[Cu^{II}L]^{2+}$ spectral changes during the experiments.

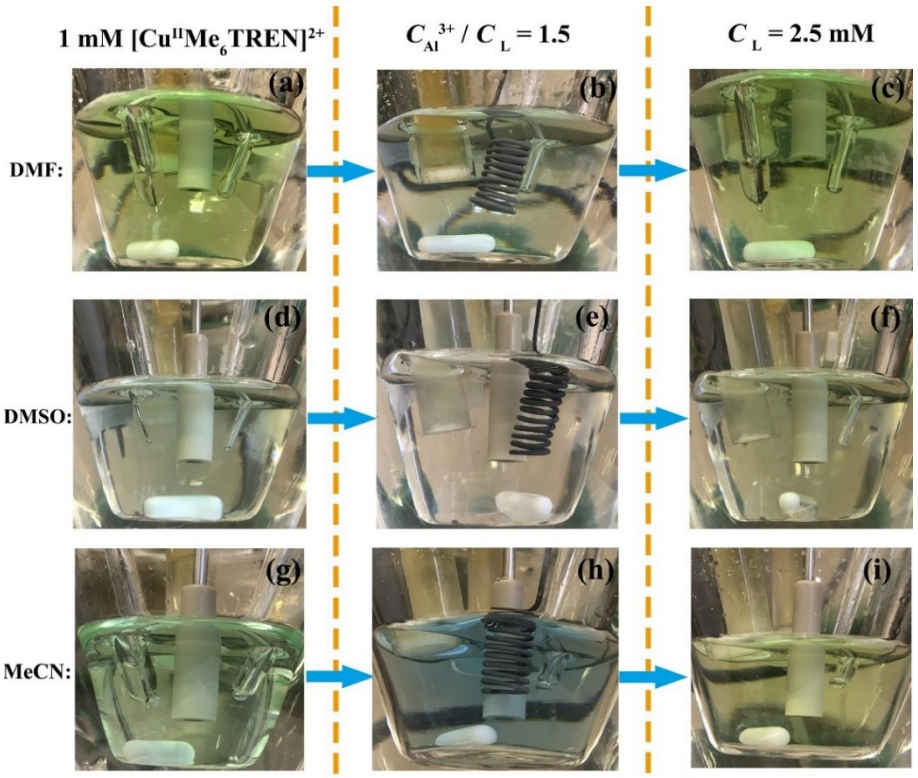

Figure 4.10 Digital photographs of 1 mM $[Cu^{II}Me_6TREN]^{2+}$ in the absence **(a,d,g)** and presence of Al^{3+} alone **(b, e, h)** or Al^{3+} and excess ligand **(c, f, i)** in DMF **(a - c)**, DMSO **(d - f)**, and MeCN **(g - i).**

Figure 4.12 shows UV-vis spectra of $Cu(OTf)_2$ and $[Cu^{II}L]^{2+}$ recorded in different solvents before and after progressive addition of Al^{3+} ions. Solvated Cu^{2+} ions showed a broad absorption band with a maximum wavelength (λ_{max}) varying between 780 nm and 894 nm, depending on solvent. When TPMA or Me_6TREN was added, the newly formed $[Cu^{II}L]^{2+}$ species showed a broad band centered around 890 nm and a shoulder around 700 nm. These spectra are consistent with published spectra for Cu^{II} complexes of trigonal bipyramidal geometry with tripodal nitrogen-based ligands such as TPMA and Me_6TREN, which typically show a broad band with λ_{max} > 800 nm corresponding to d_{xy}, d_{x^2}-d_{y^2}→d_{z^2} with a higher energy shoulder (d_{xz}, d_{yz}→d_{z^2}).[52, 57, 61, 66-68]

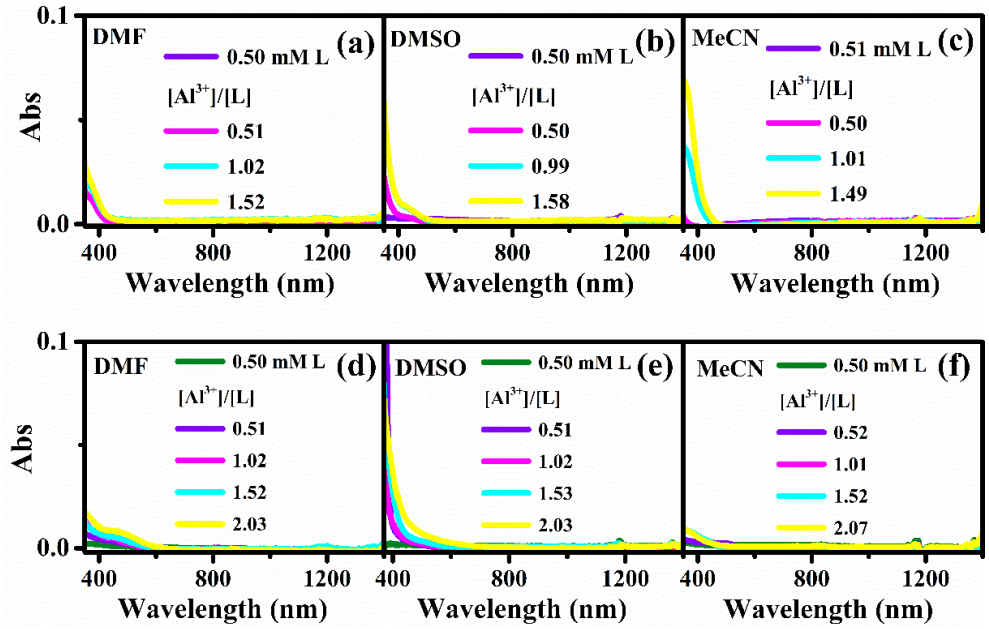

Figure 4.11 UV-vis-NIR spectra of TPMA **(a-c)** or Me_6TREN **(d-f)** in the absence and presence of Al^{3+} ions, recorded in DMF, DMSO, and MeCN in a 10 mm pathlength cuvette.

Addition of increasing amounts of Al^{3+} to solutions of $[Cu^{II}TPMA]^{2+}$ in the three investigated solvents did not cause any change to the spectra recorded in the 500-1400 nm range for $[Cu^{II}L]^{2+}$ (**Figure 4.12 a, c, e** and **Figure 4.13 a**). This agrees very well with the CV experiments: TPMA could steadily coordinate with Cu^{2+} than Al^{3+} so that $[Cu^{II}TPMA]^{2+}$ is not destroyed even in the presence of excess Al^{3+}. In the case of TPMA in MeCN, a new complex was formed, and its concentration increased with Al^{3+}, as proved by the increase of absorption intensity near the band centered around 440 nm in **Figure 4.12 e**. Conversely, the intensity of the UV-vis spectrum of $[Cu^{II}Me_6TREN]^{2+}$ progressively decreased as increasing amounts of Al^{3+} were added to the solution (**Figure 4.12 b, d, f**). In this case, Me_6TREN has higher affinity for Al^{3+} than Cu^{2+} so that a ligand exchange reaction occurs and free Cu^{2+} ions go into solution (**eq. 4-6**). When excess Al^{3+} was added, the UV-vis spectrum tended toward that recorded for solvated Cu^{2+} ions. These competitive equilibria involving the ligand, Cu^{2+} and Al^{3+} ions were well-evidenced by the decrease of absorption value at 880 nm in **Figure 4.13 b**.

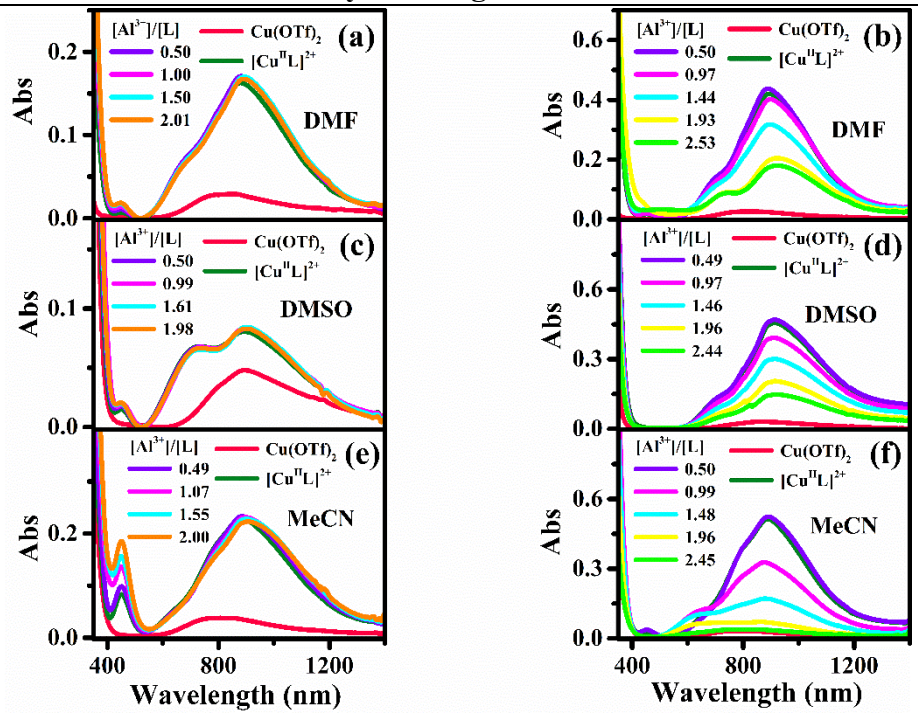

Figure 4.12 UV-vis-NIR spectra of 1 mM $Cu(OTf)_2$ recorded in DMF, DMSO, and MeCN in a 10 mm pathlength cuvette in the absence and presence of 1 mM amine ligand (L), and after further addition of Al^{3+} ions; L= TPMA **(a, c, e)** or Me_6TREN **(b, d, f)**.

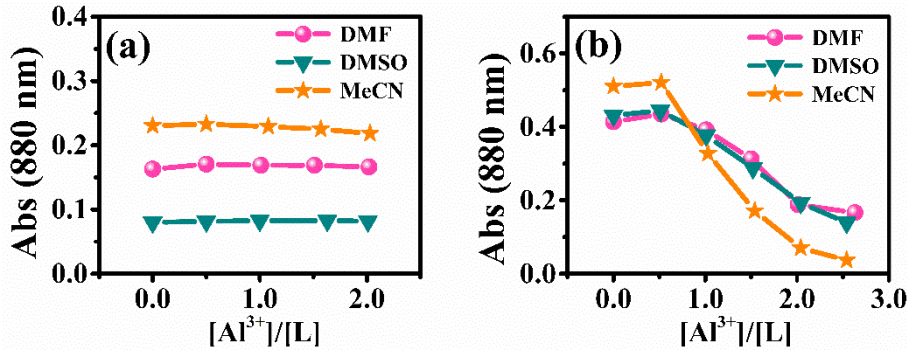

Figure 4.13 Absorbance of 1 mM $[Cu^{II}L]^{2+}$ measured at 880 nm as a function of added Al^{3+} ions for TPMA **(a)** or Me_6TREN **(b)** in different solvents, T = *25 °C*.

4.4 Conclusions

To sum up, cyclic voltammetry, linear sweep voltammetry, and UV-vis-NIR investigations on the stability of copper complexes with two amine ligands (TPMA and

Me_6TREN) in DMF, DMSO and MeCN in the presence of Al^{3+} ions have shown that $[Cu^{II}TPMA]^{2+}$ is not affected by Al^{3+} in DMF and DMSO. Both TPMA and Me_6TREN are capable of forming complexes with Al^{3+} in the selected solvents. It appears that TPMA could react with Cu^{2+} in MeCN rather than Al^{3+}, whereas competition between the metal ions becomes important when Cu^{II} is reduced to Cu^{I}, especially in the presence of high concentration of Al^{3+}. This distinctive competition reaction between the Cu^{I} and Al^{3+} on TPMA affects the activation process during *e*ATRP. In contrast, Cu complexes with Me_6TREN are destroyed by Al^{3+} in all investigated solvents. The investigations suggested that Me_6TREN forms more stable complexes with Al^{3+} than Cu^{2+} or Cu^{+}. To keep Cu^{II} and Cu^{I} complexes in solution when also Al^{3+} ions are present, enough ligand to make complexes with both metals should be added and experiments have shown that a 1:1 molar ratio between ligand and total amount of metal ions (Cu^{2+} + Al^{3+}) is enough.

References

[1]. Shipp, D. A., Reversible-deactivation radical polymerizations. *Polymer Reviews* **2011,** *51* (2), 99-103.
[2]. Matyjaszewski, K.; Gao, H.; Sumerlin, B. S.; Tsarevsky, N. V., *Reversible Deactivation Radical Polymerization: Mechanisms and Synthetic Methodologies*. American Chemical Society: 2018.
[3]. Corrigan, N.; Jung, K.; Moad, G.; Hawker, C. J.; Matyjaszewski, K.; Boyer, C., Reversible-deactivation radical polymerization (Controlled/living radical polymerization): From discovery to materials design and applications. *Progress in Polymer Science* **2020**, 101311.
[4]. Grubbs, R. B., Nitroxide-mediated radical polymerization: limitations and versatility. *Polymer Reviews* **2011,** *51* (2), 104-137.
[5]. Hurtgen, M.; Detrembleur, C.; Jerome, C.; Debuigne, A., Insight into organometallic-mediated radical polymerization. *Polymer Reviews* **2011,** *51* (2), 188-213.
[6]. Allan, L. E.; Perry, M. R.; Shaver, M. P., Organometallic mediated radical polymerization. *Progress in polymer science* **2012,** *37* (1), 127-156.
[7]. Barner-Kowollik, C., *Handbook of RAFT polymerization*. John Wiley & Sons: 2008.
[8]. Destarac, M., On the critical role of RAFT agent design in reversible addition-fragmentation chain Transfer (RAFT) polymerization. *Polymer reviews* **2011,** *51* (2), 163-187.
[9]. Semsarilar, M.; Perrier, S., 'Green'reversible addition-fragmentation chain-transfer (RAFT) polymerization. *Nature chemistry* **2010,** *2* (10), 811.
[10]. Ayres, N., Atom transfer radical polymerization: a robust and versatile route for polymer synthesis. *Polymer Reviews* **2011,** *51* (2), 138-162.
[11]. Matyjaszewski, K., Atom transfer radical polymerization (ATRP): current status and future perspectives. *Macromolecules* **2012,** *45* (10), 4015-4039.
[12]. Matyjaszewski, K.; Spanswick, J., Copper-Mediated Atom Transfer Radical Polymerization. **2012**.
[13]. Matyjaszewski, K.; Tsarevsky, N. V., Macromolecular engineering by atom transfer radical polymerization. *J Am Chem Soc* **2014,** *136* (18), 6513-33.
[14]. Matyjaszewski, K., Advanced Materials by Atom Transfer Radical Polymerization. *Adv Mater* **2018,** *30* (23), e1706441.
[15]. Pan, X.; Fantin, M.; Yuan, F.; Matyjaszewski, K., Externally controlled atom transfer radical polymerization. *Chem Soc Rev* **2018,** *47* (14), 5457-5490.
[16]. Lin, C. Y.; Coote, M. L.; Gennaro, A.; Matyjaszewski, K., Ab initio evaluation of the thermodynamic and electrochemical properties of alkyl halides and radicals and their mechanistic implications for atom transfer radical polymerization. *Journal of the American Chemical Society* **2008,** *130* (38), 12762-12774.
[17]. Braunecker, W. A.; Tsarevsky, N. V.; Gennaro, A.; Matyjaszewski, K., Thermodynamic components of the atom transfer radical polymerization equilibrium:

quantifying solvent effects. *Macromolecules* **2009,** *42* (17), 6348-6360.
[18**]**. Wang, Y.; Kwak, Y.; Buback, J.; Buback, M.; Matyjaszewski, K., Determination of ATRP equilibrium constants under polymerization conditions. *ACS Macro Letters* **2012,** *1* (12), 1367-1370.
[19**]**. Jakubowski, W.; Matyjaszewski, K., Activators regenerated by electron transfer for atom-transfer radical polymerization of (meth) acrylates and related block copolymers. *Angewandte Chemie International Edition* **2006,** *45* (27), 4482-4486.
[20**]**. Jakubowski, W.; Min, K.; Matyjaszewski, K., Activators regenerated by electron transfer for atom transfer radical polymerization of styrene. *Macromolecules* **2006,** *39* (1), 39-45.
[21**]**. Braidi, N.; Buffagni, M.; Ghelfi, F.; Parenti, F.; Gennaro, A.; Isse, A. A.; Bedogni, E.; Bonifaci, L.; Cavalca, G.; Ferrando, A., ARGET ATRP of styrene in EtOAc/EtOH using only Na2CO3 to promote the copper catalyst regeneration. *Journal of Macromolecular Science, Part A* **2021,** *58* (6), 376-386.
[22**]**. Ramu, A.; Rajendrakumar, K., Natural catalyst mediated ARGET and SARA ATRP of N-isopropylacrylamide and methyl acrylate. *Polymer Chemistry* **2020,** *11* (3), 687-694.
[23**]**. Abreu, C. M.; Mendonça, P. V.; Serra, A. n. C.; Popov, A. V.; Matyjaszewski, K.; Guliashvili, T.; Coelho, J. F., Inorganic sulfites: Efficient reducing agents and supplemental activators for atom transfer radical polymerization. *Acs Macro Letters* **2012,** *1* (11), 1308-1311.
[24**]**. Konkolewicz, D.; Wang, Y.; Krys, P.; Zhong, M.; Isse, A. A.; Gennaro, A.; Matyjaszewski, K., SARA ATRP or SET-lRP. end of controversy? *Polymer Chemistry* **2014,** *5* (15), 4396-4417.
[25**]**. Chmielarz, P.; Krys, P.; Park, S.; Matyjaszewski, K., PEO-b-PNIPAM copolymers via SARA ATRP and *e*ATRP in aqueous media. *Polymer* **2015,** *71*, 143-147.
[26**]**. Matyjaszewski, K.; Jakubowski, W.; Min, K.; Tang, W.; Huang, J.; Braunecker, W. A.; Tsarevsky, N. V., Diminishing catalyst concentration in atom transfer radical polymerization with reducing agents. *Proceedings of the National Academy of Sciences* **2006,** *103* (42), 15309-15314.
[27**]**. Konkolewicz, D.; Magenau, A. J.; Averick, S. E.; Simakova, A.; He, H.; Matyjaszewski, K., ICAR ATRP with ppm Cu Catalyst in Water. *Macromolecules* **2012,** *45* (11), 4461-4468.
[28**]**. Tsarevsky, N. V.; Matyjaszewski, K., "Green" atom transfer radical polymerization: from process design to preparation of well-defined environmentally friendly polymeric materials. *Chemical reviews* **2007,** *107* (6), 2270-2299.
[29**]**. Chen, M.; Zhong, M.; Johnson, J. A., Light-controlled radical polymerization: mechanisms, methods, and applications. *Chemical reviews* **2016,** *116* (17), 10167-10211.
[30**]**. Dadashi-Silab, S.; Doran, S.; Yagci, Y., Photoinduced electron transfer reactions for macromolecular syntheses. *Chemical reviews* **2016,** *116* (17), 10212-10275.
[31**]**. Konkolewicz, D.; Schröder, K.; Buback, J.; Bernhard, S.; Matyjaszewski, K., Visible Light and Sunlight Photoinduced ATRP with ppm of Cu Catalyst. *ACS Macro Letters* **2012,** *1* (10), 1219-1223.

[32**]**. Zhang, W.; He, J.; Lv, C.; Wang, Q.; Pang, X.; Matyjaszewski, K.; Pan, X., Atom transfer radical polymerization driven by near-infrared light with recyclable upconversion nanoparticles. *Macromolecules* **2020,** *53* (12), 4678-4684.

[33**]**. Dadashi-Silab, S.; Lorandi, F.; DiTucci, M. J.; Sun, M.; Szczepaniak, G.; Liu, T.; Matyjaszewski, K., Conjugated Cross-linked Phenothiazines as Green or Red Light Heterogeneous Photocatalysts for Copper-Catalyzed Atom Transfer Radical Polymerization. *J Am Chem Soc* **2021,** *143* (25), 9630-9638.

[34**]**. Pan, X.; Malhotra, N.; Simakova, A.; Wang, Z.; Konkolewicz, D.; Matyjaszewski, K., Photoinduced atom transfer radical polymerization with ppm-level Cu catalyst by visible light in aqueous media. *Journal of the American Chemical Society* **2015,** *137* (49), 15430-15433.

[35**]**. Xu, J.; Jung, K.; Atme, A.; Shanmugam, S.; Boyer, C., A robust and versatile photoinduced living polymerization of conjugated and unconjugated monomers and its oxygen tolerance. *Journal of the American Chemical Society* **2014,** *136* (14), 5508-5519.

[36**]**. Magenau, A. J.; Strandwitz, N. C.; Gennaro, A.; Matyjaszewski, K., Electrochemically mediated atom transfer radical polymerization. *Science* **2011,** *332* (6025), 81-4.

[37**]**. Isse, A. A.; Visona, G.; Ghelfi, F.; Roncaglia, F.; Gennaro, A., Electrochemical Approach to Copper-Catalyzed Reversed Atom Transfer Radical Cyclization. *Advanced Synthesis & Catalysis* **2015,** *357* (4), 782-792.

[38**]**. Bortolamei, N.; Isse, A. A.; Magenau, A. J.; Gennaro, A.; Matyjaszewski, K., Controlled aqueous atom transfer radical polymerization with electrochemical generation of the active catalyst. *Angewandte Chemie International Edition* **2011,** *50* (48), 11391-11394.

[39**]**. Chmielarz, P.; Fantin, M.; Park, S.; Isse, A. A.; Gennaro, A.; Magenau, A. J. D.; Sobkowiak, A.; Matyjaszewski, K., Electrochemically mediated atom transfer radical polymerization (*e*ATRP). *Progress in Polymer Science* **2017,** *69*, 47-78.

[40**]**. Lorandi, F.; Fantin, M.; Isse, A. A.; Gennaro, A., Electrochemical triggering and control of atom transfer radical polymerization. *Current Opinion in Electrochemistry* **2018,** *8*, 1-7.

[41**]**. Isse, A. A.; Gennaro, A., Electrochemistry for Atom Transfer Radical Polymerization. *The Chemical Record* **2021**.

[42**]**. Wang, Z.; Pan, X.; Li, L.; Fantin, M.; Yan, J.; Wang, Z.; Wang, Z.; Xia, H.; Matyjaszewski, K., Enhancing Mechanically Induced ATRP by Promoting Interfacial Electron Transfer from Piezoelectric Nanoparticles to Cu Catalysts. *Macromolecules* **2017,** *50* (20), 7940-7948.

[43**]**. Wang, Z.; Pan, X.; Yan, J.; Dadashi-Silab, S.; Xie, G.; Zhang, J.; Wang, Z.; Xia, H.; Matyjaszewski, K., Temporal control in mechanically controlled atom transfer radical polymerization using low ppm of Cu catalyst. *ACS Macro Letters* **2017,** *6* (5), 546-549.

[44**]**. Wang, Z.; Wang, Z.; Pan, X.; Fu, L.; Lathwal, S.; Olszewski, M.; Yan, J.; Enciso, A. E.; Wang, Z.; Xia, H., Ultrasonication-induced aqueous atom transfer radical polymerization. *ACS Macro Letters* **2018,** *7* (3), 275-280.

[45**]**. Poli, R., New Phenomena in Organometallic-Mediated Radical Polymerization (OMRP) and Perspectives for Control of Less Active Monomers. *Chemistry–A European Journal* **2015,** *21* (19), 6988-7001.
[46**]**. Park, S.; Chmielarz, P.; Gennaro, A.; Matyjaszewski, K., Simplified electrochemically mediated atom transfer radical polymerization using a sacrificial anode. *Angew Chem Int Ed Engl* **2015,** *54* (8), 2388-92.
[47**]**. Fantin, M.; Lorandi, F.; Isse, A. A.; Gennaro, A., Sustainable Electrochemically-Mediated Atom Transfer Radical Polymerization with Inexpensive Non-Platinum Electrodes. *Macromol Rapid Commun* **2016,** *37* (16), 1318-22.
[48**]**. Lorandi, F.; Fantin, M.; Isse, A. A.; Gennaro, A., Electrochemically mediated atom transfer radical polymerization of n-butyl acrylate on non-platinum cathodes. *Polymer Chemistry* **2016,** *7* (34), 5357-5365.
[49**]**. De Bon, F.; Isse, A. A.; Gennaro, A., Towards scale-up of electrochemically-mediated atom transfer radical polymerization: Use of a stainless-steel reactor as both cathode and reaction vessel. *Electrochimica Acta* **2019,** *304*, 505-512.
[50**]**. Zaborniak, I.; Chmielarz, P.; Martinez, M. R.; Wolski, K.; Wang, Z.; Matyjaszewski, K., Synthesis of high molecular weight poly(n-butyl acrylate) macromolecules via *se*ATRP: From polymer stars to molecular bottlebrushes. *European Polymer Journal* **2020,** *126*, 109566.
[51**]**. Isse, A. A.; Scialdone, O.; Galia, A.; Gennaro, A., The influence of aluminium cations on electrocarboxylation processes in undivided cells with Al sacrificial anodes. *Journal of Electroanalytical Chemistry* **2005,** *585* (2), 220-229.
[52**]**. Golub, G.; Lashaz, A.; Cohen, H.; Paoletti, P.; Bencini, A.; Valtancoli, B.; Meyerstein, D., The effect of N-methylation of tetra-aza-alkane copper complexes on the axial binding of anions. *Inorganica chimica acta* **1997,** *255* (1), 111-115.
[53**]**. Navon, N.; Golub, G.; Cohen, H.; Paoletti, P.; Valtancoli, B.; Bencini, A.; Meyerstein, D., Design of Ligands That Stabilize Cu(I) and Shift the Reduction Potential of the Cu(II/I) Couple Cathodically in Aqueous Solutions. *Inorg Chem* **1999,** *38* (15), 3484-3488.
[54**]**. Ambundo, E. A.; Deydier, M.-V.; Grall, A. J.; Aguera-Vega, N.; Dressel, L. T.; Cooper, T. H.; Heeg, M. J.; Ochrymowycz, L. A.; Rorabacher, D. B., Influence of Coordination Geometry upon Copper(II/I) Redox Potentials. Physical Parameters for Twelve Copper Tripodal Ligand Complexes. *Inorganic Chemistry* **1999,** *38* (19), 4233-4242.
[55**]**. Pintauer, T.; Matyjaszewski, K., Structural aspects of copper catalyzed atom transfer radical polymerization. *Coordination chemistry reviews* **2005,** *249* (11-12), 1155-1184.
[56**]**. Bortolamei, N.; Isse, A. A.; Di Marco, V. B.; Gennaro, A.; Matyjaszewski, K., Thermodynamic Properties of Copper Complexes Used as Catalysts in Atom Transfer Radical Polymerization. *Macromolecules* **2010,** *43* (22), 9257-9267.
[57**]**. Kaur, A.; Ribelli, T. G.; Schroder, K.; Matyjaszewski, K.; Pintauer, T., Properties and ATRP activity of copper complexes with substituted tris(2-pyridylmethyl)amine-based ligands. *Inorg Chem* **2015,** *54* (4), 1474-86.
[58**]**. Fantin, M.; Lorandi, F.; Gennaro, A.; Isse, A.; Matyjaszewski, K., Electron

Transfer Reactions in Atom Transfer Radical Polymerization. *Synthesis* **2017,** *49* (15), 3311-3322.

[59**]**. Trevisanello, E.; De Bon, F.; Daniel, G.; Lorandi, F.; Durante, C.; Isse, A. A.; Gennaro, A., Electrochemically mediated atom transfer radical polymerization of acrylonitrile and poly(acrylonitrile-b-butyl acrylate) copolymer as a precursor for N-doped mesoporous carbons. *Electrochimica Acta* **2018,** *285*, 344-354.

[60**]**. Lorandi, F.; Fantin, M.; Isse, A. A.; Gennaro, A., RDRP in the presence of Cu0: The fate of Cu(I) proves the inconsistency of SET-LRP mechanism. *Polymer* **2015,** *72*, 238-245.

[61**]**. Ribelli, T. G.; Fantin, M.; Daran, J. C.; Augustine, K. F.; Poli, R.; Matyjaszewski, K., Synthesis and Characterization of the Most Active Copper ATRP Catalyst Based on Tris[(4-dimethylaminopyridyl)methyl]amine. *J Am Chem Soc* **2018,** *140* (4), 1525-1534.

[62**]**. Karlin, K. D.; Wei, N.; Jung, B.; Kaderli, S.; Niklaus, P.; Zuberbuehler, A. D., Kinetics and thermodynamics of formation of copper-dioxygen adducts: Oxygenation of mononuclear copper (I) complexes containing tripodal tetradentate ligands. *Journal of the American Chemical Society* **1993,** *115* (21), 9506-9514.

[63**]**. De Paoli, P.; Isse, A. A.; Bortolamei, N.; Gennaro, A., New insights into the mechanism of activation of atom transfer radical polymerization by Cu (I) complexes. *Chemical Communications* **2011,** *47* (12), 3580-3582.

[64**]**. Bard, A. J.; Faulkner, L. R., Electrochemical Methods, 2nd ed. *John Wiley & Sons: New York* **2001**.

[65**]**. Swinehart, D. F., The beer-lambert law. *Journal of chemical education* **1962,** *39* (7), 333.

[66**]**. McLachlan, G. A.; Fallon, G. D.; Martin, R. L.; Spiccia, L., Synthesis, structure and properties of five-coordinate copper (II) complexes of pentadentate ligands with pyridyl pendant arms. *Inorganic Chemistry* **1995,** *34* (1), 254-261.

[67**]**. Thaler, F.; Hubbard, C. D.; Heinemann, F. W.; Van Eldik, R.; Schindler, S.; Fábián, I.; Dittler-Klingemann, A. M.; Hahn, F. E.; Orvig, C., Structural, spectroscopic, thermodynamic and kinetic properties of copper (II) complexes with tripodal tetraamines. *Inorganic chemistry* **1998,** *37* (16), 4022-4029.

[68**]**. Kaur, A.; Ribelli, T. G.; Schröder, K.; Matyjaszewski, K.; Pintauer, T., Properties and ATRP activity of copper complexes with substituted tris (2-pyridylmethyl) amine-based ligands. *Inorganic chemistry* **2015,** *54* (4), 1474-1486.

Chapter V

Simplified *e*ATRP (*se*ATRP) of *n*-butyl acrylate (*n*-BA) in organic media

Abstract

Simplified electrochemically-mediated atom transfer radical polymerization (*se*ATRP) with cheap sacrificial anodes such as aluminum has attracted a great deal of attention as one of the most powerful methods of synthesis of polymers with well-defined architecture and low dispersity. This process is more cost-effective and simpler in an undivided cell than in a two-compartment cell. In this connection, knowledge of the effect of Al^{3+} ions released from the anode on the stability and performance of typical Cu catalysts is highly desired. In this study, the stability of ternary Cu complexes with Br^- and tris(2-(dimethylamino)ethyl)amine (Me_6TREN) or tris(2-pyridylmethyl)amine (TPMA), was investigated in mixtures of *n*-butyl acrylate with DMF, DMSO, or MeCN by cyclic voltammetry and controlled-potential *e*ATRP. TPMA binds more strongly Cu^{2+} and Cu^+ than Al^{3+} in DMF and DMSO, while a ligand competition between Cu^+ and Al^{3+} ions occur in MeCN. In contrast, competitive equilibria occur between Cu and Al ions for Me_6TREN in all selected solvents, dramatically affecting the stability of the copper catalyst. Therefore, *e*ATRP of *n*-butyl acrylate catalyzed by $[Cu^{I}TPMA]^+$ in MeCN was affected by Al^{3+} ions in an undivided cell. In addition, when Me_6TREN was used, the reactions could not proceed to high conversions because Al^{3+} ions displace Cu^{2+} from the ligand. To suppress the effect of Al^{3+}, use of excess ligand and/or Br^- with respect to Cu^{II} proved to be efficient.

Keywords: *e*ATRP, copper catalysts, ligands, stability, aluminum ions

5.1 Introduction

Over the past few decades, a great deal of effort was made to develop reversible deactivation radical polymerization (RDRP) methods for the synthesis of polymers with a well-defined structure, low dispersity and predetermined composition.[1-3] Various RDRP techniques [4-14] have been developed but the last has attracted most attention because of its robustness, simplicity and applicability to a wide range of monomers and reaction media.

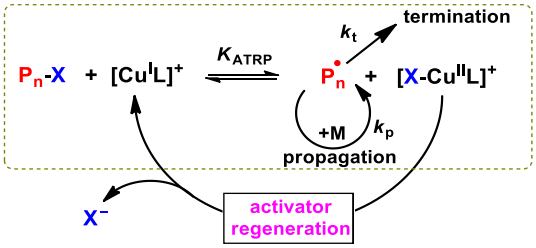

Scheme 5.1 Mechanism of traditional ATRP (dashed line) and general scheme for advanced ATRP techniques with activator regeneration.

The mechanism of traditional copper-catalyzed ATRP is shown in **Scheme 5.1** (region delimited by the dashed line).[15-16] $[Cu^IL]^+$ activates the dormant species (an activated alkyl halide, R-X, used as an initiator or a halogen-capped polymeric chain, P_n–X) by a reductive cleavage of the C-X bond, resulting in the formation of propagating radicals and the Cu complex at a higher oxidation state, i.e. $[XCu^{II}L]^+$, which acts as a deactivator. In the deactivation step, $P_n^•$ is converted back to the dormant species P_n-X while $[XCu^{II}L]^+$ is reduced to $[Cu^IL]^+$. The equilibrium is well-shifted to the left ($K_{ATRP} << 1$) so that the propagating radicals are always present in solution at a very low concentration, thus disfavoring radical-radical termination reactions.[17] Polymer chains grow as they are intermittently activated and deactivated, but most of the time they stay in the dormant state. The rate of polymerization, R_p, depends on the rate of radical propagation (k_p) as well as on the concentrations of all involved species and the ATRP equilibrium constant, as shown in **eq. 5-1.**

$$\boldsymbol{R}_P = \boldsymbol{k}_p\,[M][P_n^•] = \boldsymbol{k}_p[M]_0\,\boldsymbol{K}_{ATRP}\frac{[RX]\cdot[Cu^IL]^+}{[XCu^{II}L]^+} \qquad (5\text{-}1)$$

Traditional ATRP requires starting with air sensitive Cu^{I} at relatively high concentrations with the obvious trouble of successive workup for accurate polymer purification. Various advanced methods (mainly including chemical and physical stimuli) of ATRP aiming to avoid starting with Cu^{I} and reducing the catalyst load to ppm levels have been developed and are nowadays commonly used.[3, 18-20] These methods are based on the use of air-stable Cu^{II} and (re)generation of Cu^{I} in situ by different reduction processes. Among these techniques, electrochemically mediated ATRP (*e*ATRP) proved to have distinct advantages in controlling polymerization rate by tuning the Cu^{I} to Cu^{II} ratio through the applied potential (or current).[21-24] It has been successfully applied in ATRP of many monomers in various media.[25-28]. Typically, *e*ATRP is carried out in a divided electrochemical cell setup with Pt as both working electrode and counter electrode. Use of undivided cells with a sacrificial Al anode,[29-33] as well as inexpensive non Pt cathodes[30-31, 34] was also proposed.

Simplified *e*ATRP in undivided cells is particularly interesting for large-scale applications because of the absence of separator resistance. It has been shown, however, that *e*ATRP with sacrificial Al anodes works well only if excess amine ligand over Cu^{II} is used. There appears to be a competition between Al^{3+} ions released from the anode and copper ions for complexation with the ligand and, if excess ligand is not provided, polymerization progressively slows and stops after several hours at a moderate monomer conversion.[30] Despite the practical importance of simplified *e*ATRP in undivided cells, to the best of our knowledge, there is no systematic investigation on the stability evolution of copper catalysts during polymerization in the presence of Al^{3+} ions in common organic media. As discussed in **Chapter IV**, $[Cu^{II}TPMA]^{2+}$ is not affected by Al^{3+} in DMF and DMSO, whereas $[Cu^{II}Me_6TREN]^{2+}$ is not stable in the presence of Al^{3+}. Herein, the stability of $[BrCu^{II}L]^{+}$ with two widely used amine ligands, Me_6TREN and TPMA, in the presence of increasing amounts of Al^{3+} ions was evaluated by cyclic voltammetry in mixtures of *n*-butyl acrylate (*n*-BA) monomer with three selected organic solvents (DMF, DMSO, and MeCN). Subsequently, possible solutions to the problem of Al^{3+} interference were investigated by *e*ATRP of *n*-BA under controlled-potential electrolysis. The investigated amine ligands, the copper

catalysts, *n*-BA, and methyl 2-bromoisobutyrate (MBiB) used as the initiator are shown in **Scheme 5.2**.

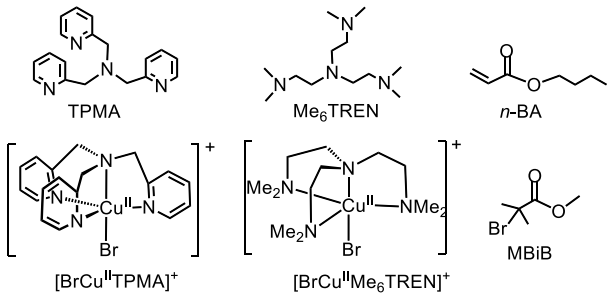

Scheme 5.2 Molecular structures of monomer, initiator, ligands and Cu(II) deactivator complexes used in this work.

5.2 Methodologies and procedures

5.2.1 Cyclic voltammetry (CV) measurements in the presence of Al^{3+}

Solutions of $[Cu^{II}L]^{2+}$ or $[BrCu^{II}L]^{+}$ in the selected solvent + 0.1 M Et_4NBF_4 were always prepared in situ starting from 1 mM $Cu(OTf)_2$, followed by addition of the ligand, L, ($[Cu^{II}]$:[L] = 1:1.05) or ligand and Et_4NBr ($[Cu^{II}]$:[L]:$[Br^-]$ = 1:1.05:1). Al^{3+} ions were introduced in the system by anodic dissolution of an Al wire immersed in the working solution containing the Cu complex while the cathode was immersed in a separated compartment containing only the electrolytic solution. The required amount of Al^{3+} (*n* mole) was prepared by applying a fixed anodic current until the passage of the theoretical charge, *Q*, according to $Q = 3nF$.[35] The effect of Al^{3+} on the voltammetric pattern of the complexes was often investigated by addition of increasing amounts of Al^{3+} ions until a two- to three-fold excess over $[Cu^{II}L]^{2+}$ (or $[BrCu^{II}L]^{+}$) was reached. After each addition of Al^{3+}, a freshly polished GC electrode was used to record voltammograms.

5.2.2 Potentiostatic *e*ATRP of *n*-BA

Electrochemically mediated polymerizations of *n*-BA in three selected organic

solvents were performed in both divided and undivided cells by controlled-potential electrolysis. A typical setup of an *e*ATRP experiment in a two-compartment cell was as follows. Et_4NBF_4 (0.65776 g, 3 mmol), CH_3CN (14.0 mL), *n*-BA (15.0 mL, 0.104 mol), and 0.5 mL of a 60 mM stock solution of $[Cu^{II}TPMA]^{2+}$ (0.03 mmol) in CH_3CN were progressively added to a seven-neck electrochemical cell maintained at 50 ˚C and under Ar flux. After purging the solution with the inert gas for ca 20 min, a CV of the copper complex was recorded on a GC disk electrode. Then 0.5 mL of a 60 mM stock solution of Et_4NBr in CH_3CN (0.03 mmol) were added and a CV was run after degassing for 5 min. Subsequently, 39.5 μL of methyl 2-bromoisobutyrate (MBiB, 0.3 mmol) were injected into the solution and a CV was recorded to verify the catalytic reaction. Then the Pt mesh working electrode and the graphite rod counter electrode, which were previously activated and positioned in the cell, were connected and the chosen potential was applied. Samples were withdrawn periodically to determine the monomer conversion by ^1H NMR, and the number average molecular weight (M_n) and molecular weight distribution ($Đ$) by gel permeation chromatograph (GPC).

A similar procedure was used for *e*ATRP in the undivided cell with the sacrificial Al anode. The Al wire was activated, immediately before use, by pickling in HCl/H_2O (1:2) and washing with double distilled water and acetone.

5.3 Results and discussion

5.3.1 Electrochemical characterization of $[Cu^{II}L]^{2+}$ and $[XCu^{II}L]^{+}$

Typically, in ATRP the reaction medium is composed of a solvent and a monomer together with the catalyst and initiator. In addition, halide ions (X^-) are released into the solution because of unavoidable termination events. Quite often, X^- is also introduced in the system as CuX_2 at the beginning of the reaction. The presence of X^- converts $[Cu^{II}L]^{2+}$ to $[XCu^{II}L]^{+}$, which plays the fundamental role of deactivating the propagating radicals (**Scheme 5.1**).[36-37] It is therefore important to evaluate the effect of Al^{3+} on the stability of $[XCu^{II}L]^{+}$ in solvent/monomer mixtures. We chose *n*-butyl

acrylate (*n*-BA), which was previously polymerized by *e*ATRP in DMF,[29-30] as a model monomer for this study and a tetraethylammonium salt (Et_4NX) as a source of bromide or chloride ions. Thus, the electrochemical performance of both binary and ternary copper complexes, $[Cu^{II}L]^{2+}$ and $[XCu^{II}L]^{+}$, were investigated in the selected solvent/monomer mixtures.

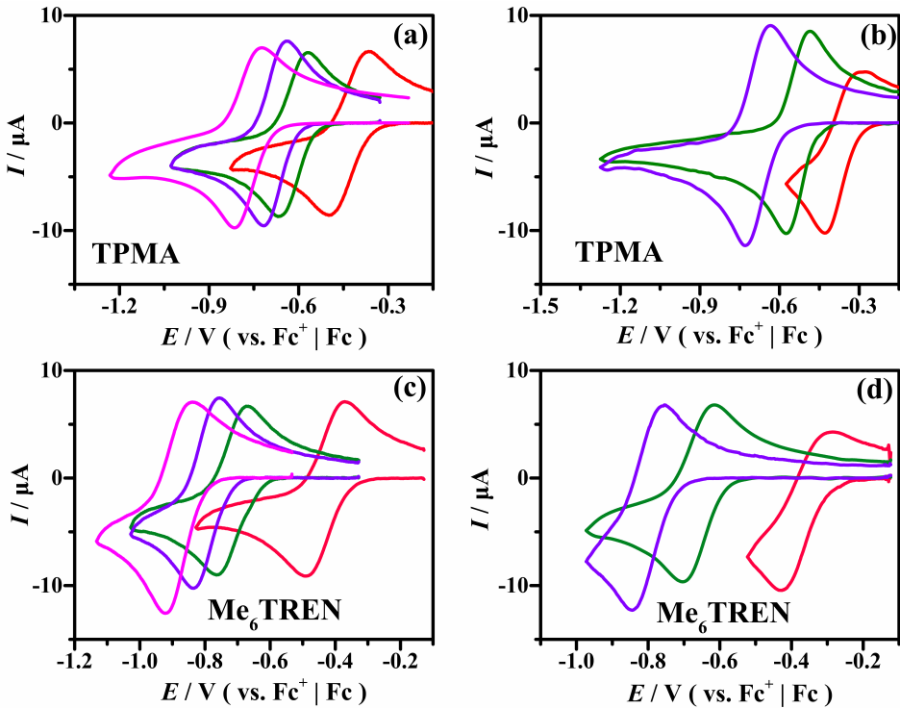

Figure 5.1 Cyclic voltammetry of 1.0 mM $Cu^{II}(OTf)_2$ (—), $[Cu^{II}L]^{2+}$ (—) and $[BrCu^{II}L]^{+}$ (—), $[ClCu^{II}L]^{+}$ (—) in pure DMSO (a, c) and 50% (v/v) DMSO/*n*-BA mixture (b, d) containing 0.1 M Et_4NBF_4 as a supporting electrolyte, recorded on a GC electrode at 0.2 V/s and $T = 25$ °C.

In general, copper(II) complexes undergo quasi-reversible one electron transfer to the corresponding Cu(I) complexes.[16, 36-38] An example of typical voltametric behavior of Cu(II) complexes in DMSO or DMSO/*n*-BA is reported in **Figure 5.1**. Starting with $Cu(OTf)_2$, the $[Cu^{II}L]^{2+}$ and $[XCu^{II}L]^{+}$ complexes were prepared in situ by consecutive addition of equimolar amounts of TPMA or Me_6TREN, and X^- (X = Cl, Br). Both $[Cu^{II}L]^{2+}$ and $[XCu^{II}L]^{+}$ are stable in DMSO or DMSO/*n*-BA mixture and exhibit a quasi-reversible peak couple. The peak couple observed for the reduction of Cu^{2+} shifts

to more negative potentials after addition of the ligand; further addition of halide ions causes further negative shift of the peak couple. The differences in current intensities are ascribed to the various diffusion coefficients of Cu^{II} species. A similar voltametric behavior was also observed in DMF and MeCN both in the absence and presence of 50 vol% *n*-BA. The standard potentials measured as $E^{\Theta} \approx E_{1/2} = (E_{pc} + E_{pa})/2$ for all investigated Cu^{II} species are summarized in **Table 5.1**.

Table 5.1 Redox properties of copper complexes and their relative stabilities in solvent or 50% (v/v) solvent/*n*-BA mixture at 25 °C.[a]

Entry	Media	Ligands	Cu^{2+}/Cu^{+}	$[Cu^{II}L]^{2+}/[Cu^{I}L]^{+}$		$[BrCu^{II}L]^{+}/[BrCu^{I}L]$		$[ClCu^{II}L]^{+}/[ClCu^{I}L]$	
			E^{Θ} (V)	E^{Θ} (V)	β^{II}/β^{I}	E^{Θ} (V)	K^{II}/K^{I}	E^{Θ} (V)	K^{II}/K^{I}
1	DMSO	TPMA	-0.425	-0.615	1.6×10^{3}	-0.678	10.1	-0.769	3.6×10^{2}
2		Me_6TREN	-0.425	-0.714	7.5×10^{4}	-0.797	22.1	-0.880	5.6×10^{2}
3	DMF/*n*-BA	TPMA	-0.282	-0.506	6.2×10^{3}	-0.704	2.2×10^{3}	-	-
4		Me_6TREN	-0.282	-0.650	1.7×10^{6}	-0.806	4.3×10^{2}	-	-
5	DMSO/*n*-BA	TPMA	-0.355	-0.532	1.0×10^{3}	-0.682	3.4×10^{2}	-	-
6		Me_6TREN	-0.355	-0.659	1.4×10^{5}	-0.799	2.3×10^{2}	-	-
7	MeCN/*n*-BA	TPMA	0.507	-0.390	1.5×10^{15}	-0.671	5.6×10^{2}	-	-
8		Me_6TREN	0.507	-0.518	2.1×10^{17}	-0.763	1.4×10^{4}	-	-

[a] Recorded at a glassy carbon working electrode, scan rate = 0.2 V/s, E^{Θ} (V) vs $Fc^{+}|Fc$.

The standard potential of the Cu^{2+}/Cu^{+} couple shifted to more negative potentials after addition of the ligand. This potential shift is a measure of the relative stability constants of $[Cu^{II}L]^{2+}$ and $[Cu^{I}L]^{+}$, β^{II} and β^{I}, respectively, according to **eq. 5-2**.

$$E^{\Theta}_{[Cu^{II}L]^{2+}/[Cu^{I}L]^{+}} = E^{\Theta}_{Cu^{2+}/Cu^{+}} - \frac{RT}{nF}\ln\frac{\beta^{II}}{\beta^{I}} \qquad (5\text{-}2)$$

where R is the universal gas constant, and F is the Faraday constant. The separate values of β^{II} or β^{I} cannot be obtained from cyclic voltammetry, but if either β^{II} or β^{I} is independently determined by other means, the remaining parameter can be easily calculated by **eq. 5-2**. As shown in **Table 5.1**, $\beta^{II} >> \beta^{I}$ was obtained as in pure solvents

(**Table 4.1**) but neither the effect of solvent type nor that of 50 vol% of *n*-BA could be easily rationalized. In addition, it is important to note that $[XCu^{II}L]^+$ has a more negative $E^{\ominus}$ value with respect to $[Cu^{II}L]^{2+}$ also in the mixture. This $E^{\ominus}$ shift is related to the relative affinity of X^- for $[Cu^{II}L]^{2+}$ and $[Cu^{I}L]^+$ according to **eq. 5-3**:

$$E^{\ominus}_{[XCu^{II}L]^+/[XCu^{I}L]} = E^{\ominus}_{[Cu^{II}L]^{2+}/[Cu^{I}L]^+} - \frac{RT}{nF}\ln\frac{K^{II}}{K^{I}} \qquad (5\text{-}3)$$

where K^{II} and K^{I} are the binding constants of X^- to $[Cu^{II}L]^{2+}$ and $[Cu^{I}L]^+$, respectively. As shown in **Figure 5.1 a, c**, $E^{\ominus}$ of $[ClCu^{II}L]^+$ is more negative than $E^{\ominus}$ of $[BrCu^{II}L]^+$, suggesting higher affinity of Cu^{II} for Cl^- than Br^-. Application of **eq. 5-3** gave $K^{II} > K^{I}$ both for Cl^- and Br^- with $K^{II}_{Br}/K^{I}_{Br} < K^{II}_{Cl}/K^{I}_{Cl}$. The observed high binding of X^- with Cu^{II} than Cu^{I} is a desirable property for ATRP catalysts. Indeed, whilst a highly stable deactivator $[XCu^{II}L]^+$ is necessary, the activation process is more efficient if the activator is mainly present as $[Cu^{I}L]^+$. We have previously shown that the presence of X^- in the reaction medium considerably lowers the activation rate, because of the formation of inactive $[XCu^{I}L]$ and $Cu^{I}X_2^-$ species.[37, 39] In addition, the effect of X^- is higher for Cl^- than for Br^- because of the higher affinity of Cu(I) for chlorides with respect to bromides.[36-37] Therefore, we used only Br^- ions in further investigations.

Comparing pure DMSO with DMSO/*n*-BA, K^{II}_{Br}/K^{I}_{Br} increases by about one order of magnitude on passing from DMSO to 50 vol% *n*-BA in DMSO (**Table 5.1, entries 1-2 vs 5-6**). In solvent/monomer mixtures, the values of K^{II}_{Br}/K^{I}_{Br} calculated by **eq. 5-3** are in the range from 2.3×10^2 to 1.4×10^4 in good agreement with literature data.[25, 36-37] This is particularly important, according to the general ATRP mechanism (**Scheme 5.1**), because it is desirable to have a deactivator complex ($[XCu^{II}L]^+$) with good stability while the activator complex should not have high affinity for halide ions to avoid speciation of Cu^{I} to produce inactive species.[36, 39-40] To summarize, the redox properties of $[XCu^{II}L]^+$ in mixtures of selected solvents (DMF, DMSO, and MeCN) with *n*-BA mixtures followed the expected behavior for ATRP catalysts in organic media.

5.3.2 Catalyst stability and Al^{3+} effect in typical ATRP conditions

The effects of Al^{3+} on the stability and performance of copper-based ATRP catalysts in monomer/solvent mixtures were investigated following the same protocol used for $[Cu^{II}L]^{2+}$ in **Chapter IV**. **Figure 5.2** shows cyclic voltammetry of Cu^{II} species in different solvent/monomer mixtures (50 vol% *n*-BA). Starting with $Cu(OTf)_2$, the binary and ternary complexes $[Cu^{II}L]^{2+}$ and $[BrCu^{II}L]^{+}$ were prepared in situ by stepwise addition of equimolar amounts of ligand and Br^{-}. After these two steps, the effect of Al^{3+} on $[BrCu^{II}L]^{+}$ was investigated. Last, the effects of additional ligand and Br^{-} were examined. The concentration of the starting Cu^{II} and its complexes in solution was fixed at 1 mM, whereas the concentrations of Al^{3+}, ligand and Br^{-} added to $[BrCu^{II}L]^{+}$ are reported in **Figure 5.2**.

When Al^{3+} was added to $[BrCu^{II}TPMA]^{+}$ in mixtures of either DMF or DMSO with 50 vol% *n*-BA, no exchange of ligand was observed just like in pure solvents (**Chapter IV, section 4.3.2**). Only a slight positive shift of the peak couple for Cu^{II}/Cu^{I} occurred. Clearly in these media, TPMA binds much better to Cu^{II} (and Cu^{I}) than to Al^{3+} but the later may be compete with the copper ions for Br^{-}, resulting in a positive shift of E^{0} of the $[BrCu^{II}L]^{+}/[BrCu^{I}L]$ couple. Further addition of ligand and Br^{-} shifted E^{0} back to its original value. In MeCN/*n*-BA, the reversible peak couple was replaced by an irreversible cathodic peak at a more positive potential when Al^{3+} ions were added. This behavior was already observed in pure MeCN and attributed to a better binding of TPMA to Al^{3+} than Cu^{+}. Addition of more ligand restored the reversible peak couple of $[BrCu^{II}TPMA]^{+}$ while further addition of Br^{-} did not cause any change.

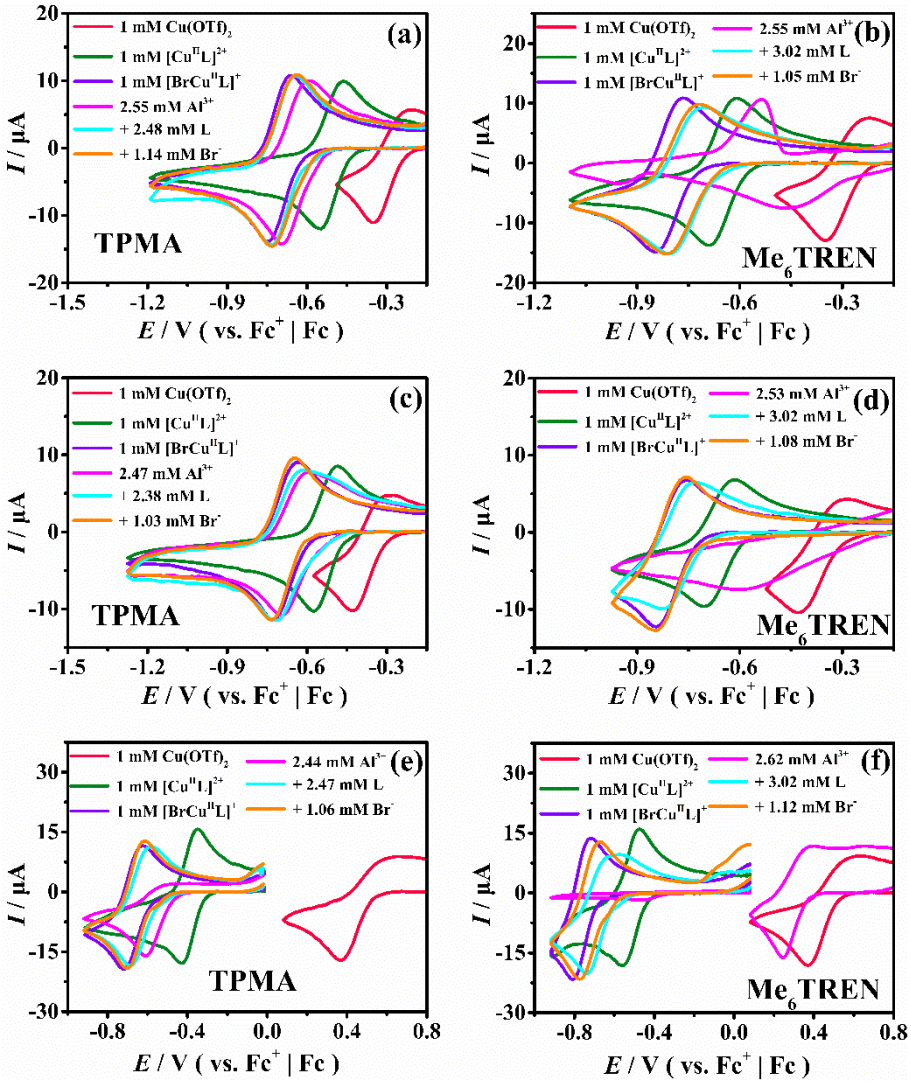

Figure 5.2 CVs of 1 mM $Cu(OTf)_2$, 1 mM $[Cu^{II}L]^{2+}$ and 1 mM $[BrCu^{II}L]^{+}$ before and after addition of Al^{3+}, followed by addition of free ligand and Et_4NBr, recorded at υ = 0.2 V s^{-1} on a GC disk in DMF **(a, b)**, DMSO **(c, d)** and MeCN **(e, f)**, with 0.1 M Et_4NBF_4 as the supporting electrolyte; the concentrations of all species added to $[BrCu^{II}L]^{+}$ are shown in the figure, T = 25 °C.

$[BrCu^{II}Me_6TREN]^{+}$ behaved in a similar way in all three solvent/monomer mixtures. It was destroyed completely in the presence of Al^{3+} as evidenced by the disappearance of its reversible peak couple and the appearance of the reduction wave of solvated Cu^{2+} ions (**Figure 5.2 b, d, and f**). When however further ligand was added to the solution, the original voltametric pattern of $[BrCu^{II}Me_6TREN]^{+}$ was restored. Addition of Br^{-} did not produce significant changes as in the case of TPMA in all

solvent/*n*-BA mixtures.

5.3.4 Potentiostatic *e*ATRP of *n*-BA in a traditional divided cell

The voltammetric and UV-vis investigations suggested that Al^{3+} ions destroy copper complexes with Me_6TREN whereas TPMA provides more stable complexes with both Cu^{II} and Cu^{I} than Al^{3+} except in MeCN and MeCN/*n*-BA. To check the effective interference of Al^{3+} on the efficiency of copper catalysts in *e*ATRP, electrochemically-mediated polymerization of 50 vol% *n*-BA in DMF, DMSO, and MeCN was studied in an undivided cell with a sacrificial Al anode. For the sake of comparison, *e*ATRP in a divided cell with a graphite anode was first carried out in each solvent. As shown in **Figure 2.6** in **Chapter II**, a conventional setup with a separated graphite anode was used. All polymerizations were run with 1 mM $[BrCu^{II}L]^+$ and 10 mM methyl 2-bromoisobutyrate (MBiB) used as an initiator and were triggered by applying $E_{app} = E_{1/2} - 60$ mV. The results of a first set of *e*ATRP experiments are summarized in **Table 5.2**, whereas monomer conversion, first-order kinetic plots and evolution of number average molecular weight (M_n) and dispersity ($Đ$) with conversion are shown in **Figure 5.3**.

High monomer conversions were obtained, and the polymer showed MWs matching the theoretical values and very low dispersity ($Đ < 1.2$) in all three selected solvents. Although the reactions were well-controlled, significant differences were observed in the overall performance of the process in different solvents. The polymerization was fastest in DMSO media, reaching 92% and 88% conversion with $[BrCu^{II}TPMA]^+$ and $[BrCu^{II}Me_6TREN]^+$, respectively (**Table 5.2, entries 3, 4**). It is important to note that although the reaction was well-controlled in DMSO, poly(*n*-butyl acrylate) (PBA) has a limited solubility in this solvent, especially at high monomer conversion. However, no phase separation was observed during electrolysis and the limited solubility did not negatively affect polymerization control, but when the stirring was stopped at the end of the experiment, the system split into two phases (see **Figure 5.4 d**), one containing DMSO/*n*-BA and catalyst, and the other mainly containing

PBA.[41-42] The reaction was also fast in DMF, 76% and 89% monomer conversions were obtained in 4 h with $[BrCu^{II}TPMA]^+$ and $[BrCu^{II}Me_6TREN]^+$, respectively. The potentiostatic *e*ATRP was slowest in MeCN, but the polymerization still proceeded with good control. GPC traces taken during *e*ATRP in all solutions were symmetrical without tailing and continuously shifted to higher molecular weights with increasing conversion, as shown in **Figure 5.4** for polymerizations catalyzed by $[BrCu^{II}Me_6TREN]^+$.

Table 5.2 Potentiostatic *e*ATRP of 50% (v/v) *n*-BA in DMF, DMSO and MeCN in a divided cell with a separated graphite anode.[a]

Entry	Solvent	Ligand	*t* (h)	*Q* (C)	Conv.[b] (%)	$10^{-3}M_{n,th}$[c]	10^{-3} M_n[d]	k_p^{app}[e] (h^{-1})	$Đ$[d]
1	DMF	TPMA	4	5.50	76	33.8	38.5	0.54	1.12
2		Me_6TREN	4	6.95	89	39.6	37.6	0.62	1.16
3	DMSO	TPMA	2	1.82	92	40.9	44.3	1.21	1.16
4		Me_6TREN	3	5.07	88	39.0	38.5	0.64	1.11
5	MeCN	TPMA	4	6.69	84	36.8	42.4	0.39	1.12
6		Me_6TREN	3	6.50	79	34.8	35.2	0.51	1.12

[a] Polymerization conditions: [*n*-BA]:[MBiB]:[$Cu(OTf)_2$]:[L]:[Et_4NBr] = 344:1:0.1:0.1:0.1, $E_{app} = E_{1/2}$ - 0.06 V, with initial $[Cu^{II}] = 10^{-3}$ M; $[Et_4NBF_4] = 0.1$ M; $V_{tot} = 30$ mL; $T = 50$ °C.

[b] Determined by ^{1}H NMR.

[c] Calculated on the basis of conversion obtained by ^{1}H NMR (i.e. $M_{n,th} = M_{MBiB} + 344 \times \text{conversion} \times M_{n\text{-BA}}$).

[d] Determined by GPC.

[e] Slope of the linear plot of ln ($[M]_0/[M]$) vs. time.

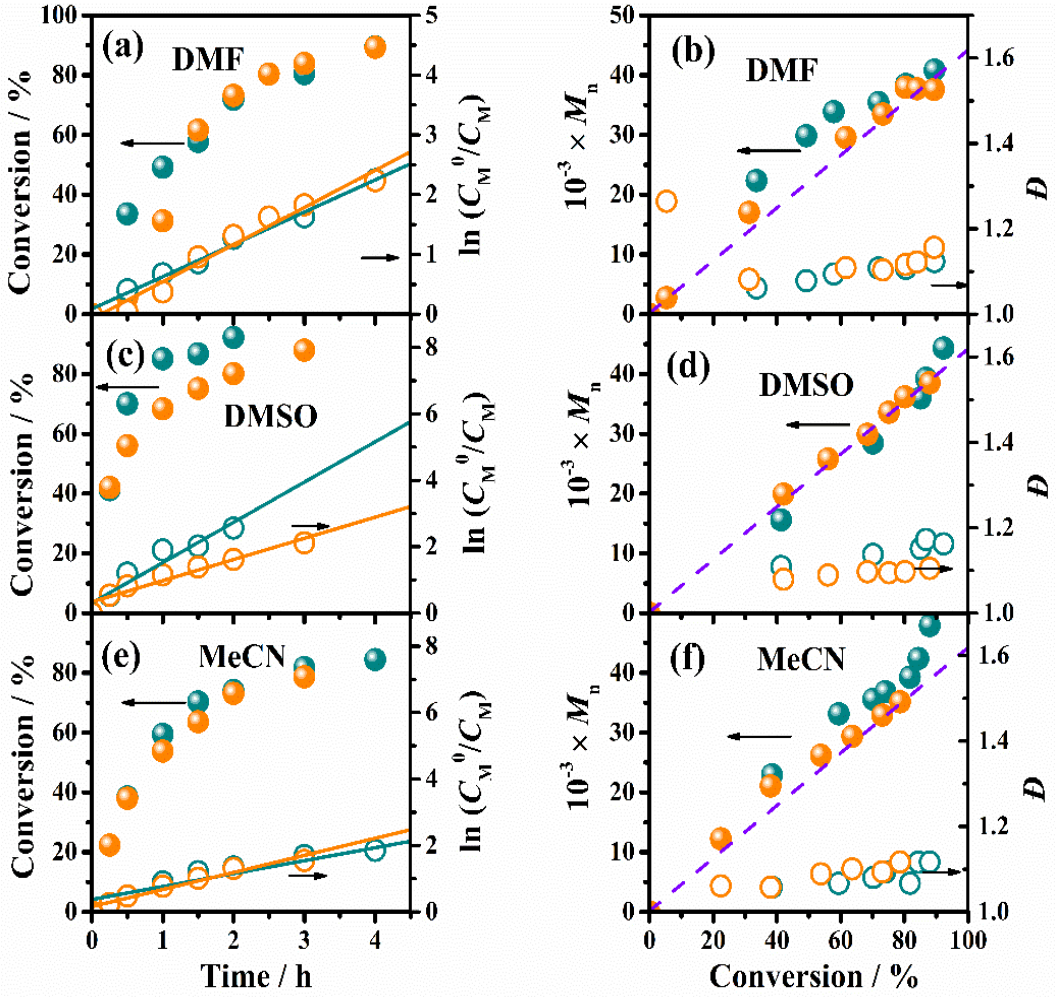

Figure 5.3 Kinetic plots and monomer conversion as a function of time **(a, c, e)** and evolution of M_n and $Đ$ with conversion **(b, d, f)** for *e*ATRP of 50 vol% *n*-BA in DMF, DMSO and MeCN with 0.1 M Et_4NBF_4, performed at $E_{app} = E_{1/2} - 0.06$ V on a Pt cathode at 50 °C in a divided cell with a separated graphite anode. Other conditions: $Cu(OTf)_2$:L:Et_4NBr = 1:1:1, when L= TPMA (green circles) and Me_6TREN (orange circles). The dashed line in b, d and f indicates $M_{n,th}$, , T = 50 °C.

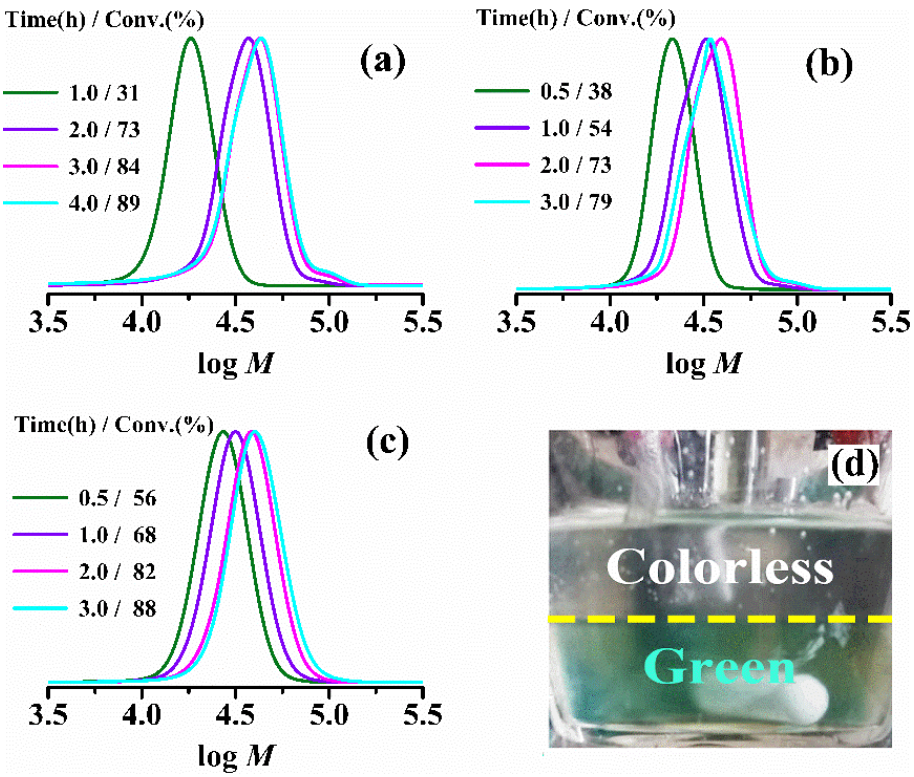

Figure 5.4 Representative GPC traces of poly(*n*-butyl acrylate) prepared by Cu-catalyzed *e*ATRP in a divided cell with a separated graphite anode. Polymerization conditions: [*n*-BA]:[MBiB]:[$Cu(OTf)_2$]:[Me_6TREN]:[Et_4NBr] = 344:1:0.1:0.1:0.1, with initial [Cu^{II}] = 10^{-3} M; $C_{Et_4NBF_4}$ = 0.1 M; V_{tot} = 30 mL; T = 50 °C; $E_{app} = E_{1/2}$ - 0.06 V. **(d)** A picture of a reaction mixture in DMSO after polymerization.

5.3.5 Potentiostatic *e*ATRP of n-BA in a simplified undivided cell with an Al sacrificial anode

With the aim of assessing the effective interference of Al^{3+} on the efficiency of copper catalysts in *e*ATRP, potentiostatic *e*ATRP of 50 vol% *n*-BA in DMF, DMSO, and MeCN was studied also in an undivided cell with a sacrificial Al anode, as shown in **Figure 5.5**. Additionally, the effects of excess ligand and Br^- with respect to $[BrCu^{II}L]^+$ were evaluated. All polymerizations were run with 1 mM $[BrCu^{II}L]^+$ and 10 mM methyl 2-bromoisobutyrate (MBiB) used as an initiator and were triggered by applying $E_{app} = E_{1/2} - 60$ mV. The results obtained with L = TPMA are collected in **Table 5.3**, whereas monomer conversion, kinetic plots and evolution of number

average molecular weight (M_n) and dispersity ($Đ$) with conversion are reported in **Figure 5.6**.

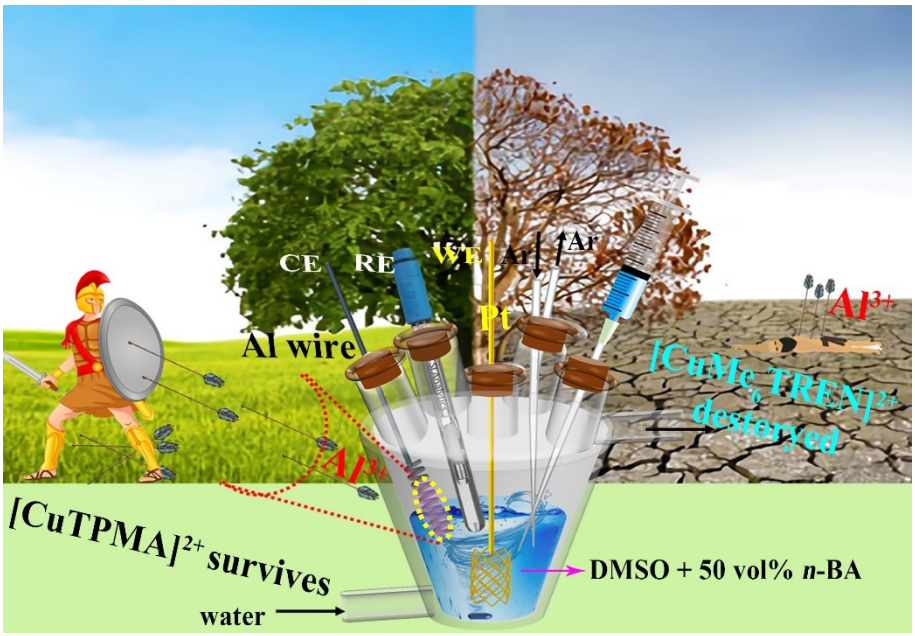

Figure 5.5 Artistic representation of *se*ATRP setup. In the cell, Al wire used as a sacrificial anode (reprinted with permission from Ref. 42. Copyright 2021, ELSEVIER).

In all solvents, polymerizations in the undivided cell were well-controlled yielding polymers with narrow molecular weight distribution ($Đ$ < 1.2) and M_n linearly increasing with conversion (**Figure 5.6**). The experimental M_n values from gel permeation chromatography (GPC) were also near the theoretical values ($M_{n,th}$) calculated from the monomer conversion. GPC traces were always monomodal shifting to higher molecular weights without tailing (**Figure 5.7**). However, the overall rate of polymerization (k_p^{app}) and hence the final conversion depended on type of solvent. In DMF and DMSO (**Table 5.3**, **entries 1-8**) conversions as high as those obtained in the divided cell (**Table 5.2, entries 1, 3**) were reached. Additionally, the presence of excess ligand and/or Br^- had no effect. As previously shown by CV and UV-vis spectroscopy, Cu/TPMA complexes in these solvents are not destroyed by the presence Al^{3+} ions. Therefore, the performance of the process in the divided cell with the Al anode was essentially the same as that in the divided cell. Since Al^{3+} did not affect the stability of

the catalyst, addition of excess TPMA and/or Br^- had little or no effect. It is noteworthy that the phase separation in DMSO was also observed when the stirring was stopped because of the limited solubility of high MW of PBA in this solvent. Also, the polymerization rate followed the same trend observed for *e*ATRPs in the divided cell, decreasing in the order: DMSO > DMF > MeCN.

Table 5.3 Potentiostatic *e*ATRP of 50% (v/v) *n*-BA in DMF, DMSO and MeCN with a Cu catalyst based on TPMA in an undivided cell with a sacrificial Al anode.[a]

Entry	Solvent	$[Cu^{II}]:[L]:[Br^-]$	t (h)	Q (C)	Conv.[b] (%)	$10^{-3}M_{n,th}$[c]	10^{-3} M_n[d]	k_p^{app}[e] (h^{-1})	$Đ$[d]
1	DMF	1:1:1	4	7.61	74	32.8	38.0	0.28	1.08
2		1:2:1	4	6.27	79	34.8	39.1	0.31	1.12
3		1:1:2	4	6.78	77	33.9	38.9	0.28	1.11
4		1:2:2	4	5.92	82	36.1	39.7	0.33	1.12
5	DMSO	1:1:1	2	4.18	88	39.0	48.5	1.19	1.16
6		1:2:1	2	2.97	94	41.3	48.1	1.51	1.16
7		1:1:2	2	3.39	93	41.1	46.4	1.45	1.17
8		1:2:2	2	3.32	94	41.6	48.9	1.52	1.17
9	MeCN	1:1:1	4	12.02	26	11.6	19.3	0.07	1.09
10		1:2:1	4	13.62	48	21.3	25.8	0.20	1.09
11		1:1:2	4	6.83	38	16.9	24.1	0.16	1.11
12		1:2:2	4	13.33	53	23.7	27.6	0.24	1.09

[a] Polymerization conditions: L= TPMA, [*n*-BA]:[MBiB]:[$Cu(OTf)_2$] = 344:1:0.1, $E_{app} = E_{1/2}$ - 0.06 V, with initial $[Cu^{II}] = 10^{-3}$ M; $[Et_4NBF_4]$ = 0.1 M; V_{tot} = 30 mL; T = 50 °C.

[b] Determined by ^{1}H NMR.

[c] Calculated on the basis of conversion obtained by ^{1}H NMR (i.e. $M_{n,th} = M_{MBiB} + 344 \times \text{conversion} \times M_{n\text{-BA}}$).

[d] Determined by GPC.

[e] Slope of the linear plot of ln ($[M]_0/[M]$) vs. time.

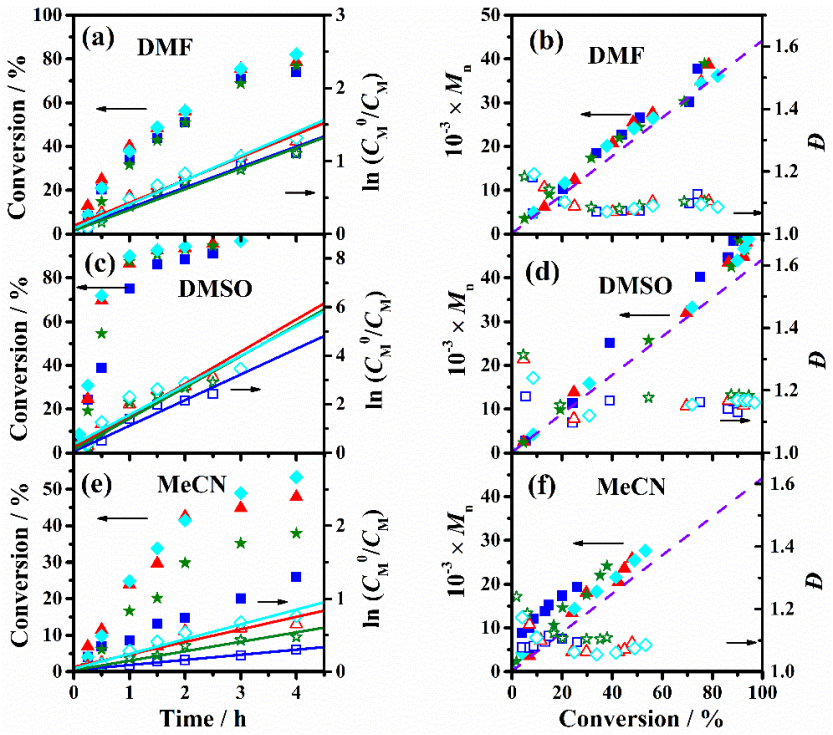

Figure 5.6 Kinetic plots and monomer conversion as a function of time **(a, c, e)** and evolution of M_n and $Đ$ with conversion **(b, d, f)** for *e*ATRP of 50 vol% *n*-BA in DMF, DMSO and MeCN with 0.1 M Et_4NBF_4, performed at $E_{app} = E_{1/2} - 0.06$ V on a Pt cathode at 50 °C in an undivided cell with a sacrificial Al anode. Other conditions: $[Cu(OTf)_2]$:[TPMA]:$[Et_4NBr]$ = 1:1:1 (■), 1:2:1 (▲), 1:1:2 (★), 1:2:2 (♦). The dashed line in **b, d** and **f** indicates $M_{n,th}$, T = 50 °C.

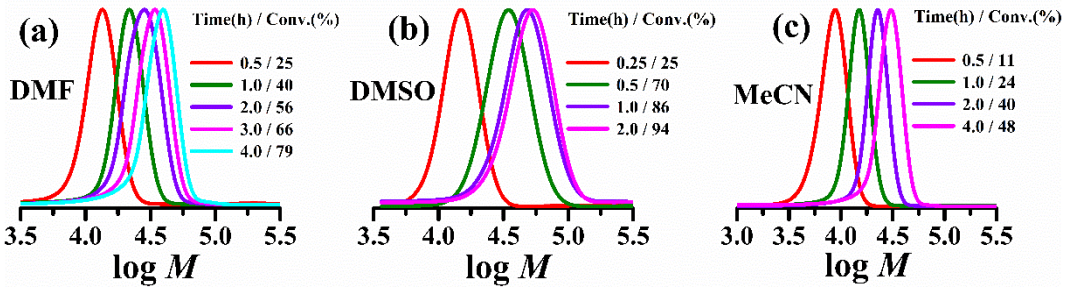

Figure 5.7 Representative GPC traces of poly(*n*-butyl acrylate) prepared by Cu-catalyzed *e*ATRP in an undivided cell with a sacrificial Al anode. Polymerization conditions: [*n*-BA]:[MBiB]:$[Cu(OTf)_2]$:[TPMA]:$[Et_4NBr]$ = 344:1:0.1:0.2:0.1, with initial $[Cu^{II}] = 10^{-3}$ M; $C_{Et_4NBF_4}$ = 0.1 M; V_{tot} = 30 mL; T = 50 °C; $E_{app} = E_{1/2}$ - 0.06 V.

In MeCN, the monomer conversion after 4 h dropped from 84% to 26% when the separated graphite anode was replaced with a sacrificial Al anode (**Table 5.2, entry 5** and **Table 5.3, entry 9**). However, the polymerization was well-controlled as evidenced by the linear first-order kinetic plot and low dispersity shown in **Figure 5.6 e and f**. Note that in **Figure 5.3 e**, data on conversion in the divided cell, which reached values as high as 84%, were omitted for clarity. The drastic drop of monomer conversion and k_p^{app} in MeCN confirms that Al^{3+} ions released at the anode destroy the catalyst, most likely when it is reduced to Cu^{I}, lowering drastically the activation rate. It appears that $[BrCu^{II}TPMA]^+$ is stable and continues to provide efficient radical deactivation, so that control over molecular weight distribution is not lost. When *e*ATRP was run with excess TPMA ($[Cu^{II}]$:[TPMA] = 1:2) both monomer conversion and k_p^{app} increased significantly, but did not reach the values observed in the divided cell. Also, excess Br^- without excess TPMA (**Table 5.3, entry 11**) improved the catalyst performance. Possibly, Br^- forms complexes with Al^{3+} reducing therefore its competition with copper for the amine ligand. The best result was obtained when both TPMA and Br^- were used in a two-fold excess with respect to Cu^{II}. However, the monomer conversion was well below that achieved in the divided cell. A large excess of TPMA would probably suppress the effect of Al^{3+} but this is not feasible as it would make the process highly costly, especially in view of process scale-up.

Polymerization of *n*-BA by *e*ATRP with Me_6TREN as the ligand was also investigated in the three selected solvents and the results are reported in **Table 5.4**. The kinetic plots and evolution of monomer conversion, M_n and dispersity during polymerization are shown in **Figure 5.8**. Again, all *e*ATRPs fulfilled the criteria of controlled polymerization. In particular, M_n increased linearly with conversion and closely matched the theoretical values, dispersity was very low, and GPC traces were monomodal (**Figure 5.9**). A first comparison between *e*ATRPs conducted in the same conditions except for the type of cell, divided with graphite anode versus undivided with Al anode, revealed that both monomer conversion and k_p^{app} dropped on passing from the divided cell to the undivided one. The effect was modest in DMF but was drastic in the other solvents, especially MeCN. Indeed, polymerization almost stopped

after 76%, 43% and 15% conversion in DMF, DMSO and MeCN, respectively. The Al^{3+} ions released from the anode destroy the Cu catalyst, the competition between the different metal ions for the ligand depending on the relative stabilities of their complexes, which is affected by the type of solvent.

Table 5.4 Potentiostatic *e*ATRP of 50% (v/v) *n*-BA in DMF, DMSO and MeCN with a Cu catalyst based on Me_6TREN in an undivided cell with a sacrificial Al anode.[a]

Entry	Solvent	$[Cu^{II}]$:[L]:$[Br^-]$	*t* (h)	*Q* (C)	Conv.[b] (%)	$10^{-3}M_{n,th}$[c]	$10^{-3}\,M_n$[d]	k_p^{app}[e] (h^{-1})	*Đ*[d]
1	DMF	1:1:1	4	5.60	73	32.3	34.3	0.58	1.16
2		1:2:1	4	5.87	88	38.8	39.0	0.81	1.12
3		1:1:2	4	5.09	87	38.4	38.8	0.35	1.12
4		1:2:2	4	7.60	90	39.7	42.3	0.41	1.15
5	DMSO	1:1:1	3	2.44	43	19.3	24.7	0.32	1.11
6		1:2:1	3	1.40	90	39.8	41.7	0.74	1.11
7		1:1:2	2.5	2.43	72	31.9	33.6	0.37	1.12
8		1:2:2	2.5	1.99	91	40.0	45.6	1.36	1.12
9	MeCN	1:1:1	3	5.32	15	6.8	9.6	0.06	1.17
10		1:2:1	3	8.80	82	36.2	43.5	0.60	1.10
11		1:1:2	2	3.98	48	21.4	29.7	0.61	1.09
12		1:2:2	3	8.32	81	35.8	40.4	0.86	1.13

[a] Polymerization conditions: L= Me_6TREN, [*n*-BA]:[MBiB]:[$Cu(OTf)_2$] = 344:1:0.1, $E_{app} = E_{1/2}$ - 0.06 V, with initial $[Cu^{II}] = 10^{-3}$ M; $[Et_4NBF_4]$ = 0.1 M; V_{tot} = 30 mL; *T* = 50 °C.

[b] Determined by ^{1}H NMR.

[c] Calculated on the basis of conversion obtained by ^{1}H NMR (i.e. $M_{n,th} = M_{MBiB} + 344 \times \text{conversion} \times M_{n\text{-BA}}$).

[d] Determined by GPC.

[e] Slope of the linear plot of ln ($[M]_0/[M]$) vs. time.

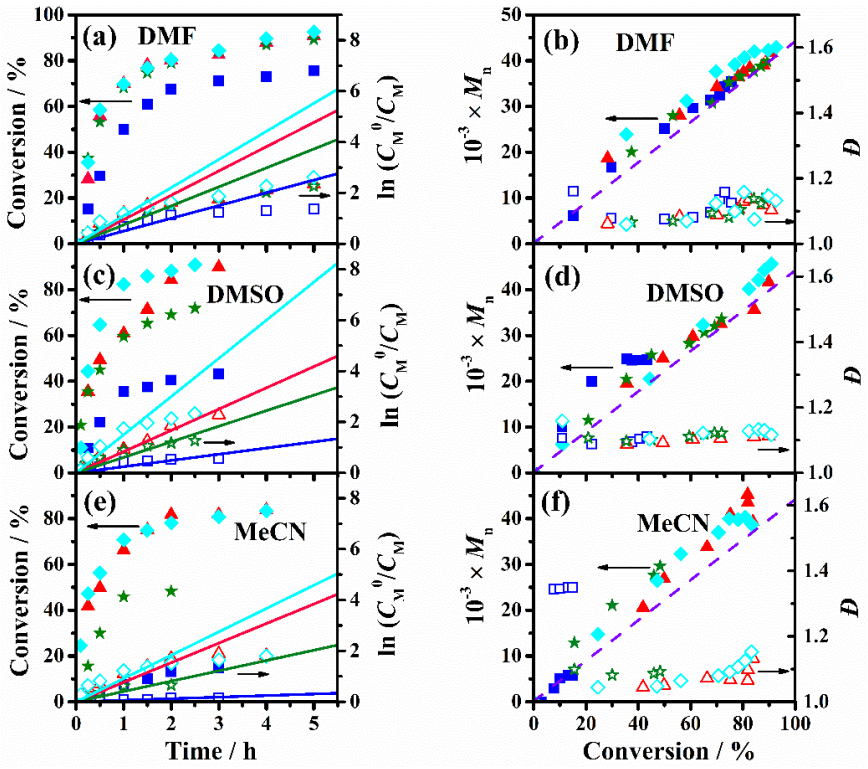

Figure 5.8 Kinetic plots and monomer conversion as a function of time **(a, c, e)** and evolution of M_n and $Đ$ with conversion **(b, d, f)** for *e*ATRP of 50 vol% *n*-BA in DMF, DMSO and MeCN with 0.1 M Et_4NBF_4, performed at $E_{app} = E_{1/2} - 0.06$ V on a Pt cathode at 50 °C in an undivided cell with a sacrifical Al anode. Other conditions: [$Cu(OTf)_2$[:[Me_6TREN]:[Et_4NBr] = 1:1:1 (■), 1:2:1 (▲), 1:1:2 (★), 1:2:2 (◆). The dashed line in **b, d** and **f** indicates $M_{n,th}$.

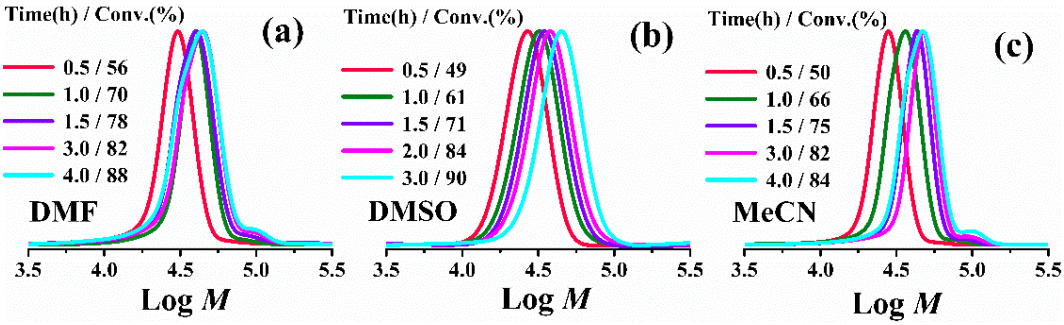

Figure 5.9 Representative GPC traces of poly(*n*-BA) prepared by Cu-catalyzed *e*ATRP in an undivided cell with a sacrificial Al anode. Polymerization conditions: [*n*-BA]:[MBiB]:[$Cu(OTf)_2$]:[Me_6TREN]:[Et_4NBr] = 344:1:0.1:0.2:0.1, with initial [Cu^{II}] = 10^{-3} M; $C_{Et_4NBF_4} = 0.1$ M; $V_{tot} = 30$ mL; $T = 50$ °C; $E_{app} = E_{1/2}$ - 0.06 V.

As with TPMA, to mitigate the detrimental effect of Al^{3+}, *e*ATRPs were run with a two-fold excess of Me_6TREN and/or Br^-. In all solvents, use of excess ligand fully suppressed the effect of Al^{3+}. The quantity of charge passed during *e*ATRP is reported in **Tables 5.2 - 5.4** (column 5). In most cases, the concentration of Al^{3+} produced at the end of *e*ATRP was lower than that of the starting Cu catalyst (1 mM). Therefore, starting with a two-fold excess of ligand over Cu^{II} ensures the presence of enough ligand for both Cu^{2+} or Cu^+ ions and Al^{3+} ions all over during electrolysis. Interestingly, moderate to high conversions in the range from 48% to 87% were obtained when only a two-fold excess of Br^- was used (**Table 5.4, entries 3, 7, 11**). When both Me_6TREN and Br^- were added in excess over Cu^{II}, the results were the same as when only excess amine ligand was used.

5.4 Conclusions

In conclusion, the stability of ternary $[BrCu^{II}L]^+$ complexes with two amine ligands (TPMA and Me_6TREN) in DMF, DMSO and MeCN in the presence of Al^{3+} ions were investigated via cyclic voltammetry, showing that $[BrCu^{II}TPMA]^+$ is not affected by Al^{3+} in DMF and DMSO. It appears that TPMA prefers binding to Cu^{2+} than to Al^{3+} also in MeCN, whereas the competition between the metals becomes important when Cu^{II} is reduced to Cu^{I}. In contrast, Cu complexes with Me_6TREN are destroyed by Al^{3+} in all investigated media. The investigations suggested that Me_6TREN forms more stable complexes with Al^{3+} than Cu^{2+} or Cu^+. To prevent Cu^{II} and Cu^{I} complexes in solvent/monomer mixtures from decomposition when also Al^{3+} ions are present, enough ligand and/or Br^- to make complexes with both metals should be added.

The competition between Al^{3+} and Cu^{2+} (and Cu^+) ions also has a negative impact on electrochemically-mediated ATRP if a simplified setup with a sacrificial Al anode in an undivided cell is used. *e*ATRP experiments of 50 vol% *n*-BA in DMF, DMSO and MeCN with Cu catalysts based on both ligands confirmed that TPMA prefers binding to Cu^{2+} ions than to Al^{3+} in DMF and DMSO and therefore the polymerization

was not affected by Al^{3+} ions released from the anode. Conversely, the catalytic performance of the system became heavily compromised in all solvents when Me_6TREN or TPMA in MeCN was used in the undivided cell. The interference of Al^{3+} during *e*ATRP could be suppressed by adding excess amine ligand. It is noteworthy that a large excess of ligand, which would otherwise make the process highly costly, is not required; an amount of excess ligand not necessarily exceeding the quantity of Al^{3+} ions produced during electrolysis can suffice. Interestingly, using a two-fold excess of Br^- without excess ligand was found to be beneficial although it could not fully restore the efficiency of the Cu catalysts.

Further development of *e*ATRP with special emphasis on making it as simple and handy as possible is desirable to enhance the potentiality of the method. Using cells without separators is of course important but care must be exercised on the compatibility between the catalyst and sacrificial anode. Here, we show that TPMA is compatible with the use of Al anode in an undivided cell, provided that DMF or DMSO is used as a solvent.

References

[1**]**. Shipp, D. A., Reversible-deactivation radical polymerizations. *Polymer Reviews* **2011,** *51* (2), 99-103.
[2**]**. Matyjaszewski, K.; Gao, H.; Sumerlin, B. S.; Tsarevsky, N. V., *Reversible Deactivation Radical Polymerization: Mechanisms and Synthetic Methodologies*. American Chemical Society: 2018.
[3**]**. Corrigan, N.; Jung, K.; Moad, G.; Hawker, C. J.; Matyjaszewski, K.; Boyer, C., Reversible-deactivation radical polymerization (Controlled/living radical polymerization): From discovery to materials design and applications. *Progress in Polymer Science* **2020**, 101311.
[4**]**. Ohno, K.; Tsujii, Y.; Fukuda, T., Mechanism and kinetics of nitroxide-controlled free radical polymerization. Thermal decomposition of 2, 2, 6, 6-tetramethyl-1-polystyroxypiperidines. *Macromolecules* **1997,** *30* (8), 2503-2506.
[5**]**. Grubbs, R. B., Nitroxide-mediated radical polymerization: limitations and versatility. *Polymer Reviews* **2011,** *51* (2), 104-137.
[6**]**. Hurtgen, M.; Detrembleur, C.; Jerome, C.; Debuigne, A., Insight into organometallic-mediated radical polymerization. *Polymer Reviews* **2011,** *51* (2), 188-213.
[7**]**. Debuigne, A.; Poli, R.; Jérôme, C.; Jérôme, R.; Detrembleur, C., Overview of cobalt-mediated radical polymerization: Roots, state of the art and future prospects. *Progress in Polymer Science* **2009,** *34* (3), 211-239.
[8**]**. Poli, R., New Phenomena in Organometallic-Mediated Radical Polymerization (OMRP) and Perspectives for Control of Less Active Monomers. *Chemistry–A European Journal* **2015,** *21* (19), 6988-7001.
[9**]**. Destarac, M., On the critical role of RAFT agent design in reversible addition-fragmentation chain Transfer (RAFT) polymerization. *Polymer reviews* **2011,** *51* (2), 163-187.
[10**]**. Barner-Kowollik, C., *Handbook of RAFT polymerization*. John Wiley & Sons: 2008.
[11**]**. Semsarilar, M.; Perrier, S., 'Green'reversible addition-fragmentation chain-transfer (RAFT) polymerization. *Nature chemistry* **2010,** *2* (10), 811.
[12**]**. Wang, J.-S.; Matyjaszewski, K., Controlled/" living" radical polymerization. atom transfer radical polymerization in the presence of transition-metal complexes. *Journal of the American Chemical Society* **1995,** *117* (20), 5614-5615.
[13**]**. Ayres, N., Atom transfer radical polymerization: a robust and versatile route for polymer synthesis. *Polymer Reviews* **2011,** *51* (2), 138-162.
[14**]**. Matyjaszewski, K., Atom transfer radical polymerization (ATRP): current status and future perspectives. *Macromolecules* **2012,** *45* (10), 4015-4039.
[15**]**. Lin, C. Y.; Coote, M. L.; Gennaro, A.; Matyjaszewski, K., Ab initio evaluation of the thermodynamic and electrochemical properties of alkyl halides and radicals and their mechanistic implications for atom transfer radical polymerization. *Journal of the*

American Chemical Society **2008,** *130* (38), 12762-12774.
[16**]**. Isse, A. A.; Bortolamei, N.; De Paoli, P.; Gennaro, A., On the mechanism of activation of copper-catalyzed atom transfer radical polymerization. *Electrochimica Acta* **2013,** *110*, 655-662.
[17**]**. Tang, W.; Kwak, Y.; Braunecker, W.; Tsarevsky, N. V.; Coote, M. L.; Matyjaszewski, K., Understanding atom transfer radical polymerization: effect of ligand and initiator structures on the equilibrium constants. *Journal of the American Chemical Society* **2008,** *130* (32), 10702-10713.
[18**]**. Pan, X.; Fantin, M.; Yuan, F.; Matyjaszewski, K., Externally controlled atom transfer radical polymerization. *Chem Soc Rev* **2018,** *47* (14), 5457-5490.
[19**]**. Krys, P.; Matyjaszewski, K., Kinetics of Atom Transfer Radical Polymerization. *European Polymer Journal* **2017,** *89*, 482-523.
[20**]**. Parkatzidis, K.; Wang, H. S.; Truong, N. P.; Anastasaki, A., Recent developments and future challenges in controlled radical polymerization: a 2020 update. *Chem* **2020**.
[21**]**. Magenau, A. J.; Strandwitz, N. C.; Gennaro, A.; Matyjaszewski, K., Electrochemically mediated atom transfer radical polymerization. *Science* **2011,** *332* (6025), 81-4.
[22**]**. Chmielarz, P.; Fantin, M.; Park, S.; Isse, A. A.; Gennaro, A.; Magenau, A. J. D.; Sobkowiak, A.; Matyjaszewski, K., Electrochemically mediated atom transfer radical polymerization (*e*ATRP). *Progress in Polymer Science* **2017,** *69*, 47-78.
[23**]**. Isse, A. A.; Gennaro, A., Electrochemistry for Atom Transfer Radical Polymerization. *The Chemical Record* **2021**.
[24**]**. Lorandi, F.; Fantin, M.; Isse, A. A.; Gennaro, A., Electrochemical triggering and control of atom transfer radical polymerization. *Current Opinion in Electrochemistry* **2018,** *8*, 1-7.
[25**]**. Trevisanello, E.; De Bon, F.; Daniel, G.; Lorandi, F.; Durante, C.; Isse, A. A.; Gennaro, A., Electrochemically mediated atom transfer radical polymerization of acrylonitrile and poly(acrylonitrile-b-butyl acrylate) copolymer as a precursor for N-doped mesoporous carbons. *Electrochimica Acta* **2018,** *285*, 344-354.
[26**]**. Chmielarz, P.; Park, S.; Simakova, A.; Matyjaszewski, K., Electrochemically mediated ATRP of acrylamides in water. *Polymer* **2015,** *60*, 302-307.
[27**]**. Fantin, M.; Chmielarz, P.; Wang, Y.; Lorandi, F.; Isse, A. A.; Gennaro, A.; Matyjaszewski, K., Harnessing the interaction between surfactant and hydrophilic catalyst to control *e*ATRP in miniemulsion. *Macromolecules* **2017,** *50* (9), 3726-2732.
[28**]**. Lorandi, F.; De Bon, F.; Fantin, M.; Isse, A. A.; Gennaro, A., Electrochemical characterization of common catalysts and initiators for atom transfer radical polymerization in [BMIm][OTf]. *Electrochemistry Communications* **2017,** *77*, 116-119.
[29**]**. Park, S.; Chmielarz, P.; Gennaro, A.; Matyjaszewski, K., Simplified electrochemically mediated atom transfer radical polymerization using a sacrificial anode. *Angew Chem Int Ed Engl* **2015,** *54* (8), 2388-92.
[30**]**. Lorandi, F.; Fantin, M.; Isse, A. A.; Gennaro, A., Electrochemically mediated atom transfer radical polymerization of n-butyl acrylate on non-platinum cathodes. *Polymer Chemistry* **2016,** *7* (34), 5357-5365.
[31**]**. De Bon, F.; Isse, A. A.; Gennaro, A., Towards scale-up of electrochemically-

mediated atom transfer radical polymerization: Use of a stainless-steel reactor as both cathode and reaction vessel. *Electrochimica Acta* **2019,** *304*, 505-512.
[32**]**. Chmielarz, P.; Sobkowiak, A.; Matyjaszewski, K., A simplified electrochemically mediated ATRP synthesis of PEO-b-PMMA copolymers. *Polymer* **2015,** *77*, 266-271.
[33**]**. Zaborniak, I.; Chmielarz, P.; Martinez, M. R.; Wolski, K.; Wang, Z.; Matyjaszewski, K., Synthesis of high molecular weight poly(n-butyl acrylate) macromolecules via *se*ATRP: From polymer stars to molecular bottlebrushes. *European Polymer Journal* **2020,** *126*, 109566.
[34**]**. Fantin, M.; Lorandi, F.; Isse, A. A.; Gennaro, A., Sustainable Electrochemically-Mediated Atom Transfer Radical Polymerization with Inexpensive Non-Platinum Electrodes. *Macromol Rapid Commun* **2016,** *37* (16), 1318-22.
[35**]**. Isse, A. A.; Scialdone, O.; Galia, A.; Gennaro, A., The influence of aluminium cations on electrocarboxylation processes in undivided cells with Al sacrificial anodes. *Journal of Electroanalytical Chemistry* **2005,** *585* (2), 220-229.
[36**]**. Bortolamei, N.; Isse, A. A.; Di Marco, V. B.; Gennaro, A.; Matyjaszewski, K., Thermodynamic Properties of Copper Complexes Used as Catalysts in Atom Transfer Radical Polymerization. *Macromolecules* **2010,** *43* (22), 9257-9267.
[37**]**. Lorandi, F.; Fantin, M.; Isse, A. A.; Gennaro, A., RDRP in the presence of Cu0: The fate of Cu (I) proves the inconsistency of SET-LRP mechanism. *Polymer* **2015,** *72*, 238-245.
[38**]**. Qiu, J.; Matyjaszewski, K.; Thouin, L.; Amatore, C., Cyclic voltammetric studies of copper complexes catalyzing atom transfer radical polymerization. *Macromolecular Chemistry and Physics* **2000,** *201* (14), 1625-1631.
[39**]**. De Paoli, P.; Isse, A. A.; Bortolamei, N.; Gennaro, A., New insights into the mechanism of activation of atom transfer radical polymerization by Cu (I) complexes. *Chemical Communications* **2011,** *47* (12), 3580-3582.
[40**]**. De Bon, F.; Carlan, G. M.; Tognella, E.; Isse, A. A., Exploring Electrochemically Mediated ATRP of Styrene. *Processes* **2021,** *9* (8), 1327.
[41**]**. Boyer, C.; Atme, A.; Waldron, C.; Anastasaki, A.; Wilson, P.; Zetterlund, P. B.; Haddleton, D.; Whittaker, M. R., Copper(0)- mediated radical polymerisation in a self-generating biphasic system. *Polymer Chemistry* **2013,** *4* (1), 106-112.
[42**]**. Luo, J.; Durante, C.; Gennaro, A.; Isse, A. A., Electrochemical study of the effect of Al^{3+} on the stability and performance of Cu-based ATRP catalysts in organic media. *Electrochimica Acta* **2021,** *388*, 138589.

Chapter VI

Electrochemical study of the effect of Al^{3+} on Cu-based ATRP catalysts in water

Abstract

Aqueous controlled electrochemically-mediated atom transfer radical polymerization (*e*ATRP) is a powerful technique for the preparation of water-soluble multi-functional polymers for applications in various fields. However, the thermodynamic stabilities of copper-based ATRP catalysts are affected by the solution pH and use of a two-compartment setup results in cost burden, especially in view of industrial scale-up. Recently, *e*ATRP performed in nonaqueous solutions in a simplified undivided cell (termed *se*ATRP) with an inexpensive metal anode such as aluminum attracted a great deal of attention, while there has been almost no relative report on the investigation of *se*ATRP in aqueous media. Thus, the study of the impacts of anodic dissolution of Al on two commonly used copper amine catalysts ($[Cu^{II}L]^{2+}$, L = TPMA and Me_6TREN) in water were investigated by cyclic voltammetry and UV-vis-NIR spectroscopy. Obvious interaction between Me_6TREN and Al^{3+}, hence a significant fraction of $[Cu^{II}Me_6TREN]^{2+}$ undergoing exchange of the ligand with Al^{3+}, was observed. Also, reduction of Cu^{2+} and $[Cu^{II}Me_6TREN]^{2+}$ to Cu^0 by Al leading to irreversible depletion of copper ions was found. Surface morphology and composition of the Al electrode were also characterized by scanning electron microscope (SEM), providing evidence of the formation of Cu on its surface after the electrolysis process in a $[Cu^{II}Me_6TREN]^{2+}$ solution. A slow chemical reaction between $[Cu^{II}TPMA]^{2+}$ and active Al caused a slight loss (~10%) of the catalyst. These competitive equilibria between Cu and Al ions for ligands were effectively suppressed by adding excess ligands.

Keywords: copper complex, aqueous solution, stability, aluminum ions

6.1 Introduction

Atom transfer radical polymerization (ATRP, **Scheme 4.1**) is a robust and highly versatile method that has been successfully employed for the preparation of various advanced materials with controlled architecture. Using ppm levels of copper/amine catalysts with strong catalytic activities permits more environmentally benign ATRP procedures in various media, especially in water.[1-4] In the past two decades, a multitude of advanced ATRP approaches were rapidly developed with the aim of employing very low catalyst loads; these methods start with air-stable copper(II) complexes, which are activated in situ through chemical methods or external physical stimuli.[2, 5-12] One of the most studied and popular approaches is electrochemically mediated ATRP (*e*ATRP, **Scheme 2.1**), which offers multiple readily adjustable parameters for controlling the desired concentration of activator and deactivator species at the working electrode surface.[6, 13-21] Moreover, the conventional *e*ATRP performed in a two-compartment setup with a separated expensive platinum anode was improved by a simplified undivided cell with a low-cost sacrificial Al anode.[16, 18, 22-28] Concurrently, the system resistance was reduced by working in a one-compartment setup. It is favorable for diverse fields of academic study and industrial applications for large-scale production. However, most of these studies were performed in organic solvents,[16, 18, 22, 24-26, 28] while only few cases are reported in aqueous solutions[23] and miniemulsion.[27]

Marco Fantin *et al*. investigated the *e*ATRP of oligo(ethylene oxide) methyl ether methacrylate (OEOMA) in both divided and undivided cells with a sacrificial Al anode in water on various cathodes such as glassy carbon, Au, Ti, Ni, NiCr and SS304.[23] Using the ternary complex $[BrCu^{II}TPMA]^+$ as a deactivator, high monomer conversion (~98%) with low polymer dispersity ($Đ$ < 1.2) was reached in ~ 4 h, although conducting an ATRP in water provides several intriguing challenges.[23, 29-34] Additionally, it was found that these electrodes neither release harmful ions in solution nor react directly with the C-X chain end and can be reused several times. Moreover,

the ratio of $[Cu^{I}L]^{+}/[XCu^{II}L]^{+}$ could be regulated by the applied potential or current, thus the overall rate of polymerization could be finely tuned by modulating some experimental parameters (**eq. 4-2)**. In spite of these brilliant outcomes, several shortcomings exist: only one aromatic amine ligand (TPMA) was tested, and the effects of the ions released from the Al anode on the catalyst stability were not examined. Thus, it is very meaningful to broaden the exploration of the ligand type and examine the effects of the anodic dissolution of Al on catalyst stabilities to provide a set of guidelines for a well-controlled aqueous ATRP in a simplified electrochemical setup.

Herein, this Chapter is aimed to provide some insights into the effect of anodic dissolution of Al on the ATRP catalyst in aqueous media. In order to attain a deeper understanding of the mechanism, with particular attention to the reasons for the stability loss of the catalyst, a systematic investigation was carried out with two highly catalytic copper-amine complexes ($[Cu^{II}L]^{2+}$, L = TPMA and Me_6TREN) in aqueous solutions. In particular, the interactions of free ligands with Al^{3+} and competitive complexation equilibria involving Al^{3+} and copper complexes were estimated via cyclic voltammetry and UV-vis-NIR spectroscopy. Additionally, the morphology of the Al electrode before and after experiments was characterized by the means of SEM. The results of these studies will give us a set of guidelines for the setup of efficient, controlled polymerizations by *se*ATRP in water.

6.2 Methodologies and procedures

6.2.1 CV measurements in the presence of Al^{3+}

Solutions of $[Cu^{II}L]^{2+}$ in water + 0.1 M Et_4NBF_4 were always prepared in situ starting from 1 mM $Cu(OTf)_2$, followed by addition of the ligand (L, $[Cu^{II}]$:[L] = 1:1.05). The desired quantity of Al^{3+} ions was then introduced in the system by anodic dissolution of an Al wire immersed in the working solution containing the Cu complex while the cathode was immersed in a separated compartment containing only the electrolytic solution. The required amount of Al^{3+} (*n* mol) was prepared by applying a

fixed anodic current until the passage of the theoretical charge, Q, according to $Q = 3nF$.[35] The effect of Al^{3+} on the voltammetric pattern of the complexes was often investigated by addition of increasing amounts of Al^{3+} until a two- to three-fold excess over $[Cu^{II}L]^{2+}$ was reached. Strictly speaking, the factors of GC passivation and the difference between the theoretical and real content of Al^{3+} released during the anodic dissolution process cannot be completely excluded. Fortunately, we only investigate the variation trends of different species. After each addition of either Al^{3+} or excess ligand, a freshly polished GC electrode was used to record cyclic voltammetry.Therefore, The reproducibility of the results was less affected.

6.2.2 UV – vis-NIR absorption spectroscopy measurements

The interactions between Al^{3+} and ligands and the competition between Cu^{2+} and Al^{3+} ions for the ligands were also investigated by UV-vis-NIR spectroscopy. Typically, after every addition and CV measurement, a fixed volume of the solution was withdrawn by a pipette and transferred to a 10 mm optical path length quartz cuvette. Subsequently, the UV-vis-NIR spectrum of every sample was recorded by using air as internal standard and was repeated at least two times.

6.2.3 SEM-EDX characterizations and analysis

With the aim of further understanding the mechanism, the surface morphology of the Al wire was characterized after electrolysis in the $[Cu^{II}L]^{2+}$ solution and for comparison without electrolysis but after dipping the Al wire in the blank solution. In addition, elemental analysis was evaluated and based on at least 3 different selected regions for each sample and the results were reported as average values.

6.3 Results and discussion

6.3.1 Interaction between amine ligands and Al^{3+}

The obvious competition between Al^{3+} ions and copper ions for the ligands was

systemically explored in some commonly used organic solvents in **Chapters IV** and **V**, showing that Al^{3+} ions can destroy copper complexes and therefore stop polymerization after a low conversion. Thus, it's necessary to investigate the possible interactions between Al^{3+} and TPMA or Me_6TREN in aqueous solutions as well. Initially, as shown in **Figure 6.1 a, b**, the electrochemical behaviors of TPMA and Me_6TREN in the absence and presence of Al^{3+} ions were examined on a freshly polished electrode surface. An irreversible oxidation peak was found for TPMA and Me_6TREN at about 1.13V and 0.91V, respectively. As in DMF, DMSO and MeCN, the oxidation peak of Me_6TREN decreased and disappeared with increasing concentration of Al^{3+}, while the CV response of TPMA remained unchanged. In this experiment, Al^{3+} ions were prepared in situ by anodic dissolution of an Al wire immersed in a solution containing the ligand. However, similar results were obtained when the Al wire was eliminated and Al^{3+} ions were added from a stock solution prepared in advance (**Figure 6.1 c, d**). The observed decrease of peak intensity for Me_6TREN is clear evidence of the formation of new Al^{3+} species with the ligand, no matter how the Al^{3+} ions were introduced into the cell.

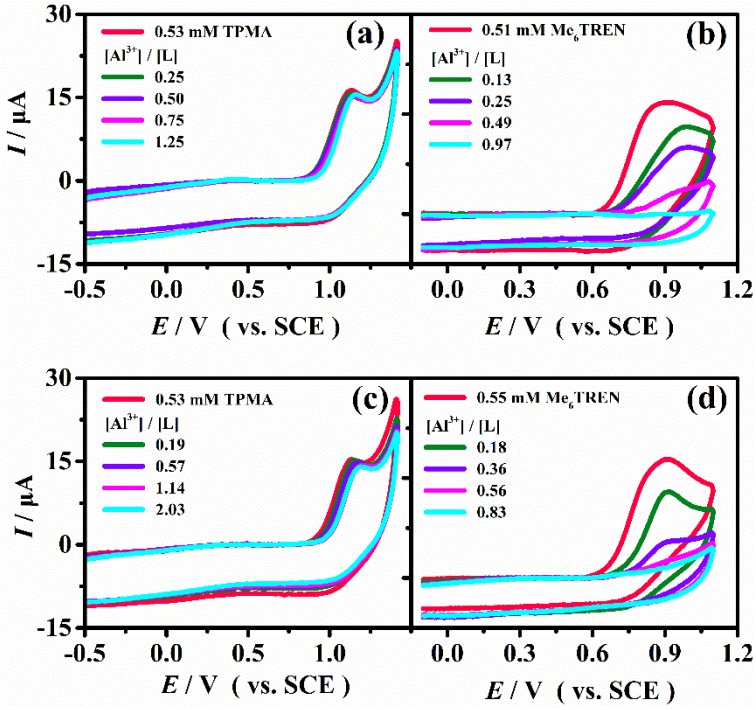

Figure 6.1 CVs of TPMA and Me_6TREN in the absence and presence of Al^{3+}, generated

in situ via electrolysis (a, b) or added from a stock solution (c, d), in H_2O + 0.1 M Et_4NBF_4, recorded on a GC disk at $\upsilon = 0.2$ Vs^{-1}, $T = 25$ °C.

The oxidation peaks of both ligands were investigated at different sweep rates, showing that they remain irreversible even at relatively high scan rates. Analysis of E_p and $\Delta E_{p/2} = E_p - E_{p/2}$ **(eq. 6-1)** as a function of υ showed a straight line for E_p vs. log υ and a roughly constant $\triangle E_{p/2}$; examples of the trends of Ep and $\triangle E_{p/2}$ are shown in **Figure 6.2** for Me_6TREN. The values of the transfer coefficient α calculated from the slope of the line and from $\triangle E_{p/2}$ for Me_6TREN and TPMA were 0.29 and 0.26, respectively. The very low α value in water points out that the oxidation reaction is kinetically controlled by a slow electron transfer (ET) process.[36-39]

$$\triangle E_{p/2} = E_{P/2} - E_P = 1.857RT/\alpha F = 0.0477/\alpha \qquad \text{at } 25\ ^oC \qquad (6\text{-}1)$$

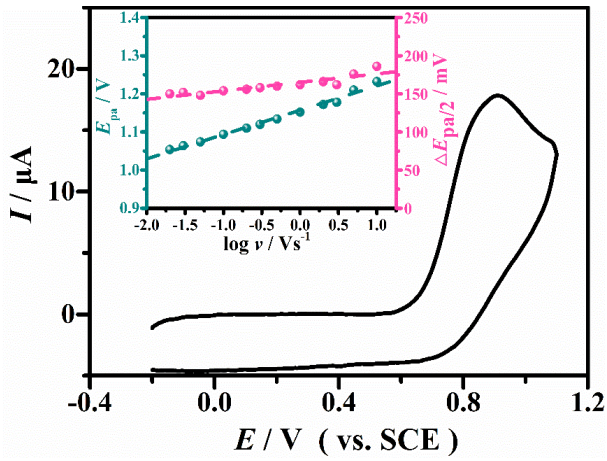

Figure 6.2 CVs of 0.5 mM Me_6TREN in H_2O + 0.1 M Et_4NBF_4, recorded on a GC disk at $\upsilon = 0.2$ Vs^{-1}, $T = 25$ °C. The inset shows dependence of E_p and $\triangle E_{p/2}$ on scan rate.

6.3.2 Effect of Al^{3+} on the stability of Cu^{2+} and $[Cu^{II}L]^{2+}$

Cu^{2+} and Cu^{+} ions combine with tetradentate amine ligands (TPMA and Me_6TREN) to form $[Cu^{II}L]^{2+}$ and $[Cu^{I}L]^{+}$, respectively, as indicated in **Scheme 6.1**. **Figure 6.3** shows CVs of copper (II) trifluoromethanesulfonate ($Cu(OTf)_2$) before and after addition of TPMA or Me_6TREN and further progressive addition of Al^{3+} ions. The

Al^{3+} ions were either prepared in situ via the electrolysis of an Al wire (**Figure 6.3 a, c**) or added from a stock solution (**Figure 6.3 b, d**). The solvated Cu^{2+} ions presented a peak couple with a big separation, ΔE_p = 94 mV at 0.2 Vs^{-1} and a half-wave potential around -0.087 V vs. SCE. Thus a quasi-reversible redox reaction takes place in water for the solvated of Cu^{2+}/Cu^{+} couple. Addition of an equimolar quantity of ligand quantitatively converted Cu^{2+} to $[Cu^{II}L]^{2+}$; the peak couple at -0.087 disappeared while a new peak couple with a narrower peak separation appeared at more negative potentials. The electron transfer process is faster for the $[Cu^{II}L]^{2+}/[Cu^{I}L]^{+}$ couple than for the solvated ions. The redox potentials measured for Cu^{2+}/Cu^{+} were negatively shifted by 0.277 V and 0.324 V after addition of TPMA and Me_6TREN, i.e., from -0.087 V to -0.364 V and -0.411 V, respectively. These remarkably negative shifts indicate that both ligands stabilize Cu^{2+} better than Cu^{+}, and $[Cu^{I}Me_6TREN]^{+}$ is a stronger reducing agent than $[Cu^{I}TPMA]^{+}$.

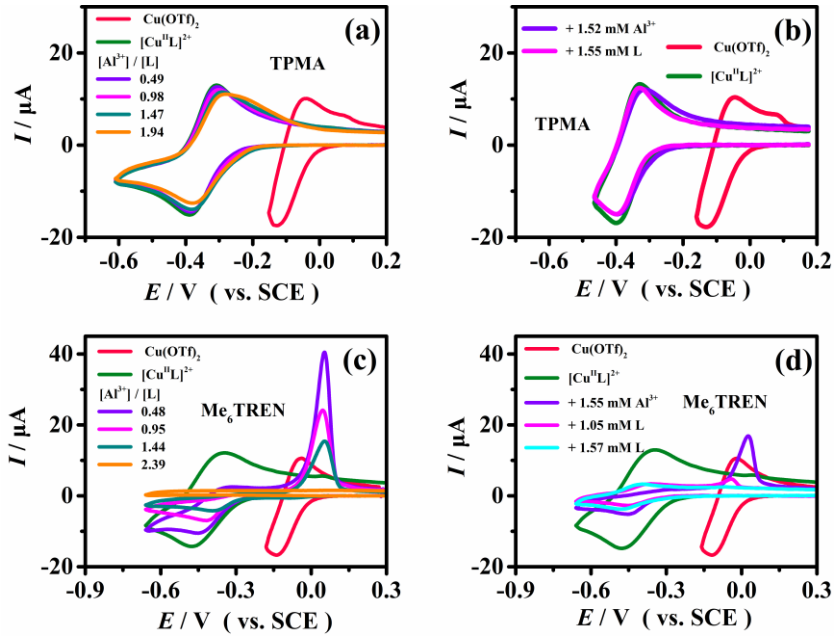

Figure 6.3 CVs of 1 mM $Cu(OTf)_2$ and 1 mM $[Cu^{II}L]^{2+}$ before and after stepwise addition of Al^{3+} and ligand (L) for L= TPMA **(a-b)** and Me_6TREN **(c-d)**, recorded at υ = 0.2 V s^{-1} on a GC disk in H_2O + 0.1 M Et_4NBF_4, T = 25 °C.

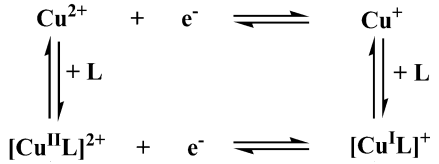

Scheme 6.1 Redox and complexation equilibria involving Cu^{2+} and Cu^{+} ions.

Addition of progressively increasing amounts of Al^{3+} to the working solution by anodic dissolution of an Al wire immersed in solution had completely different effects for the two ligands. In the case of TPMA, no remarkable changes occurred to the CV response of $[Cu^{II}TPMA]^{2+}$. It continued to exhibit a quasi-reversible redox feature in the presence of Al^{3+}. $E^{\ominus}_{[Cu^{II}L]^{2+}/[Cu^{I}L]^{+}}$ can be obtained according to $E^{\ominus} \approx E_{1/2} = (E_{pc} + E_{pa})/2$, where E_{pc} and E_{pa} stand for the cathodic and anodic peak potentials, respectively. $E^{\ominus}_{[Cu^{II}L]^{2+}/[Cu^{I}L]^{+}}$ shifted slightly to more positive potentials (from -0.364 V to -0.346 V) when $[Al^{3+}]$/[TPMA] was varied from 0 to 1.94. Also, a slight decrease of the cathodic peak current was observed. Addition of excess ligand to a solution of $[Cu^{II}L]^{2+}$ containing Al^{3+} ions had no significant effect since Al^{3+} did not destroy $[Cu^{II}L]^{2+}$ (**Figure 6.3 b**).

Conversely, a different situation was observed for Me_6TREN (**Figure 6.3 c**). The reversible peak couple decreased in intensity and eventually disappeared as the quantity of added Al^{3+} ions was increased. This circumstance was possibly due to the instability of the binary copper complex during anodic dissolution of Al. Furthermore, the rapid decay of the peak couple for $[Cu^{II}Me_6TREN]^{2+}/[Cu^{I}Me_6TREN]^{+}$ was accompanied by the appearance of a sharp anodic stripping peak around 0.05 V. These observations clearly prove the instability of Cu/Me_6TREN complexes in the presence of Al^{3+} ions in aqueous solutions. A possible explanation of the observed phenomena could be given if one assumes that Me_6TREN forms a stronger complex with Al^{3+} than with Cu^{2+} and Cu^{+}. A ligand exchange reaction takes place when Al^{3+} ions are added to the solution so that both $[Cu^{II}Me_6TREN]^{2+}$ and electrogenerated $[Cu^{I}Me_6TREN]^{+}$ are destroyed:

$$[Cu^{II}Me_6TREN]^{2+} + Al^{3+} \rightleftharpoons [Al^{III}Me_6TREN]^{3+} + Cu^{2+} \quad (6\text{-}2)$$

$$[Cu^{I}Me_6TREN]^{+} + Al^{3+} \rightleftharpoons [Al^{III}Me_6TREN]^{3+} + Cu^{+} \quad (6\text{-}3)$$

However, free Cu^{2+} ions could not be observed in solution. Indeed, during Al^{3+} addition experiments, the peak couple at -0.087 for the Cu^{2+}/Cu^{+} redox couple never appeared. During Al^{3+} additions, the cathodic peak for $[Cu^{II}Me_6TREN]^{2+}$ reduction decreased gradually with the increasing concentration of Al^{3+}, while the anodic peak disappeared immediately. This clearly indicates that $[Cu^{I}Me_6TREN]^{+}$ immediately exchanges the ligand with Al^{3+}. Another piece of evidence for fast kinetics of this reaction comes from the dependence of the anodic stripping peak at 0.05 V on added Al^{3+} concentration. It decreases as the amount of added Al^{3+} is increased. At the end, when excess Al^{3+} over $[Cu^{II}Me_6TREN]^{2+}$ was added, neither the peak couple of $[Cu^{II}Me_6TREN]^{2+}/[Cu^{I}Me_6TREN]^{+}$ nor that of Cu^{2+}/Cu^{+} was present. Also, the anodic stripping peak disappeared (**Figure 6.3 c**). It appears that no Cu(II) species is present in solution. This is confirmed by an attempt to restore the $[Cu^{II}Me_6TREN]^{2+}/[Cu^{I}Me_6TREN]^{+}$ peak couple by addition of excess ligand after a series of Al^{3+} additions. As shown in **Figure 6.3 d** no signal recovery was observed after addition. Neglecting at the moment the fate of Cu^{2+} from reaction **6-2**, the experimental observations fit very well the following sequence of reactions:

$$[Cu^{II}Me_6TREN]^{2+} + e^{-} \rightleftharpoons [Cu^{I}Me_6TREN]^{+} \quad (6\text{-}4)$$

$$[Cu^{I}Me_6TREN]^{+} + Al^{3+} \rightleftharpoons [Al^{III}Me_6TREN]^{3+} + Cu^{+} \quad (6\text{-}3)$$

$$Cu^{+} + e^{-} \rightleftharpoons Cu^{0} \quad (6\text{-}5)$$

$$Cu^{0} \rightleftharpoons Cu^{2+} + 2\,e^{-} \quad (6\text{-}6)$$

Although a clear evidence of Cu^{2+} formation is missing, it is doubtless that the concentration of $[Cu^{II}M_6TREN]^{2+}$ in solution decreases as the quantity of added Al^{3+} is increased. Anyway, electroreduction of the remaining $[Cu^{II}M_6TREN]^{2+}$ triggers a

sequence of reactions (**eqs. 6-3 to 6-5**) leading to the formation of a copper deposit on the GC electrode. The quantity of the deposited metal, which is proportional to the anodic stripping peak current, decreases as the starting amount of $[Cu^{II}M_6TREN]^{2+}$ decreases.

An intriguing issue of the above described system is the complete disappearance of all Cu(II) species from the solution. As shown in **Figure 6.3 d**, the quasi-reversible peak couple of $[Cu^{II}Me_6TREN]^{2+}$ could not be recovered after addition of excess ligand. This behavior clearly differs from what was observed in DMF at the same conditions (except for the solvent) reported in **Chapter IV**, in which total regeneration of $[Cu^{II}Me_6TREN]^{2+}$ was observed after addition of excess ligand.[18, 28] Side reactions involving the active Al wire must be considered. Indeed, a homogenous brown–red layer was observed on the immersed Al wire surface after the experiment. In addition, the solution color changed from green before immersion of Al to colorless after the experiment of Al^{3+} addition by electrolysis.

6.3.3 Reaction of Al with Cu^{2+} and $[Cu^{II}L]^{2+}$ in water

To better understand the possible side reactions consuming Cu(II) species during the anodic dissolution step, several parallel experiments were designed and carried out to confirm the hypothesis of Al acting as a reducing agent for Cu(II), converting it to metallic Cu according reaction **(6-7)** and/or reaction **(6-2)** followed by reaction **(6-8)**:

$$3[Cu^{II}Me_6TREN]^{2+} + 2Al \rightleftharpoons 2[Al^{III}Me_6TREN]^{3+} + 3Cu \quad (6\text{-}7)$$

$$[Cu^{II}Me_6TREN]^{2+} + Al^{3+} \rightleftharpoons [Al^{III}Me_6TREN]^{3+} + Cu^{2+} \quad (6\text{-}2)$$

$$3Cu^{2+} + 2Al \rightleftharpoons 2Al^{3+} + 3Cu \quad (6\text{-}8)$$

For comparison, four experiments with an activated Al wire were performed. In three experiments the wire was immersed in a solution containing Cu(II) species ($Cu(OTf)_2$, $[Cu^{II}TPMA]^{2+}$ or $[Cu^{II}Me_6TREN]^{2+}$) and CVs were periodically recorded

to evaluate Cu(II) concentration. In the fourth experiment, the Al wire was immersed in a $Cu(OTf)_2$ solution and a constant anodic current was applied, and again CVs of the system were periodically recorded. As shown in **Figure 6.4 a**, a spontaneous reaction between Cu^{2+} and Al occurred with continuous decrease of Cu^{2+} concentration until after 90 min the reaction stopped due to the exhaustion of Cu^{2+}. In addition, a metallic copper deposit was observed on the surface of the Al surface. These observations clearly point out reduction of $[Cu^{II}Me_6TREN]^{2+}$ and Cu^{2+} by Al. The standard Gibbs energy of reaction (**6-8**), $\Delta G^{\ominus}_{6\text{-}8}$, can be calculated from the standard reduction potentials of Al^{3+} and Cu^{2+}, which correspond to − 1.66 V vs. SHE and 0.34 V vs. SHE, respectively. This gives $\Delta G^{\ominus}_{6\text{-}8}$ = -1157.8 kJ/mol. Estimation of $\Delta G^{\ominus}_{6\text{-}7}$ needs data on the stability constants of $[Cu^{II}Me_6TREN]^{2+}$ and $[Al^{III}Me_6TREN]^{3+}$ in water, which are not available. However, considering that Me_6TREN gives a more stable complex with Al^{3+} than with Cu^{2+}, it is likely that reduction of $[Cu^{II}Me_6TREN]^{2+}$ by Al is a spontaneous reaction, that is, $\Delta G^{\ominus}_{6\text{-}7} < 0$.

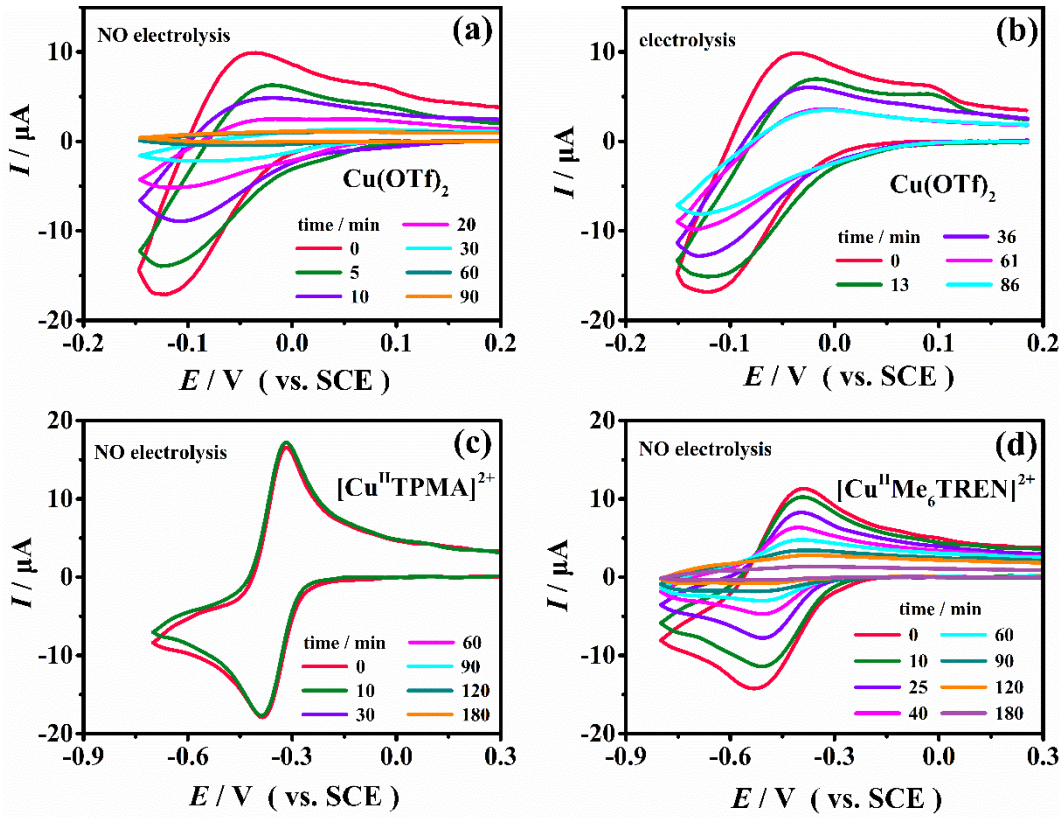

Figure 6.4 CVs of 1 mM $Cu(OTf)_2$ or 1 mM $[Cu^{II}L]^{2+}$ before and after immersion of

an activated Al wire into the solution without (**a, c,** and **d**) and with (**b**) anodic dissolution of Al by electrolysis, recorded at different time intervals at $\upsilon = 0.2$ Vs^{-1} on a GC disk in H_2O + 0.1 M Et_4NBF_4, $T = 25$ °C. During the CV measurements, the Al wires were lifted up and remained above the solution level.

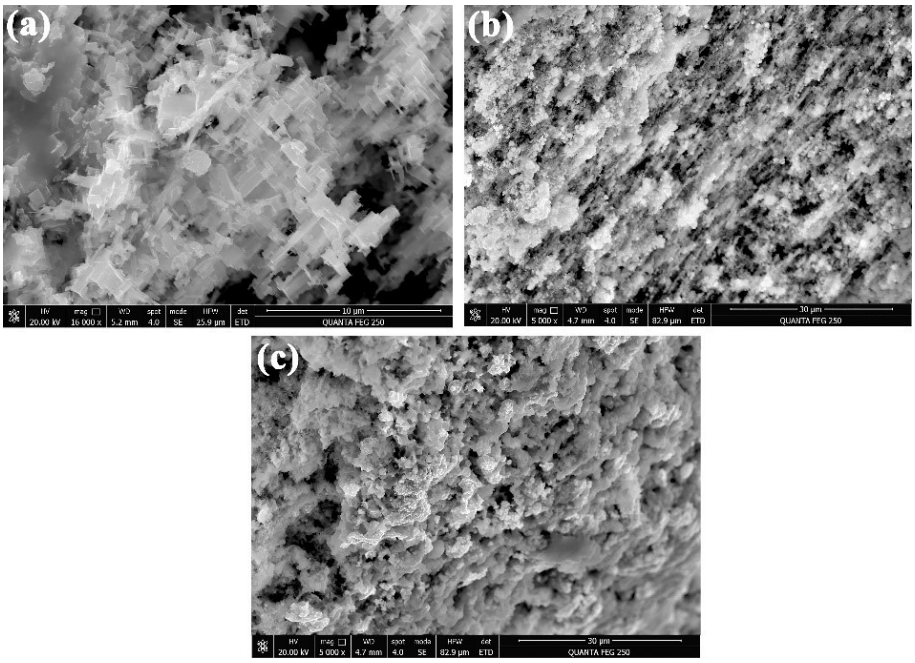

Figure 6.5 SEM images of the initial Al electrode **(a)** and after immersion in a $Cu(OTf)_2$ solution and application of an anodic current for 86 mins **(b)** or after immersing for 90 mins without electrolysis in a $Cu(OTf)_2$ solution of the same composition **(c)**.

Depletion of Cu^{2+} from the solution was, however, slower in the presence of applied current, **Figure 6.4 b**. In addition, SEM EDX elemental analyses of the Al electrode after the experiments (**Figure 6.5, Table 6.1**) showed significant differences in terms of both morphology and surface content of Al. In **Figure 6.5 b, c**, serious corrosion of the metal surface with many micro-grade pores was observed, especially in the case of electrolysis; the presence of the same elements at different contents were also confirmed.

Figure 6.4 shows also Al dipping experiments in the presence of a ligand. When TPMA was used, negligible variation of $[Cu^{II}TPMA]^{2+}$ concentration was observed after 3 hours (**Figure 6.4 c**), while $[Cu^{II}Me_6TREN]^{2+}$ was completely consumed in the

same period of time (**Figure 6.4 d)**. Such a big difference in reactivity is possibly related to the previously observed difference of reactivity of Al^{3+} ions with the two ligands. Indeed, Al^{3+} forms a very stable complex with Me_6TREN, whereas it does not react with TPMA. This means while reaction (**6-7**) is probably spontaneous, the corresponding reaction with TPMA is not thermodynamically favorable.

Table 6.1 Elemental analysis of Al surface in **Figure 6.5** via SEM-EDX

Elements	Blank Al		After electrolysis		Immersion without electrolysis	
	Wt%	At%	Wt%	At%	Wt%	At%
C	2.4	4.94	4.3	8.7	4.6	10.4
O	10.0	15.35	14.3	21.7	20.3	34.5
Al	87.6	79.71	74.8	67.1	39.4	39.7
Cu	-	-	6.6	2.5	35.7	15.3

The decay rates of $Cu(OTf)_2$ and $[Cu^{II}L]^{2+}$ in the presence of Al with or without electrolysis can be roughly estimated using the cathodic peak currents according to Randles–Sevcik equation (**eq. 6-9**).[40]

$$I_p = 0.4463\,(\frac{F^3}{RT})^{1/2} \times n^{3/2} A C D^{1/2} \upsilon^{1/2} \qquad (6\text{-}9)$$

where I_p is peak current (A), F is Faraday constant, R is gas constant, T is temperature, n is number of electrons transferred in the reaction, A is electrode area, C is substance concentration, υ is the scan rate. In the dipping experiments described above, all parameters in **eq. 6-9** are constant, except C. Thus, the concentration can be written as:

$$C = z\, I_p \qquad (6\text{-}10)$$

where z is equal to $1/(0.4463\,(\frac{F^3}{RT})^{1/2} \times n^{3/2} A D^{1/2} \upsilon^{1/2})$. Assuming that $[Cu^{II}Me_6TREN]^{2+}$ mainly disappears via reaction **6-7**, the kinetics of the process was analyzed according to a first-order rate law. Thus, after t min, the reactant concentration can be calculated as follows:

$$\int_{C_0}^{C_t} dC = -\int_0^t k\, dt \quad (6\text{-}11)$$

$$C = C_0\, e^{-kt} \quad (6\text{-}12)$$

where C_0, C_t are the concentrations of $Cu(OTf)_2$ or $[Cu^{II}L]^{2+}$ at 0 min and t min, respectively, k is the rate constant (1/min). Introducing **eq. 6-10** in **eq. 6-12** and rearranging gives:

$$\ln\frac{C_0}{C_t} = \ln\frac{I_{p,0}}{I_{p,t}} = k\,t \quad (6\text{-}13)$$

Figure 6.6 shows linear plots based on **eq. 6-13** for $Cu(OTf)_2$ and $[Cu^{II}L]^{2+}$. Higher rate constants were obtained for reactions without applied anodic current on the Al wire than when the Al wire was working also as an anode. Also, free Cu^{2+} ions reacted faster than $[Cu^{II}Me_6TREN]^{2+}$. The rate constants obtained for the reduction of Cu^{2+} ions and $[Cu^{II}Me_6TREN]^{2+}$ by an active Al wire without applied anodic current were 0.059 ± 0.001 min^{-1} and 0.022 ± 0.001 min^{-1}, respectively. The obtained difference of k values (0.059 ± 0.001 min^{-1} for $Cu(OTf)_2$ and 0.022 ± 0.001 min^{-1} for $[Cu^{II}Me_6TREN]^{2+}$) agrees well with the previous results observed in **Figure 6.4**.

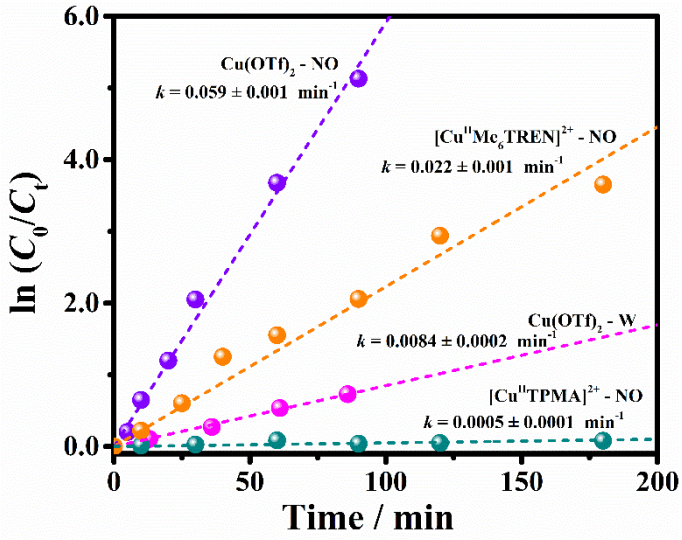

Figure 6.6 Linear plots of $\ln(C_0/C_t)$ as a function of reaction time with the best fit lines for $Cu(OTf)_2$ and $[Cu^{II}L]^{2+}$ in the presence of Al without or with electrolysis in water.

6.3.4 UV-vis-NIR analysis of L, Cu^{2+}, and $[Cu^{II}L]^{2+}$ in the presence of Al^{3+}

During the CV experiments aimed to analyze the effect of Al wire and Al^{3+} ions on the stability of $[Cu^{II}L]^{2+}$, significant changes of solution color were observed. For example, the color of $[Cu^{II}Me_6TREN]^{2+}$ solution slowly faded and nearly disappeared when the ratio of added Al^{3+} to ligand reached 1.55, as shown in **Figure 6.7 a, b**. This apparent color changes could not be fully restored after addition of excess ligand to the solution (**Figure 6.7 c, d**), which again indicates that Cu(II) has been lost during the experiment. Thus, the depletion of $[Cu^{II}L]^{2+}$ in the presence of Al wire in aqueous solutions was also investigated by UV-vis-NIR spectroscopy. For comparison, spectra of the ligands in the presence of increasing Al^{3+} ions were first recorded. No significant absorption peaks were observed for TPMA or Me_6TREN in the presence of Al^{3+} in the UV-vis-NIR region from 330 to 1350 nm (**Figure 6.8 a, b**) despite the interactions of Al^{3+} with Me_6TREN shown in **Figure 6.1 b and d**. Similar to solvated Cu^{2+} ions in organic media, a broad absorption band of Cu^{2+} was also found in water with a maximum wavelength (λ_{max}) at about 880 nm. Analogously, when TPMA or Me_6TREN was added, two typical d → d transitions were observed in the NIR and visible regions [41-44]: a lower energy band centered around 905 nm and a higher energy, less intense shoulder around 685 nm. This result is in accordance with literature reports and is attributed to the effect of distorted trigonal bipyramidal geometry of the copper complexes with tripodal nitrogen-based ligands.[41-43, 45]

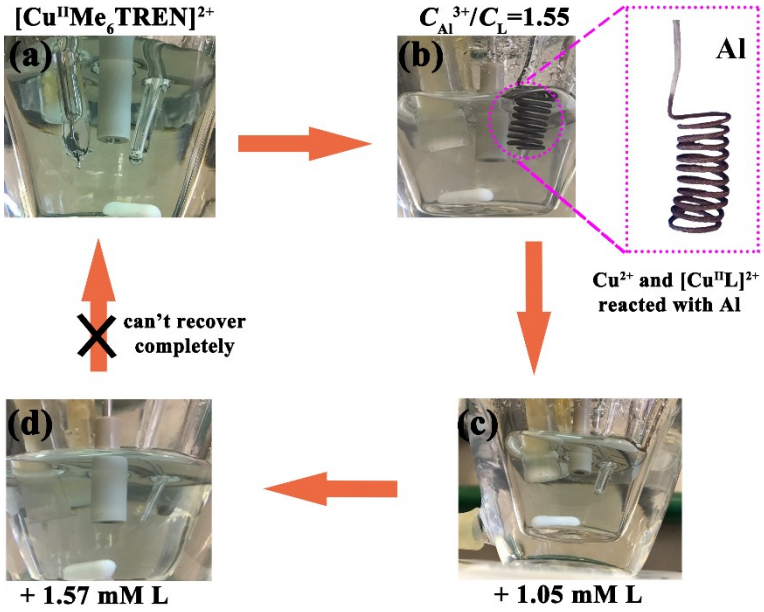

Figure 6.7 Digital photographs of 1 mM $[Cu^{II}Me_6TREN]^{2+}$ in the absence **(a)** and presence of Al^{3+} alone **(b)** or Al^{3+} and excess ligand **(c-d)** in aqueous solutions. The inset in **(b)** shows the Al electrode with a brown-red layer covering the surface of the spiral coil after electrolysis.

Based on Beer–Lambert law (**eq. 4-13**),[46] the slight loss (~10%) of the absorption intensity of $[Cu^{II}TPMA]^{2+}$ in **Figure 6.8 c** is probably indicative of a slow chemical reaction during anodic dissolution of Al. This is in line with the CV experiments above. Conversely, the intensity of the spectrum of $[Cu^{II}Me_6TREN]^{2+}$ rapidly decreased and finally disappeared as the electrolysis was protracted (**Figure 6.8 d**). A fast chemical reaction of Al^{3+} and active Al with $[Cu^{II}Me_6TREN]^{2+}$ occurred during electrolysis. A direct evidence of the reaction between metallic Al and $[Cu^{II}Me_6TREN]^{2+}$ was also observed in **Figure 6.7 b**. The complicated equilibria involving the ligand, Cu^{2+} and Al^{3+} ions were well-evidenced by the decrease of absorption at 880 nm (**Figure 6.8 e**).

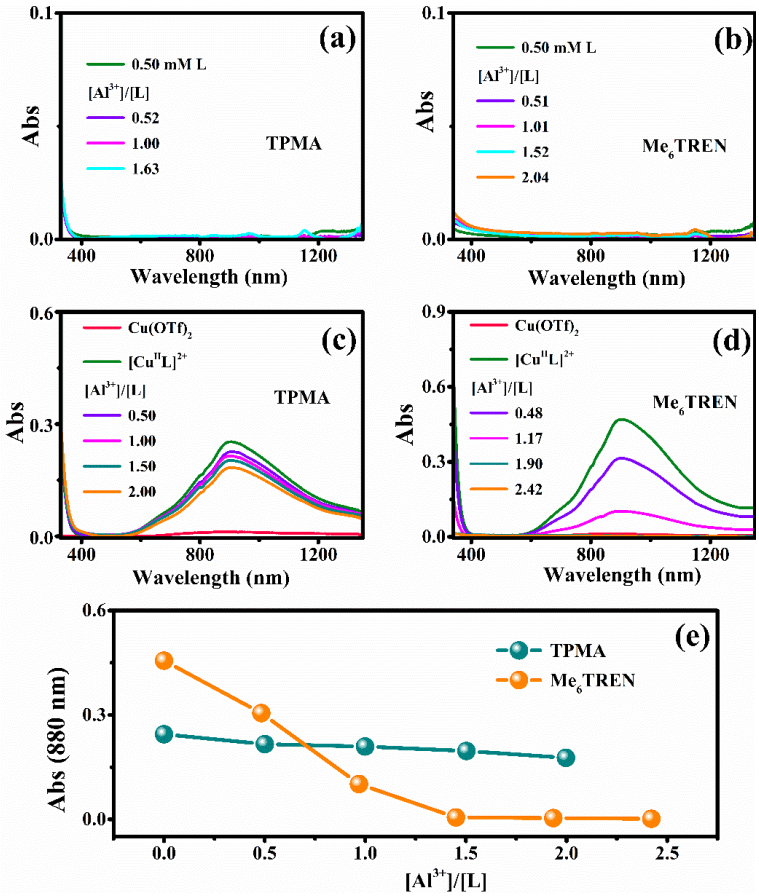

Figure 6.8 UV-vis-NIR spectra of TPMA **(a)** or Me_6TREN **(b)**, and 1 mM $Cu(OTf)_2$ and $[Cu^{II}L]^{2+}$ **(c-d)**, in the absence and presence of increasing amounts of Al^{3+} ions, recorded in aqueous solutions in a 10 mm pathlength cuvette. **(e)** Absorbance of 1 mM $[Cu^{II}L]^{2+}$ measured at 880 nm as a function of the ratio of added Al^{3+} ions to the ligands.

6.4 Conclusions

In conclusion, evaluation of $[Cu^{II}L]^{2+}$ stabilities in the presence of anodic dissolution of Al in aqueous solutions gives results similar to those found in DMF and DMSO. A big fraction of $[Cu^{II}TPMA]^{2+}$ remained unchanged in water containing Al^{3+} ions, clearly indicating that this complex is highly stable in such conditions. The slight loss (~10%) of $[Cu^{II}TPMA]^{2+}$ is probably indicative of a slow chemical reaction in the presence of high concentration of Al^{3+} ions. Conversely, the copper complex coordinated to Me_6TREN showed a completely different stability as compared to TPMA. Cyclic voltammetry and UV-vis-NIR investigations showed that not only

$[Cu^{I}Me_6TREN]^{+}$ but also $[Cu^{II}Me_6TREN]^{2+}$ is rapidly destroyed by Al^{3+}, which displace the ligand from copper, forming more stable complexes. In addition, Cu^{2+} and $[Cu^{II}Me_6TREN]^{2+}$ react spontaneously with active Al, leading to irreversible consumption of Cu(II) and formation of a metallic copper deposit on the Al surface. Usually, the competitive chemical reactions involving Cu^{2+}, Al^{3+} and amine ligands can be effectively suppressed by the addition of excess ligand. Despite this, $[Cu^{II}Me_6TREN]^{2+}$ could not be recovered completely even in the presence of a large excess of ligand because of the irreversible depletion Cu(II) during the anodic dissolution of Al in water. These investigations helped us understand the mechanism of the reactions of Cu^{2+} ions and/or complexes with Al^{3+} and Al surface in water. The obtained results will be of great help for the setup of aqueous *e*ATRP with Al sacrificial anodes.

References

[1**]**. Ayres, N., Atom transfer radical polymerization: a robust and versatile route for polymer synthesis. *Polymer Reviews* **2011,** *51* (2), 138-162.
[2**]**. Matyjaszewski, K., Atom transfer radical polymerization (ATRP): current status and future perspectives. *Macromolecules* **2012,** *45* (10), 4015-4039.
[3**]**. Matyjaszewski, K.; Tsarevsky, N. V., Macromolecular engineering by atom transfer radical polymerization. *J Am Chem Soc* **2014,** *136* (18), 6513-33.
[4**]**. Matyjaszewski, K., Advanced Materials by Atom Transfer Radical Polymerization. *Adv Mater* **2018,** *30* (23), e1706441.
[5**]**. Krys, P.; Matyjaszewski, K., Kinetics of Atom Transfer Radical Polymerization. *European Polymer Journal* **2017,** *89*, 482-523.
[6**]**. Pan, X.; Fantin, M.; Yuan, F.; Matyjaszewski, K., Externally controlled atom transfer radical polymerization. *Chem Soc Rev* **2018,** *47* (14), 5457-5490.
[7**]**. Ma, Q.; Song, J.; Liao, S., Metal-free atom transfer radical polymerization with ppm catalyst loading under sunlight. *Nat Commun* **2021,** *12* (1), 429.
[8**]**. Tsarevsky, N. V.; Matyjaszewski, K., "Green" atom transfer radical polymerization: from process design to preparation of well-defined environmentally friendly polymeric materials. *Chemical reviews* **2007,** *107* (6), 2270-2299.
[9**]**. Semsarilar, M.; Perrier, S., 'Green'reversible addition-fragmentation chain-transfer (RAFT) polymerization. *Nature chemistry* **2010,** *2* (10), 811.
[10**]**. Konkolewicz, D.; Magenau, A. J.; Averick, S. E.; Simakova, A.; He, H.; Matyjaszewski, K., ICAR ATRP with ppm Cu Catalyst in Water. *Macromolecules* **2012,** *45* (11), 4461-4468.
[11**]**. Jakubowski, W.; Min, K.; Matyjaszewski, K., Activators regenerated by electron transfer for atom transfer radical polymerization of styrene. *Macromolecules* **2006,** *39* (1), 39-45.
[12**]**. Abreu, C. M.; Mendonça, P. V.; Serra, A. n. C.; Popov, A. V.; Matyjaszewski, K.; Guliashvili, T.; Coelho, J. F., Inorganic sulfites: Efficient reducing agents and supplemental activators for atom transfer radical polymerization. *Acs Macro Letters* **2012,** *1* (11), 1308-1311.
[13**]**. Magenau, A. J.; Strandwitz, N. C.; Gennaro, A.; Matyjaszewski, K., Electrochemically mediated atom transfer radical polymerization. *Science* **2011,** *332* (6025), 81-4.
[14**]**. Li, B.; Yu, B.; Huck, W. T. S.; Zhou, F.; Liu, W., Electrochemically Induced Surface-Initiated Atom-Transfer Radical Polymerization. *Angewandte Chemie International Edition* **2012,** *51* (21), 5092-5095.
[15**]**. Magenau, A. J. D.; Bortolamei, N.; Frick, E.; Park, S.; Gennaro, A.; Matyjaszewski, K., Investigation of Electrochemically Mediated Atom Transfer Radical Polymerization. *Macromolecules* **2013,** *46* (11), 4346-4353.
[16**]**. Park, S.; Chmielarz, P.; Gennaro, A.; Matyjaszewski, K., Simplified electrochemically mediated atom transfer radical polymerization using a sacrificial

anode. *Angew Chem Int Ed Engl* **2015,** *54* (8), 2388-92.
[17**]**. Fantin, M.; Park, S.; Wang, Y.; Matyjaszewski, K., Electrochemical atom transfer radical polymerization in miniemulsion with a dual catalytic system. *Macromolecules* **2016,** *49* (23), 8838-8847.
[18**]**. Lorandi, F.; Fantin, M.; Isse, A. A.; Gennaro, A., Electrochemically mediated atom transfer radical polymerization of n-butyl acrylate on non-platinum cathodes. *Polymer Chemistry* **2016,** *7* (34), 5357-5365.
[19**]**. Chmielarz, P.; Fantin, M.; Park, S.; Isse, A. A.; Gennaro, A.; Magenau, A. J. D.; Sobkowiak, A.; Matyjaszewski, K., Electrochemically mediated atom transfer radical polymerization (*e*ATRP). *Progress in Polymer Science* **2017,** *69*, 47-78.
[20**]**. Lorandi, F.; Fantin, M.; Isse, A. A.; Gennaro, A., Electrochemical triggering and control of atom transfer radical polymerization. *Current Opinion in Electrochemistry* **2018,** *8*, 1-7.
[21**]**. Isse, A. A.; Gennaro, A., Electrochemistry for Atom Transfer Radical Polymerization. *The Chemical Record* **2021**.
[22**]**. Chmielarz, P.; Sobkowiak, A.; Matyjaszewski, K., A simplified electrochemically mediated ATRP synthesis of PEO-b-PMMA copolymers. *Polymer* **2015,** *77*, 266-271.
[23**]**. Fantin, M.; Lorandi, F.; Isse, A. A.; Gennaro, A., Sustainable Electrochemically-Mediated Atom Transfer Radical Polymerization with Inexpensive Non-Platinum Electrodes. *Macromol Rapid Commun* **2016,** *37* (16), 1318-22.
[24**]**. Chmielarz, P.; Sobkowiak, A., Ultralow ppm *se*ATRP synthesis of PEO-b-PBA copolymers. *Journal of Polymer Research* **2017,** *24* (5).
[25**]**. De Bon, F.; Isse, A. A.; Gennaro, A., Towards scale-up of electrochemically-mediated atom transfer radical polymerization: Use of a stainless-steel reactor as both cathode and reaction vessel. *Electrochimica Acta* **2019,** *304*, 505-512.
[26**]**. Zaborniak, I.; Chmielarz, P.; Martinez, M. R.; Wolski, K.; Wang, Z.; Matyjaszewski, K., Synthesis of high molecular weight poly(n-butyl acrylate) macromolecules via *se*ATRP: From polymer stars to molecular bottlebrushes. *European Polymer Journal* **2020,** *126*, 109566.
[27**]**. Zaborniak, I.; Chmielarz, P., Miniemulsion switchable electrolysis under constant current conditions. *Polymers for Advanced Technologies* **2020,** *31* (11), 2806-2815.
[28**]**. Luo, J.; Durante, C.; Gennaro, A.; Isse, A. A., Electrochemical study of the effect of Al3+ on the stability and performance of Cu-based ATRP catalysts in organic media. *Electrochimica Acta* **2021,** *388*, 138589.
[29**]**. Braunecker, W. A.; Tsarevsky, N. V.; Gennaro, A.; Matyjaszewski, K., Thermodynamic components of the atom transfer radical polymerization equilibrium: quantifying solvent effects. *Macromolecules* **2009,** *42* (17), 6348-6360.
[30**]**. Konkolewicz, D.; Krys, P.; Góis, J. R.; Mendonca, P. V.; Zhong, M.; Wang, Y.; Gennaro, A.; Isse, A. A.; Fantin, M.; Matyjaszewski, K., Aqueous RDRP in the presence of Cu0: The exceptional activity of CuI confirms the SARA ATRP mechanism. *Macromolecules* **2014,** *47* (2), 560-570.
[31**]**. Tsarevsky, N. V.; Pintauer, T.; Matyjaszewski, K., Deactivation efficiency and degree of control over polymerization in ATRP in protic solvents. *Macromolecules* **2004,** *37* (26), 9768-9778.

[32**]**. Min, K.; Matyjaszewski, K., Atom transfer radical polymerization in aqueous dispersed media. *Open Chemistry* **2009,** *7* (4), 657-674.
[33**]**. Fantin, M.; Isse, A. A.; Gennaro, A.; Matyjaszewski, K., Understanding the Fundamentals of Aqueous ATRP and Defining Conditions for Better Control. *Macromolecules* **2015,** *48* (19), 6862-6875.
[34**]**. Fantin, M.; Isse, A. A.; Matyjaszewski, K.; Gennaro, A., ATRP in Water: Kinetic Analysis of Active and Super-Active Catalysts for Enhanced Polymerization Control. *Macromolecules* **2017,** *50* (7), 2696-2705.
[35**]**. Isse, A. A.; Scialdone, O.; Galia, A.; Gennaro, A., The influence of aluminium cations on electrocarboxylation processes in undivided cells with Al sacrificial anodes. *Journal of Electroanalytical Chemistry* **2005,** *585* (2), 220-229.
[36**]**. Isse, A. A.; Mussini, P. R.; Gennaro, A., New Insights into Electrocatalysis and Dissociative Electron Transfer Mechanisms: The Case of Aromatic Bromides. *Journal of Physical Chemistry C* **2009,** *113* (33), 14983-14992.
[37**]**. Savéant, J.-M., *Elements of molecular and biomolecular electrochemistry: an electrochemical approach to electron transfer chemistry*. John Wiley 2006; Vol. 13.
[38**]**. Andrieux, C. P.; Blocman, C.; Dumas-Bouchiat, J. M.; Saveant, J. M., Heterogeneous and homogeneous electron transfers to aromatic halides. An electrochemical redox catalysis study in the halobenzene and halopyridine series. *Journal of the American Chemical Society* **1979,** *101* (13), 3431-3441.
[39**]**. Isse, A. A.; Gennaro, A.; Lin, C. Y.; Hodgson, J. L.; Coote, M. L.; Guliashvili, T., Mechanism of carbon-halogen bond reductive cleavage in activated alkyl halide initiators relevant to living radical polymerization: theoretical and experimental study. *J Am Chem Soc* **2011,** *133* (16), 6254-64.
[40**]**. Bard, A. J.; Faulkner, L. R., Electrochemical Methods, 2nd ed. *John Wiley & Sons: New York* **2001**.
[41**]**. Golub, G.; Lashaz, A.; Cohen, H.; Paoletti, P.; AndreaBencini; Valtancoli, B.; Meyerstein, D., The effect of N-methylation of tetra-aza-alkane copper complexes on the axial binding of anions-annotated. *Inorganica Chimica Acta* **1997**.
[42**]**. Ribelli, T. G.; Fantin, M.; Daran, J. C.; Poli, R.; Matyjaszewski, K., Synthesis and Characterization of the Most Active Copper ATRP Catalyst Based on Tris[(4-dimethylaminopyridyl)methyl]amine. *J Am Chem Soc* **2018,** *140* (4), 1525-1534.
[43**]**. McLachlan, G. A.; Fallon, G. D.; Martin, R. L.; Spiccia, L., Synthesis, structure and properties of five-coordinate copper (II) complexes of pentadentate ligands with pyridyl pendant arms. *Inorganic Chemistry* **1995,** *34* (1), 254-261.
[44**]**. Kaur, A.; Ribelli, T. G.; Schroder, K.; Matyjaszewski, K.; Pintauer, T., Properties and ATRP activity of copper complexes with substituted tris(2-pyridylmethyl)amine-based ligands. *Inorg Chem* **2015,** *54* (4), 1474-86.
[45**]**. Thaler, F.; Hubbard, C. D.; Heinemann, F. W.; Van Eldik, R.; Schindler, S.; Fábián, I.; Dittler-Klingemann, A. M.; Hahn, F. E.; Orvig, C., Structural, spectroscopic, thermodynamic and kinetic properties of copper (II) complexes with tripodal tetraamines. *Inorganic chemistry* **1998,** *37* (16), 4022-4029.
[46**]**. Swinehart, D. F., The beer-lambert law. *Journal of chemical education* **1962,** *39* (7), 333.

Chapter VII

*e*ATRP in aqueous media

Abstract

Simplified electrochemically-mediated atom transfer radical polymerization (*se*ATRP) with a sacrificial Al anode in an undivided cell in aqueous solutions was systematically investigated. Cyclic voltammetry investigations and controlled-potential *e*ATRP experiments have shown that various factors such as pH, Al^{3+} ions released from the anode, and the active Al electrode have negative impacts on the stability of copper catalysts ($[Cu^{II}L]^{2+}$, L= tris(2-(dimethylamino)ethyl)amine, Me_6TREN or tris(2-pyridylmethyl)amine, TPMA). The instability of the catalysts, especially $[Cu^{II}Me_6TREN]^{2+}$ at low pH and high concentration of Al^{3+} ions was attributed to ligand protonation and copper complex dissociation. In addition, as shown in **Chapter VI**, both $[Cu^{II}Me_6TREN]^{2+}$ and free Cu^{2+} can react with the Al surface, resulting in a fast irreversible consumption of Cu(II). Loss of a small fraction of $[Cu^{II}TPMA]^{2+}$ in the presence of Al^{3+} was confirmed again by *se*ATRP of oligo(ethylene oxide) methyl ether methacrylate (OEOMA) performed in an undivided cell. The reaction was well-controlled and reached high monomer conversion within 4 h, yielding a polymer with low dispersity ($Đ$ = 1.23). Conversely, *se*ATRP with $[Cu^{II}Me_6TREN]^{2+}$ conducted in the same conditions was slower, reaching only 59% conversion after 4 h; also, the produced polymer dispersity was significantly higher (1.46 instead of 1.23). As in the case of organic media, monomer conversion, molecular weights, and polymerization rate were significantly improved by the addition of excess ligand.

Keywords: copper complex, stability, anodic dissolution, pH, controlled *se*ATRP

7.1 Introduction

Atom transfer radical polymerization (ATRP) is one of the most studied and versatile methods of reversible deactivation radical polymerization, which has been successfully employed for the preparation of a large variety of functional polymers of diverse topology.[1-8] The process is well-controlled by an equilibrium (K_{ATRP}, **eq. 4-1**) between active propagating radicals and dormant polymer chains, catalyzed by copper complexes with polydentate amine ligands (**Scheme 4.1**). With the aim of avoiding starting with oxygen-sensitive Cu(I) complexes, minimizing side reactions and reducing the catalyst loading, various advanced methods of ATRP have been developed in the last two decades.[3, 6, 9-10] Among them, electrochemically mediated ATRP (*e*ATRP) attracted much attention.[11-15]

Traditionally, *e*ATRP was carried out in a two-compartment cell with Pt working and counter electrodes, a setup that is not much appealing for large scale applications because of the costly Pt electrodes and the additional energy consumption required to overcome the resistance of the separator. More recently, a simplified setup (*se*ATRP) using a sacrificial anode such as Al and inexpensive non noble metals in an undivided cell has been developed and used in organic solvents, aqueous media, and miniemulsion under both potentiostatic and galvanostatic conditions.[12, 16-20] Furthermore, a decrease in the energy consumption was observed due to the absence of separator resistance in a one-compartment system. Despite the practical importance of *se*ATRP and the investigations discussed in **Chapters IV-VI**, to the best of our knowledge, there is no systematic investigation on the stability of copper catalysts during polymerization in the presence of anodic dissolution of Al in aqueous media. Moreover, as shown in **Chapter VI**, the aqueous chemistry of aluminum is especially complex in ATRP conditions, as it involves not only chemical reaction and electrochemical reaction, but also the formation of new aluminum complex and metallic copper and probably modification of solution pH.

$$Đ = \frac{M_w}{M_n} = 1 + \left(\frac{k_p[RX]_0}{k_{deact}[XCu^{II}L]^{2+}}\right)\left(\frac{2}{Conv.} - 1\right) \quad (7\text{-}1)$$

Water as an environmentally benign solvent is highly appealing for many chemical processes including radical polymerization. However, the stability of the deactivator complex ($[XCu^{II}L]^+$) is quite low in aqueous media. There are several reports showing that the halidophilicity (K_X, X = Br^- or Cl^-) of $[Cu^{II}L]^{2+}$ in organic solvents containing added water decreases significantly as the amount of water in the mixture is increased.[21-27] K_X depends upon the nature of the ligand L and the metal and drastically decreases in aqueous media as compared to organic solvents. Therefore, an important issue of ATRP in water-rich mixtures or pure water is the dissociation of $[XCu^{II}L]^+$ to X^- and $[Cu^{II}L]^{2+}$, which cannot deactivate radicals. Low deactivator concentration leads to increased dispersity of the produced polymer (**eq. 7-1**).[25] There are three general ways to improve the control over polymerization in protic media: (i) selecting appropriate ATRP catalysts that possess high K_X, (ii) use of a system containing large amounts of deactivator, or (iii) addition of excess halide ions to the system. Usually, the utilization of the last two methods has been demonstrated in several systems, especially addition of a large excess of halide salts to guarantee enough deactivators in solution.[25, 28-31] On the other hand, Cu^I complexes are generally unstable in aqueous media and tend to disproportionate. Specifically, $[Cu^IMe_6TREN]^+$ disproportionates faster than $[Cu^ITPMA]^+$, especially in acidic environmens.[4, 30, 32] In addition, the stability of copper complexes in aqueous media strongly depends on pH.[30]

This chapter focuses on *se*ATRP with a sacrificial Al anode in aqueous media. According to previous experience in the literature and the results reported in **Chapter V**, a series of experiments were designed and conducted to explore the stability and catalytic activity of $[Cu^{II}L]^{2+}$ (TPMA or Me_6TREN), in the presence of a large excess of Br^- ions, under anodic dissolution of Al in typical ATRP conditions. Additionally, the effects of pH variations during the anodic dissolution of Al electrolysis step on the stability of copper complexes were taken into consideration and evaluated. The potential chemical reactions of activated Al metal with Cu^{2+} ions and $[Cu^{II}L]^+$ in

water/monomer mixtures were investigated by cyclic voltammetry. Subsequently, the morphologies as well as composition variations of Al surface before and after electrolysis were analyzed through SEM-EDX. Possible solutions to the issues induced by anodic dissolution of Al were investigated by potentiostatic *e*ATRP of OEOMA and *N,N*-dimethyl acrylamide (DMA).

7.2 Methodologies and procedures

7.2.1 CV measurements in the presence of Al^{3+}

Solutions of $[Cu^{II}L]^{2+}$ in H_2O + OEOMA (10%, v/v) with 0.1 M Et_4NBr were always prepared in situ starting from 1 mM $Cu(OTf)_2$, followed by addition of the ligand (L = TPMA or Me_6TREN, and $[Cu^{II}]$:[L] = 1:1.05). Al^{3+} ions were introduced in the system by anodic dissolution of an Al wire immersed in the working solution containing the Cu complex. This was done by a constant current electrolysis, which was stopped after the passage of a charge corresponding to the required amount of Al^{3+} ions. The effect of Al^{3+} on the voltammetric pattern of the ternary complexes was often investigated by addition of increasing amounts of Al^{3+} until a ~2.5-fold excess over $[XCu^{II}L]^{+}$ was reached. After each Al^{3+} addition, a freshly polished GC electrode was used to record voltammograms. Moreover, the pH of the solution was measured and recorded after every addition step.

Additionally, the kinetics of direct reaction between Al immersed in solution and $[Cu^{II}L]^{2+}$ was evaluated by recording the voltammetric pattern of $[Cu^{II}L]^{2+}$ as a function of immersion time. The morphology and surface compositions of Al surface were characterized via SEM-EDX technique.

7.2.2 Potentiostatic *e*ATRP of oigo(ethylene oxide) methyl ether methacrylate (OEOMA) and *N, N*-dimethylacrylamide (DMA)

Electrochemically mediated polymerizations of OEOMA or DMA in aqueous solutions were performed in both divided and undivided cells by controlled-potential

electrolysis. A typical setup of an *e*ATRP experiment in a two-compartment cell was as follows. Et_4NBr (0.6435 g, 3.0 mmol), double distilled water (26.4 mL), OEOMA (3.0 mL, 6.48 mmol) or DMA (3.0 mL, 28.8 mmol), 0.6 mL of DMF used as an internal standard for NMR analysis (Et_4N^+ from the supporting electrolyte was used as internal standard in divided cells), $Cu(OTf)_2$ (11.07 mg, 0.03 mmol) and TPMA (9.33 mg, 0.03 mmol) were progressively added to a seven-neck electrochemical cell maintained at 25 ˚C or 0 ˚C and under Ar flux. After purging the solution with the inert gas for ca. 20 min, a CV of the copper complex was recorded on a GC disk electrode. Then 2-hydroxyethyl 2-bromoisobutyrate (HEBiB) (9.2 μL, 0.06 mmol) was injected into the solution and a CV was recorded to verify the catalytic reaction. Then the Pt mesh working electrode and the graphite rod counter electrode, which were previously activated and positioned in the cell, were connected and the chosen potential was applied. Samples were withdrawn periodically to determine the monomer conversion by ^1H NMR, and the number average molecular weight (M_n) and molecular weight distribution (Đ) by gel permeation chromatography (GPC).

7.3 Results and discussion

7.3.1 Effect of pH, Br^- ions, and monomer on the properties of $[Cu^{II}L]^{2+}$

Before *e*ATRP experiments, we have to carefully assess the effects of pH and concentration of Br^- ions on the redox performance of copper complexes in pure water as well as in water/monomer mixtures. In water, pH is a fundamental parameter that in general may drastically affect the properties of the catalyst system and the polymerization process. In addition, besides the chemical reaction involving the active Al and copper species, other side reactions occurring during anodic dissolution should also be taken into account. For example, Al^{3+} is a Lewis acid[33-34] and as such can react with water to form different aluminum hydroxides, further changing the solution pH.[35-37]

In detail, at the anode surface, anodic dissolution of activated Al generates Al^{3+} in

solution. Then, Al^{3+} ions combine with H_2O to form aluminum hydroxides and H^+. In the working solution, in general, different Al^{3+} species (Al^{3+}, $Al(OH)^{2+}$, $Al(OH)_2^+$, $Al(OH)_3$ as well as $Al(OH)_4^-$) are formed depending on pH.[35–37] Specially at pH ≤ 3, only solvated Al^{3+} ions are present. If pH is in the 3~8 range, monomeric and polymeric hydroxoaluminum ions are present (**eqs. 7-2 to 7-4**). As the pH rises $Al(OH)_3$ starts precipitating. At pH ≥ 8, the colloidal $Al(OH)_3$ particles are dissolved by the formation of soluble $Al(OH)_4^-$ species (**eq. 7-5**). Moreover, pH variations could also cause speciation of Cu(II) species in solution, due to ligand protonation at low pH (**eq. 7-6**) or formation of $[Cu^{II}L(OH)]^+$ at high pH (**eq. 7-7**).[30, 38] These two circumstances decrease the stability of the complex stability.

$$Al^{3+} + H_2O \longrightarrow Al(OH)^{2+} + H^+ \quad (7\text{-}2)$$

$$Al(OH)^{2+} + H_2O \longrightarrow Al(OH)_2^+ + H^+ \quad (7\text{-}3)$$

$$Al(OH)_2^+ + H_2O \longrightarrow Al(OH)_{3\,(s)} + H^+ \quad (7\text{-}4)$$

$$Al(OH)_{3\,(s)} + H_2O \longrightarrow Al(OH)_4^- + H^+ \quad (7\text{-}5)$$

$$L + H_3O^+ \rightleftharpoons LH^+ + H_2O \quad (7\text{-}6)$$

$$[Cu^{II}L]^{2+} + OH^- \rightleftharpoons [Cu^{II}L(OH)]^+ \quad (7\text{-}7)$$

Figure 7.1 a, b shows examples of typical CVs of $[Cu^{II}L]^{2+}$ systems at different pH values in water. Generally, $[Cu^{II}L]^{2+}$ complexes undergo a quasi-reversible one electron transfer reaction to form $[Cu^{I}L]^+$ at the electrode surface. The voltammetric pattern is affected by the pH. In the case of TPMA, a single peak couple is observed in the rough pH range of 3 ~ 10, whereas loss of reversibility, a new cathodic peak at -0.56 V and an anodic stripping peak at ca. 0.1 V for Cu^0 oxidation were observed at pH = 2.2. This points out dissociation of $[Cu^{I}TPMA]^+$ with release of free solvated copper ions, which are reduced to Cu^0 at extremely low pH values. More or less a similar behavior was observed with $[Cu^{II}Me_6TREN]^{2+}$ although the pH range of complex stability was narrower with respect to the $[Cu^{II}TPMA]^{2+}/[Cu^{I}TPMA]^+$ couple. Therefore, both high and low pH values are not favorable for *e*ATRP.

The standard potential (E^e) of the $[Cu^{II}L]^{2+}/[Cu^{I}L]^+$ couple can be estimated from

cyclic voltammetry as the half-sum of the cathodic potential (E_{pc}) and anodic peak potential (E_{pa}), $E^{\ominus} \approx E_{1/2} = (E_{pc} + E_{pa})/2$. Obviously, $E^{\ominus}$ shifted to more negative potentials upon increasing pH. A similar trend has already been observed in water in previous works.[30, 39]

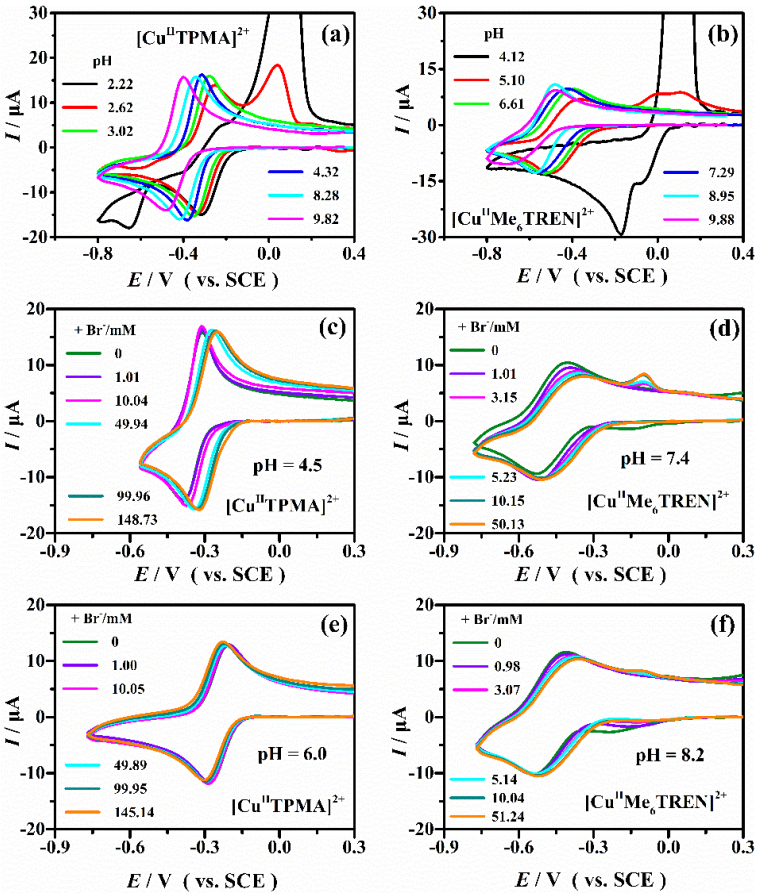

Figure 7.1 CV curves of 1 mM $[Cu^{II}TPMA]^{2+}$ and $[Cu^{II}Me_6TREN]^{2+}$, recorded at 0.2 Vs^{-1} at different pH values **(a-b)** and in the presence of Br^- **(c-d)** in H_2O + 0.1 M Et_4NBF_4 or in H_2O + 10% OEOMA (v/v) **(e-f)**. Values of pH and Br^- concentration are reported in the legends. In figures **c-f**, the initial pH values of unbuffered solutions are reported, $T = 25$ °C.

The affinity of Br^- ion for copper complexes (halidophilicity) plays an important role in ATRP processes due to the formation of deactivator $[XCu^{II}L]^+$. It can be evaluated on the basis of a thermochemical cycle involving the reactions in **Scheme 7.1** and **eq. 5-3**. In pure water, CV of both $[Cu^{II}TPMA]^{2+}$ and $[Cu^{II}Me_6TREN]^{2+}$ (**Figure 7.1 c, d**) showed a positive shift of the reversible peak couple after addition of

increasing amounts of Br^- to the solution, indicating that the Br^- ions stabilize Cu^I species more than Cu^{II}. However, in water + 10% OEOMA (v/v), a very small negative shift was found for $[Cu^{II}TPMA]^{2+}$, whereas a slight positive shift was observed for $[Cu^{II}Me_6TREN]^{2+}$ (**Figure 7.1 e, f**). Similar trends were observed in our previous work.[30] The voltametric behavior of $[Cu^{II}TPMA]^{2+}$ and $[Cu^{II}Me_6TREN]^{2+}$ in the presence of excess Br^- ions was investigated in H_2O + 10% OEOMA (v/v) also at different pH values, as shown in **Figure 7.2**. For both complexes the same behavior found in pure water was observed. Decreasing the pH of $[Cu^{II}TPMA]^{2+}$ solution close to 3 caused ligand protonation and $[Cu^{I}TPMA]^{+}$ dissociation and decomplexation in a short time. The free Cu^+ ions generated in the decomposition process were reduced at the electrode to form a metallic copper deposit (**Figure 7.2 a**). Consequently, a new oxidation peak with high intensity occurred at ca -0.06 V, which is attributed to anodic stripping of electrodeposited Cu^0. The same phenomena occurred also for Me_6TREN (**Figure 7.2 b**). When the pH was decreased to below 5, ligand protonation resulted in partial decomposition of $[Cu^{II}Me_6TREN]^{2+}$. In this circumstance, two cathodic peaks corresponding to the reduction of free Cu^{2+} ions and the remaining $[Cu^{II}Me_6TREN]^{2+}$ were observed. At pH = 4.10, $[Cu^{II}Me_6TREN]^{2+}$ was almost completely decomposed to Cu^{2+} and protonated ligand. The free solvated Cu^{2+} was reduced to Cu^+ and then to metallic Cu deposited on the electrode surface.[4, 30, 32] Thus, three cathodic peaks were found at pH = 4.65, but only two at pH = 4.1, in both cases followed by an anodic stripping peak ca -0.06 V and an oxidation peak at 0.25 V.

In addition, E^e of the redox $[Cu^{II}L]^{2+}/[Cu^{I}L]^{+}$ couple shifted to more negative potentials as the pH was increased

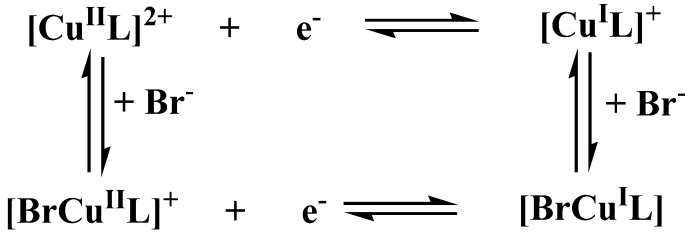

Scheme 7.1 Equilibria between binary/ternary copper complexes.

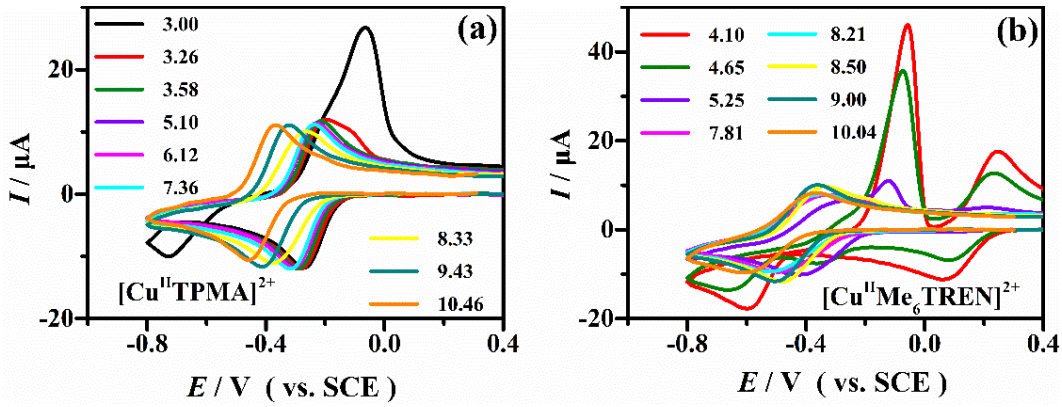

Figure 7.2 CV curves of 1 mM $[Cu^{II}TPMA]^{2+}$ **(a)** and $[Cu^{II}Me_6TREN]^{2+}$ **(b)**, recorded at 0.2 Vs^{-1} at different pH values in unbuffered H_2O + 10% OEOMA (v/v) + 0.1 M, *T* = 25 °C. The legends show the pH values.

7.3.2 Effect of anodic dissolution of Al on catalyst stability in H_2O/OEOMA

During a simplified *e*ATRP using a sacrificial Al anode in aqueous media, the anodic dissolution process affects the pH by the formation of aluminum hydroxide compounds, as in electrocoagulation (EC).[35, 40-41] Both high and low pH circumstances are unfavorable for obtaining a well-controlled polymerization in aqueous solutions due to the formation of $[Cu^{II}L(OH)]^+$ at high pH and decomposition of $[Cu^{II}L]^{2+}$ at low pH. Therefore, the effect of anodic dissolution of Al on the stability of copper-based ATRP catalysts must be investigated in solvent/monomer mixtures. **Figure 7.3** presents typical CVs of copper species in 10% OEOMA (v/v) + 0.1 M Et_4NBr solution followed by stepwise addition of ligand and Al^{3+} generated in situ. Here we simply used Al^{3+} to indicate all kinds of aluminum species present in the system. The required amount of Al^{3+} was theoretically calculated from the passage of the charge. The concentration of the starting Cu^{II} and its complexes in solution was fixed at 1 mM, whereas the concentrations of Al^{3+} and ligands are shown in the figures. **Figure 7.3** reports also the pH values measured after each addition step.

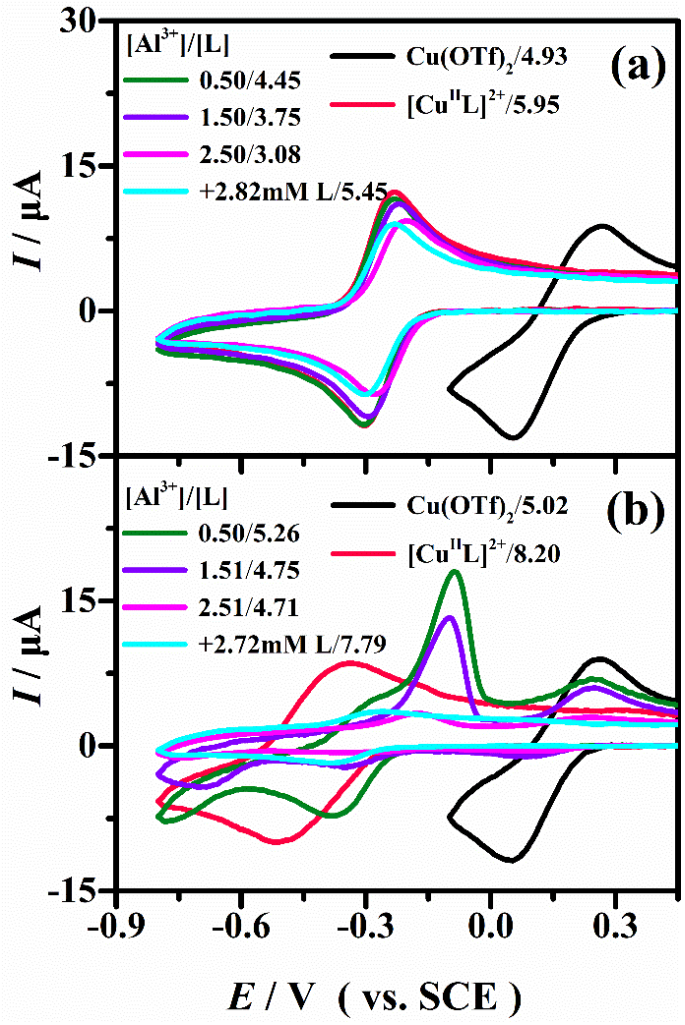

Figure 7.3 CVs of 1 mM $Cu(OTf)_2$ and 1 mM $[Cu^{II}L]^{2+}$ with L = TPMA **(a)** and Me_6TREN **(b)**, recorded at $v = 0.2$ Vs^{-1}, $T = 25$ °C on a GC disk before and after addition of Al^{3+} ions produced in situ in H_2O + 0.1 M Et_4NBr, followed by further addition of excess ligand; the pH values are shown behind the oblique lines in the legends.

The standard potentials (E^{Θ}) and the anodic to cathodic peak separations (ΔE_p) are reported in **Table 7.1**. After addition of TPMA and Me_6TREN to a solution with $[Cu^{2+}]$ = [L], the pH changed from 5 to 6 and 8.2, respectively. E^{Θ} of Cu^{2+}/Cu^{+} shifted from 0.155 V in the absence of ligand to -0.268 V and -0.425 V after addition of TPMA and Me_6TREN, respectively, which agrees well with our previously reported data.[30] ΔE_p measured for Cu^{2+}/Cu^{+} changed from 206 mV to 72 mV for $[Cu^{II}TPMA]^{2+}/[Cu^{I}TPMA]^{+}$ and to 182 mV for $[Cu^{II}Me_6TREN]^{2+}/[Cu^{I}Me_6TREN]^{+}$.

Table 7.1 E^{Θ} and ΔE_p of copper species in solvent/monomer mixtures with 0.1 M Et_4NBr at 25 °C.[a]

Entry	Ligand	Cu^{2+}/Cu^{+}		$[Cu^{II}L]^{2+}/[Cu^{I}L]^{+}$		Excess ligand	
		E^{Θ} (V)	ΔE_p (V)	E^{Θ} (V)	ΔE_p (V)	E^{Θ} (V)	ΔE_p (V)
1	TPMA	0.155	0.206	-0.268	0.072	-0.266	0.068
2	Me_6TREN	0.155	0.206	-0.425	0.182	-0.323	0.122
3[b]	Me_6TREN	0.155	0.206	-0.428	0.180	-0.382	0.112
4[c]	Me_6TREN	0.155	0.206	-0.432	0.178	-0.388	0.112

[a] 90/10 (v/v) monomer mixtures, scan rate = 0.2 V/s, E^{Θ} (V) vs SCE, $\Delta E_p = E_{pa} - E_{pc}$.

[b] The use of Al^{3+} ions from a stock solution replaced in situ anodic Al dissolution .

[c] $AlCl_3$ was used.

In the case of $[Cu^{II}TPMA]^{2+}$ (**Figure 7.3 a**), progressive addition of Al^{3+} by in situ anodic dissolution of Al caused a slight decrease of the intensity of the quasi-reversible peak couple for Cu(II)/Cu(I), which also shifted slightly to more positive potentials. Moreover, the pH decreased by almost 3 units reaching pH = 3.08 when the $[Al^{3+}]/[L]$ ratio changed from 0 to 2.50. When excess TPMA was added, the pH increased to about its initial value. These results demonstrate that both Al^{3+} and TPMA have a significant effect on pH variation. Notably, the stability of the binary complexes $[Cu^{II}TPMA]^{2+}$ and $[Cu^{I}TPMA]^{+}$, and the corresponding ternary complexes with Br^{-} was not compromised at pH values as low as 3.08. It can be deduced from the small decrease of current intensity that a small amount $[Cu^{II}TPMA]^{2+}$ undergoes decomposition due to ligand protonation, followed by reduction of free Cu^{2+} by Al:

$$3Cu^{2+} + 2Al^{0} \longrightarrow 2Al^{3+} + 3Cu^{0} \qquad (7\text{-}10)$$

In **Figure 7.3 b**, the single peak couple for the quasi-reversible reduction of $[Cu^{II}Me_6TREN]^{2+}$ (and also $[BrCu^{II}Me_6TREN]^{+}$) was replaced by three cathodic peaks and two anodic peaks as the $[Al^{3+}]/[Me_6TREN]$ ratio was increased from 0 to 2.51. However, all peaks gradually decreased in height with time and nearly disappeared at

the end of the experiment. This behavior was previously observed for $[Cu^{II}Me_6TREN]^{2+}$ in pure water (**Figure 6.3 b**). Moreover, after the experiment, a brown-red deposit on the surface of the Al spiral coil was observed, and the initial green color of the solution disappeared. These changes point out instability of the copper complex coordinated with Me_6TREN during the Al anodization process. As described above, Al^{3+} can associate to the ligand, but also can lower solution pH. When Al electrolysis started, released Al^{3+} ions reacted with water to form various aluminum hydroxide species. This enhanced the concentration of protons in solution, hence decreasing solution pH. At the initial solution pH of 8.2, a mixture of $[Cu^{II}Me_6TREN]^{2+}$ and $[Cu^{II}Me_6TREN\text{-}OH]^{+}$ co-existed in the solution according to speciation diagram reported by Golub et al. in H_2O + 0.15 M $NaClO_4$.[38] During Al^{3+} addition by electrolysis, the pH changed from 8.20 to 4.71. $[Cu^{II}Me_6TREN]^{2+}$ stability is highly sensitive to the pH and when this was decreased by Al^{3+} addition, spontaneous protonation of Me_6TREN took place, leading to release of free Cu^{2+} ions in solution. According to the distribution diagram, $[Cu^{II}Me_6TREN]^{2+}$ complexes are subjected to significant dissociation when pH becomes lower than 5, and only Cu^{2+} ions exist at pH ≤ 3.5. Moreover, formation of a strong complex between Al^{3+} and Me_6TREN could accelerate the dissociation equilibrium of $[Cu^{II}Me_6TREN]^{2+}$. It is worth noting that at the end of this experiment only a very small amount of Cu(II) species was present in solution. This is probably due to reduction of Cu^{2+} and $[Cu^{II}Me_6TREN]^{2+}$ by Al (**eqs. 7-10 and 7-11**), as was previously observed in pure water.

$$3[Cu^{II}Me_6TREN]^{2+} + 2Al \longrightarrow 2[Al^{III}Me_6TREN]^{3+} + 3Cu^{0} + Me_6TREN \quad (7\text{-}11)$$

Thus, two parallel experiments were conducted to confirm this hypothesis by immersion of two identical Al wires in equimolar solutions of Cu^{2+} and $[Cu^{II}Me_6TREN]^{2+}$, respectively. Examples of typical CVs are reported in **Figure 7.4**, whereas values of I_{pc} measured for Cu^{II} as a function of time are collected in **Table 7.2**. The rate constants of Cu^{2+} and $[Cu^{II}Me_6TREN]^{2+}$ decay were evaluated using the cathodic peak currents according to **eq. 6-13 (Figure 7.5**) and the values obtained for Cu^{2+} and $[Cu^{II}Me_6TREN]^{2+}$ were 0.051 ± 0.001 min^{-1}, 0.022 ± 0.001 min^{-1}, respectively.

The reaction of Al with Cu^{2+} was about 2.3 times faster than with $[Cu^{II}Me_6TREN]^{2+}$. This result is similar to what was observed in pure water (**Figure 6.6**). In addition, the same brown-red color was observed again on both Al surfaces. It can be concluded that both solution pH and active Al affect the deactivator stability.

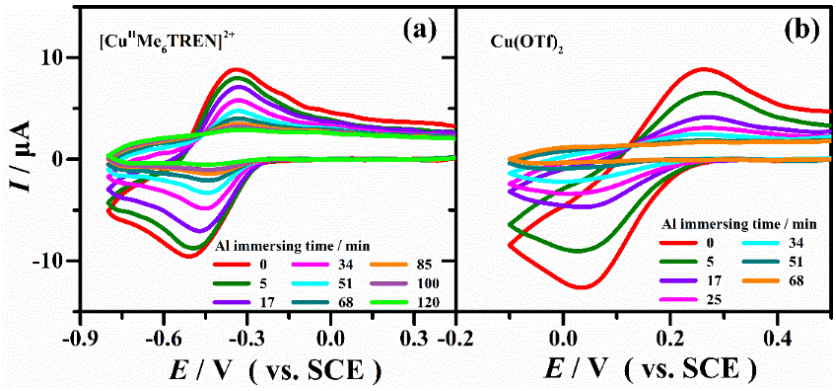

Figure 7.4 CVs of 1 mM $[Cu^{II}Me_6TREN]^{2+}$ **(a)** and $Cu(OTf)_2$ **(b)** in H_2O + 10% OEOMA (v/v) + 0.1 M Et_4NBr, recorded at $v = 0.2$ Vs^{-1} on a GC disk at $T = 25$ °C after immersion of an Al wire.

Table 7.2 Cathodic peak currents from CVs of 1 mM $[Cu^{II}Me_6TREN]^{2+}$ and 1 mM $Cu(OTf)_2$ in in the presence of Al wire (**Figure 7.4**).

NO.	$[Cu^{II}Me_6TREN]^{2+}$		$Cu(OTf)_2$	
	Time/min	$-I_{pc}$/µA	Time/min	$-I_{pc}$/µA
1	0	9.58	0	12.64
2	5	8.73	5	9.04
3	17	7.05	17	4.70
4	34	4.86	25	3.41
5	51	3.30	34	2.22
6	68	2.09	51	0.94
7	85	1.44	68	0.39
8	100	1.03		
9	120	0.55		

When more ligand was added to the solutions of $[Cu^{II}TPMA]^{2+}$ and $[Cu^{II}Me_6TREN]^{2+}$ after progressive Al^{3+} addition by Al anodization, as shown in **Figure 7.3**, the pH was shifted back to values close to those of the starting solutions. In addition, both the standard potential and voltammetric pattern of $[Cu^{II}TPMA]^{2+}$ were almost recovered except the peak currents (**Table 7.1, entry 1**). But for $[Cu^{II}Me_6TREN]^{2+}$, E^{Θ} shifted to less negative potentials while the original voltammetric pattern was not fully recovered because of the conversion of $[Cu^{II}L]^{2+}$ to Cu^0 (**Table 7.1, entry 2**).

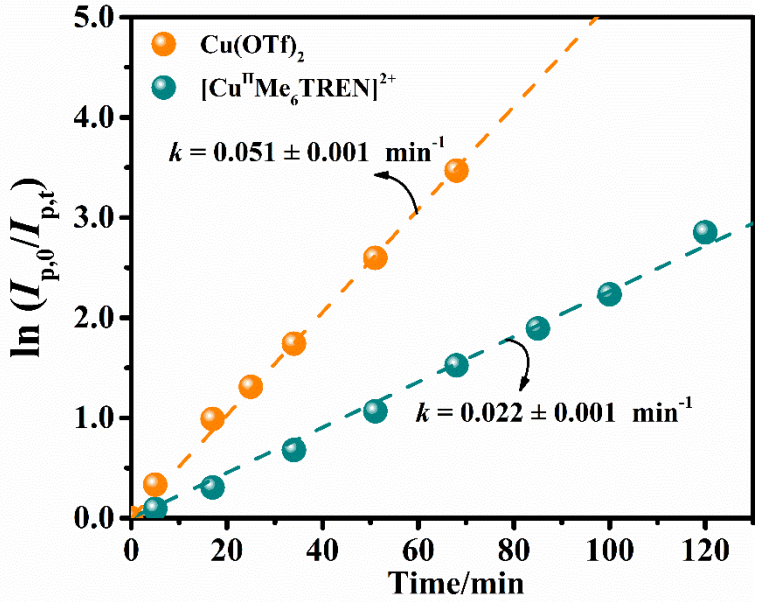

Figure 7.5 Linear plots of $\ln(I_{p,0}/I_{p,t})$ as a function of time with the best fitting lines for $Cu(OTf)_2$ and $[Cu^{II}Me_6TREN]^{2+}$ in the presence of an Al wire without electrolysis in H_2O + 10% OEOMA (v/v) + 0.1 M Et_4NBr.

To evaluate the contribution of active Al surface to $[Cu^{II}Me_6TREN]^{2+}$ destruction during electrolysis, the method of Al^{3+} addition was changed. A stock solution of Al^{3+} ions was prepared by anodic dissolution of Al in H_2O + 10% OEOMA (v/v). Then the effect of Al^{3+} on the stability of copper complexes was investigated by making additions of Al^{3+} ions from the stock solution. Examples of typical CVs are reported in **Figure 7.6 a**. A decrease of the peak couple for $[Cu^{II}Me_6TREN]^{2+}/[Cu^{I}Me_6TREN]^{+}$ and the appearance of Cu^{2+}/Cu^{+} peak couple together with a new irreversible cathodic peak and

an anodic stripping peak were observed when 0.5 mM Al^{3+} was added to 1 mM $[Cu^{II}Me_6TREN]^{2+}$. This clearly evidences the occurrence of ligand exchange between Cu^{2+} and Al^{3+} ions. After addition of 1.5-fold Al^{3+}, no residual Cu(II) complex could be observed in solution, as shown by the disappearance of its peak couple (**Figure 7.6 a**). Further addition of Al^{3+} up to a 2.5-fold excess over $[Cu^{II}L]^{2+}$, which decreased the pH to 3.8, did not cause any change to the voltametric pattern. When Me_6TREN was added to this solution, the original voltammetric pattern of $[Cu^{II}Me_6TREN]^{2+}$ was restored without any free Cu^{2+} remaining in the solution. However, there are three distinct changes on the peak couple: (i) increased peak currents, (ii) positive shift of $E_{1/2}$ and (iii) reduced peak separation (ΔE_p) (**Table 7.1, entry 3**). These changes can be attributed to a change of Cu(II) speciation in solution. The staring Cu(II)/Me_6TREN solution was a mixture of $[Cu^{II}L]^{2+}$, $[HO\text{-}Cu^{II}L]^{+}$ and $[Br\text{-}Cu^{II}L]^{+}$ and the observed peak couple was composed of overlapping peaks. It appears that in the presence of excess ligand, $[Cu^{II}L]^{2+}$ prevails over other species and therefore the system exhibits a clean redox signal.

The same experiment was repeated by using $AlCl_3$ as a source of Al^{3+} ions and essentially the same result was obtained (**Figure 7.6 b** and **Table 7.1, entry 4**).

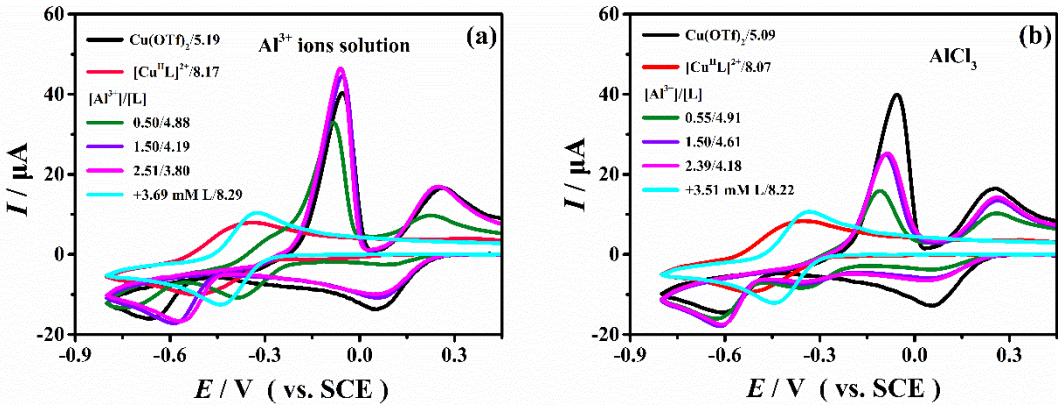

Figure 7.6 CVs of 1 mM Cu^{2+} and 1mM $[Cu^{II}Me_6TREN]^{2+}$ before and after addition of Al^{3+} ions **(a)** from a stock solution or **(b)** as $AlCl_3$, recorded at $v = 0.2$ Vs^{-1}, $T = 25$ °C on a GC disk in H_2O + 10% OEOMA (v/v) + with 0.1 M Et_4NBr; the pH values are shown behind the oblique line in the figures.

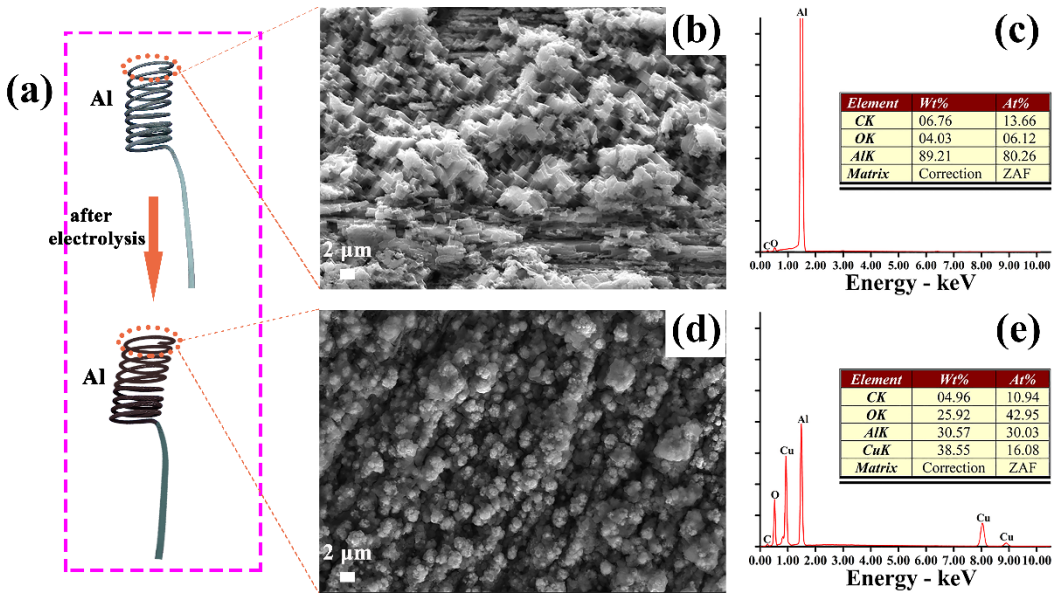

Figure 7.7 (a) Digital photograph of an Al wire before and after anodic dissolution in a solution of $[Cu^{II}Me_6TREN]^{2+}$. **(b)** SEM image and **(c)** surface elemental analysis of an Al wire in H_2O + 10% OEOMA (v/v) + 0.1 M Et_4NBr in the absence of copper catalyst. **(d)** SEM image and **(e)** surface elemental analysis of an Al wire after anodic dissolution in a solution of $[Cu^{II}Me_6TREN]^{2+}$ in H_2O + 10% OEOMA (v/v) + 0.1 M Et_4NBr.

It is clear that both Al^{3+} and Al wire contribute to the process of $[Cu^{II}L]^{2+}$ destruction. Nevertheless, whilst Al^{3+} destroys the copper complex by a ligand exchange mechanism whereby Cu^{2+} ions accumulate in solution, metallic Al eliminates all copper species from the solution. It is noteworthy that in both pure water and water/OEOMA (10%, v/v) mixture, containing 0.1 M Et_4NBr, a brown-red color was observed on the Al surface after the experiments (**Figure 7.7 a**). For comparison, **Figure 7.7 b, d** shows SEM images of an Al wire etched by diluted HCl solution and the same wire after anodic dissolution in a solution of $[Cu^{II}Me_6TREN]^{2+}$ in H_2O + 10% OEOMA (v/v) + 0.1 M Et_4NBr. A great deal of uneven "defects" – artificial active sites and a regular matrix array with well-defined crystallographic directions were observed. Elemental analysis of representative selected areas showed three main elements (**Figure 7.7 c**). Carbon and oxygen probably originate from acetone and H_2O, although

some surface oxides may also contribute. Acetone was used to store the samples until characterization. In effect, we only focused on Al and Cu contents. This analysis revealed that no copper was present on the blank Al sample. In contrast, SEM analysis of the Al wire that was anodized in the presence of copper complex showed rough morphologies and homogenous micro grade size particles, which were attributed to the anodic corrosion and chemical reactions (**Figure 7.7 d**). Moreover, a decrease of Al wt% from 89.21 to 30.57 and an increase of Cu wt% from 0 to 38.55 were observed (**Figure 7.7 e**). The O wt% increased presumably because of Cu and Al oxidation in the air.

Two more experiments were done to complete the set of tests designed to shed light on Cu(II) disappearance in the presence of Al. In the first experiment, the surface of an Al wire used as a source of Al^{3+} ions during CV analysis of $[Cu^{II}TPMA]^{2+}$ in H_2O + 10% OEOMA (v/v) + 0.1 M Et_4NBr was analyzed. The other experiment was the analysis of the surface of an Al wire that was immersed for 120 min in a solution of $[Cu^{II}Me_6TREN]^{2+}$ in H_2O + 10% OEOMA (v/v) + 0.1 M Et_4NBr. SEM images and surface elemental analysis of both wires are reported in **Figure 7.8**. SEM images of the Al wire after the experiment with $[Cu^{II}TPMA]^{2+}$ show a large number of scattered and small size particles concentrated on the higher hill edges and only minute amounts on the low-lying areas (marked by pink dash cycles), and also clear crystallographic edges. Moreover, it is important to note that, in comparison with the Al surface of the blank experiment (**Figure 7.7 c**), the Al wt% decreased while Cu was deposited on the surface. However, the wt% of Cu was considerably lower than what was observed in a similar experiment with $[Cu^{II}Me_6TREN]^{2+}$ (**Figure 7.7 e**). These results clearly point out that Al reduces also $[Cu^{II}TPMA]^{2+}$ to some extent but this complex is more stable than $[Cu^{II}Me_6TREN]^{2+}$.

Figure 7.8 b, d and e shows the SEM images and elemental analysis of the wire after immersion in a $[Cu^{II}Me_6TREN]^{2+}$ without electrolysis. A high amount of Cu was observed on the Al surface. The Cu wt% was however lower than in the case of the analogous experiment with anodic dissolution of the Al wire (**Figure 7.7 e**).

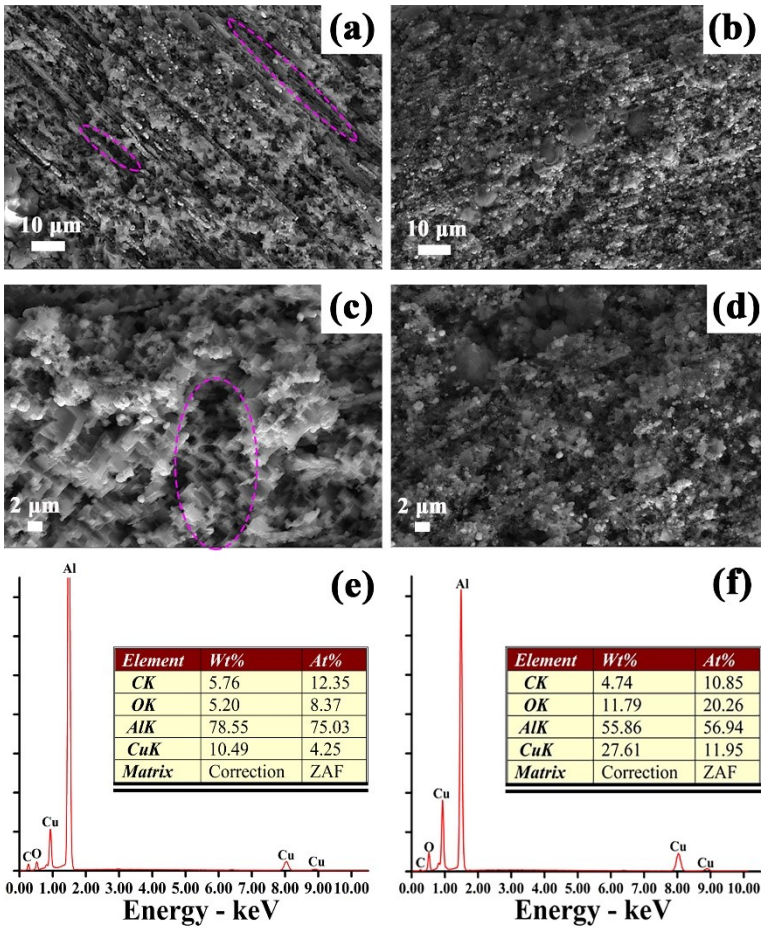

Figure 7.8 SEM images at different magnifications and surface elemental analysis (average of dots) of an Al wire after anodic dissolution in the presence of $[Cu^{II}TPMA]^{2+}$ **(a, c, e)**, or after immersion for 120 min in a solution of $[Cu^{II}Me_6TREN]^{2+}$ without electrolysis **(b, d, f)**; both solutions were 1 mM $[Cu^{II}L]^{2+}$ in H_2O + 10% OEOMA (v/v) + 0.1 M Et_4NBr.

It is evident from this set of surface analysis experiments that Cu(II) disappears through reduction to metallic Cu by Al. This reaction depends on the ligand type and is affected by solution pH. Indeed, a small loss of Cu(II) was found in all experiments with TPMA. In contrast, when Me_6TREN was used as a ligand, a massive loss of Cu(II) was always observed. The reaction was found to be slower when an anodic current was not applied to the Al wire. It is likely that Al reduces $[Cu^{II}L]^{2+}$ (**eq. 7-11**) to Cu^0, but certainly the analogous reaction of free Cu^{2+} is more favorable and faster. During anodic dissolution of Al, hydrolysis of Al^{3+} lowers solution pH, which helps destroy $[Cu^{II}L]^{2+}$

via ligand protonation. The so generated Cu^{2+} ions then undergo galvanic displacement with Al. This reaction route is more important for Me_6TREN than TPMA as the former is a much stronger base than the latter and is almost completely protonated at pH < 3.5.

7.3.3 Potentiostatic *e*ATRP of OEOMA in divided and undivided cells

The investigations described in the previous sections revealed that both Al and Al^{3+} ions have significant negative effects on copper complex stability, regardless of whether pure water or a water/monomer mixture is used. $[Cu^{II}TPMA]^{2+}$ only marginally decomposes in the presence of anodic dissolution of Al, whereas $[Cu^{II}Me_6TREN]^{2+}$ is completely lost. These findings suggest that aqueous *se*ATRP with a sacrificial Al anode will suffer from catalyst loss, especially with Me_6TREN as a ligand. Nevertheless, the degree of interference of anodic dissolution of Al on $[Cu^{II}L]^{2+}$ catalytic efficiency in *e*ATRP must be evaluated by electrochemically-mediated polymerization. To this end, *e*ATRP of two monomers, namely, oligo(ethylene oxide) methyl ether methacrylate (OEOMA) and *N,N*-dimethylacrylamide (DMA) in water were comparatively investigated in both divided and undivided cells. All polymerizations were performed with 1 mM $[Cu^{II}L]^{2+}$, 2 mM 2-hydroxyethyl 2-bromoisobutyrate (HEBiB) as initiator, and 0.1 M Et_4NBr used as electrolyte and bromide source. They were triggered by applying a predesigned potential around $E_{1/2}$ of the catalyst.

Figure 7.9. shows CVs of $[Cu^{II}L]^{2+}$ in H_2O + 10% OEOMA (v/v) + 0.1 M Et_4NBr. Voltammogramms recorded both before and after *e*ATRP are reported. Before polymerization, both catalysts exhibit the characteristic peak couple for the Cu(II)/Cu(I) couple in the absence of the initiator. When HEBiB is added, the quasi-reversible peak couple is replaced by an irreversible catalytic reduction peak. A fixed applied potential close to catalyst $E_{1/2}$ was applied to trigger polymerization (see arrows in **Figure 7.9**). The applied potential (E_{app}) fixes the Cu^{II} to Cu^{I} ratio at the electrode surface, according to Nernst equation:

$$E_{app} = E_{1/2} + \frac{RT}{nF} \ln \frac{C_{[Cu^{II}L]^{2+}}}{C_{[Cu^{I}L]^{+}}} \quad (7\text{-}12)$$

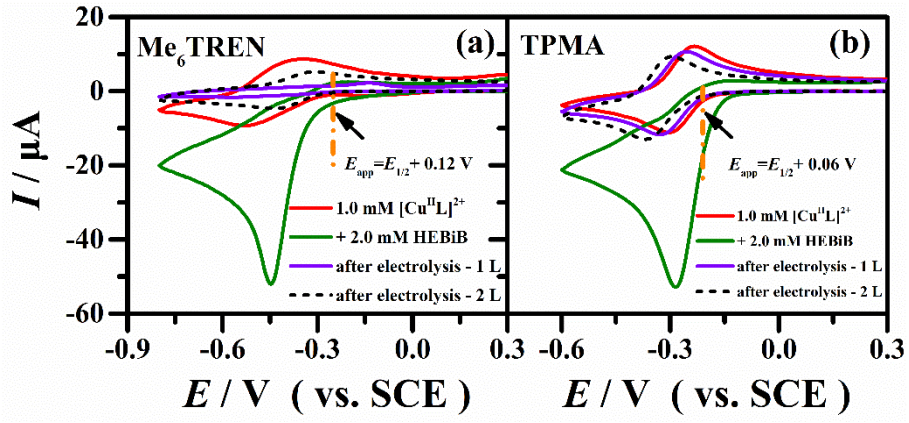

Figure 7.9 Cyclic voltammetry of 1 mM $[Cu^{II}L]^{2+}$ in H_2O + 10 vol% OEOMA + 0.1 M Et_4NBr, recorded for L= Me_6TREN **(a)** and TPMA **(b)** at T = 25 °C, v = 0.2 V/s. The violet (▬) and dashed black (- - - -) traces are CVs of two separate experiments with $[Cu^{2+}]$:[L] = 1:1 and 1:2, respectively. The arrows indicate applied potential.

The results of a first series of experiments, with $[Cu^{II}Me_6TREN]^{2+}$ as the catalyst and OEOMA as the monomer, are summarized in **Table 7.3**. At $E_{app} = E_{1/2} + 0.06$ V, the $C_{[Cu^{II}L]^{2+}}/C_{[Cu^{I}L]^{+}}$ ratio near the electrode is around 10. Although a continuous generation of a small quantity of $[Cu^{I}L]^{+}$ is achieved under this condition, the reaction was fast, reaching 99.8% monomer conversion after 3 h, but control over polymer molecular weight and dispersity was not good (**Table 7.3, entry 1**). When the same experiment was repeated in the undivided cell, the result was worse: the reaction was slower (lower k_p^{app}) and the dispersity of the polymer was higher (**Table 7.3, entry 2**). In addition, copper deposits were observed on both the Pt cathode and Al anode, clearly showing that $[Cu^{II}Me_6TREN]^{2+}$ stability was seriously affected by the presence of the Al anode and the Al^{3+} ions released in solution. According to the total charge passed at the end of the experiment, ca 0.5 mM Al^{3+} ions were generated in the solution. Thus, as could be predicted on the basis of the previously discussed investigations, the catalyst was destroyed and free Cu^{2+} ions were mainly electroreduced to a Cu^0 deposit on the

Pt cathode and in part reduced via galvanic displacement at the Al surface. Besides the colored deposits on the electrodes, the disappearance of Cu(II) during *e*ATRP was demonstrated by the absence of the peak couple for $[Cu^{II}L]^{2+}/[Cu^{I}L]^{+}$ at the end of polymerization (**Figure 7.9 a, violet trace**). Repeating the same experiment in the undivided cell with a 2-fold excess of ligand over Cu^{2+}, the polymerization control was just slightly improved but remained unsatisfactory (**Table 7.3, entry 3**).

Table 7.3 Potentiostatic *e*ATRP of 10% (v/v) OEOMA + H_2O with $[Cu^{II}Me_6TREN]^{2+}$.[a]

Entry	Anode	ΔE [b] (V)	$[Cu^{2+}]$:[L]	Conv.[c] (%)	t (h)	Q (C)	10^{-3} $M_{n,th}$ [d]	10^{-3} M_n [e]	k_p^{app} [f] (h^{-1})	$Đ$ [e]	$[Al^{3+}]_{th}$ [g]
1	Gr [h]	0.06	1:1	99.8	3	5.29	53.8	157.0	1.13	1.58	-
2	Al		1:1	88.7	3	4.28	47.9	118.4	0.74	1.98	0.49
3	Al		1:2	97.5	5	7.49	52.6	172.6	1.23	1.69	0.86
4	Gr [h]	0.12	1:1	93.9	4	5.16	49.6	79.7	0.65	1.35	-
5	Al		1:1	59.4	4	4.52	31.4	65.6	0.24	1.46	0.52
6	Al		1:2	98.4	4	7.99	52.5	122.9	1.04	1.40	0.92

[a]Polymerization conditions: [OEOMA]:[HEBiB]:[$Cu(OTf)_2$] = 107.5:1.0:0.5, with initial [$Cu(OTf)_2$] = 1.0 mM; [Et_4NBr] = 0.1 M; V_{tot} = 30 mL; T = 25 °C. [b]$\Delta E = E_{app} - E_{1/2}$. [c]Determined by ^{1}H NMR. [d]Calculated on the basis of conversion obtained by ^{1}H NMR (i.e. $M_{n,th} = M_{HEBiB} + 107.5 \times \text{conversion} \times M_{OEOMA}$). [e]Determined by GPC. [f]Slope of the linear plot of ln ($[M]_0/[M]$) vs. time. [g]$[Al^{3+}]_{th}$ (mM) = $Q/(3 \cdot F \cdot V)$, where F is the Faraday constant, 96485.332 C/mol, V = 30 mL.

Usually, the polymer dispersity can be reduced by either using a higher deactivator ($[BrCu^{II}L]^{+}$) concentration (**eq. 7-1**) and/or a more positive E_{app} value, each essentially increasing the effective concentration of $[BrCu^{II}L]^{+}$ in the reaction medium. At $E_{app} = E_{1/2} + 0.12$ V, the ratio of $[Cu^{II}L]^{2+}$ to $[Cu^{I}L]^{+}$ concentrations is ca 100. Repeating the *e*ATRP experiments at $E_{app} = E_{1/2} + 0.12$ V, under otherwise identical conditions, the polymerization rate decreased because of the ultra-low concentration of activator species $[Cu^{I}L]^{+}$. However, the polymerization control was improved as evidenced by the linear first-order kinetic plot and low dispersity shown in **Table 7.3 entries 4-6** and **Figure 7.10 a, b**. The experimental M_n values directly obtained from GPC measurements were linearly increasing with conversion, but were higher than the

theoretical values ($M_{n,th}$). In the undivided cell, the monomer conversion after 4 h dramatically dropped from 93.9% to 59.4% when the separated graphite anode was replaced with a sacrificial Al anode (**Table 7.3, entries 4, 5**). However, the polymer molecular weight distribution $Đ$ decreased a lot in comparison to the *se*ATRP conducted at the more negative applied potential (**Table 7.3, entry 2),** and the polymerization was well-controlled as evidenced by the linear first-order kinetic plot in **Figure 7.10 a, b**. When *e*ATRP at $E_{app} = E_{1/2} + 0.12$ V was run with excess Me_6TREN ($[Cu^{II}]$:[Me_6TREN] = 1:2), the monomer conversion reached 98.4% after 4 h and M_n and k_p^{app} increased significantly (**Table 7.3, entry 6**). Furthermore, addition of excess ligand provided lower M_w/M_n values ($Đ < 1.5$) at identical $[BrCu^{II}L]^+$ concentration. GPC traces indicated successful polymerization of the monomer, as a clean monomodal shift of the MW peak toward higher MW values was observed (**Figure 7.11 a**).

It is also important to mention that the surfaces of both the Pt and Al electrodes were covered by a layer of a colored substance after polymerization, as shown in **Figure 7.12**. In the divided cell, only a small part of Pt surface was covered by a light red layer, while full coverage was observed for both Pt and Al surfaces in undivided cells without excess Me_6TREN. Additionally, the quasi-reversible peak couple of $[Cu^{II}L]^{2+}/[Cu^{I}L]^+$ disappeared after polymerization, as shown in **Figure 7.9 a**. When excess ligand over Cu^{2+} was used in undivided cells, no colored deposit was found on the Al surface, but it could still be observed on the Pt surface. In this case, the voltametric pattern of $[Cu^{II}L]^{2+}$ was observed after polymerization. The Al^{3+} ions combine with the free ligand to form a stable complex rather than react with the Cu(II) complex. These results suggested that Cu(II) complexes with Me_6TREN were destroyed during *e*ATRP with anodic dissolution of Al, in good agreement with the CV results. As in the case of organic media, monomer conversion, molecular weights, and polymerization rate were significantly improved by the addition of excess ligand.

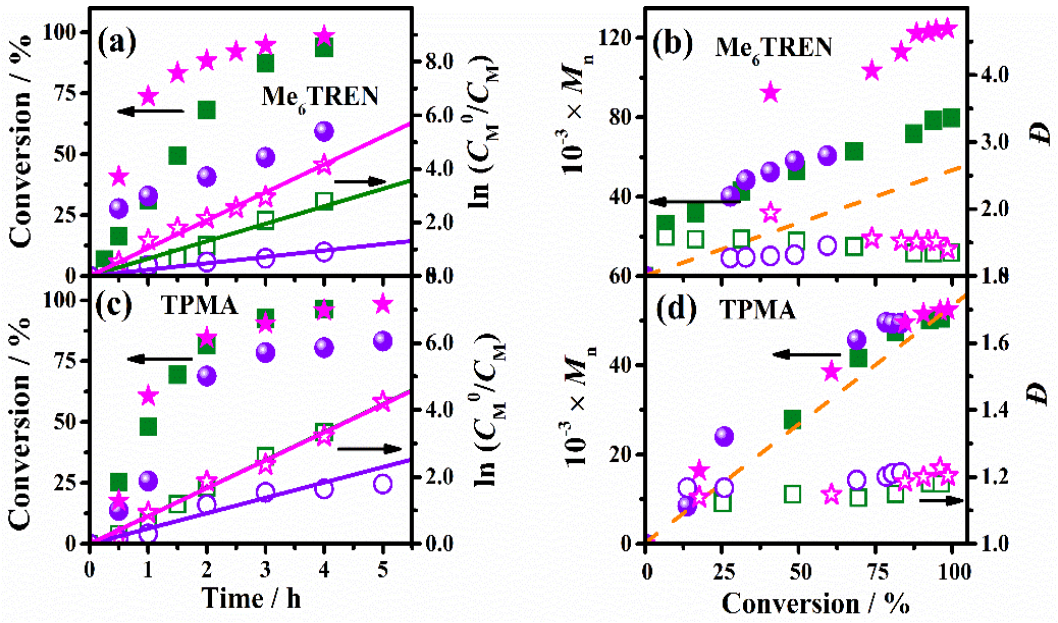

Figure 7.10 Kinetic plots and monomer conversion as a function of time and evolution of M_n and $Đ$ with conversion for *e*ATRP of 10 vol% OEOMA in H_2O + 0.1 M Et_4NBr with 1 mM $[Cu^{II}L]^{2+}$, performed on a Pt cathode at 25 °C at $E_{app} = E_{1/2} + 0.06$ V for L = TPMA **(a, b)** or $E_{app} = E_{1/2} + 0.12$ V for L = Me_6TREN **(c, d)**. Other conditions: divided cell with a graphite anode and $Cu(OTf)_2$:L = 1:1 (■); undivided cell with an Al anode and $[Cu(OTf)_2]$:[L] = 1:1 (●), 1: 2 (★). The dashed line in c and d indicates $M_{n,th}$.

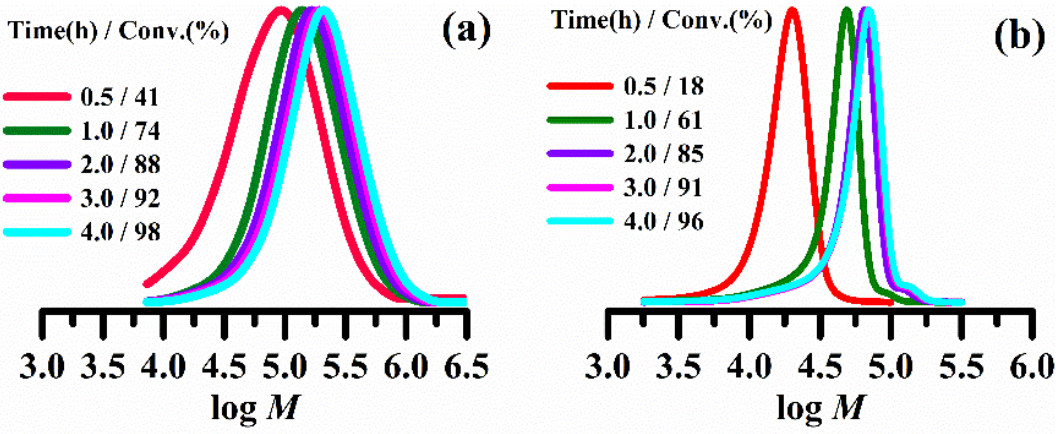

Figure 7.11 Representative GPC traces of POEOMA prepared by *e*ATRP of 10% (v/v) OEOMA at 25 °C in H_2O + 0.1 M Et_4NBr in an undivided cell with a sacrificial Al wire anode. Polymerization conditions: E_{app} - $E_{1/2} = 0.12$ V for Me_6TREN **(a)**, 0.06 V for TPMA **(b)**; HEBiB/$Cu(OTf)_2$/L = 1/0.5/1, with initial $[Cu^{II}] = 10^{-3}$ M; $V_{tot} = 30$ mL.

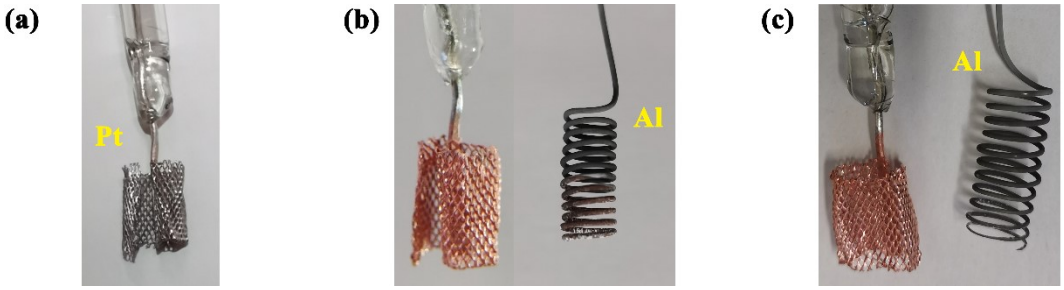

Figure 7.12 Digital images of Pt and Al electrodes after *e*ATRP of 10% (v/v) OEOMA in H_2O + 0.1 M Et_4NBr at $E_{app} = E_{1/2} + 0.12$ V, with 1 mM $[Cu^{II}Me_6TREN]^{2+}$ catalyst in divided cell **(a)** and undivided cell with $[Cu(OTf)_2]$:$[Me_6TREN]$ = 1:1 **(b)**, 1:2 **(c)**.

Analogous experiments were carried out by using TPMA instead of Me_6TREN as a ligand. *e*ATRP of OEOMA with $[Cu^{II}TPMA]^{2+}$ in both types of cell behaved better than with $[Cu^{II}Me_6TREN]^{2+}$ when the $E_{app} = E_{1/2} + 0.06$ V was applied. Use of a sacrificial Al anode in *e*ATRP of OEOMA with $[Cu^{II}TPMA]^{2+}$ had little effect on the polymerization and polymer dispersity (**Figure 7.10 c-d**). M_n increased linearly with conversion and closely matched $M_{n,th}$. The monomer conversion after 4 h dropped from 96.4% to 80.6% when a sacrificial Al anode was used in place of a separated graphite electrode, and the overall rate of polymerization (k_p^{app}) decreased by ca 50% (**Table 7.4, entries 1, 2**). At the end of this experiment, no significant colored substance was observed on Al and Pt surfaces. In addition, the voltammetric pattern of $[Cu^{II}TPMA]^{2+}$ remained essentially unaffected (**Figure 7.9 b**). When the experiment in the undivided cell was repeated with a two-fold excess of TPMA over Cu^{2+}, both monomer conversion and k_p^{app} were recovered (**Table 7.4 entry 3**); also, a regular shift of narrow GPC traces to higher MWs was observed (**Figure 7.11 b**). The differences between these two experiments were probably caused by the small dissociation of $[Cu^{II}TPMA]^{+}$ during polymerization. Theoretically, the concentrations of Al^{3+} ions released in the two experiments were 0.45 mM and 0.53 mM, which have little effects on the catalyst stability as was previously shown by CV analysis. The small improvement of the *e*ATRP process in the presence of excess TPMA is because the free ligand suppresses $[Cu^{II}TPMA]^{2+}$ dissociation.

Table 7.4 Potentiostatic *e*ATRP of 10% (v/v) OEOMA + H_2O with $[Cu^{II}TPMA]^{2+}$.[a]

Entry	Anode	$[Cu^{2+}]$:[L]	Q (C)	Conv.[b] (%)	10^{-3} $M_{n,th}$ [c]	10^{-3} M_n [d]	k_p^{app} [e] (h^{-1})	$Đ$ [d]	$[Al^{3+}]_{th}$ [f]
1	Gr[g]	1:1	3.31	96.4	52.0	51.6	0.83	1.19	-
2	Al	1:1	3.92	80.6	43.5	49.4	0.46	1.23	0.45
3	Al	1:2	4.64	96.0	51.8	52.3	0.83	1.21	0.53

[a]Polymerization conditions: [OEOMA]:[HEBiB]:[$Cu(OTf)_2$] = 107.5:1.0:0.5, $E_{app} = E_{1/2} + 0.06$ V with initial [$Cu(OTf)_2$] = 1.0 mM; [Et_4NBr] = 0.1 M; V_{tot} = 30 mL; T = 25 °C, t = 4 h. [b]Determined by ^{1}H NMR. [c]Calculated on the basis of conversion obtained by ^{1}H NMR (i.e. $M_{n,th} = M_{HEBiB} + 107.5 \times \text{conversion} \times M_{OEOMA}$). [d]Determined by GPC. [e]Slope of the linear plot of ln ($[M]_0/[M]$) vs. time. [f]$[Al^{3+}]_{th}$ (mM) = $Q/(3 \cdot F \cdot V)$, where F is the Faraday constant, 96485.332 C/mol, V = 30 mL. [g]Graphite anode in a separated anodic compartment.

7.3.4 Potentiostatic *e*ATRP of DMA in divided and undivided cells

Poly(*N,N*-dimethylacrylamide) is a non-ionic, water-soluble and biocompatible monomer and its polymerization may be tailored to meet a broad range of applications.[42-45] *N,N*-dimethylacrylamide (DMA) polymerization catalyzed by copper complexes has been studied systematically via various RDRP methods.[46-54] Chmielarz et al. reported that *e*ATRP exhibits extreme sensibility to ligand structure in the case of polymerization of acrylamides[55], and De Bon et al. successfully synthesized PDMA via *e*ATRP in water in a divided cell with three types of ligands.[53] Therefore, *e*ATRP of DMA with two widely used catalyst systems ($[Cu^{II}TPMA]^{2+}$ and $[Cu^{II}Me_6TREN]^{2+}$) were performed in two different types of cells, and the results are summarized in **Table 7.5**. The voltammetric patterns of catalysts before and after polymerization and the E_{app} for each complex are indicated in the **Figure 7.13**. The kinetic plots and evolution of monomer conversion, M_n and Đ during polymerization are shown in **Figure 7.14**.

Table 7.5 Potentiostatic *e*ATRP of 10% (v/v) DMA + H_2O with $[Cu^{II}TPMA]^{2+}$ and $[Cu^{II}Me_6TREN]^{2+}$.[a]

Entry	Anode	L	ΔE[b] (V)	T (°C)	t (h)	Q (C)	Conv.[c] (%)	10^{-3} $M_{n,th}$[d]	10^{-3} M_n[e]	k_p^{app} [f] (h^{-1})	$Đ$ [e]
1	Gr [g]	Me_6TREN	0.06	25	2	1.68	16.9	9.04	14.4	0.12	2.03
2	Gr [g]		0.06	0	2	0.36	96.6	46.0	81.8	1.62	1.61
3	Gr [g]		0.03	0	2	0.53	97.3	46.3	73.5	1.88	1.23
4	Al		0.03	0	2	0.47	99.1	47.2	68.0	2.34	1.21
5	Gr [g]	TPMA	0	0	6	2.86	28.9	13.1	12.9	0.07	1.84
6	Al		0	0	6	2.55	26.0	12.5	12.6	0.08	1.41

[a]Polymerization conditions: [DMA]:[HEBiB]:$[Cu(OTf)_2]$:[L]= 449:1.0:0.5:0.5, with initial $[Cu(OTf)_2] = 10^{-3}$ M; $[Et_4NBr] = 0.1$ M; $V_{tot} = 30$ mL. [b]$\Delta E = E_{app} - E_{1/2}$. [c]Determined by ^{1}H NMR. [d]Calculated on the basis of conversion obtained by ^{1}H NMR (i.e. $M_{n,th} = M_{HEBiB} + 449 \times$ conversion $\times M_{DMA}$). [e]Determined by GPC. [f]Slope of the linear plot of $\ln([M]_0/[M])$ vs. time. [g]Graphite anode in a separated anodic compartment.

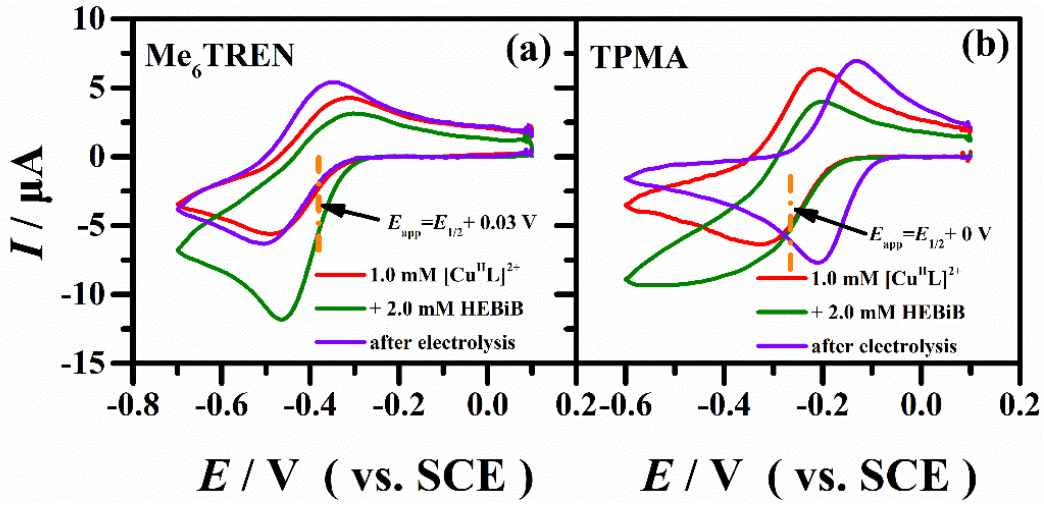

Figure 7.13 Cyclic voltammetry results of 1 mM $[Cu^{II}L]^{2+}$ in H_2O + 10 vol% DMA + 0.1 M Et_4NBr recorded at T = 0 °C and v = 0.2 V/s before *e*ATRP in the absence (—) and presence of HEBiB (—), and after electrolysis (—) for L= Me_6TREN **(a)** and TPMA **(b)** with the ratio of $[Cu(OTf)_2]$:[L] = 1:1 in an undivided cell. Arrows indicate applied potential.

A reversible voltammetric pattern was observed for $[Cu^{II}L]^{2+}$, indicating that both Cu(II) and the corresponding Cu(I) complexes are stable in H_2O + 10 vol% DMA (**Figure 7.13**). The standard reduction potentials ($E_{1/2}$) of $[Cu^{II}L]^{2+}$ are -0.402 V and -0.268 V vs SCE for L = Me_6TREN and TPMA, respectively, in line with our previous work.[53] Addition of 2 mM HEBiB caused a remarkable increase of the cathodic peak current and a decrease of the anodic one in the case of L = Me_6TREN, indicating the establishment of the so-called electrocatalytic (EC', an electron transfer followed by a catalytic chemical reaction) behavior.[56-57] Conversely, the voltammetric pattern of $[Cu^{II}TPMA]^{2+}$ was not significantly modified by the addition of a 2-fold excess of initiator, confirming that activation of HEBiB by $[Cu^{I}TPMA]^{+}$ is a slow reaction.[53] According to the CVs of $[Cu^{II}L]^{2+}$ in the presence of initiator in the mixture, it was demonstrated that stable $[Cu^{I}Me_6TREN]^{+}$ can react rapidly with HEBiB and regenerate $[Cu^{II}Me_6TREN]^{2+}$ which diffuses back to the electrode to be reduced again. The observed difference of behavior between TPMA and Me_6TREN in H_2O/DMA agrees well with the results reported by Chmielarz et al. who found the apparent propagation rate constant (k_p^{app}) of acrylamide with $[Cu^{II}Me_6TREN]^{2+}$ was 44 times higher than that with $[Cu^{II}TPMA]^{2+}$.[55]

A well-controlled ATRP of DMA in aqueous media is challenging due to several factors including a potential deactivation of the catalyst, fast activation, and loss of halide chain end functionality.[46-47, 50, 53, 55, 58] The effect of reaction temperature on DMA polymerization was initially evaluated at room (25 °C) and low (0 °C) temperatures at $E_{app} = E_{1/2}$ + 0.06 V in H_2O + 10 vol% DMA mixture solution in a divided cell (**Table 7.5, entries 1, 2**). Bad control with low conversion (16.9%), and low k_p^{app} were observed for *e*ATRP of DMA at 25 °C after 2 h, yielding a low molecular weight polymer with high Đ. Moreover, as the molecular weight distribution peak in GPC moved toward high molecular weights, some tailing could be seen, suggesting small amounts of dead chains generated by radical-radical terminations. Polymerization was uncontrolled mainly because of loss of chain-end functionality by a cyclization reaction.[46, 50, 53, 59-60] When the temperature was lowered to 0 °C, monomer conversion reached 96.6% after 2 h and evolution of M_n with conversion followed the theoretical

prediction (**Table 7.5, entries 1** and **2, Figure 7.14 a, b**). But the experimental molecular weights deviated from the theoretical values at high conversions and also the polymer dispersity increased at conversion > 85%, reaching 1.61 at the end of polymerization. Shifting E_{app} to more negative potentials increases the amount of Cu(II) converted to Cu(I) and this increases the rate of the activation reaction between Cu(I) and the dormant species. In fact, the apparent polymerization rate constant k_p^{app} and polymer dispersity Đ were obviously improved when the applied potential was changed to $E_{app} = E_{1/2} + 0.03$ V (**Table 7.5**, **entry 3** and **Figure 7.14 a, b**).

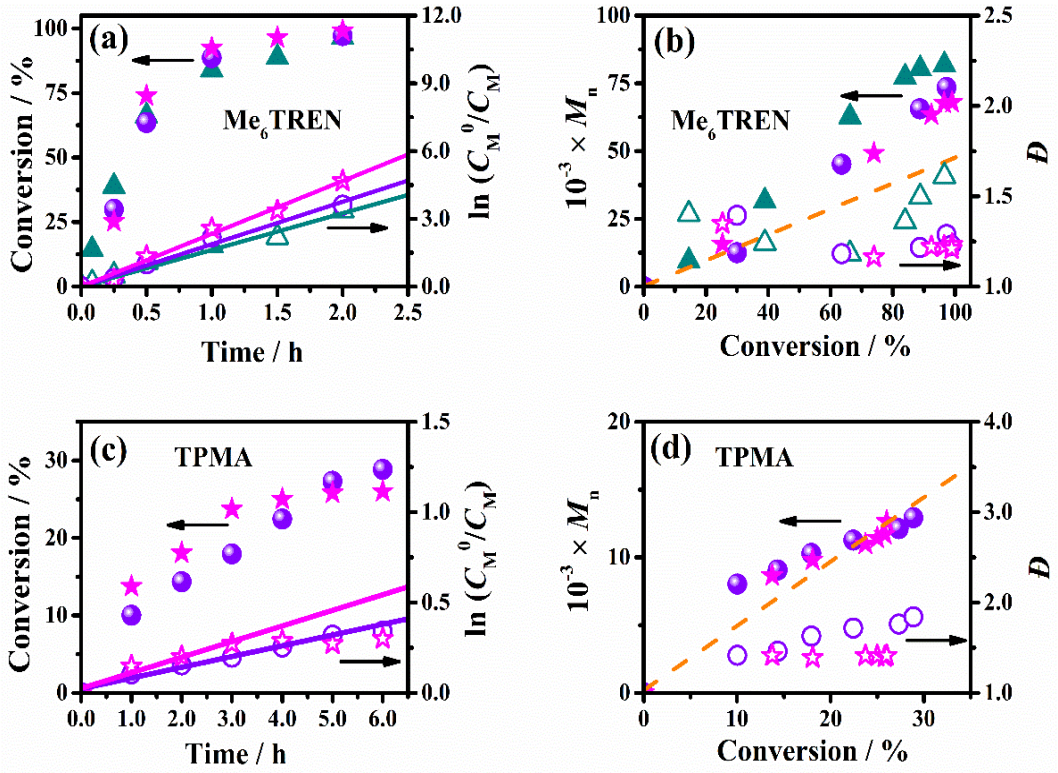

Figure 7.14 Kinetic plots and monomer conversion as a function of time and evolution of M_n and $Đ$ with conversion for *e*ATRP of 10 vol% DMA in H_2O + 0.1 M Et_4NBr, performed on a Pt cathode at 0 °C with $[Cu^{II}Me_6TREN]^{2+}$ **(a, b)** or $[Cu^{II}TPMA]^{2+}$ at $E_{app} = E_{1/2}$ **(c, d)**. Other conditions: divided cell with a graphite anode and $Cu(OTf)_2$:TPMA = 1:1 (●); $Cu(OTf)_2$:Me_6TREN = 1:1 at $E_{app} = E_{1/2} + 0.06$ V (▲) or 0.03 V (●), undivided cell with an Al anode and $[Cu(OTf)_2]$:[L] = 1:1 (★) , T = 25 °C. The dashed lines in c and d indicate $M_{n,th}$.

The difficulty of controlling *e*ATRP of DMA does not probably arise from fast radical-radical termination reactions. A more likely reaction, which has been reasonably proposed in the literature on polymerization of DMA, is an intramolecular cyclization reaction leading to loss of the C-Br chain-end functionality, especially at high monomer conversion even if a low temperature (0 °C) is used.[50, 53, 55, 61] The monomer conversion and k_p^{app} improved when the separated graphite anode was replaced with a sacrificial Al anode in an undivided cell (**Table 7.5, entry 4**). Moreover, the polymerization was well-controlled as evidenced by the linear first-order kinetic plot and low dispersity shown in **Figure 7.14 a, b**, and the GPC traces which were always monomodal, continuously shifting to higher molecular weights without tailing (**Figure 7.15 a**).

In contrast to *e*ATRP of OEOMA in the undivided cell, no marked colored layer was observed on the Al surface after the polymerization of DMA with $[Cu^{II}Me_6TREN]^{2+}$. A quasi-reversible peak couple of $[Cu^{II}Me_6TREN]^{2+}/[Cu^{I}Me_6TREN]^{+}$ was found after polymerization (**Figure 7.13 a**). This demonstrates that Al has some positive effects on the polymerization of DMA with $[Cu^{II}Me_6TREN]^{2+}$ in an undivided cell even without excess ligand.

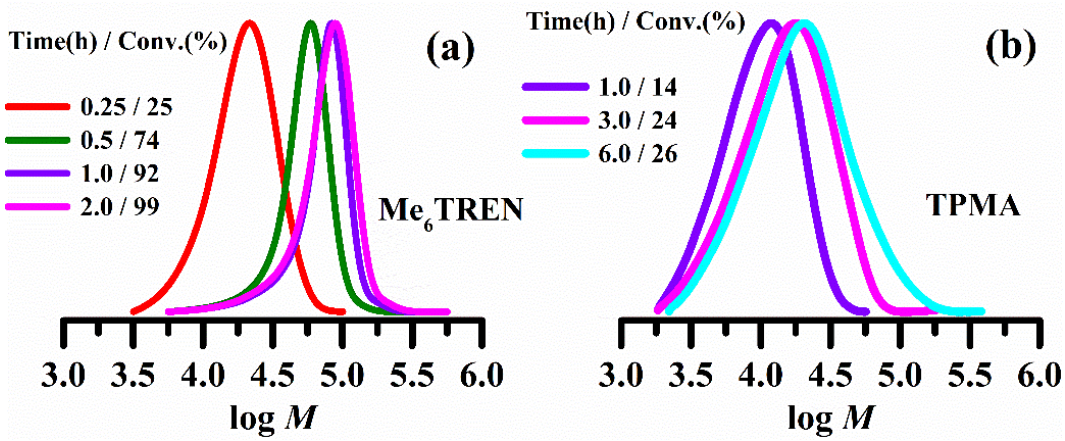

Figure 7.15 Representative GPC traces of PDMA prepared by *e*ATRP at 0 °C in H_2O +10% (v/v) DMA + 0.1 M Et_4NBr in an undivided cell with a sacrificial Al anode. Polymerization conditions: $E_{app} - E_{1/2} = 0.03$ V **(a)**, 0 V **(b)**, HEBiB/$Cu(OTf)_2$/L = 1/0.5/1, with initial $[Cu^{II}] = 10^{-3}$ M; $V_{tot} = 30$ mL, $T = 25$ °C.

Conversely, *e*ATRP catalyzed by $[Cu^{II}TPMA]^{2+}$ was very slow (**Figure 7.14 c, d**), yielding a polymer with high dispersity and broad GPC traces (**Figure 7.15 b**). Monomer conversion was quite low, reaching only 26~28.9% in six hours in both kinds of cell (**Table 7.5 entries 5**, **6**). This is opposite of the normal behavior of $[Cu^{II}TPMA]^{2+}$, which is one of the best catalysts for *e*ATRP in aqueous media. As shown in **Figure 7.13 b**, activation of the initiator HEBiB by $[Cu^{I}TPMA]^{+}$ is quite slow, even if tertiary initiators usually have high activation rate constants. It is also important to mention that the dispersity in the undivided cell was lower than that in the divided one, which could be attributed to the beneficial effect of Al^{3+} already observed with $[Cu^{II}Me_6TREN]^{2+}$. The voltametric pattern of $[Cu^{II}TPMA]^{2+}$ was recorded after polymerization and a quasi-reversible peak couple was observed without evident loss of the starting copper complex. Overall, the results obtained in this study provide interesting guidelines for electrochemically mediated polymerization of water-soluble monomers in undivided cells with a sacrificial anode.

7.4 Conclusions

The stability of copper complexes with TPMA and Me_6TREN in water and water/monomer mixtures under anodic dissolution of Al were evaluated systematically via cyclic voltammetry and surface characterization methods. Both $[Cu^{II}TPMA]^{2+}$ and $[BrCu^{II}TPMA]^{+}$ are little affected by Al^{3+} ions and Al in both reaction media. Only a small fraction of complexes (<10%) suffered from dissociation and released free solvated Cu^{2+} ions, which can react with Al to form Cu^0. Me_6TREN prefers binding to Al^{3+} than Cu^{2+} or Cu^{+} to form more stable complexes in both types of reaction media. It is noteworthy that both Al and Al^{3+} can destroy Cu complexes coordinated with Me_6TREN. In practical, the strong Lewis acid Al^{3+} generated by anodic dissolution of Al electrode undergoes hydrolysis, changing the solution pH to values as low as 3. $[Cu^{II}Me_6TREN]^{2+}$ is not stable at this low pH and dissociates to free Cu^{2+} ions and protonated ligand. It was observed that both free solvated Cu^{2+} ions and $[Cu^{II}Me_6TREN]^{2+}$ can be reduced to metallic Cu^0 by Al and the reaction of Cu^{2+} was

ca 2 times faster than that of the copper complex in H_2O + 10% (v/v) OEOMA. Therefore, the copper complexes could not be restored completely when at the end of the experiment excess ligand was added to the solution, due to the irreversible conversion of Cu(II) to a metallic deposit on the Al surface.

The stability of copper complexes is critically important in ATRP. Electrochemically mediated ATRP of 10 vol% OEOMA or DMA with two copper complexes was investigated in a simplified setup with a sacrificial Al anode. In the case of $[Cu^{II}TPMA]^{2+}$, the catalyst maintained its activity during *e*ATRP of OEOMA, with only a slight negative impact of Al^{3+} ions in the undivided cell, which was successfully suppressed by using a two-fold excess ligand over Cu^{2+}. The stability and performance of $[Cu^{II}TPMA]^{2+}$ were not impacted by anodic dissolution of Al in H_2O + 10% (v/v) DMA. However, the catalytic efficiency of $[Cu^{II}TPMA]^{2+}$ on DMA polymerization was very low, even in the absence of anodic dissolution of Al.

In contrast to $[Cu^{II}TPMA]^{2+}$, the catalytic performance of the system became heavily compromised when Me_6TREN was used in the polymerization of OEOMA in the undivided cell; the catalyst was lost during *e*ATRP and a copper deposit was observed on both the Pt cathode and Al anode. This deterioration could be avoided by using a two-fold excess of Me_6TREN over Cu^{2+}. It is worth noting that, with $[Cu^{II}Me_6TREN]^{2+}$ as the catalyst, *e*ATRP of DMA was fast and well-controlled in the undivided cell without using excess ligand with respect to Cu^{2+}. It appears that the strong Lewis acid nature of Al^{3+} likely plays a key role on well-controlled polymerization of DMA in the undivided cell.

References

[1**]**. Patten, T. E.; Xia, J.; Abernathy, T.; Matyjaszewski, K., Polymers with very low polydispersities from atom transfer radical polymerization. *Science* **1996,** *272* (5263), 866-868.
[2**]**. Braunecker, W. A.; Matyjaszewski, K., Controlled/living radical polymerization: Features, developments, and perspectives. *Progress in Polymer Science* **2007,** *32* (1), 93-146.
[3**]**. Ayres, N., Atom transfer radical polymerization: a robust and versatile route for polymer synthesis. *Polymer Reviews* **2011,** *51* (2), 138-162.
[4**]**. Matyjaszewski, K., Atom transfer radical polymerization (ATRP): current status and future perspectives. *Macromolecules* **2012,** *45* (10), 4015-4039.
[5**]**. Ribelli, T. G.; Konkolewicz, D.; Bernhard, S.; Matyjaszewski, K., How are radicals (re) generated in photochemical ATRP? *Journal of the American Chemical Society* **2014,** *136* (38), 13303-13312.
[6**]**. Corrigan, N.; Jung, K.; Moad, G.; Hawker, C. J.; Matyjaszewski, K.; Boyer, C., Reversible-deactivation radical polymerization (Controlled/living radical polymerization): From discovery to materials design and applications. *Progress in Polymer Science* **2020**, 101311.
[7**]**. Messina, M. S.; Messina, K. M.; Bhattacharya, A.; Montgomery, H. R.; Maynard, H. D., Preparation of biomolecule-polymer conjugates by grafting-from using ATRP, RAFT, or ROMP. *Progress in Polymer Science* **2020,** *100*, 101186.
[8**]**. Matyjaszewski, K., Advanced Materials by Atom Transfer Radical Polymerization. *Adv Mater* **2018,** *30* (23), e1706441.
[9**]**. Krys, P.; Matyjaszewski, K., Kinetics of Atom Transfer Radical Polymerization. *European Polymer Journal* **2017,** *89*, 482-523.
[10**]**. Pan, X.; Fantin, M.; Yuan, F.; Matyjaszewski, K., Externally controlled atom transfer radical polymerization. *Chem Soc Rev* **2018,** *47* (14), 5457-5490.
[11**]**. Magenau, A. J.; Strandwitz, N. C.; Gennaro, A.; Matyjaszewski, K., Electrochemically mediated atom transfer radical polymerization. *Science* **2011,** *332* (6025), 81-4.
[12**]**. Park, S.; Chmielarz, P.; Gennaro, A.; Matyjaszewski, K., Simplified electrochemically mediated atom transfer radical polymerization using a sacrificial anode. *Angew Chem Int Ed Engl* **2015,** *54* (8), 2388-92.
[13**]**. Chmielarz, P.; Fantin, M.; Park, S.; Isse, A. A.; Gennaro, A.; Magenau, A. J. D.; Sobkowiak, A.; Matyjaszewski, K., Electrochemically mediated atom transfer radical polymerization (*e*ATRP). *Progress in Polymer Science* **2017,** *69*, 47-78.
[14**]**. Lorandi, F.; Fantin, M.; Isse, A. A.; Gennaro, A., Electrochemical triggering and control of atom transfer radical polymerization. *Current Opinion in Electrochemistry* **2018,** *8*, 1-7.
[15**]**. Isse, A. A.; Gennaro, A., Electrochemistry for Atom Transfer Radical Polymerization. *The Chemical Record* **2021**.

[16**]**. Fantin, M.; Lorandi, F.; Isse, A. A.; Gennaro, A., Sustainable Electrochemically-Mediated Atom Transfer Radical Polymerization with Inexpensive Non-Platinum Electrodes. *Macromol Rapid Commun* **2016,** *37* (16), 1318-22.
[17**]**. Lorandi, F.; Fantin, M.; Isse, A. A.; Gennaro, A., Electrochemically mediated atom transfer radical polymerization of n-butyl acrylate on non-platinum cathodes. *Polymer Chemistry* **2016,** *7* (34), 5357-5365.
[18**]**. Chmielarz, P., Synthesis of naringin-based polymer brushes via seATRP. *Polymers for Advanced Technologies* **2018,** *29* (1), 470-480.
[19**]**. Zaborniak, I.; Chmielarz, P., Miniemulsion switchable electrolysis under constant current conditions. *Polymers for Advanced Technologies* **2020,** *31* (11), 2806-2815.
[20**]**. Luo, J.; Durante, C.; Gennaro, A.; Isse, A. A., Electrochemical study of the effect of Al^{3+} on the stability and performance of Cu-based ATRP catalysts in organic media. *Electrochimica Acta* **2021,** *388*, 138589.
[21**]**. Perrier, S.; Armes, S. P.; Wang, X.; Malet, F.; Haddleton, D. M., Copper (I)-mediated radical polymerization of methacrylates in aqueous solution. *Journal of Polymer Science Part A: Polymer Chemistry* **2001,** *39* (10), 1696-1707.
[22**]**. Tsarevsky, N.; McKenzie, B.; Tang, W.; Matyjaszewski, K. In *Tuning the activity and performance of the catalyst in atom transfer radical polymerization and general rules for catalyst selection*, Abstracts of papers of the American Chemical Society, Amer Chemical Soc 1155 16th ST, NW, Washington, DC 20036 USA: 2005; pp 4018.
[23**]**. Paneva, D.; Mespouille, L.; Manolova, N.; Degée, P.; Rashkov, I.; Dubois, P., Preparation of Well-Defined Poly [(ethylene oxide)-block-(sodium 2-acrylamido-2-methyl-1-propane sulfonate)] Diblock Copolymers by Water-Based Atom Transfer Radical Polymerization. *Macromolecular rapid communications* **2006,** *27* (17), 1489-1494.
[24**]**. Tsarevsky, N. V.; Braunecker, W. A.; Vacca, A.; Gans, P.; Matyjaszewski, K. In *Competitive equilibria in atom transfer radical polymerization*, Macromolecular symposia, Wiley Online Library: 2007; pp 60-70.
[25**]**. Tsarevsky, N. V.; Matyjaszewski, K., "Green" atom transfer radical polymerization: from process design to preparation of well-defined environmentally friendly polymeric materials. *Chemical reviews* **2007,** *107* (6), 2270-2299.
[26**]**. Braunecker, W. A.; Tsarevsky, N. V.; Gennaro, A.; Matyjaszewski, K., Thermodynamic components of the atom transfer radical polymerization equilibrium: quantifying solvent effects. *Macromolecules* **2009,** *42* (17), 6348-6360.
[27**]**. Pavan, P.; Lorandi, F.; De Bon, F.; Gennaro, A.; Isse, A. A., Enhancement of the Rate of Atom Transfer Radical Polymerization in Organic Solvents by Addition of Water: An Electrochemical Study. *ChemElectroChem* **2021,** *8* (13), 2450-2458.
[28**]**. Min, K.; Matyjaszewski, K., Atom transfer radical polymerization in aqueous dispersed media. *Open Chemistry* **2009,** *7* (4), 657-674.
[29**]**. Bortolamei, N.; Isse, A. A.; Magenau, A. J.; Gennaro, A.; Matyjaszewski, K., Controlled aqueous atom transfer radical polymerization with electrochemical generation of the active catalyst. *Angewandte Chemie International Edition* **2011,** *50* (48), 11391-11394.
[30**]**. Fantin, M.; Isse, A. A.; Gennaro, A.; Matyjaszewski, K., Understanding the

Fundamentals of Aqueous ATRP and Defining Conditions for Better Control. *Macromolecules* **2015,** *48* (19), 6862-6875.
[31**]**. Fantin, M.; Isse, A. A.; Matyjaszewski, K.; Gennaro, A., ATRP in Water: Kinetic Analysis of Active and Super-Active Catalysts for Enhanced Polymerization Control. *Macromolecules* **2017,** *50* (7), 2696-2705.
[32**]**. Liarou, E.; Han, Y.; Sanchez, A. M.; Walker, M.; Haddleton, D. M., Rapidly self-deoxygenating controlled radical polymerization in water via in situ disproportionation of Cu (I). *Chemical science* **2020,** *11* (20), 5257-5266.
[33**]**. Mitchell, L.; Williamson, P.; Ehrlichová, B.; Anderson, A. E.; Seymour, V. R.; Ashbrook, S. E.; Acerbi, N.; Daniels, L.; Walton, R.; Clarke, M. L., Mixed-metal MIL-100 (Sc, M)(M= Al, Cr, Fe) for Lewis acid catalysis and Tandem C− C bond formation and alcohol oxidation. *Chemistry-A European Journal* **2014**.
[34**]**. Piovano, A.; Thushara, K.; Morra, E.; Chiesa, M.; Groppo, E., Unraveling the catalytic synergy between Ti3+ and Al3+ sites on a chlorinated Al2O3: a tandem approach to branched polyethylene. *Angewandte Chemie* **2016,** *128* (37), 11369-11372.
[35**]**. izares, P. C.; Martı´nez, F.; Jime´nez, C.; Lobato, J.; Rodrigo*, a. M. A., Comparison of the aluminum speciation in chemical and electrochemical dosing processes-annotated. *Ind. Eng. Chem. Res.* **2006,** *45*, 8749-8756.
[36**]**. Thakur, L. S.; Mondal, P., Simultaneous arsenic and fluoride removal from synthetic and real groundwater by electrocoagulation process: Parametric and cost evaluation. *J Environ Manage* **2017,** *190*, 102-112.
[37**]**. Sandoval, M. A.; Fuentes, R.; Thiam, A.; Salazar, R., Arsenic and fluoride removal by electrocoagulation process: A general review. *Sci Total Environ* **2021,** *753*, 142108.
[38**]**. Golub, G.; Lashaz, A.; Cohen, H.; Paoletti, P.; AndreaBencini; Valtancoli, B.; Meyerstein, D., The effect of N-methylation of tetra-aza-alkane copper complexes on the axial binding of anions-annotated. *Inorganica Chimica Acta* **1997**.
[39**]**. McLachlan, G. A.; Fallon, G. D.; Martin, R. L.; Spiccia, L., Synthesis, structure and properties of five-coordinate copper (II) complexes of pentadentate ligands with pyridyl pendant arms. *Inorganic Chemistry* **1995,** *34* (1), 254-261.
[40**]**. Emamjomeh, M. M.; Sivakumar, M., Review of pollutants removed by electrocoagulation and electrocoagulation/flotation processes. *Journal of environmental management* **2009,** *90* (5), 1663-1679.
[41**]**. Mansouri, K.; Ibrik, K.; Bensalah, N.; Abdel-Wahab, A., Anodic Dissolution of Pure Aluminum during Electrocoagulation Process: Influence of Supporting Electrolyte, Initial pH, and Current Density. *Industrial & Engineering Chemistry Research* **2011,** *50* (23), 13362-13372.
[42**]**. Yeh, J.-C.; Hsu, Y.-T.; Su, C.-M.; Wang, M.-C.; Lee, T.-H.; Lou, S.-L., Preparation and characterization of biocompatible and thermoresponsive micelles based on poly (N-isopropylacrylamide-co-N, N-dimethylacrylamide) grafted on polysuccinimide for drug delivery. *Journal of biomaterials applications* **2014,** *29* (3), 442-453.
[43**]**. Bashir, S.; Omar, F. S.; Hina, M.; Numan, A.; Iqbal, J.; Ramesh, S.; Ramesh, K., Synthesis and characterization of hybrid poly (N, N-dimethylacrylamide) composite hydrogel electrolytes and their performance in supercapacitor. *Electrochimica Acta* **2020,** *332*, 135438.

[44**]**. Plucinski, A.; Willersinn, J.; Lira, R. B.; Dimova, R.; Schmidt, B. V., Aggregation and Crosslinking of Poly (N, N-dimethylacrylamide)-b-pullulan Double Hydrophilic Block Copolymers. *Macromolecular Chemistry and Physics* **2020,** *221* (13), 2000053.
[45**]**. Pidhatika, B.; Zhao, N.; Zinggeler, M.; Rühe, J., Surface-attached dual-functional hydrogel for controlled cell adhesion based on poly (N, N-dimethylacrylamide). *Journal of Polymer Research* **2019,** *26* (3), 1-12.
[46**]**. Mircea Teodorescu; KrzysztofMatyjaszewski, Macromol. Rapid Commun_Controlled polymerization of DMAA by ATRP. *Macromol. Rapid Commun.* **2000,** *21* (4), 190-194.
[47**]**. Ding, S.; Radosz, M.; Shen, Y., Atom Transfer Radical Polymerization of N,N-Dimethylacrylamide. *Macromolecular Rapid Communications* **2004,** *25* (5), 632-636.
[48**]**. Alsubaie, F.; Anastasaki, A.; Wilson, P.; Haddleton, D. M., Sequence-controlled multi-block copolymerization of acrylamides via aqueous SET-LRP at 0 °C. *Polymer Chemistry* **2015,** *6* (3), 406-417.
[49**]**. Wu, Z.; Peng, C.-H.; Fu, X., Tacticity control approached by visible-light induced organocobalt-mediated radical polymerization: the synthesis of crystalline poly (N, N-dimethylacrylamide) with high isotacticity. *Polymer Chemistry* **2020,** *11* (27), 4387-4395.
[50**]**. Rademacher, J. T.; Baum, M.; Pallack, M. E.; Brittain*, W. J., Atom Transfer Radical Polymerization of N,N-Dimethylacrylamide. *Macromolecules* **2000,** *33*, 284-288.
[51**]**. Donovan, M. S.; Sanford, T. A.; Lowe, A. B.; Sumerlin, B. S.; Mitsukami, Y.; McCormick*, C. L., RAFT Polymerization of N,N-Dimethylacrylamide in Water. *Macromolecules* **2002,** *35*, 4570-4572.
[52**]**. Donovan, M. S.; Lowe, A. B.; Sumerlin, B. S.; McCormick*, C. L., Raft Polymerization of N,N-Dimethylacrylamide Utilizing Novel Chain Transfer Agents Tailored for High Reinitiation Efficiency and Structural Control. *Macromolecules* **2002,** *35*, 4123-4132.
[53**]**. De Bon, F.; Marenzi, S.; Isse, A. A.; Durante, C.; Gennaro, A., Electrochemically Mediated Aqueous Atom Transfer Radical Polymerization of N, N-Dimethylacrylamide. *ChemElectroChem* **2020,** *7* (6), 1378-1388.
[54**]**. Lutz, J.-F. o.; Neugebauer, D.; Matyjaszewski, K., Stereoblock Copolymers and Tacticity Control in Controlled/ Living Radical Polymerization. *J. AM. CHEM. SOC.* **2003,** *125*, 6986-6993.
[55**]**. Chmielarz, P.; Park, S.; Simakova, A.; Matyjaszewski, K., Electrochemically mediated ATRP of acrylamides in water. *Polymer* **2015,** *60*, 302-307.
[56**]**. Bard, A. J.; Faulkner, L. R., Fundamentals and Applications, New York: Wiley, 2001. Springer: 2002.
[57**]**. Bell, C. A.; Bernhardt, P. V.; Monteiro, M. J., A rapid electrochemical method for determining rate coefficients for copper-catalyzed polymerizations. *J Am Chem Soc* **2011,** *133* (31), 11944-7.
[58**]**. Tsarevsky, N. V.; Pintauer, T.; Matyjaszewski, K., Deactivation efficiency and degree of control over polymerization in ATRP in protic solvents. *Macromolecules* **2004,** *37* (26), 9768-9778.

[59**]**. Teodorescu, M.; Matyjaszewski, K., Atom transfer radical polymerization of (meth) acrylamides. *Macromolecules* **1999,** *32* (15), 4826-4831.
[60**]**. Herberg, A.; Yu, X.; Kuckling, D., End group stability of atom transfer radical polymerization (ATRP)-synthesized poly (N-isopropylacrylamide): Perspectives for diblock copolymer synthesis. *Polymers* **2019,** *11* (4), 678.
[61**]**. Herberg, A.; Yu, X.; Kuckling, D., End Group Stability of Atom Transfer Radical Polymerization (ATRP)-Synthesized Poly(N-isopropylacrylamide): Perspectives for Diblock Copolymer Synthesis. *Polymers* **2019,** *11* (4).

Chapter VIII

Use of common inorganic salts to suppress the effects of Al anodic dissolution in *se*ATRP

Abstract

As discussed in **Chapters IV-VII**, Al^{3+} ions generated by anodic dissolution of Al in simplified electrochemically-mediated atom transfer radical polymerization (*se*ATRP) with a sacrificial Al anode are engaged in competitive complexation equilibria with Cu^{2+} (and Cu^{+}) for amine ligands. This undesired competition has so far been suppressed by addiing excess of the costly ligand. The possibility of using inexpensive sodium salts to suppress the competitive equilibria triggered by the presence of Al^{3+} was explored as well. In aqueous media, addition of basic salts (Na_3PO_4, Na_2CO_3, $NaHCO_3$, and NaOH) not only could effectively suppress the competitive complexation equilibria involving Al^{3+} and copper ions with Me_6TREN, but also recovered the pH. In particular, addition of 3.0 mM Na_2CO_3 significantly enhanced the molecular weight distribution and the polymerization rate of OEOMA catalyzed by $[Cu^{II}Me_6TREN]^{2+}$ in water in an undivided cell with a sacrificial Al anode. The stability of copper complexes with Me_6TREN in organic solvents (DMF, DMSO, and MeCN) in the presence of Al^{3+} was also investigated and effectively improved by the addition of a small quantity of Na_2CO_3. However, it is important to mention that the amount of CO_3^{2-} must be strictly controlled with respect to Al^{3+} ions, otherwise, it can combine with $[Cu^{II}Me_6TREN]^{2+}$ to form a new more stable complex $[CO_3Cu^{II}Me_6TREN]$8 with a more negative redox potential.

Keywords: $[Cu^{II}Me_6TREN]^{2+}$, stability, aluminum ions, carbonate ions, *se*ATRP

8.1 Introduction

The environmentally benign and versatile *se*ATRP with a sacrificial Al anode in an undivided cell has attracted considerable attention in the preparation of various advanced polymer materials with controlled architecture.[1-8] A simplified cell setup with a Pt cathode and a sacrificial Al anode reduces process cost by partially removing the costly platinum electrode from the system and eliminating the cell separator. However, the Al^{3+} ions released from anodic dissolution of Al wire would decrease the stability of $[Cu^{II}Me_6TREN]^{2+}$ in both organic solvents and aqueous solutions, according to the literature and the results reported in **Chapters IV-VII** of this thesis.[3, 5, 8] Copper catalysts based on TPMA tolerate the presence of Al^{3+} in DMF, DMSO and water, but not in MeCN. As shown in **Chapters IV** and **V**, $[Cu^{I}TPMA]^{+}$ rapidly undergoes ligand exchange with Al^{3+} ions in MeCN. To eliminate the deleterious effect of Al^{3+} on copper catalysts, excess ligand over $[Cu^{II}L]^{2+}$ has been used.[3, 5, 8] Nonetheless, addition of excess ligand will result in an economic burden, further limiting the industrial scale-up production. It is therefore necessary to look for other novel approaches not involving costly reagents.

Zhu's group reported a significant dual enhancement of polymerization rate and controllability over molecular weight of poly methyl methacrylate (PMMA) or poly styrene (PS) via iron-mediated AGET ATRP after addition of small amounts of inorganic bases (i.e., NaOH, Na_3PO_4, $NaHCO_3$, and Na_2CO_3).[9-11] Moreover, the effect of the amount of $NaHCO_3$ and Na_2CO_3 on AGET ATRP of MMA with iron complex as catalysts and vitamin C as reducing agent were further investigated.[12-13] The polymerization rate was enhanced significantly in the presence of tiny amounts of a base and water. The introduction of a tiny amount of water not only is helpful to dissolve these two sodium salts, but also has a positive effect on polymerization equilibrium, as reported in several papers.[12, 14-16] Furthermore, Na_2CO_3 can efficiently decrease the redox potential of the catalyst.[12, 17] Despite these advantages on iron-catalyzed AGET ATRP, a long induction period (~9 h) was observed in the AGET

ATRP of methyl acrylate (MA) catalyzed by $CuBr_2$/bpy in DMF when ethylene glycol (EG) was used as a reducing agent in the presence of small quantity of Na_2CO_3.[17] This was attributed to the low reduction rate of $CuBr_2$/bpy catalyst in the presence of ethylene glycol (EG) and low solubility of Na_2CO_3 in DMF. Buffagni et al. reported an ARGET ATRP of styrene with various carbonate salts as reducing agents, both alone and paired with ascorbic acid (AA) in a green solvent mixture of EtOAc/EtOH.[18-19] In addition, the introduction of a small quantity of H_2O accelerated the activation of the catalyst and increased the solubility of Na_2CO_3. Matyjaszewski's group deeply explored the catalytic mechanism of Na_2CO_3 and obtained rapid sono-ATRP of MA in DMSO (80% conversion in < 2 h) with excellent control of molecular weights and low dispersity ($Đ$ < 1.2).[20] Superfine Na_2CO_3 particles were gained through an ultra-sonication process, which also indirectly improved the solubility of Na_2CO_3. Ultrasound was used to convert the in situ formed $[CO_3Cu^{II}TPMA]$ complex into $[Cu^{I}TPMA]^+$ activator and a carbonate radical anion. The latter was scavenged by DMSO which was oxidized to dimethyl sulfone. Inspired by these outcomes, various sodium salts were investigated in *se*ATRP.

Therefore, in this Chapter, experiments with 14 different sodium salts were designed and conducted to recover the voltammetric pattern of $[Cu^{II}Me_6TREN]^{2+}$ and pH in water in the presence of Al^{3+}. Moreover, *se*ATRP of OEOMA with $[Cu^{II}Me_6TREN]^{2+}$ catalyst was carried out in the presence of different amounts of Na_2CO_3. In particular, the effects of Na_2CO_3 on $[Cu^{II}Me_6TREN]^{2+}$ in organic media (DMF, DMSO, and MeCN) in the presence of Al^{3+} ions were also explored via voltammetric methods. A small quantity of a concentrated Na_2CO_3 aqueous solution (2.0 M or 4.0 M) was added to the organic solution under investigation.

8.2 Methodologies and procedures

8.2.1 Typical CV measurements of $[Cu^{II}Me_6TREN]^{2+}$ in the presence of Al^{3+}

Solutions of $[Cu^{II}Me_6TREN]^{2+}$ in water + 0.1 M Et_4NBF_4 were always prepared

in situ starting from 1 mM $Cu(OTf)_2$, followed by addition of Me_6TREN ($[Cu^{II}]$:[Me_6TREN] = 1:1.05). The desired quantity of Al^{3+} ions was then injected using a 30.16 mM $Al(BF_4)_3$ stock solution, which was prepared by anodic dissolution of an Al wire in H_2O + 0.1 M Et_4NBF_4 and the quantity (n mol) of electrogenerated Al^{3+} ions was calculated from the consumed charge, Q, according to $Q = 3nF$.[21] The effect of Al^{3+} on the voltammetric pattern of the complexes was investigated by addition of increasing amounts of Al^{3+}. Fourteen sodium salts were investigated to explore the possibility of mitigating or suppressing the effect of Al^{3+} on the stability of copper complexes with Me_6TREN. After each addition of either Al^{3+} or a sodium salt, a freshly polished GC electrode was used to record cyclic voltammetry. Therefore, the reproducibility of the results was less affected. At the end of each experiment in organic media, the potential of the reference electrode (Ag/AgI/0.1 M *n*-Bu_4NI in DMF) was calibrated against the ferrocenium/ferrocene couple (Fc^+/Fc).

8.2.2 Typical linear sweep voltammetry (LSV) pattern measurements

Solutions of $[Cu^{II}Me_6TREN]^{2+}$ in organic solvents + 0.1 M Et_4NBF_4 in a tightly sealed cell were always prepared by addition of 0.5 mM $Cu(OTf)_2$, followed by adding Me_6TREN ($[Cu^{II}]$:[Me_6TREN] = 1:1.05). Al^{3+} ions were introduced by injecting a small volume of stock Al^{3+} solution. The effect of Al^{3+} on the voltammetric pattern of the complexes was investigated by addition of increasing amounts of Al^{3+}. And then different amounts of Na_2CO_3 were added to restore the initial $[Cu^{II}Me_6TREN]^{2+}$ pattern. At the end of each experiment, the potential of the reference electrode (Ag/AgI/0.1 M *n*-Bu_4NI in DMF) was calibrated against the ferrocenium/ferrocene couple (Fc^+/Fc).

8.2.3 Potentiostatic *e*ATRP of oigo(ethyleneoxide) methyl ether methacrylate (OEOMA)

Electrochemically mediated polymerizations of OEOMA in aqueous solutions were performed in an undivided cell by controlled-potential electrolysis. A typical setup of an *e*ATRP experiment was as follows. Et_4NBr (0.6435 g, 3.0 mmol), double distilled

water (26.4 mL), OEOMA (3.0 mL, 6.48 mmol), 0.6 mL of DMF used as an internal standard for NMR analysis, $Cu(OTf)_2$ (11.07 mg, 0.03 mmol), Me_6TREN (8.7 μL, 0.03 mmol), and the desired amount of a 2 M Na_2CO_3 (0, 7.5, 15, or 45 μL) were progressively added to a seven-neck electrochemical cell maintained at 25 ˚C and under Ar flux. After purging the solution with the inert gas for ca. 20 min, a CV of the copper complex was recorded on a GC disk electrode. Then 2-hydroxyethyl 2-bromoisobutyrate (HEBiB) (9.2 μL, 0.06 mmol) was injected into the solution and a CV was recorded to verify the catalytic reaction. Then the Pt mesh working electrode and the Al counter electrode, which were previously activated and positioned in the cell, were connected and the chosen potential was applied. Samples were withdrawn periodically to determine the monomer conversion by ^1H NMR, and the number average molecular weight (M_n) and molecular weight distribution (Đ) by gel permeation chromatography (GPC).

8.3 Results and discussion

8.3.1 CV measurements of $[Cu^{II}Me_6TREN]^{2+}$ in the presence of Al^{3+} and different sodium salts in water

As discussed in **Chapters IV-VII**, copper complexes with TPMA are stable in DMF, DMSO, and water even in the presence of a high concentration of Al^{3+} ions. Conversely, copper complexes with Me_6TREN are not stable in all investigated solvents. Therefore, in this last part of the work, we focused on evaluating the voltammetric behavior of $[Cu^{II}Me_6TREN]^{2+}$ in the presence of Al^{3+} ions and various inorganic salts. $[Cu^{II}Me_6TREN]^{2+}$ complex was prepared in situ by mixing equimolar amounts of $Cu(OTf)_2$ and Me_6TREN. **Figure 8.1** shows typical CVs of $[Cu^{II}Me_6TREN]^{2+}$ before and after addition of Al^{3+} ions, and after further progressive addition of NaBr, Na_2HPO_4, and Na_2CO_3. Reported in the figure are also the pH values measured after each addition step.

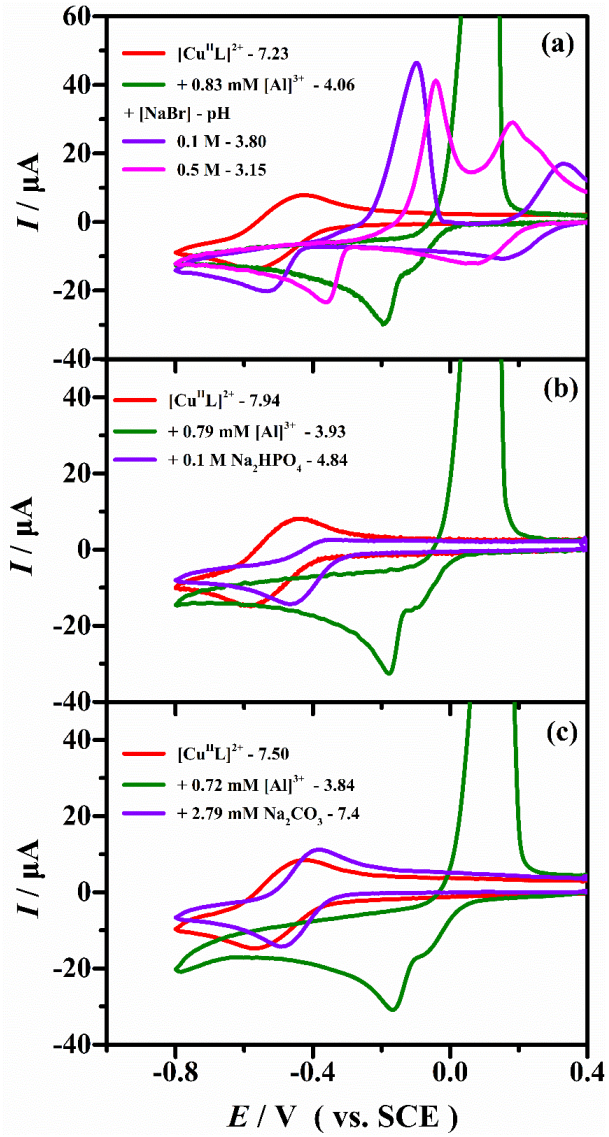

Figure 8.1 Typical CV curves of 1 mM $[Cu^{II}Me_6TREN]^{2+}$ in the absence and presence of Al^{3+} ions added from a stock solution, and after further addition of **(a)** NaBr, **(b)** Na_2HPO_4, or **(c)** Na_2CO_3, recorded at 0.2 Vs^{-1} in H_2O + 0.1 M Et_4NBF_4, T = 25 °C. The concentrations of the added sodium salts and the measured pH values are reported in the legends.

A quasi-reversible redox reaction takes place for the $[Cu^{II}L]^{2+}/[Cu^{I}L]^{+}$ couple. After the addition of a certain amount of Al^{3+} ions from a stock solution, the pH shifted from ~7.5 to ~3.9 and the quasi-reversible peak couple of $[Cu^{II}L]^{2+}/[Cu^{I}L]^{+}$ disappeared. $[Cu^{II}Me_6TREN]^{2+}$ was fully dissociated with release of free solvated Cu^{2+} ions. Consequently, two ill-separated cathodic peaks followed by a huge anodic stripping

peak in the reverse scan were observed. These are attributed to a two consecutive one-electron reduction steps of Cu^{2+} to electrodeposited Cu^0 and a two-electron anodic stripping of Cu^0 to Cu^{2+}. This behavior was already observed for $[Cu^{II}Me_6TREN]^{2+}$ in H_2O + 10% (v/v) OEOMA + 0.1 M Et_4NBr after addition of Al^{3+} ions or $AlCl_3$ (**Figure 7.6**). After the addition of a certain quantity of a sodium salt, three different results were generally obtained: i) only pH recovery, ii) both pH and voltammetric pattern were restored, and iii) neither the pH nor the voltammetric pattern was recovered. The various tested sodium salts and the obtained results are listed in **Table 8.1**. Moreover, three representative examples (NaBr, Na_2HPO_4, and Na_2CO_3) are illustrated in **Figure 8.1.**

Table 8.1 pH and CV recovery results of $[Cu^{II}Me_6TREN]^{2+}$ in the presence of Al^{3+} by the addition of various sodium salts.[a]

Entry	Sodium salts	pH	CV	Both pH and CV
1	Na_3PO_4	✔	✔	✔
2	Na_2HPO_4	✔	✘	✘
3	NaH_2PO_4	✘	✘	✘
4	Na_2CO_3	✔	✔	✔
5	$NaHCO_3$	✔	✔	✔
6	NaF	✔	✘	✘
7	NaCl	✘	✘	✘
8	NaBr	✘	✘	✘
9	NaI	✘	✘	✘
10	NaOH	✔	✔	✔
11	$NaNO_3$	✘	✘	✘
12	Na_2SO_4	✘	✘	✘
13	$NaClO_4$	✘	✘	✘
14	CH_3COONa	✔	✘	✘

[a] ✔ indicates recovery, ✘ indicates no recovery.

Addition of PO_4^{3-}, CO_3^{2-}, HCO_3^- and OH^- ions could recover not only the pH but also the voltammetric pattern of $[Cu^{II}Me_6TREN]^{2+}$, as the example of CO_3^{2-} presented in **Figure 8.1 c** illustrates. Due to the lower basicity of HCO_3^- than CO_3^{2-}, a large amount of HCO_3^- had to be added to restore the pH and voltametric pattern of $[Cu^{II}Me_6TREN]^{2+}$ solution. F^-, HPO_4^{2-}, and CH_3COO^- ions could recover the pH but not the CV pattern of $[Cu^{II}Me_6TREN]^{2+}$. When increasing amounts of these anions were added to the solution, the cathodic peak of $[Cu^{II}Me_6TREN]^{2+}$ was gradually restored, while the anodic peak did not appear, as the representative case with HPO_4^{2-} shows in **Figure 8.1 b**. Neither the voltammetric pattern of $[Cu^{II}Me_6TREN]^{2+}$ nor the pH was restored by adding $H_2PO_4^-$, NO_3^-, SO_4^{2-}, ClO_4^-, and halide ions (Cl^-, Br^-, I^-), as in the case of Br^- shown in **Figure 8.1 a**.

8.3.2 Potentiostatic *e*ATRP of OEOMA in an undivided cell with Al anode

To verify the positive effects of addition of anions on polymerization with a sacrificial anode, *se*ATRP experiments on OEOMA in an undivided cell were performed in the presence of CO_3^{2-}. For comparison, a blank experiment without added Na_2CO_3 was first carried out. Then, the same experiment was repeated with increasing amounts of Na_2CO_3 from 0 to 3.0 mM. The results of *se*ATRP experiments are summarized in **Table 8.2**, whereas monomer conversion and first-order kinetic plots are shown in **Figure 8.2**.

When the polymerization was performed in the absence of Na_2CO_3 (**Table 8.2 entry 1**), the previously reported results (**Table 7.3, entry 5)** were confirmed. The reaction was quite slow and the dispersity of the obtained polymer was high. Addition of Na_2CO_3 significantly improved the performance of the process. Both the apparent propagation rate constant (k_p^{app}) and conversion increased with increasing Na_2CO_3 concentration, while the polymer dispersity decreased. This improvement on polymerization control could also be observed by the GPC traces shown in **Figure 8.3**. The monomer conversion, molecular weights, the polymer dispersity and polymerization rate were obviously improved in the presence of Na_2CO_3, which is well

consistent with literature reports on other ATRP methods.[9-13, 17-20, 22]

Table 8.2 Potentiostatic *se*ATRP of 10% (v/v) OEOMA in H_2O with $[Cu^{II}Me_6TREN]^{2+}$.[a]

Entry	$[Na_2CO_3]$ (mM)	t (h)	Conv.[b] (%)	Q (C)	10^{-3} $M_{n,th}$ [c]	10^{-3} M_n [d]	k_p^{app} [e] (h^{-1})	$Đ$ [d]	$[Al^{3+}]_{th}$ [f]
1	0.0	4	53	1.5	26.3	55.0	0.19	1.65	0.17
2	0.5	4	74	2.3	39.5	89.7	0.33	1.53	0.26
3	1.0	3	>99	4.5	53.4	115.9	1.28	1.41	0.52
4	3.0	4	>99	5.4	53.3	154.3	0.54	1.38	0.62

[a]Polymerization conditions: [OEOMA]:[HEBiB]:[$Cu(OTf)_2$]:[Me_6TREN] = 107.5:1.0:0.5:0.5, with initial [$Cu(OTf)_2$] = 1.0 mM; [Et_4NBr] = 0.1 M; *se*ATRP under constant potential conditions (WE = Pt mesh with surface area ~ 6 cm^2, CE = Al, RE = SCE), $E_{app} = E_{1/2} + 0.12$, V_{tot} = 30 mL, T = 25 °C. [b]Determined by ^1H NMR. [c]Calculated on the basis of conversion obtained by ^1H NMR (i.e. $M_{n,th} = M_{HEBiB} + 107.5 \times \text{conversion} \times M_{OEOMA}$). [d]Determined by GPC. [e]Slope of the linear plot of ln ($[M]_0/[M]$) vs. time. [f]$[Al^{3+}]_{th}$ (mM) = $Q/(3 \cdot F \cdot V)$, where F is the Faraday constant, 96485.332 C/mol, V = 30 mL.

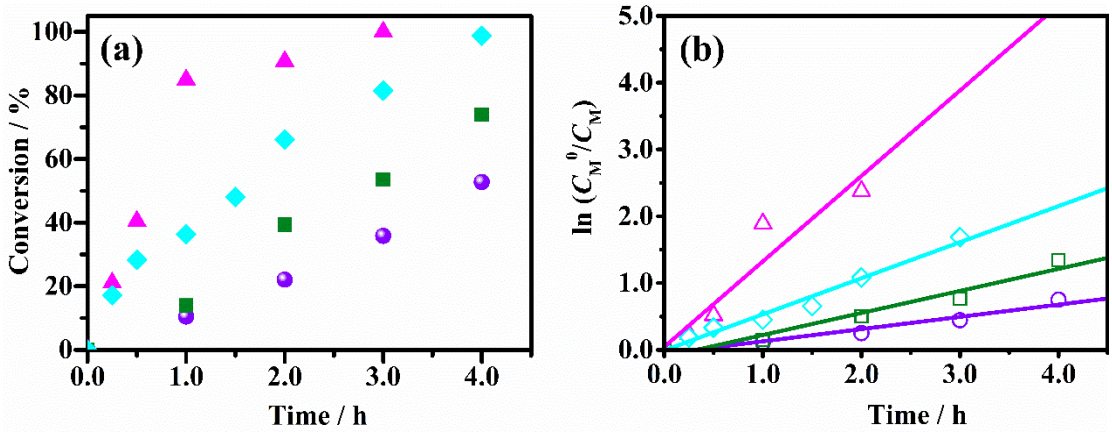

Figure 8.2 (a) Monomer conversion and **(b)** kinetic plots as a function of time for *e*ATRP of 10 vol% OEOMA in H_2O + 0.1 M Et_4NBr, performed at $E_{app} = E_{1/2} + 0.12$V on a Pt cathode at 25 °C in an undivided cell with a sacrificial anode Al. Other conditions: [OEOMA]:[HEBiB]:[$Cu(OTf)_2$]:[Me_6TREN]:[Na_2CO_3] = 215:2:1:1:x, with x = 0 (●), 0.5 (■), 1.0 (▲), and 3.0 (♦) and [$Cu(OTf)_2$] = 1 mM.

During *se*ATRP experiments performed in the presence of Na_2CO_3, the Al^{3+} ions

released from the anode combine with carbonate ions to form colloidal particles in solution and on the Al surface. As shown in **Figure 8.3 b**, white colloidal particles could be observed in solution after polymerization. When the solution was left to stand for several minutes without shaking, a clear white precipitate could be observed. When the *se*ATRP is triggered in the presence of Na_2CO_3, the Al^{3+} ions generated at the anode are immediately quenched by CO_3^{2-} to form insoluble $Al_2(CO_3)_3$. This preserves solution pH and hence catalyst stability. Indeed, at the end of polymerization, the solution had the bright blue color, typical of $[Cu^{II}L]^{2+}$ (**Figure 8.3 b**).

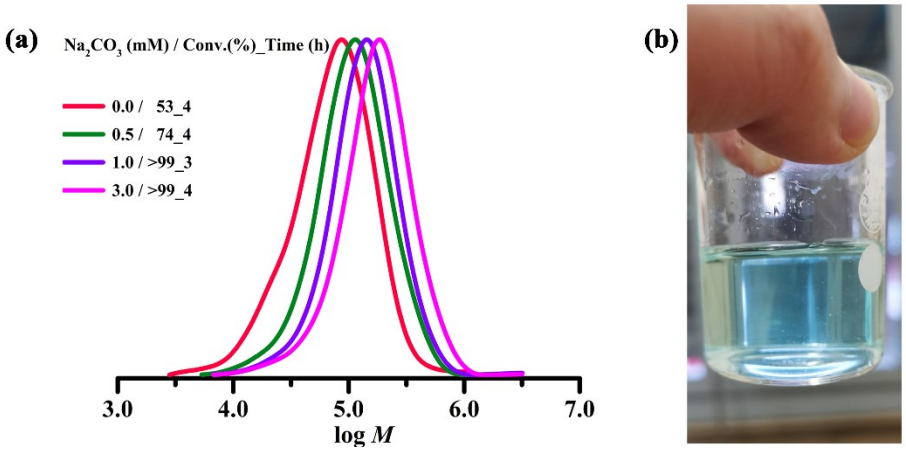

Figure 8.3 (a) Representative GPC traces of POEOMA prepared by Cu-catalyzed *e*ATRP in an undivided cell with a sacrificial anode Al. Polymerization conditions: [OEOMA]:[HEBiB]:[$Cu(OTf)_2$]:[Me_6TREN]:[Na_2CO_3] = 215:2:1:1:x (x = 0, 0.5, 1.0, and 3.0), with initial $[Cu^{II}] = 10^{-3}$ M; $C_{Et_4NBr} = 0.1$ M; $V_{tot} = 30$ mL; $T = 25$ °C; $E_{app} = E_{1/2} + 0.12$ V. **(b)** The digital image of the mixture after polymerization when x = 3.0.

8.3.3 CV measurements of $[Cu^{II}Me_6TREN]^{2+}$ in the presence of Al^{3+} and Na_2CO_3 in organic media

The voltammetric behavior of $[Cu^{II}Me_6TREN]^{2+}$ was also investigated in organic solvents, such as DMF, DMSO, and MeCN, with the progressive addition of Al^{3+} and Na_2CO_3. **Figure 8.4 a, c, and e** shows CVs of $Cu(OTf)_2$ in organic solvents before and after addition of the amine ligand, and after further progressive addition of Al^{3+} ions. A remarkable negative shift of the redox peak couple of Cu^{II}/Cu^{I} was observed after

addition of an equimolar amount of Me_6TREN in each solvent; rapid reaction of the ligand with Cu^{2+} produced $[Cu^{II}Me_6TREN]^{2+}$, which exhibited its typical voltammetric pattern. When subsequently Al^{3+} ions were added, the competition between Al^{3+} and Cu^{2+} shifted the ligand from Cu^{2+} to Al^{3+} via a ligand exchange equilibrium (**eq. 4-6**). Consequently, the reversible peak couple for $[Cu^{II}L]^{2+}/[Cu^{I}L]^{+}$ gradually decayed in current intensity until disappearance, while the peak couple for solvated Cu^{2+} ions appeared and increased in height. These findings agree well with the results reported in Chapter IV (**Figure 4.5 b, d, and f**).

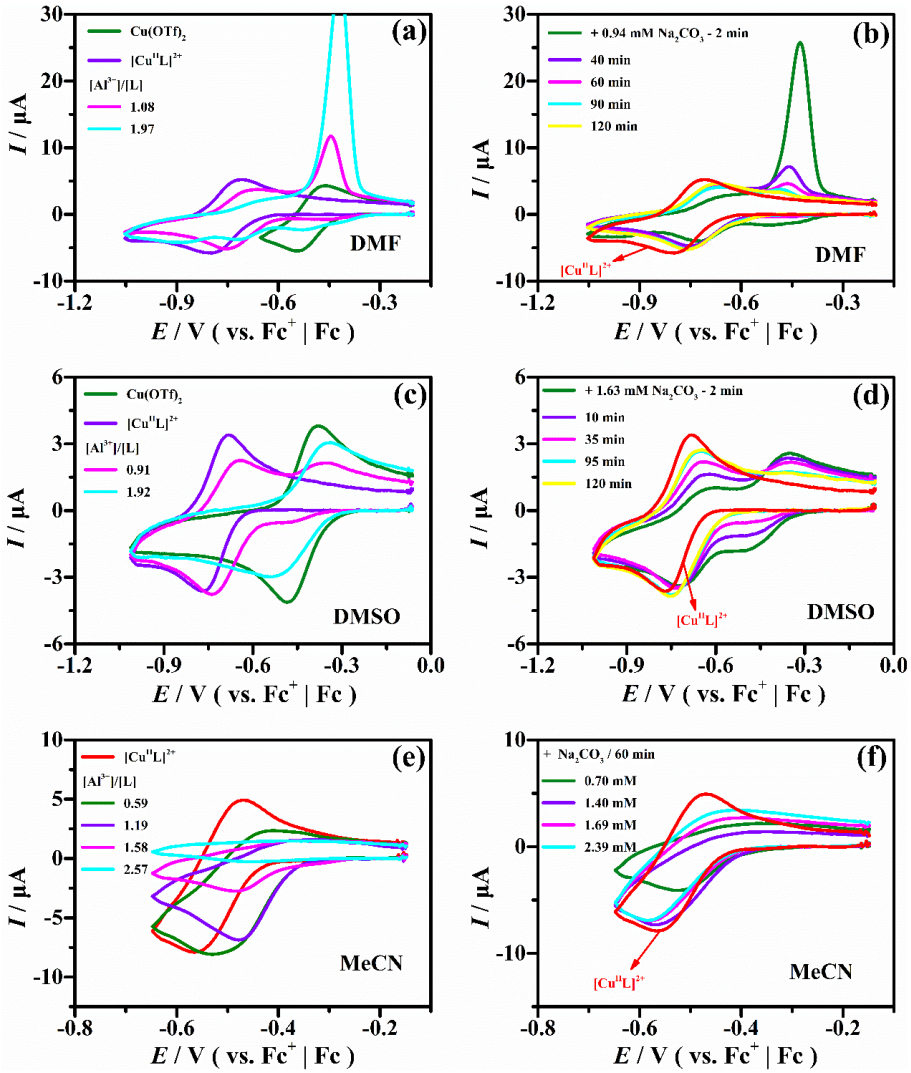

Figure 8.4 CVs of 0.5 mM $Cu(OTf)_2$ and 0.5 mM $[Cu^{II}L]^{2+}$ before and after stepwise addition of Al^{3+} and Na_2CO_3 solutions, recorded at $\upsilon = 0.2$ V s^{-1} on a GC disk in DMF (a, b), DMSO (c, d) and MeCN (e, f), with 0.1 M Et_4NBF_4 as the supporting electrolyte,

T = 25 °C.

Due to the poor solubility of solid Na_2CO_3 in organic solvents, Na_2CO_3 was added from a concentrated stock solution of the salt in water. Despite this expedient, a white Na_2CO_3 precipitate immediately formed after injection. However, the solid was dispersed in the solution as tiny particles which slowly dissolved and reacted with Al^{3+}, thus shifting the ligand exchange equilibrium back to $[Cu^{II}Me_6TREN]^{2+}$. Therefore, the voltammetric pattern of $[Cu^{II}Me_6TREN]^{2+}$ slowly recovered nearly to the initial state, as shown in **Figure 8.4 b, d, and f**. This effect was stronger in DMF and DMSO than in MeCN. Indeed, not only the recovery period was shorter but also the required quantity of Na_2CO_3 was lower in DMF and DMSO than in MeCN. This difference of behavior likely arises from Na_2CO_3 solubility differences in the three solvents.

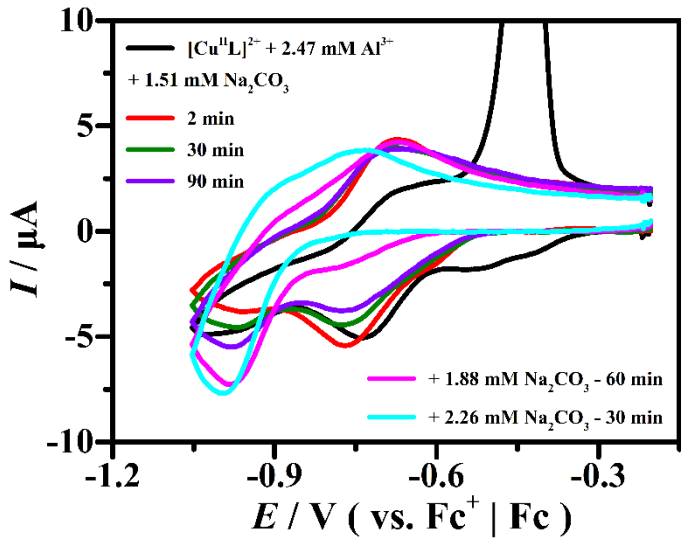

Figure 8.5 CVs of 0.5 mM $[Cu^{II}Me_6TREN]^{2+}$ + 2.47 mM Al^{3+} ions before and after addition of different amounts of Na_2CO_3, recorded at υ = 0.2 V s^{-1} on a GC disk in DMF + 0.1 M Et_4NBF_4 as the supporting electrolyte, T = 25 °C.

It is important to mention that carbonate ions can combine with $[Cu^{II}Me_6TREN]^{2+}$ as a ligand. **Figure 8.5** shows CVs of $[Cu^{II}Me_6TREN]^{2+}$ + Al^{3+}, recorded after addition of different amounts of Na_2CO_3. When 1.51 mM Na_2CO_3 was added the quasi-reversible peak couple of $[Cu^{II}L]^{2+}/[Cu^{I}L]^{+}$ was initially recovered but after few minutes the cathodic peak was split into two cathodic peaks at ca -0.77 V and -0.98 V,

while the anodic peak remained unchanged. It can be assumed that the less negative cathodic peak and the anodic peak are for the redox reaction of the $[Cu^{II}Me_6TREN]^{2+}/[Cu^{I}Me_6TREN]^{+}$ couple. The more negative cathodic peak can be assigned to a new Cu(II) complex between CO_3^{2-} and $[Cu^{II}Me_6TREN]^{2+}$. The quantity of this new complex in solution increases at the detriment of $[Cu^{II}Me_6TREN]^{2+}$ as the amount of added Na_2CO_3 is increased. This agrees very well with the outcomes obtained in DMSO with $Cu(OTf)_2$/TPMA reported by Matyjaszewski *et al.*[20] Therefore, the quantity of Na_2CO_3 must be strictly controlled with respect to the Al^{3+}, especially during polymerization.

To further confirm that addition of Na_2CO_3 effectively recovers $[Cu^{II}Me_6TREN]^{2+}$ after dissociation caused by the presence of Al^{3+} ions, one more experiment was carried out in DMF. A solution of 0.5 mM $[Cu^{II}Me_6TREN]^{2+}$ was prepared and variations of the complex concentration were monitored by chronoamperometry (CA) under steady state conditions. Cyclic voltammetry and linear sweep voltammetry at a RDE of the starting $[Cu^{II}Me_6TREN]^{2+}$ solution in DMF + 0.1 M Et_4NBF_4 are reported in **Figure 8.6 a** and **b**. They show a quasi-reversible peak couple and a well-defined cathodic wave. The figure shows also CV and LSV of $Cu(OTf)_2$. Solvated free Cu^{2+} ions undergo two consecutive one-electrode reduction processes leading to electrodeposition of metallic copper on the GC surface.

A CA experiment was performed for $[Cu^{II}Me_6TREN]^{2+}$, with a potential step from -0.3 V, where no reduction process occurs at the electrode, to a value (-0.93 V) in the plateau region where the electrode process has the maximum reduction rate, producing a limiting current (I_L). After remaining in this state for ca 840s, a solution of Al^{3+} ions was injected. This caused a steep increase of I_L to a constant value within 334 s (**Figure 8.6 c**). This is due to the two-electron reduction of free solvated Cu^{2+} arising from decomposition of $[Cu^{II}Me_6TREN]^{2+}$ in the presence of a 3-fold excess of Al^{3+} with respect to the copper complex. Subsquently, the current decreased instantaneously by about 50% in ca 1 min when 5.5 µL of a Na_2CO_3 solution (4 M) was injected. After this injection, the current increased slowly due to the gradual dissolution of Na_2CO_3, but when another 5.5 µL were added, I_L rapidly increased nearly to the initial value in less

than 30 s, indicating almost full recovery of $[Cu^{II}Me_6TREN]^{2+}$. A further slow decrease of the current, which at the end reached a limiting current roughly equal to the initial I_L value, was observed. CV and LSV recorded at the end of the experiment showed the presence of a new reduction wave attributable to $[CO_3Cu^{II}Me_6TREN]^{+}$ formed in the presence of excess CO_3^{2-}. Furthermore, loss and recovery of $[Cu^{II}Me_6TREN]^{2+}$ were confirmed by changes of solution color from light green of the starting solution to colorless and finally to light yellow, as the inserts of **Figure 8.6 c** show.

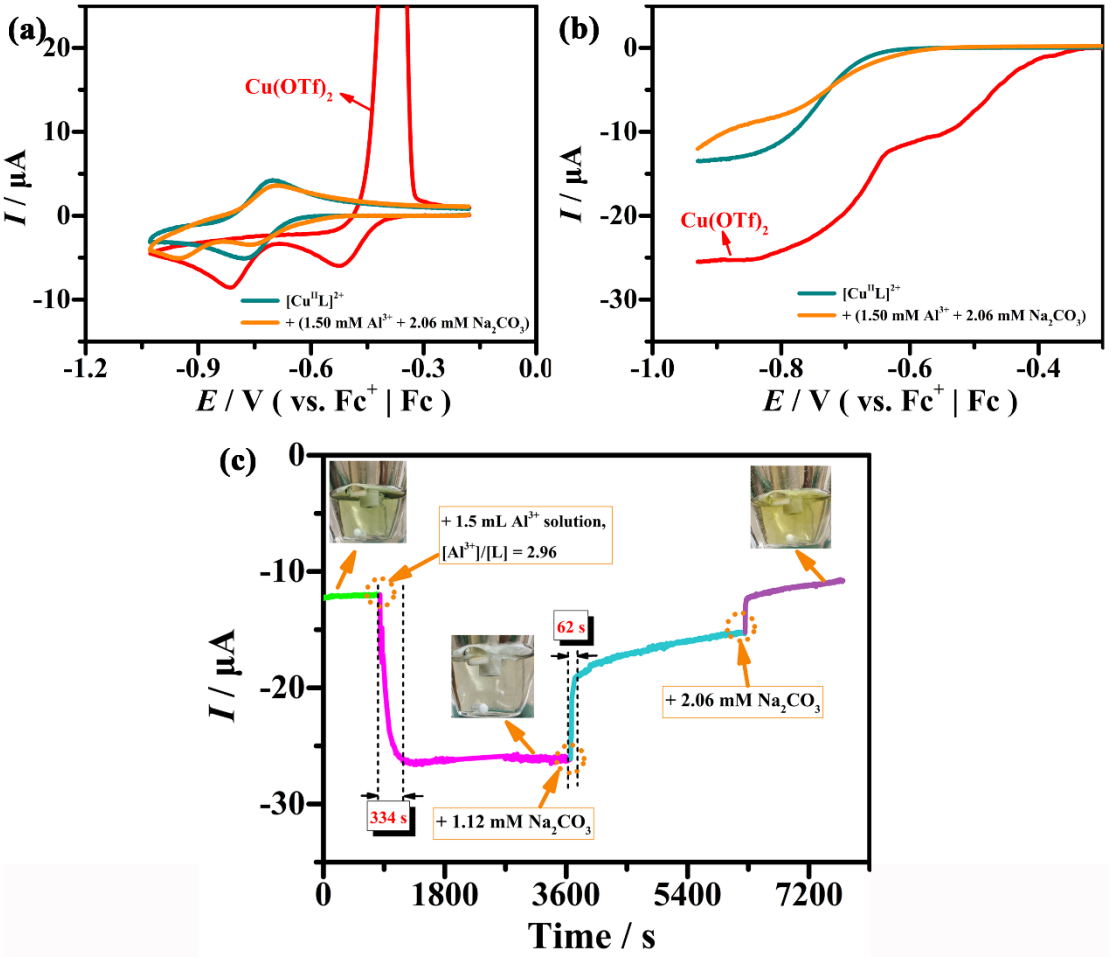

Figure 8.6 (a) CVs and (b) LSVs of 0.5 mM $Cu(OTf)_2$ before and after addition of equimolar Me_6TREN, 1.5 mL of 21.5 mM Al^{3+} ions and two consecutive additions of 5.5 µL of 4.0 M Na_2CO_3, recorded in DMF + 0.1 M Et_4NBF_4 at $\upsilon = 0.2$ Vs^{-1} on a GC disk, υ = 0.005 V s^{-1} and ω = 2500 rpm on a rotating disc electrode. (c) Chronoamperometry of 0.5 mM $[Cu^{II}Me_6TREN]^{2+}$ in DMF + 0.1 M Et_4NBF_4 at a rotating disc electrode at $\upsilon = 0.005$ V s^{-1} and ω = 2500 rpm before and after addition of Al^{3+} ions, followed by Na_2CO_3. $T = 25$ °C.

8.4 Conclusions

In order to find an economical approach to suppress the competition between Al^{3+} and Cu^{2+} for Me_6TREN, the last part of my PhD thesis focused on the investigation of the stability of copper complexes with Me_6TREN in the presence of Al^{3+} ions and common sodium salts containing different anions. Interesting results were obtained with Na_2CO_3. In comparison with the costly ligand, Na_2CO_3 is an inexpensive additive that can effectively safeguard the stability of $[Cu^{II}Me_6TREN]^{2+}$ in both organic (DMF, DMSO, and MeCN) and aqueous media containing Al^{3+}; it acts also as a buffer in aqueous media, restoring the initial pH of the system. In addition, the *e*ATRP of OEOMA in water was significantly improved by the addition of 3 mM Na_2CO_3. However, the carbonate ions can further react with copper complexes to form a more stable complex if a large excess of the salt is used. Therefore, the amount of Na_2CO_3 must be strictly controlled to guarantee enough copper catalyst species for the *e*ATRP equilibrium.

References

[1]. Park, S.; Chmielarz, P.; Gennaro, A.; Matyjaszewski, K., Simplified electrochemically mediated atom transfer radical polymerization using a sacrificial anode. *Angew Chem Int Ed Engl* **2015,** *54* (8), 2388-92.
[2]. Fantin, M.; Lorandi, F.; Isse, A. A.; Gennaro, A., Sustainable Electrochemically-Mediated Atom Transfer Radical Polymerization with Inexpensive Non-Platinum Electrodes. *Macromol Rapid Commun* **2016,** *37* (16), 1318-22.
[3]. Lorandi, F.; Fantin, M.; Isse, A. A.; Gennaro, A., Electrochemically mediated atom transfer radical polymerization of n-butyl acrylate on non-platinum cathodes. *Polymer Chemistry* **2016,** *7* (34), 5357-5365.
[4]. Matyjaszewski, K., Advanced Materials by Atom Transfer Radical Polymerization. *Adv Mater* **2018,** *30* (23), e1706441.
[5]. De Bon, F.; Isse, A. A.; Gennaro, A., Towards scale-up of electrochemically-mediated atom transfer radical polymerization: Use of a stainless-steel reactor as both cathode and reaction vessel. *Electrochimica Acta* **2019,** *304*, 505-512.
[6]. Zaborniak, I.; Chmielarz, P., Miniemulsion switchable electrolysis under constant current conditions. *Polymers for Advanced Technologies* **2020,** *31* (11), 2806-2815.
[7]. Zaborniak, I.; Chmielarz, P.; Martinez, M. R.; Wolski, K.; Wang, Z.; Matyjaszewski, K., Synthesis of high molecular weight poly(n-butyl acrylate) macromolecules via *se*ATRP: From polymer stars to molecular bottlebrushes. *European Polymer Journal* **2020,** *126*, 109566.
[8]. Luo, J.; Durante, C.; Gennaro, A.; Isse, A. A., Electrochemical study of the effect of Al^{3+} on the stability and performance of Cu-based ATRP catalysts in organic media. *Electrochimica Acta* **2021,** *388*, 138589.
[9]. Bai, L.; Zhang, L.; Zhang, Z.; Zhu, J.; Zhou, N.; Cheng, Z.; Zhu, X., Rate-enhanced ATRP in the presence of catalytic amounts of base: An example of iron-mediated AGET ATRP of MMA. *Journal of Polymer Science Part A: Polymer Chemistry* **2011,** *49* (18), 3980-3987.
[10]. Bai, L.; Zhang, L.; Zhang, Z.; Tu, Y.; Zhou, N.; Cheng, Z.; Zhu, X., Iron-mediated AGET ATRP of styrene in the presence of catalytic amounts of base. *Macromolecules* **2010,** *43* (22), 9283-9290.
[11]. Guo, T.; Zhang, L.; Jiang, H.; Zhang, Z.; Zhu, J.; Cheng, Z.; Zhu, X., Catalytic amounts of sodium hydroxide as additives for iron-mediated AGET ATRP of MMA. *Polymer Chemistry* **2011,** *2* (10), 2385-2390.
[12]. He, W.; Zhang, L.; Bai, L.; Zhang, Z.; Zhu, J.; Cheng, Z.; Zhu, X., Iron-mediated AGET ATRP of Methyl Methacrylate in the Presence of Catalytic Amounts of Base. *Macromolecular Chemistry and Physics* **2011,** *212* (14), 1474-1480.
[13]. Wang, G.-X.; Lu, M.; Hou, Z.-H.; Wu, H., Homogeneous Fe-Mediated AGET ATRP of Methyl Methacrylate in PEG-400 in the Presence of Na_2CO_3. *Journal of Macromolecular Science, Part A* **2015,** *52* (3), 186-192.
[14]. Pavan, P.; Lorandi, F.; De Bon, F.; Gennaro, A.; Isse, A. A., Enhancement of the

Rate of Atom Transfer Radical Polymerization in Organic Solvents by Addition of Water: An Electrochemical Study. *ChemElectroChem* **2021,** *8* (13), 2450-2458.
[15**]**. Fantin, M.; Isse, A. A.; Matyjaszewski, K.; Gennaro, A., ATRP in Water: Kinetic Analysis of Active and Super-Active Catalysts for Enhanced Polymerization Control. *Macromolecules* **2017,** *50* (7), 2696-2705.
[16**]**. Wang, Z.; Wang, Z.; Pan, X.; Fu, L.; Lathwal, S.; Olszewski, M.; Yan, J.; Enciso, A. E.; Wang, Z.; Xia, H., Ultrasonication-induced aqueous atom transfer radical polymerization. *ACS Macro Letters* **2018,** *7* (3), 275-280.
[17**]**. Wang, Y.; Li, X.; Du, F.; Yu, H.; Jin, B.; Bai, R., Use of alcohols as reducing agents for synthesis of well-defined polymers by AGET-ATRP. *Chemical Communications* **2012,** *48* (22), 2800-2802.
[18**]**. Borsari, M.; Braidi, N.; Buffagni, M.; Ghelfi, F.; Parenti, F.; Porcelli, N.; Serafini, G.; Isse, A. A.; Bonifaci, L.; Cavalca, G., Copper-catalyzed ARGET ATRP of styrene from ethyl α-haloisobutyrate in EtOAc/EtOH, using ascorbic acid/Na_2CO_3 as reducing system. *European Polymer Journal* **2021**, 110675.
[19**]**. Braidi, N.; Buffagni, M.; Ghelfi, F.; Parenti, F.; Gennaro, A.; Isse, A. A.; Bedogni, E.; Bonifaci, L.; Cavalca, G.; Ferrando, A., ARGET ATRP of styrene in EtOAc/EtOH using only Na_2CO_3 to promote the copper catalyst regeneration. *Journal of Macromolecular Science, Part A* **2021,** *58* (6), 376-386.
[20**]**. Wang, Z.; Lorandi, F.; Fantin, M.; Wang, Z.; Yan, J.; Wang, Z.; Xia, H.; Matyjaszewski, K., Atom transfer radical polymerization enabled by sonochemically labile Cu-carbonate species. *ACS Macro Letters* **2019,** *8* (2), 161-165.
[21**]**. Isse, A. A.; Scialdone, O.; Galia, A.; Gennaro, A., The influence of aluminium cations on electrocarboxylation processes in undivided cells with Al sacrificial anodes. *Journal of Electroanalytical Chemistry* **2005,** *585* (2), 220-229.
[22**]**. Bruns, N.; Renggli, K.; Seidi, F.; Kali, G., Atom transfer radical polymerization with protein-conjugated catalysts: easy removal of copper traces and controlled radical polymerizations in protein nanoreactors. *Polymer Preprints/American Chemical Society, Division of Polymer Chemistry* **2011,** *52*, 521-522.

Conclusions and outlook

The research activity carried out over the course of the PhD activity focused on exploring the application of sacrificial aluminum anode in electrochemically mediated atom transfer radical polymerization (*e*ATRP) in undivided cells and comparing it with a traditional two-compartment setup. The effects of anodic dissolution of Al in various media (DMF, DMSO, MeCN, and water) were deeply investigated on the stabilities of two highly catalytic copper complexes and their performances in well-controlled ATRP processes.

In this thesis, **Chapter I** overviewed the chronological development of reversible deactivation radical polymerization (RDRP) methods, focusing on NMP, OMRP, RAFT and ATRP.[1] **Chapter II** systematically reviewed the application of electrochemical skills in ATRP,[2-4] including investigations on reaction dynamics and determination of the most relevant parameters. In addition, the characteristics of simplified *e*ATRP (*se*ATRP) were outlined and its major shortcomings, which were the main topic of my PhD work, were pointed out. **Chapter III** briefly described the materials, instruments and experimental methods used during the thesis.

The second part (**Chapters IV** and **V**) deeply explored the impacts of Al^{3+} ions released from the Al anode on the stability of copper complexes ($[Cu^{II}L]^{2+}$ and $[BrCu^{II}L]^{+}$, L =TPMA, Me_6TREN) and their performances in *se*ATRP processes in organic solvents (DMF, DMSO, and MeCN). Both TPMA and Me_6TREN are capable of forming complexes with Al^{3+} and copper ions. The outcomes of cyclic voltammetry, linear sweep voltammetry, and UV-vis-NIR investigations in **Chapter IV** have shown that $[Cu^{II}TPMA]^{2+}$ is not affected by Al^{3+} in DMF and DMSO. It may also be concluded

that the stability of the complexes formed by Al^{3+} and copper ions with TPMA in MeCN follows the order: $[Cu^{II}TPMA]^{2+}$ > $[Al^{III}TPMA]^{3+}$ > $[Cu^{I}TPMA]^{+}$. This distinctive competition reaction between the Cu^{+} and Al^{3+} ions on TPMA affects the activation process during *e*ATRP. Conversely, Cu complexes with Me_6TREN are not stable in the presence of Al^{3+} in all investigated solvents, as the ligand shows higher affinity for Al^{3+} than for Cu^{2+} or Cu^{+}.

The above investigation was extended to typical ATRP conditions, i.e., solvent/monomer mixtures, using *n*-butyl acrylate (*n*-BA) as a model monomer (**Chapter V**). The results were essentially the same as in pure solvents: $[BrCu^{II}TPMA]^{+}$ was not affected by addition of Al^{3+} ions, whereas $[BrCu^{I}TPMA]^{+}$ was stable in mixtures of *n*-BA with DMF or DMSO, but instable in *n*-BA/MeCN. The competition between Cu^{+} and Al^{3+} ions for TPMA was further investigated in *n*-BA/MeCN. Copper complexes with Me_6TREN were fully destroyed by Al^{3+} in all investigated media. These detrimental competitive equilibria could be effectively suppressed by the addition of excess ligand. This is consistent with our previous work.[5-6] The competition between Al^{3+} and copper ions has also a negative impact on *e*ATRP performed in an undivided cell with a sacrificial Al anode. *e*ATRP experiments of 50 vol% *n*-BA in DMF, DMSO with TPMA performed in an undivided cell with a sacrificial Al anode were not affected by Al^{3+} ions released from the anode. Conversely, the catalytic performance of the system became heavily compromised when Me_6TREN in all solvents or TPMA in MeCN was used in the undivided cell. The interference of Al^{3+} ions during *e*ATRP could be suppressed by adding excess amine ligand. Interestingly, using a two-fold excess of Br^{-} without excess of ligand was found to be beneficial although it could not fully restore the efficiency of the Cu catalysts.

The third part (**Chapters VI** and **VII**) of the thesis evaluated $[Cu^{II}L]^{2+}$ stability in the presence of anodic dissolution of Al in aqueous solutions. For $[Cu^{II}TPMA]^{2+}$, the same behavior observed in DMF and DMSO, where a large amount of the catalyst remained stable, was found in water in the presence of high concentration of Al^{3+} ions. Conversely, the copper complex with Me_6TREN showed poor stability and decomposed in the presence of Al^{3+}. In addition, solvated Cu^{2+} ions and $[Cu^{II}Me_6TREN]^{2+}$ react

spontaneously with the Al surface, leading to irreversible depletion of Cu(II), which is converted to a metallic copper deposit on the Al surface. Again, use of excess ligand high enough to make complexes with both Al^{3+} and Cu^{2+} ions was found to effectively suppress the competition between the metal ions.

As shown in **Chapter VII**, both $[Cu^{II}TPMA]^{2+}$ and $[BrCu^{II}TPMA]^{+}$ are little affected by Al^{3+} ions and Al in both water and water/monomer mixtures. Only a small fraction of complexes (<10%) suffered from dissociation and released free solvated Cu^{2+} ions, which can react with Al to form Cu^{0}. However, both Al and Al^{3+} can destroy Cu complexes coordinated with Me_6TREN. In addition, the solution pH changed to values as low as 3 by the strong Lewis acid Al^{3+} released by anodic dissolution. $[Cu^{II}Me_6TREN]^{2+}$ is not stable at this low pH and dissociates to free Cu^{2+} ions and protonated ligand. As in pure water, both free solvated Cu^{2+} ions and $[Cu^{II}Me_6TREN]^{2+}$ can be reduced to Cu^{0} by Al and the reaction of Cu^{2+} was ca 2 times faster than that of the copper complex in H_2O + 10% (v/v) OEOMA. Therefore, the copper complexes could not be restored completely at the end of the experiment when excess ligand was added to the solution.

For *e*ATRP of 10 vol% OEOMA or DMA, $[Cu^{II}TPMA]^{2+}$ can maintain its activity during *e*ATRP of OEOMA, with only a slight negative impact of Al^{3+} ions in the undivided cell, which was successfully suppressed by using a two-fold excess of ligand over Cu^{2+}. However, the catalytic efficiency of $[Cu^{II}TPMA]^{2+}$ on DMA polymerization was very low, even in the absence of anodic dissolution of Al. In contrast to $[Cu^{II}TPMA]^{2+}$, the catalytic performance of $[Cu^{II}Me_6TREN]^{2+}$ was heavily compromised in the polymerization of OEOMA in the undivided cell, and the deposition of metallic copper was observed on both the Pt cathode and Al anode. This deterioration could be avoided by using a two-fold excess of Me_6TREN over Cu^{2+}. *e*ATRP of DMA with $[Cu^{II}Me_6TREN]^{2+}$ as the catalyst was fast and well-controlled in the undivided cell without using excess ligand. This is probably due to the strong Lewis acid nature of Al^{3+}, which appears to play a key role on well-controlled polymerization of DMA in the undivided cell.

It is noteworthy that a large excess of ligand, which would make the process highly

costly, especially for large-scale industrial production, is not an ideal solution. Therefore, in order to find a more economical approach to suppress the competition between Al^{3+} and Cu^{2+} for the ligand, the last part of the thesis focused on the investigation of the stability of copper complexes with Me_6TREN in the presence of Al^{3+} ions and common sodium salts containing different anions. As reported in **Chapter VIII**, results of particular interest were obtained with Na_2CO_3. In comparison with the ligand, Na_2CO_3 is an inexpensive additive that can effectively restore the stability of $[Cu^{II}Me_6TREN]^{2+}$ in both organic (DMF, DMSO, and MeCN) and aqueous media containing Al^{3+}; it acts also as a buffer in aqueous media, restoring the initial pH of the system. Moreover, *se*ATRP of OEOMA was significantly improved by addition of 3.0 mM Na_2CO_3. However, the carbonate ions can further react with copper complexes to form a more stable complex if a large excess Na_2CO_3 is added.*[7]* Therefore, the amount of Na_2CO_3 must be strictly controlled to guarantee enough copper catalyst species for the *e*ATRP equilibrium.

Overall, the results obtained in this thesis provide some insight into the mechanism of the reactions of Cu^{2+} ions and/or complexes with Al^{3+} ions produced by anodic dissolution of Al in various media. The obtained results will be of great help for the investigation of *se*ATRP with other sacrificial anodes such as Fe, Ni, Mg, Zn, etc. Using cells without separators is of course important but care must be exercised on the compatibility between the catalyst and the sacrificial anode. Here, we show that TPMA is compatible with the use of Al anode in an undivided cell, provided that DMF, DMSO, or water is used as solvent. In contrast, competition reactions leading to loss of catalyst occur for Me_6TREN, in all selected solvents, and for TPMA in MeCN. These reactions could be avoided by the addition of excess of ligand and/or Br^-, or Na_2CO_3 as an ideal low-cost inorganic additive. However, one significant drawback of Na_2CO_3 is its low solubility in organic solvents. This problem will likely be circumvented by employing carbonate salts with good solubility in organic solvents. In the near future, the robust development of *se*ATRP polymerization study will facilitate the preparation of polymers with various architectures and functionalities, thus enabling the synthesis of functional materials used in diverse fields.

Reference

[1**]**. Corrigan, N.; Jung, K.; Moad, G.; Hawker, C. J.; Matyjaszewski, K.; Boyer, C., Reversible-deactivation radical polymerization (Controlled/living radical polymerization): From discovery to materials design and applications. *Progress in Polymer Science* **2020**, 101311.

[2**]**. Pan, X.; Fantin, M.; Yuan, F.; Matyjaszewski, K., Externally controlled atom transfer radical polymerization. *Chemical Society Reviews* **2018,** *47* (14), 5457-5490.

[3**]**. Isse, A. A.; Gennaro, A., Electrochemistry for Atom Transfer Radical Polymerization. *The Chemical Record* **2021**.

[4**]**. Chmielarz, P.; Fantin, M.; Park, S.; Isse, A. A.; Gennaro, A.; Magenau, A. J. D.; Sobkowiak, A.; Matyjaszewski, K., Electrochemically mediated atom transfer radical polymerization (*e*ATRP). *Progress in Polymer Science* **2017,** *69*, 47-78.

[5**]**. Lorandi, F.; Fantin, M.; Isse, A. A.; Gennaro, A., Electrochemically mediated atom transfer radical polymerization of n-butyl acrylate on non-platinum cathodes. *Polymer Chemistry* **2016,** *7* (34), 5357-5365.

[6**]**. De Bon, F.; Isse, A. A.; Gennaro, A., Towards scale-up of electrochemically-mediated atom transfer radical polymerization: Use of a stainless-steel reactor as both cathode and reaction vessel. *Electrochimica Acta* **2019,** *304*, 505-512.

[7**]**. Wang, Z.; Lorandi, F.; Fantin, M.; Wang, Z.; Yan, J.; Wang, Z.; Xia, H.; Matyjaszewski, K., Atom transfer radical polymerization enabled by sonochemically labile Cu-carbonate species. *ACS Macro Letters* **2019,** *8* (2), 161-165.

Appendix

Glossary of Acronyms

CRP: controlled radical polymerization
ATRP: atom transfer radical polymerization
*e*ATRP: electrochemically mediated atom transfer radical polymerization
RDRP: reversible-deactivation radical polymerization
NMP: nitroxide-mediated (radical) polymerization
OMRP: organometallic-mediated radical polymerization
RAFT: reversible addition-fragmentation chain transfer
*se*ATRP: simplified *e*ATRP
TPMA: tris(2-pyridylmethyl)amine
PLP: pulse laser photolysis
R-T: a macroradical reacts with a transfer agent
LRP: a living radical polymerization
CLRP: controlled/living radical polymerization
IUPAC: the international union of pure and applied chemistry
SRMP: stable radical mediated polymerization
DTRP: degenerative-transfer radical polymerization
DT: degenerative transfer
CSIRO: the Commonwealth Scientific and Industrial Research Organization
PS: the synthesis of polystyrene
BPO: benzoyl peroxide
PRE: persistent radical effect
BDE: the bond dissociation energy
TIPNO: 2,2,5-trimethyl-4-phenyl-3-azahexane-N-oxy
RT: reversible termination
CCT: catalytic chain transfer
CMRP: cobalt-mediated radical polymerization
TERP: organotellurium-mediated radical polymerization

SBRP：organostibine-mediated radical polymerization
BIRP：organobismuthine-mediated radical polymerization
CSIRO：the Commonwealth Scientific and Industrial Research Organization
CTA：chain transfer agents
TPP：tetraphenylporphyrin
BA： *n*-butyl acrylate
APS：ammonium persulfate
CTA： chain transfer agent
SFS：sodium formaldehyde sulfoxylate
PET-RAFT：photoinduced electron transfer RAFT
ATRA：atom transfer radical addition
PRE：the persistent radical effect
CRT：catalytic radical termination
DCF：dead chain fraction
ISET：inner-sphere electron transfer
AT： atom transfer
ISET-AT：inner sphere electron transfer or atom transfer
SET-LRP：single electron transfer LRP

TMEDA：*N*, *N*, *N*′, *N*′-tetramethylethylenediamine

TREN：tris(2-aminoethyl)amine
Cyclam：tetraazacyclotetradecane
Me_4Cyclam：1,4,8,11-tetraazacyclotetradecane
PMDETA：*N*, *N*, *N*', *N*', *N*''-pentamethyldiethylenetriamine
HMTETA：1,1,4,7,10,10-hexamethyl triethylenetetramine
Me_6TREN：tris(2-(dimethylamino)ethyl) amine
EBiB： ethyl α-bromoisobutyrate
TEMPO：2,2,6,6-tetramethylpiperidine-1-oxyl
SR&NI：simultaneous reverse and normal initiation
ARGET：activators regenerated by electron transfer
AGET：activators generated by electron transfer
SARA：Supplemental activator and reducing agent
ICAR：initiators for continuous activator regeneration
*photo*ATRP：photochemically mediated ATRP
*mechano*ATRP：mechanically mediated ATRP
CQ：camphorquinone
Bzh：benzhydrol
BP：benzophenone
CV：cyclic voltammetry
LSV：linear sweep voltammetry
CA：chronoamperometry
CP：chronopotentiometry

WE：working electrode
CE：counter electrode
RE：reference electrode
SI- *e*ATRP：surface-initiated *e*ATRP
CHE：catalytic halogen exchange
DMA：dimethylacrylamide
SCE：saturated calomel electrode
GC：glassy carbon
CA：chronoamperometry
GPC：gel permeation chromatography
MW：the molecular weight
RID：refractive index detector
NMR：Nuclear magnetic resonance
SEM：scanning electron microscopy
RDRP：reversible deactivation radical polymerization
n-BA：*n*-butyl acrylate
MBiB： methyl 2-bromoisobutyrate
PBA： poly(*n*-butyl acrylate)
OEOMA：oligo(ethylene oxide) methyl ether methacrylate
HEBiB：2-hydroxyethyl 2-bromoisobutyrate
EC：electrocoagulation

Publications:

1. **Luo, J.**; Durante, C.; Gennaro, A.; Isse, A. A., Electrochemical study of the effect of Al^{3+} on the stability and performance of Cu-based ATRP catalysts in organic media. Electrochim. Acta 2021, 388, 138589.
2. **Luo, J.,** M. Fantin, C. Durante, A. Gennaro, A. A. Isse, Impact of Al anode on Cu-based *e*ATRP in aqueous solution. To be submitted soon.
3. **Luo, J.**; Miriam Chavez, Gennaro, A.; Isse, A. A., Use of common inorganic salts to suppress the effects of Al anodic dissolution in simplified electrochemically mediated atom transfer radical polymerization. In preparation.

Acknowledgements

There is no way to stop the flight of time. I have passed three unforgettable years in the second-oldest university, Padova University, in Italy. During these years, I have gained knowledge and have met a lot of kind people who helped me a lot in various aspects.

First and foremost, I would like to express my most sincere gratitude towards Prof. Armando Gennaro and Prof. Abdirisak Ahmed Isse for providing me such a great opportunity to conduct my research in the top group of *Electrocatalysis and Applied Electrochemistry Group* (EAEG). Until now, the clear scene still comes out that when I first arrived at the Padova bus station and saw Prof. Armando Gennaro stood on the step waiting for my arrival, which was deeply recorded in my brain and shocked my heart. Many thanks to his amiable help, which let me fast integrate into the life in Padova University. In addition, I also received some constructive guidance from him on my PhD projects. Although he retired during my second year of PhD, we can still meet each other in the laboratory. His attitude towards work deeply touched me and let me work harder.

I deeply acknowledge my advisor, Prof. Abdirisak Ahmed Isse, for his careful guidance and patience to me throughout the three years. Therefore, I gained a lot of knowledge of electrochemistry and *e*ATRP from our every insightful discussion and his rich experience. His enthusiasm, inspiration diligence and rigorous attitude towards scientific research, have been of great affects and value for me, which I am sure will influence my future work even after I leave Padova University. Without his huge support and tremendous help, I would have not been able to enter the field of *e*ATRP research. I am deeply impressed by his strict spirits on each inconspicuous detail of the

experiment results and how patiently explained to me again and again until I understand it completely. I benefited a lot from his kind guidance especially in my last two years of PhD study. Thus, he is not only my research advisor, but also a role model and a good friend. I full-heartedly thank him again for his guidance, encouragement and support during my three years here at EAEG group, otherwise, I do not know if I can finish my study.

I've come across many great colleagues during my PhD. In particular, many thanks to Prof. Christian Durante, Dr. Alessandro Facchin, Dr. Marco Mazzucato, Luca Rosato and other EAEG members for their significant contributions and help no matter on the experiments or laboratory life and also for building such creative, supportive, caring and hard-working environments. In addition, many thanks to my friend Yanchao Lyu, Chuanyu Sun, Dr. Miriam Chavez, Jiaying Yu, Teng Ma, Jiajia Ran, Jenny Jenny, Roberto Ravazzolo, Carlo Buffatti, Carlo Giraldin, Alessandro Viel, Margherita Sabbion, Elena Pellegrin, etc., who gave me a lot of confidence and help when I was in a tough moment on experiment and low mood. Meanwhile, I must present many thanks to my country and the China Scholarship Council (CSC) for giving me an opportunity to study abroad and providing scholarships.

Last but not the least, I appreciate the unconditional supports and care, especially during this difficult pandemic, from my wife and son, Xing Xu, Jingxi Luo, my parents, Zihua Liu, Jiankang Luo, my mother-in-law, Xiaoping Liu, my older brother and sister-in-law, Chao Luo, Tiantian Zhang. They shared my happiness and sorrow during the three years of my PhD study. Just a few words are far from enough to express my gratitude for their selfless contribution, my wife is a superstar in my heart, who spends a lot of energy to take care of our lovely son with my mother-in-law. Due to the separation, I missed many first times of the growth road of my son and felt deep guilt for him. Thanks to my parents, older brother and sister-in-law, who also give a lot of help and cares to my little family so that I can study without any misgivings. Therefore, I would have never achieved what I have gained without their love and support. In addition, this paper is also to commemorate my dearest father-in-law Maocheng Xu, who passed away in 2018 before I married his favorite daughter and studied abroad.